istituto nazionale di fisica nucleare
laboratori nazionali di frascati

2013
ANNUAL REPORT

ATLAS

A. Annovi, M. Antonelli(Resp.), A. Balla(Tech.),
M.M. Beretta, H. Bilokon, C. Brutti,
E. Capitolo(Tech.), C. Capoccia(Tech.), A. Castegnaro(Laur.),
S. Cerioni (Tech.), V. Chiarella, M. Curatolo,
R. Di Nardo(Ass. Ric.), M. Dreucci, B. Esposito, M. Gatta (Tech.), C. Gatti,
P.F. Laurelli, C. La Storia(laur.), S. Lauciani(Tech.), F. Lucchesi(laur.)
G. Maccarrone, A. Martini, G. Mancini(dott.), G. Nicoletti, G. Pileggi (Tech.),
B. Ponzio(Tech.), K. Prokofiev, V. Russo(Tech.), A. Sansoni,V. Santini(laur.)
M. Testa, P. P. Valentini, T. Vassilieva (Tech.), E. Vilucchi, G. Volpi.

In collaboration with:
Centro di Calcolo:
M. Pistoni, D. Spigone

April 4, 2014

1 Introduction

After the discovery of the Higgs boson the group analysis activity has been focused on the determination of the Higgs properties. We benefit of the matured expertize on performances. Missing Transverse Energy measurement is one of the main object used in the WW channel, and muon reconstruction (efficiency, momentum calibration, etc) is crucial for the 4 lepton channel. These contributions have been made possible also thanks to the reliability and the innovative tools available on the LNF Tier2 where novel analysis method have been tested for the first time. In parallel with the data taking activity, including shifts and maintenance, we are deeply involved in two upgrade Phase I activities the Fast TracK (FTK) for the upgrade of the trigger system, and the new Small Wheel for the upgrade of the muon system.

1.1 Evidence of the spin-0 nature of the Higgs boson.

In order to confirm that the new discovered Higgs boson is the one predicted by the Standard Model, the measurement of its spin and parity is needed. In 2012 and 2013 Frascati group was strongly involved in the study of the spin an parity of the new discovered Higgs Boson with the $H \to ZZ^* \to 4\ell$ channel and in the combination with the $H{\to}\gamma\gamma H{\to}WW^*{\to}\ell\nu\ell\nu$ channels results. In the Standard Model the J^{CP} of the Higgs boson is predicted to be 0^{++}. The Standard Model spin–parity $J^P = 0^+$ hypothesis has been compared with alternative hypotheses using the Higgs boson decays $H{\to}\gamma\gamma$, $H \to ZZ^* \to 4\ell$ and $H{\to}WW^*{\to}\ell\nu\ell\nu$, as well as the combination of these channels. The 0^- spin–parity hypothesis, corresponding to a pseudoscalar (without CP mixing) produced through gluon-gluon fusion, has been tested only using the $H \to ZZ^*$. For the 1^+ and 1^- hypotheses[1] (corresponding to an exotic vector or pseudovector particle) the $H \to ZZ^*$ and $H \to WW^*$ channels are combined. In this case only the quark-antiquark annihilation production process is considered, since the Landau-Yang theorem also forbids the production of a spin–1 particle through the fusion of two on-shell gluons. For the 2^+ hypothesis, despite the large numbers of spin–2 models, a graviton-inspired tensor with minimal couplings to SM particles has been chosen. In this case both quark-antiquark annihilation and gluon fusion are considered and the study is performed as the function of $q\bar{q}$ annihilation, $f_{q\bar{q}}$, since the experimental observables are sensitive to the different polarizations. For the 2^+ hypothesis test, all the three decay modes have been used. The experimental observables sensitive to the spin and parity of the Higgs boson used in the various analysis are used to create a binned spin–parity dependent likelihood function $\mathcal{L}(J^P, \mu, \vec{\theta})$. The test statistic q used to distinguish between

[1] The spin-1 hypothesis is strongly disfavoured by the observation of the $H{\to}\gamma\gamma$ decay

the two signal spin–parity hypotheses is based on a ratio of likelihoods:

$$q = \log \frac{\mathcal{L}(J^P = 0^+, \hat{\hat{\mu}}_{0^+}, \hat{\hat{\theta}}_{0^+})}{\mathcal{L}(J^P_{\mathrm{alt}}, \hat{\hat{\mu}}_{J^P_{\mathrm{alt}}}, \hat{\hat{\theta}}_{J^P_{\mathrm{alt}}})} , \tag{1}$$

where $\mathcal{L}(J^P, \hat{\hat{\mu}}_{J^P}, \hat{\hat{\theta}}_{J^P})$ is the maximum likelihood estimator, evaluated under either the 0^+ or the J^P_{alt} spin–parity hypothesis. The $\hat{\hat{\mu}}_{J^P}$, $\hat{\hat{\theta}}_{J^P}$ represent the values of the signal strength and nuisance parameters fitted to the data under each J^P hypothesis. The distribution of the test statistic q (obtained from MC pseudo–experiments) is used to determine the corresopnding p_0-values $p_0(0^+)$ and $p_0(J^P_{\mathrm{alt}})$. The exclusion of the alternative J^P_{alt} hypothesis in favour of the Standard Model 0^+ hypothesis is evaluated in terms of the corresponding $\mathrm{CL_s}(J^P_{\mathrm{alt}})$, defined as:

$$\mathrm{CL_s}(J^P_{\mathrm{alt}}) = \frac{p_0(J^P_{\mathrm{alt}})}{1 - p_0(0^+)} . \tag{2}$$

1.1.1 $H \rightarrow \gamma\gamma$ analysis

The $H \rightarrow \gamma\gamma$ channels, that has a signal–to–background ratio of about 3%, is sensitive to the spin of the Higgs boson. In particular the spin information can be derived from the distribution of the the cosine of the polar angle θ^* of the two photons with respect to the z-axis of the Collins-Soper frame.

$$|\cos\theta^*| = \frac{|\sinh(\Delta\eta^{\gamma\gamma})|}{\sqrt{1 + (p_T^{\gamma\gamma}/m_{\gamma\gamma})^2}} \frac{2 p_T^{\gamma 1} p_T^{\gamma 2}}{m^2_{\gamma\gamma}} ,$$

Events are selected by requiring two photons with $E_{\mathrm{T}} > 35, 25$ GeV. This channel has a large background, dominated by non-resonant diphoton production, whose distribution in $|\cos\theta^*|$ is intermediate between those expected for $J^P = 0^+$ and $J^P = 2^+$. Both $m_{\gamma\gamma}$ and $|\cos\theta^*|$ are used in the final fit with the former providing separation between signal and background and the latter providing separation between the two spin hypotheses considered. The background distributions for $|\cos\theta^*|$ are derived directly from the observed data, using the two mass sidebands 105 GeV $< m_{\gamma\gamma} <$ 122 GeV and 130 GeV $< m_{\gamma\gamma} <$ 160 GeV. For the signal, the same pdf to model $m_{\gamma\gamma}$ (sum of a Crystal Ball and a Gaussian component) is used for both spin hypotheses while the $m_{\gamma\gamma}$ background shape is modeled by a fifth–order polynomial with coefficients fitted to the data. The fit to data is carried out simultaneously in the signal region and the two sideband regions. In the signal region, the likelihood is a function of the two discriminant variables $m_{\gamma\gamma}$ and $|\cos\theta^*|$, while in the sidebands only $m_{\gamma\gamma}$ is considered. The data distribution of $|\cos\theta^*|$ in the signal region (122 GeV $< m_{\gamma\gamma} <$ 130 GeV) compared with MC expectation for a $J^P = 0^+$ hypothesis for the signal is shown in figure 1.

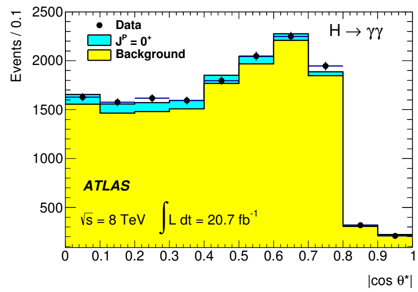

Figure 1: Distribution of $|\cos\theta^*|$ for events that fulfill the requirement 122 GeV $< m_{\gamma\gamma} <$ 130 GeV. The data (dots) are overlaid with the projection of the signal (blue/dark band) and background (yellow/light histogram) components obtained from the inclusive fit of the data under the spin–0 hypothesis.

1.1.2 $H \rightarrow ZZ^*$ analysis

The $H \rightarrow ZZ^{(*)} \rightarrow l^+l^-l'^+l'^-$ with l, l'=e or μ decay channel provide a good sensitivity for the SM Higgs boson search over a wide mass range. The main advantages for this channel are the purity (S/B∼1) and the possibility to fully reconstruct the 4-lepton final state that allows to have access to several observables dependent on the spin and parity of the Higgs boson. The kinematic observables sensitive to the J^P nature of the Higgs boson are: the reconstructed masses m_{12} and m_{34} of the two Z boson candidates (Z_1 and Z_2); the angle θ_1 (θ_2) between the negatively charged final-state lepton in the Z_1 (Z_2) rest frame and the direction of flight of the Z_1 (Z_2) boson in the four-leptons rest frame; the angle Φ between the decay planes defined by the two lepton pairs coming from the Z decays in the four-lepton rest frame; the angle Φ_1 between the decay plane of the leading lepton pair and a plane defined by the momentum of the Z_1 in the four-lepton rest frame and the direction of the beam axis; the production angle θ^* of the Z_1 defined in the four-lepton rest frame. These variables have been reconstructed for all the candidates (43 in data) within the 4–lepton invariant mass 115 GeV $< m_{4\ell} <$ 130 GeV that passes the inclusive $H \rightarrow ZZ^* \rightarrow 4\ell$ event selection described in [1]. The main backgrounds in this channel are the irreducible ZZ^* background and the reducible $t\bar{t}$, $Zb\bar{b}$ and Z+jets backgrounds. The former is estimated from MC simulation while the latter from corresponding control regions in data. In order to discriminate between pairs of J^P hypotheses, a multivariate discriminant based on a boosted decision tree (BDT) has been used, trained on the simulated signal events using the discriminating variable described above. Decicated BDTs have been trained for the separation between the SM $J^P = 0^+$ hypothesis and all the considered alternative J^P hypotheses: $J^P = 0^-$, 1^+, 1^-, 2^+. Figure 2 shows the BDT discriminant distributions for the $J^P = 0^+$ versus $J^P = 0^-$ and the

$J^P = 0^+$ versus $J^P = 1^+$ hypotheses. The distribution of the BDT output is used as a discriminant observable in the likelihood defined above.

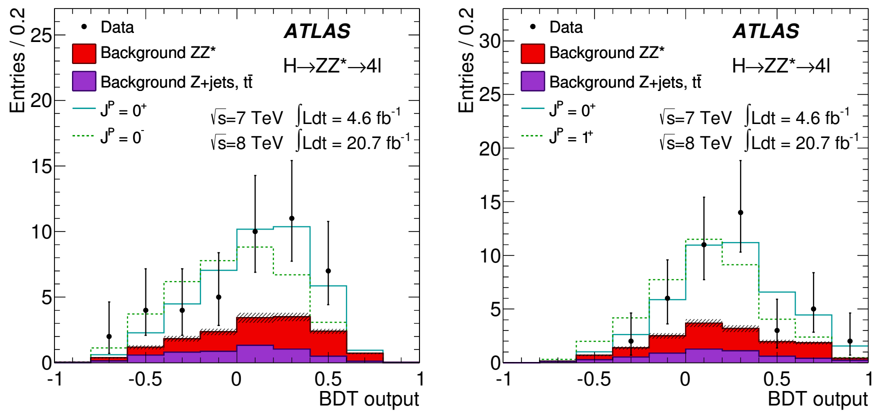

(a) (b)

Figure 2: Distributions of the BDT output for data (points with error bars) and expectations based on MC simulation (histograms). The distribution of each discriminant is shown for a pair of spin and parity hypotheses for the signal: $J^P = 0^+$ (solid line) and $J^P = 0^-$ (dashed line) in (a), $J^P = 0^+$ (solid line) and $J^P = 1^+$ (dashed line) in (b).

1.1.3 $H \to WW^*$ analysis

The analysis of the spin and parity in the $H \to WW^* \to \ell\nu\ell\nu$ channel is restricted to events containing two leptons of different flavour (one electron and one muon) and no observed jets with $p_{\rm T} > 25$ GeV within $|\eta| < 2.5$ or with $p_{\rm T} > 30$ GeV within $2.5 < |\eta| < 4.5$. The leading lepton is required to have $p_{\rm T} > 25$ GeV and the sub-leading lepton $p_{\rm T} > 15$ GeV. The major sources of background after the dilepton selection are: Z/γ^*+jets, diboson (WW, WZ/γ^*, ZZ/γ^*), top-quark ($t\bar{t}$ and single top) production, and W bosons produced in association with hadronic jets where a jet is misidentified as a lepton. Multi-jet and Z/γ^* events are suppressed by requiring relative missing transverse momentum $E_{\rm T,rel}^{\rm miss}$ above 20 GeV. The additional requirements on the dilepton invariant mass $m_{\ell\ell} < 80$ GeVand $\Delta\phi_{\ell\ell} < 2.8$ reduce the WW continuum background. The contributions from WW, top-quark and Z+jets processes are normalised to observed rates in control regions. After all the selections are expected to be selected 170 events from the SM Higgs boson signal and about 3300 events from background processes. The observed selected events in data are 3615. The most sensitive variables to the spin of the Higgs boson are the the dilepton invariant mass $m_{\ell\ell}$, the azimuthal separation of the two leptons $\Delta\phi_{\ell\ell}$ and, in a minor way, the dilepton transverse momentum $p_{\mathrm{T}}^{\ell\ell}$. A BDT is trained using the variables described above and, in addition, the transverse mass of the dilepton and missing momentum system m_{T} is included in order to maximize the separation between backgrounds and signals. Two separate BDT classifiers are developed for each hypothesis test: one classifier is trained to distinguish the $J^P = 0^+$ signal from the sum of all backgrounds while the second classifier separates the alternative spin–parity hypothesis ($J^P = 2^+$, 1^+ or 1^-) from the sum of all backgrounds. The 2–D distribution of the two BDTs is used in the binned likelihood fit to test the compatibility of the data with the $J^P = 0^+$, 1^+, 1^-or 2^+ hypotheses. Figure 3 shows the remapped 2–D BDT output distributions after background subtraction.

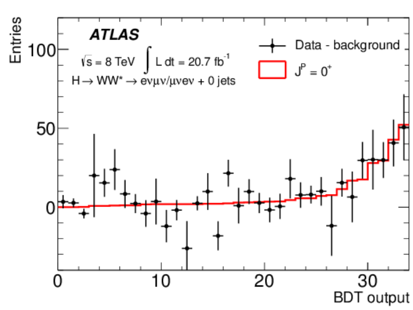

(a)

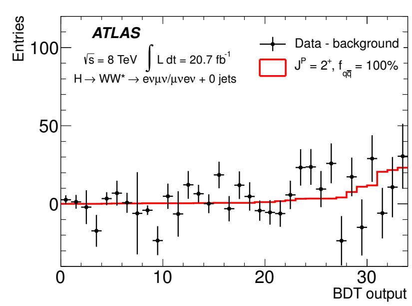

(b)

Figure 3: One-dimensional distributions of the outputs of the BDT for the $H \to WW^*$ channel after background subtraction, using best-fit values for (a) $J^P = 0^+$ and (b) $J^P = 2^+$ with $f_{q\bar{q}} = 100\%$ hypotheses.

1.1.4 Results

Test of SM $J^P = 0^+$ against $J^P = 0^-$

The expected and observed exclusion limits of the $J^P = 0^-$ hypothesis obtained with the $H \to ZZ^* \to 4\ell$ alone are summarised in figure 4(a). The data are in agreement with the $J^P = 0^+$ hypothesis with the $J^P = 0^-$ hypothesis excluded at 97.8% CL.

Test of SM $J^P = 0^+$ against $J^P = 1^+$

The expected and observed exclusion limits of the $J^P = 1^+$ hypothesis obtained form the combination of the $H \to ZZ^* \to 4\ell$ and $H{\to}WW^*{\to}\ell\nu\ell\nu$ are summarised in figure 4(a). For both channels, the data are in agreement with the $J^P = 0^+$ hypothesis while the $J^P = 1^+$ hypothesis is excluded at 99.8% CL from the $H \to ZZ^* \to 4\ell$ channel and at 92% CL from the $H{\to}WW^*{\to}\ell\nu\ell\nu$. The combination of the two channels exclude the $J^P = 1^+$ hypothesis at 99.97% CL.

Test of SM $J^P = 0^+$ against $J^P = 1^-$

The expected and observed exclusion limits of the $J^P = 1^-$ hypothesis obtained form the combination of the $H \to ZZ^* \to 4\ell$ and $H \to WW^* \to \ell\nu\ell\nu$ are summarised in figure 4(a). For both channels, the data are in agreement with the $J^P = 0^+$ hypothesis while the $J^P = 1^+$ hypothesis is excluded at 94% CL from the $H \to ZZ^* \to 4\ell$ channel and at 98% CL from the $H \to WW^* \to \ell\nu\ell\nu$. The combination of the two channels exclude the $J^P = 1^+$ hypothesis at 99.7% CL.

Test of SM $J^P = 0^+$ against $J^P = 2^+$

The expected and observed exclusion limits of the $J^P = 2^+$ hypotheses combining $H \to ZZ^* \to 4\ell$, $H \to WW^* \to \ell\nu\ell\nu$ and $H \to \gamma\gamma$ channels for all the $f_{q\bar{q}}$ values considered are reported in figure 4 (b). For all three channels, the results are in agreement with the spin–0 hypothesis. Moreover the data are in good agreement with the Standard Model $J^P = 0^+$ hypothesis over all the tested $f_{q\bar{q}}$ values. The observed exclusion of the $J^P = 2^+$ hypothesis in favour of the SM $J^P = 0^+$ hypothesis exceeds 99.9% CL for all the $f_{q\bar{q}}$ values.

1.2 Prospects for measurements of the HZZ vertex tensor structure in $H \to ZZ^* \to 4\ell$ decay channel

In order to further establish the Standard Model nature of the discovered boson, a study of its CP-nature should be performed. Indeed, theories with extended Higgs sector often require a presence of several CP-even and CP-odd Higgs bosons. In such cases, the mixing is possible and physical bosons with mixed CP could exist. While the new resonance described in the Section 1.1 is demonstrated to be dominantly CP-even, it can still contain a small admixture of a CP-odd state.

The invariant amplitude describing the interaction of a spin-0 particle and and two spin-one gauge bosons can be presented through the polarisation vectors of the gauge bosons ϵ_1 and ϵ_2:

$$A(H \to VV) \sim (a_1 M_H^2 g_{\mu\nu} + a_2(q_1+q_2)_\mu(q_1+q_2)_\nu + a_3\epsilon_{\mu\nu\alpha\beta}q_1^\alpha q_2^\beta)\epsilon_1^{*\mu}\epsilon_2^{*\nu}. \quad (3)$$

Here the q_1 and q_2 are the four momenta of the gauge bosons. Two out of the three couplings a_1, a_2 and a_3 can in general be complex numbers. The couplings a_1 and a_2 describe the tree-level and loop-induced interaction of a CP-even particle with two gauge bosons. The a_3 is responsible for the interaction of a CP-odd particle. The CP-conserving tree-level Standard Model is given by $a_1 = 1$ and $a_{2,3} = 0$. The CP violation in the Higgs sector can be generated requiring the simultaneous presence of of the a_3 and either a_1 or a_2. The observation of a significant a_2 in HZZ decay, on the other hand, will demonstrate the presence of higher order loop processes beyond those predicted by the Standard Model.

Another form of the amplitude (3) can be found in Refs. [2] and [3]. Here four couplings g_1, g_2, g_3 and g_4 are introduced with the following

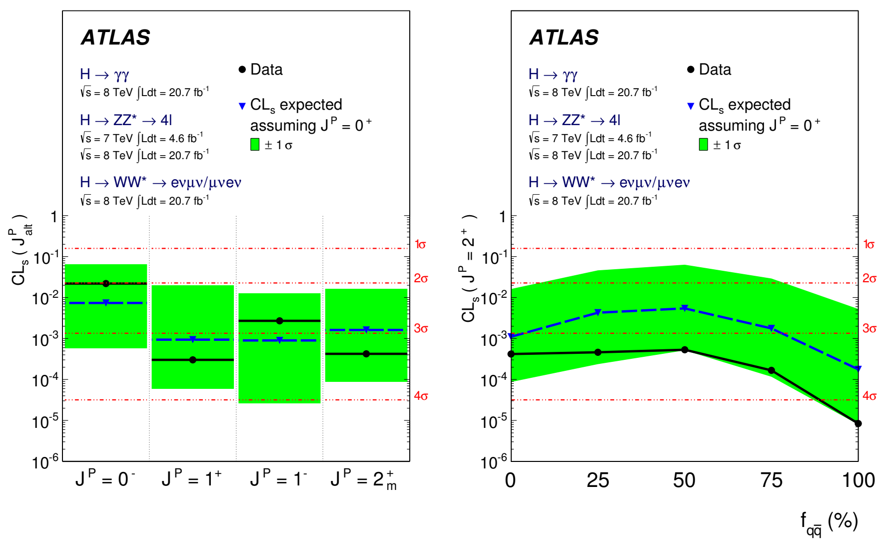

(a) (b)

Figure 4: (a)Expected (blue triangles/dashed lines) and observed (black circles/solid lines) confidence level CLs for alternative spin–parity hypotheses assuming a $J^P = 0^+$ signal. The green band represents the 68% CLs(J^P_{alt}) expected exclusion range for a signal with assumed 0^+For the spin–2 hypothesis, the results for the specific $J^P = 2^+_m$ model($f_{q\bar{q}}$ =4%), are shown. On the right y–axis, the corresponding numbers of Gaussian standard deviations are given, using the one-sided convention.
(b) Expected and observed confidence levels for $J^P = 2^+$ hypothesis for different $f_{q\bar{q}}$ values assuming a $J^P = 0^+$ signal.

momentum-dependent relation to a_1, a_2 and a_3:

$$a_1 = g_1 \frac{m_V^2}{m_H^2} + \frac{s}{m_H^2}\left(2g_2 + g_3 \frac{s}{\Lambda^2}\right); \;\; a_2 = -\left(2g_2 + g_3 \frac{s}{\Lambda^2}\right); \;\; a_3 = -2g_4, \quad (4)$$

where m_V is the mass of the gauge boson, $s = q_1 q_2$ and Λ is the new physics scale. Up to the normalisation factor, the Standard Model at tree-level corresponds to $g_1 = 1$ and $g_2 = g_3 = g_4 = 0$.
During 2013, our group has investigated the sensitivity of the ATLAS experiment to non-Standard Model contributions to the HZZ vertex for 300 fb^{-1} and 3000 fb^{-1} of the High-Luminosity LHC data. The obtained results allowed to set the expected exclusion limits for $|g_2|/g_1$, $|g_4|/g_1$. The dependence of the corresponding exclusion limits on the complex structure of g_2 and g_4 was also investigated.

1.2.1 Analysis

To obtain the limits on possible presence of g_2 and g_4 couplings in HVV decay amplitude, our group has used a so-called Matrix-element observable fit method further described in [7]. This method is based on Monte Carlo modelling of the expected signal at each bin of the $(\Re(g_i)/g_1, \Im(g_i)/g_1)$ plane, where g_i represents g_2 or g_4.
The signal samples representing the decays of Higgs bosons with $m_H = 125.5$ GeV were generated using the JHU 3.1.8 Monte Carlo generator [4]. The production was only performed for one set of tensor couplings: $g_1 = 1$, $g_2 = 1 + i$, $g_4 = 1 + i$. All other configurations of couplings are obtained by re-weighting this base sample at generator level using the target to base ratios of the corresponding Matrix Elements calculated at Leading Order. For this calculation, the JHUGenME [4] was used.
At the next stage a of the analysis, a special set of observables sensitive to the presence and structure of g_2 and g_4 is defined. These observables are constructed using the Leading Order Matrix element calculation mentioned above. The full list of observables used in our analysis is presented in the Table 1. In order to suppress the ZZ^* background and thus to further increase the signal-to-background ratio, a dedicated Boosted Decision Tree (BDT) is trained for each final state: $4e$, 4μ, $2e2\mu$ and $2\mu2e$. The training is performed on the common set of variables independent on the CP state of the signal under study. Combined with the calculated CP-sensitive observables, these BDTs are used to create two dimensional signal and background distributions for each final state and bin.
At the last stage of the analysis the normalised signal and background expectations in each $(\Re(g_i)/g_1, \Im(g_i)/g_1)$ bin and final state are compared to a test Monte Carlo data sample containing both signal and background. The test signal samples are produced independently from the base signal sample used for re-weighting. For each test Monte Carlo data sample, an Asimov dataset [5] normalised to the expected event yield is produced. The comparison of test data to the alternative Monte Carlo distribution in each bin

Observable	Sensitivity
$\ln \frac{\lvert\mathrm{ME}(g_1=1,g_2=0,g_4=0)\rvert^2}{\lvert\mathrm{ME}(g_1=0,g_2=0,g_4=1)\rvert^2}$	$\lvert g_4\rvert/g_1$
$\ln \frac{\lvert\mathrm{ME}(g_1=1,g_2=0,g_4=-2+2i)\rvert^2}{\lvert\mathrm{ME}(g_1=1,g_2=0,g_4=2+2i)\rvert^2}$	$\Re(g_4)/g_1$
$\ln \frac{\lvert\mathrm{ME}(g_1=1,g_2=0,g_4=2-2i)\rvert^2}{\lvert\mathrm{ME}(g_1=1,g_2=0,g_4=2+2i)\rvert^2}$	$\Im(g_4)/g_1$
$\ln \frac{\lvert\mathrm{ME}(g_1=1,g_2=0,g_4=0)\rvert^2}{\lvert\mathrm{ME}(g_1=1,g_2=1,g_4=0)\rvert^2}$	$\lvert g_2\rvert/g_1$
$\ln \frac{\lvert\mathrm{ME}(g_1=1,g_2=-1+i,g_4=0)\rvert^2}{\lvert\mathrm{ME}(g_1=1,g_2=1+i,g_4=0)\rvert^2}$	$\Re(g_2)/g_1$
$\ln \frac{\lvert\mathrm{ME}(g_1=1,g_2=1-i,g_4=0)\rvert^2}{\lvert\mathrm{ME}(g_1=1,g_2=1+i,g_4=0i)\rvert^2}$	$\Im(g_2)/g_1$

Table 1: Definitions of observables sensitive to the presence and structure of g_2 and g_4 considered in the current analysis. The direction in which each observable has the strongest sensitivity is listed.

of the $(\Re(g_i)/g_1, \Im(g_i)/g_1)$ plane is performed by a likelihood fit. During the fit, for each final state, the total number of signal events is fixed to its expected value while the overall signal strength and the total number of background events are treated as free parameters. After the likelihood fit of the injected sample is performed for each bin of the $(\Re(g_i)/g_1, \Im(g_i)/g_1)$ plane, the corresponding negative log-likelihood values are plotted in a two-dimensional histogram and the global minimum is found.
In order to test the sensitivity of the method to both Standard Model and CP-mixing signals, a series of closure tests are performed. The full fit machinery is applied to a set of dedicated test samples. The superimposed exclusion contours for observables sensitive to g_2 and g_4 complex structure are presented in Fig. 5 for several test data samples at 3000 fb^{-1}. It is noted that in all cases the fit converges close to the injected value independently of the complex structure of the couplings under study.

1.2.2 Results

To compare with previous publications by CMS [6], the results of this analysis are expressed in the $(f_{g_2}, f_{g_4}, \phi_{g_2}, \phi_{g_4})$ parametrization proposed in [3]:

$$f_{g_i} = \frac{|g_i|^2\sigma_i}{|g_1|^2\sigma_1 + |g_2|^2\sigma_2 + |g_4|^2\sigma_4}; \quad \phi_{g_i} = \arg\left(\frac{g_i}{g_1}\right). \tag{5}$$

The following conversion formulae is used:

$$f_{g_i} = \frac{r_{i1}^2}{1 + r_{i1}^2}, \quad \phi_{g_i} = \arg\left(\frac{g_i}{g_1}\right), \tag{6}$$

where $r_{31}^2 \approx 0.16\frac{|g_4|^2}{|g_1|^2}$ and $r_{21}^2 \approx 0.382\frac{|g_2|^2}{|g_1|^2}$. The numerical coefficients are obtained by calculating the respective cross-sections obtained from the JHU Monte Carlo generator.

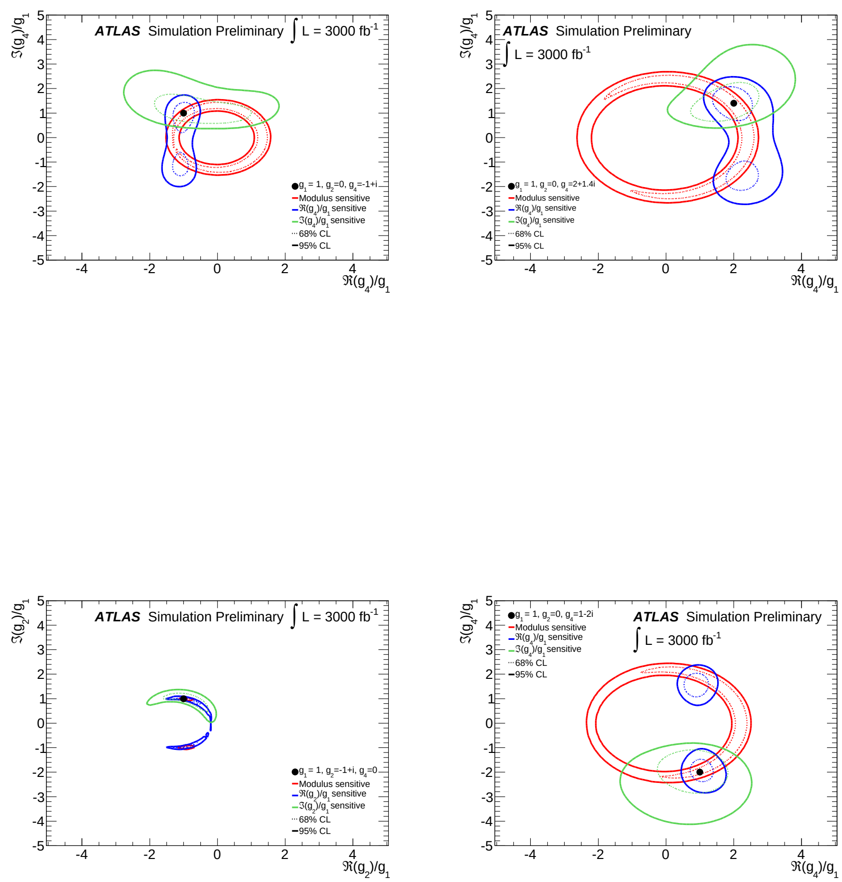

Figure 5: Superimposed 68% and 95% CL exclusion contours for observables sensitive to the complex structure of the g_2 and g_4. The contours are calculated for 3000 fb^{-1}. The selection of couplings for each injected signal sample is mentioned in the legend and indicated as a black dot on the corresponding plot.

The final exclusion limits on (f_{g_4}, ϕ_{g_4}) and (f_{g_2}, ϕ_{g_2}) planes obtained with the ME-observable fit for the Standard Model Higgs signal are presented in Fig. 6. The results are shown for 300 fb^{-1} and 3000 fb^{-1}. The parameter space outside of the shaded area is excluded at 95% CL. A summary of expected limits on f_{g_2} and f_{g_4} for 300 fb^{-1} and 3000 fb^{-1} produced with the ME-observable fit are presented in the Table 2. It can be noted that the

Luminosity	f_{g_4}	f_{g_2}
300 fb^{-1}	0.15	0.43
3000 fb^{-1}	0.037	0.20

Table 2: Expected 95% CL upper limits on f_{g_2} and f_{g_4} for 300 fb^{-1} and 3000 fb^{-1} produced with the ME-observable fit

obtained results allow for sensitive tests of the tensor structure of the $H \to ZZ^*$ couplings at the luminosities to be collected before the end of the LHC programme: 300 fb^{-1}. At present our group proceeds in deploying the ME-observable analysis at the data collected during run-I of the LHC: 25 fb^{-1}. The obtained results are expected to be published before the end of 2014.

1.3 Preparation of ATLAS Track and Vertex reconstruction software for the LHC run-II

During 2013 our group continued the preparation of ATLAS software for offline track and vertex reconstruction for the LHC run-II. In particular, a new algorithm for the reconstruction of primary vertices was designed and implemented.
The analysis of the run-I data has shown that the present primary vertex reconstruction strategy is not robust against the pile-up conditions of the LHC. Significant loss of the reconstruction efficiency was observed already at instant luminosities corresponding to 20 simultaneous *pp* collisions in the same bunch crossing [8]. The main source of the losses was identified to be the merges of nearby primary vertices, which reduce the reconstruction efficiency and often shadow the signal collision.
In order to recover the missing efficiency at the LHC run-II (expecting about $60-70$ *pp* collisions in the same bunch crossing), a new vertex reconstruction strategy was proposed. Its central part is the vertex seeding algorithm based on medical imaging technique [9]. This technique was proven to be very efficient in early association of charged tracks to potential vertex candidates. The preliminary Monte Carlo test have shown the possibility to recover the majority of merged vertices. The corresponding reconstruction efficiency stays constant with the number of *pp* collisions per bunch crossing for the luminosities expected for the LHC run-II.
In addition to the development of the new algorithm for the primary vertex reconstruction, our group has taken an important responsibility in development of the new ATLAS Event Data Model. Before the LHC run-II,

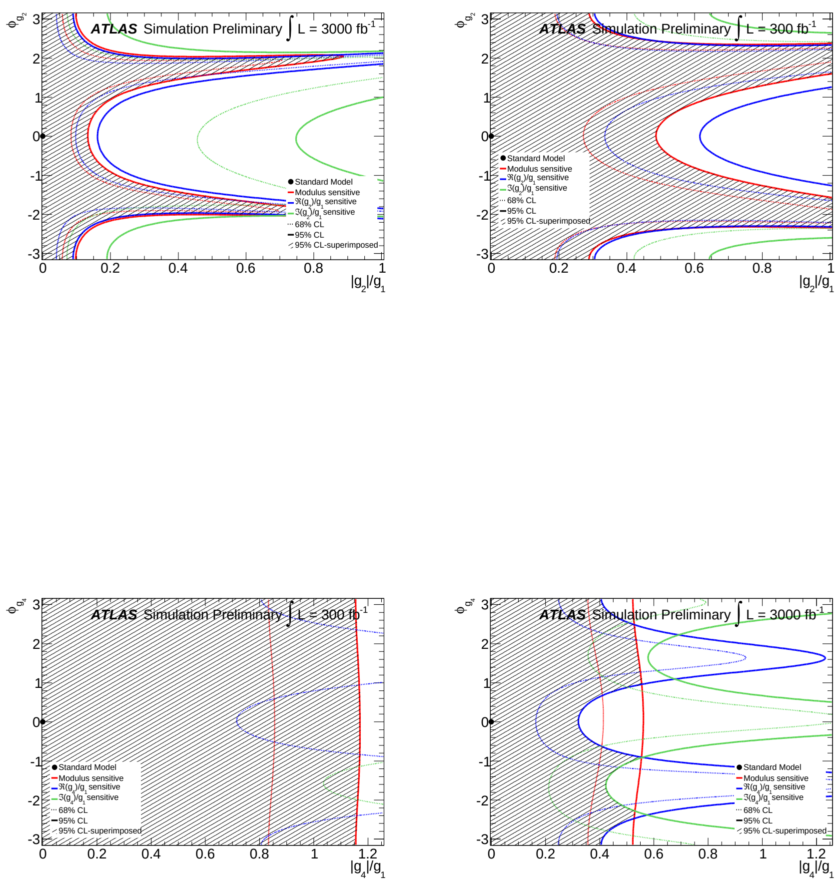

Figure 6: Couplings exclusion limits for 300 fb^{-1} and 3000 fb^{-1} obtained with the ME-observable fit for the Standard Model Higgs signal. The parameter space outside of the shaded area is excluded at 95% CL. **Top row:** Results of the g_2-sensitive fits projected onto the (f_{g_2}, ϕ_{g_2}) plane. **Bottom row:** Results of the g_4-sensitive fits projected onto the (f_{g_4}, ϕ_{g_4}) plane.

the software description of reconstructed physics objects will be changed and the new xAOD data format will be introduced. Contrary to the previous ATLAS data models, the xAOD us a ROOT-readable format, like D3PD, yet it allows for re-reconstruction of vertices inside Athena like ESD and AOD.
In order to ensure this functionality, during 2013, our group participated in the design and implementations of xAOD packages, responsible for description of charged and neutral tracks, particles and vertices. The design process is now finished and reconstruction algorithms are being updated accordingly. In the coming months, data reconstruction and analysis using new Data Model will tested on the dedicated Monte Carlo samples.

2 Particle Flow Reconstruction and PileUp suppression

The increase of luminosity for for RunII, corresponding to up to 80 mean interaction per bunch crossing, will induce serious degradation of the jets and $\not{E}_T$ resolutions and increase in fake rate contamination from Pileup jets. Standard ATLAS reconstruction exploits several techniques to mitigate Pileup effects in the jets and in the $\not{E}_T$ reconstruction. These techniques are aimed to improve resolution and reduce the fake rate of jet and $\not{E}_T$. One well established approach is calorimeter based and uses the "Jet Area" method[15], which basically evaluates the average energy Pileup contribution under the area of the jet and subtract it. This approach has the intrinsic limitation to not be able to capture local Pileup fluctuations, limiting therefore the resolution improvements and the rejection of Pileup jets. Other local approaches based on tracks have been develop to reduce Pileup jets rate. They exploit the possibility of extrapolating the tracks to the interaction vertex and therefore to identify a signal jet coming from the hard scatter vertex from the Pileup Jets coming from other Pileup vertices, using a so called Jet Vertex Fraction (JVF) cut. Even if those techniques are track-based, the constituents of the jets are calorimeter clusters. Therefore, no improvement in the resolution of jets is expected and signal jets will still suffer resolution degradation from Pileup contamination.
To face the future unprecedented Pileup conditions a Particle-Flow reconstruction has been revisited and developed within the collaboration. This kind of reconstruction can maximally mitigate Pileup effect by exploiting the correlations among the inner detector and the calorimeter. Through the association between tracks and calorimeter deposits and the track pointing to the interactions vertices, calorimeter energy deposits coming from Pileup interactions can be removed in the jets and $\not{E}_T$ reconstruction. Large improvements in resolutions and fake rate reduction can be therefore achieved. Recent studies of the Particle-Flow performances using the MonteCarlo samples and data collected in 2012 have been performed so far, showing an improvement of the jets and $\not{E}_T$ resolution and more stable behavior with

increasing Pileup contamination and a better Pileup jets rejection. This effort is going on and aims to provide an alternative jet/MET reconstruction for the next data taking during the RunII.
Figure 7 shows the fractional resolution of calorimeter based standard jets (black), calorimeter based standard jets with improved average track-based calibration (magenta) and Particle-Flow jets, based on tracks and calorimeter signals.

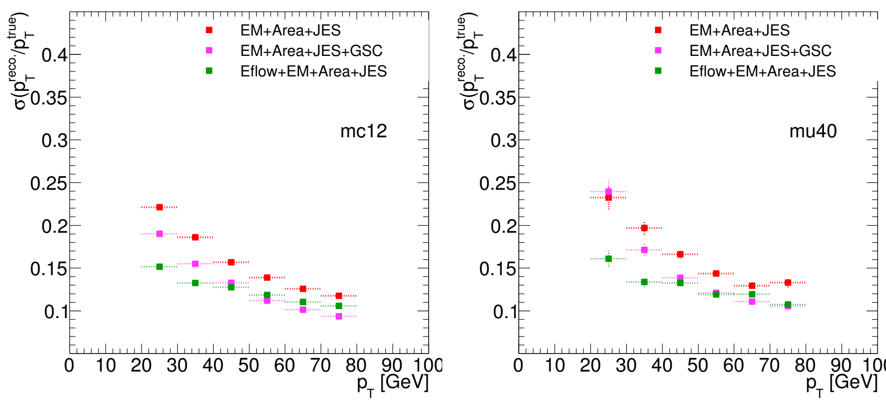

Figure 7: Fractional resolution of calorimeter based standard jets (black), calorimeter based standard jets with improved average track-based calibration (magenta) and Particle-Flow jets, based on tracks and calorimeter signals

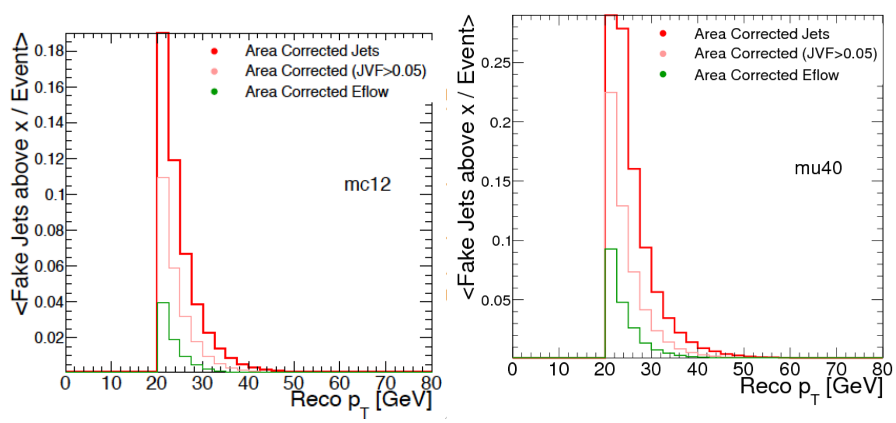

Figure 8: Fake rate of calorimeter based standard jets (red), calorimeter based standard tagged as jets from the hard scatter vertex using track information(pink), and p-flow jets (green), based on tracks and calorimeter signals

Figure 9 shows the fake rate, i.e. the rate of jets not associated to truth jets coming from the hard scatter collision, for various jet reconstructions: calorimeter based standard jets (red), calorimeter based standard tagged as jets from the hard scatter vertex using track information (pink), and Particle-Flow jets (green), based on tracks and calorimeter signals. In Both Figures 7 and 9, the left plot corresponds to the 2012 Pileup conditions, with a maximum of 30 mean interactions per bunch crossing, the right plot uses the simulated events with 40 mean interactions per bunch crossing.
The improvements in the jets performances have a direct impact on the $\not{E}_T$ reconstruction. The Particle Flow $\not{E}_T$ is reconstructed from the vectorial sum of physics objects: jets reconstructed using Particle Flow, leptons, photons and of tracks and clusters not belonging to the previous physics objects. Figure 9 shows the $\not{E}_T$ resolution versus the reconstructed numbers of primary vertices in $Z \to \mu\mu$ and $t\bar{t}$ events. The black and gray points correspond to the reconstruction without any Pileup suppression. Green and blue points are obtained using calorimeter based jets with a JVF track-based cut to tag jets from the hard scatter vertex. Red and Magenta points correspond to the Particle Flow $\not{E}_T$ reconstruction with a JVF cut.

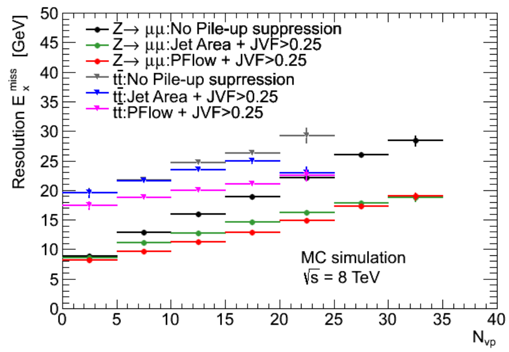

Figure 9: $\not{E}_T$ resolution versus the reconstructed numbers of primary vertex in $Z \to \mu\mu$ and $t\bar{t}$ events

3 Tier-2

During the year 2013 the Frascati's Tier-2 successfully and continuously performed all the typical activities of an ATLAS Tier-2: Monte Carlo production and users and physics groups analysis. With the exception of the first two weeks of January, when the site was shut down for the infrastructure works of the conditioning system, LNF Tier-2 has worked continuously, as we can see from the chart fig.10 left,

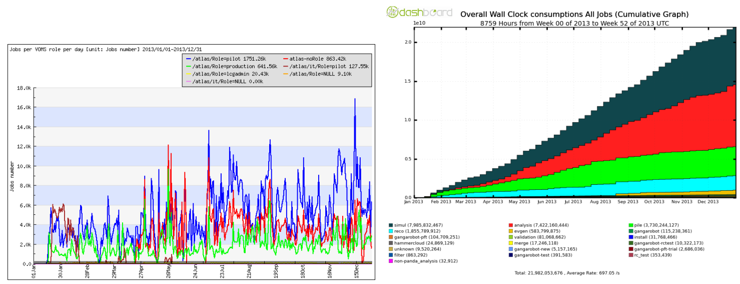

Figure 10: left: Activities performed at LNF Tier-2 during year 2013; right: Wall clock time of all jobs at LNF Tier-2 in 2013

which highlights the different activities performed in the Tier-2 in 2013. Moreover, the efficiency of the site was always maintained above 90%, so it received the greatest share of data consistent with its size. Figure 10 right reports the overall wall clock consumptions of all jobs at Frascati Tier-2, while the number of all jobs run at Frascati Tier-2 is reported in figure 11.

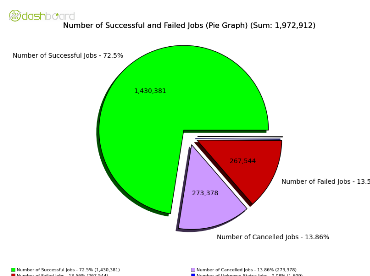

Figure 11: : Jobs run at Frascati's Tier-2 in 2013

Among the most significant activities that involved the Tier-2 and Tier-3 staff we can mention the participation in the INFN computing PRIN with the test activity of analysis tool PROOF on Demand (PoD). This activity was started in 2012 and was made in collaboration with CERN developers and the other ATLAS Italian Tier-2s, where Frascati has assumed the role of leader for all testing activities of POD in the ATLAS Italian group.
In the work of 2012 we investigated the usage of PoD to enable PROOF-based analysis on Tier-2 facilities using the PoD/gLite plug-in interface, [**?**]. In the new work of 2013, [**?**], we present the status of the investigations using the new developed PoD/PanDA plug-in to start a PROOF clusters on PanDA-managedresources, testing the system with three different real analyses of ATLAS users. So we used all the main components of the ATLAS analysis chain to evaluate the potential of PROOF-based analysis on the non-dedicated resources of an ATLAS Tier. In the work data were accessed using two different protocols: XRootD and file protocol. The former in the site where

the SRM interface is Disk Pool Manager (DPM) and the latter where the SRM interface is StoRM with GPFS filesystem. We first describe the results of some benchmark tests we run on the ATLAS Italian Tier-1 and Tier-2s sites and at CERN. Then, we compare the results of different types of analysis, comparing performances accessing data in relation to different types of SRM interfaces and accessing data with XRootD in the LAN and in the WAN using FAX: the ATLAS XROOTDstorage federation infrastructure. Then we successfully run real analysis examples at the same time of usual activities of an ATLAS Tier-2, competing with other users for analysis resources.
Below 13 some plot of benchmark tests run to test the time necessary to allocate a PROOF cluster on a Tier (12) and some benchmarck test of input data access (XRootD and GPFS in LAN) using two similar input datataset (D3PD). In 14 the plot of input access performance running two analysis with same type of input dataset, but with a different approach for the code. We also considered a third use case, still a real analysis, that uses a different sample that affects storage access performances, therefore representing a verydifferent use case of the PROOF cluster, mixed with the Grid resources accessed in a standard way.

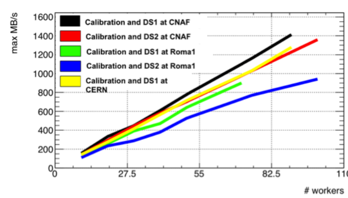

Figure 12: left: Startup latency at Tier-1/CNAF (left); right: Average startup latency.

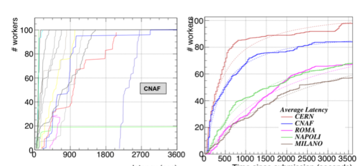

Figure 13: Max MB/s in function of number of allocated workers with input calibration DS1 and DS2 at CNAF, Roma1 and CERN.

Finally we should mention the review of Tier-2s required by the Giunta Esecutiva dell'INFN in 2013. For this review any INFN site hosting an LHC Tier-2 had draw up a document which, for Frascati [?], includes a full description of the infrastructure hosting the Tier-2 (new hall calculation, electrical and air-conditioning) and all activities (internal and external to the laboratories and INFN) that have seen the Tier-2 involved as infrastructure, as

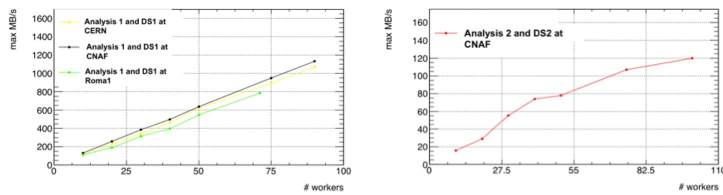

Figure 14: left: Max MB/s in function of number of workers running analysis 1 in different sites; right:Average MB/s in function of number of workers at CNAF running analysis 2.

dedicated staff and analysis groups. The review process will be completed in early 2014.

4 FTK

The trigger is a fundamental part of any experiment at hadron colliders. It is needed to select on-line the interesting low cross-section physics from the huge QCD background.
Experience at high luminosity hadron collider experiments shows that controlling trigger rates at high instantaneous luminosity can be extremely challenging. As the luminosity increases, physics goals change in response to new discoveries, and detector aging. It is thus essential that the trigger system be flexible and robust, and redundant and significant operating margin.
Providing high quality track reconstruction over the full ATLAS Inner Detector by the start of processing in the level-2 computer farm can be an important element in achieving these goals.
With the goal to improve and make more robust the ATLAS trigger, during summer 2007 the group joined the Fast-Track (FTK) proposal for “A hardware track finder for the ATLAS trigger”. This is a proposal to build a hardware track finder as an upgrade to the ATLAS trigger. It will provide global reconstruction of tracks above 1 GeV/c in the silicon detectors, with high quality helix parameters, by the beginning of level-2 trigger processing.
FTK can be particularly important for the selection of 3rd-generation fermions (b and τ). These have enormous background from QCD jets, which can be quickly rejected in level-2 if reconstructed tracks are available early. This R&D proposal was completed with the submission of the FTK Technical Proposal that was finally approved by the ATLAS collaboration meeting in June 2011.
We are continuing the design and prototyping R&D aiming to prepare the FastTrack Technical Design Report to be submitted in Spring 2013.
The FTK processor performs pattern recognition with a custom device called the Associative Memory (AM). It is an array of VLSI chips that stores pre-calculated trajectories for a ultra-fast comparison with data. The first way to reduce the combinatorial at high luminosity is to work with better

resolution in the AM. In order to do that, we will need a new AM chip with a high density of patterns, so that all possible tracks with a thinner resolution can be stored in the AM. Even with better resolution the number of candidate tracks that the AM will find at these high instantaneous luminosities will be very large. For this reason we redesigned the FTK architecture to increase the internal parallelism and data-flow to accommodate a larger flux of data.
For this purpose it was essential a new ideas. The efficiency curves for patterns is slowly increasing for efficiencies above 70%. This is due to the fact that many low probability patterns are needed to gain the missing efficiency. This is a consequence of the fact that the AM performs pattern recognition with a fixed resolution. We developed the idea of variable resolution patterns that increases the equivalent number of pattern per AMchip by a factor 3-5 with a corresponding reduction in hardware size
[doi:10.1109/ANIMMA.2011.6172856].
In the beginning of 2013 we have completed the design of a new miniasic whos aim was Testing SERDES IP and new AM core architecture. The AMchip04 was a chip with 8 times 16 bits parallel input buses that runs at 100 MHz. The main reason for the change is that the reduction in the core VDD from the standard 1.2V to 0.8V meant several different power domains within the chip. This implies many more power pins and a package change from the TQFP208 in the AMchip04 to FBGA23x23 for AMchip05. Most of these pins are devoted to the different power supply voltages and ground, as shown in figure 15. In the few remaining pins we have to accommodate all the input and output buses, the clock and the control pins. There are not enough pins to accommodate parallel buses, so we have to use high speed serialized input and output. The main requirements for the SERDES are:

- data rate of at least 2Gbps
- separate serializer and deserializer macros
- 32bit input/output buses
- driver and receiver circuits compatible with standard LVDS
- 8b/10b encode/decode capability
- comma detection and word alignment
- BIST capability for fast debugging
- low power

The LNF contribution to this task was the integration of the SERDES IP in the miniasic and the development and implementation and simulation of the communication protocol. The final layout of the chip is shown in figure 16, in which you can see in the to part of the chip the SERDES IP and in the bottom area there are the memory core architecture that has to be tested.
In 2013, after completion of the miniasic design, we have started the design of the AMchip05 layout. The aim af this new chip was to reduce the power

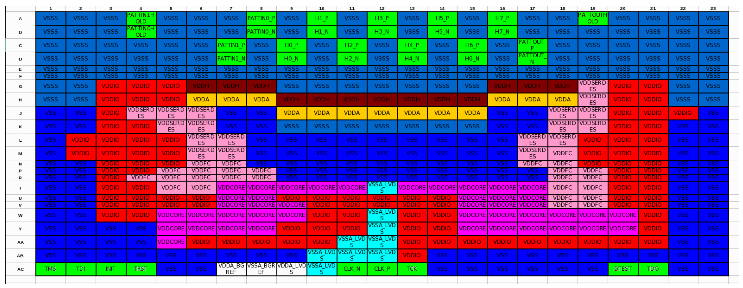

Figure 15: Sketch of the AMchip05 BGA package. The green rectangles are signal pins while all others are gounds and power supplies.

consumption as much as possible using special architectural solutions.
Moreover we want to build a small version of the final AMchip with all the functionality and final package. To reduce the power we could apply several different strategies:

1. Reduce the full custom core power supply voltage from 1.2V to 0.8V
2. Reduce the CAM layer matchline capacity (length)
3. Reduce the CAM layer matchline voltage swing from 1.2V to 0.8V
4. Reduce the bitline capacity (length)
5. Reduce the bitline voltage swing from 1.2V to 0.8V

What we wanted to avoid is reducing the clock frequency below 100MHz. As can be seen from this list, there are two different ways to control the power consumption, reduce the net capacity and their voltage swing. This is because the dynamic power consumption is dominated by the charging and discharging of line capacitance, which can be expressed by the following equation:

$$P_{Cap} = C_{line} V_{DD}^2 f \tag{7}$$

where C_{line} is the capacitance of the net, V_{DD} is the power supply voltage and f is the switching frequency of the line.
In Frascati we have designed the Low Voltage CAM cells 17.
Reducing the capacitance of the nets means reducing their length and their coupling with neighboring nets, in particular the power supply (VDD) and ground (GND). This can be achieved by properly designing the CAM cell layout. Figure 17 shows a layout example of the NOR CAM cell, in which the two memory cells are designed one over the other instead side by side as in the AMchip04 memory core. The match line path is shown in white.
The other way to reduce power consumption is to decrease the power supply voltage. However this raises speed problems, since reducing VDD increase the

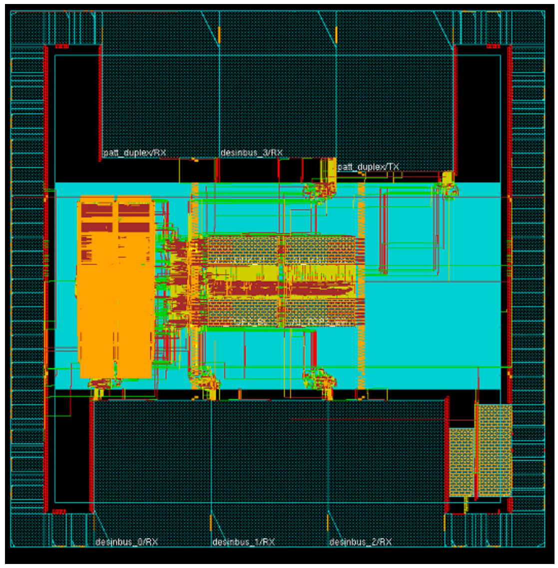

Figure 16: Layout of the miniasic.

MOS channel resistance and reduces the MOS speed. In order to maintain the circuit speed it is neecessary to use low threshold transistors instead of standard ones. Moreover, to reduce the voltage drop through the MOS channel resistance it is necessary to increase the MOS channel width and then increase the transistor area. Taking into account all of these design considerations, we arrived at the design of figure 18.
As can be seen in the figure, in order to maintain the circuit speed an additional current generator is inserted between the NAND and NOR memory cells. Previous versions of the memory layer (figure **??**) had only one current generator at the input of the NAND type memory cells. Due to all these improvements the area is increased by about 12 %.
To conclude, starting from the good results obtained in the miniasic test, we began to design the AMchip05 in TSMC 65nm technology. In this chip there will be 8 hit buses, 2 pattern-in and 1 pattern-out buses, one input 100MHz LVDS clock plus single-ended control signals: JTAG Init, Dtest, Holds.
As stated in the previous section all the input and output buses are serialized and deserialized at 2Gbs. Moreover due to the high number of power supply regions we have to pay particular attention to the floor plan of the chip.
Figure 19 shows the floor plan for the AMchip05 in which the various blocks in the chip are seen. In particular the high frequency input and output buses are aligned on the top, while the bottom is devoted to the various memory core architectures that we want to test.
In 2013, in parallel to the activity on the AMchip design we have finalized the design of the final version of the FTK IM board, that is used to clusterize the

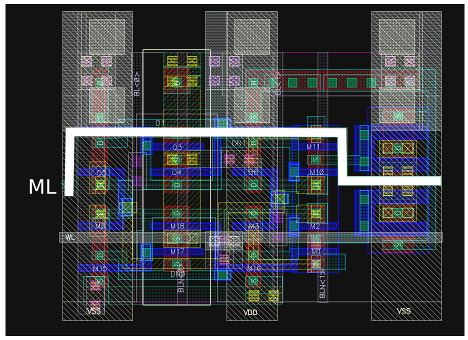

Figure 17: Nor type cell layout for AMchip05.

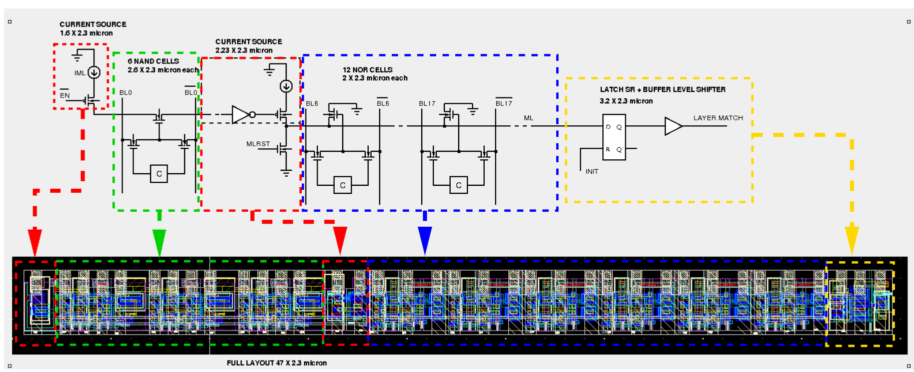

Figure 18: AMchip05 CAM layer schematic and layout.

data coming from inner tracker of the ATLAS experiment. The design of this board was started in the past year and due to some major changes in the motherboard needs to be finalized, and some part redesigned.
In partucular the connector used to connect the mezzanine to the motherboard was changed to the standard FMC HPC. This kind of connector allow high speed communication between the two boards and the pinout was defined by international standard association, in this way we can use one FPGA evaluation board to test the mezzanine without the needed of the motherboard.
All the new layout of the PCB was done in collaboration with japanese reseachers of WASEDA university.
This work was completed by the end of the summer and then a pre-production and tests was done in japan. The new mezzanine, see figure 20, works as aspected and now is mounted in the FTK demonstrator at CERN. Some further minor tests and development has to be done in 2014.

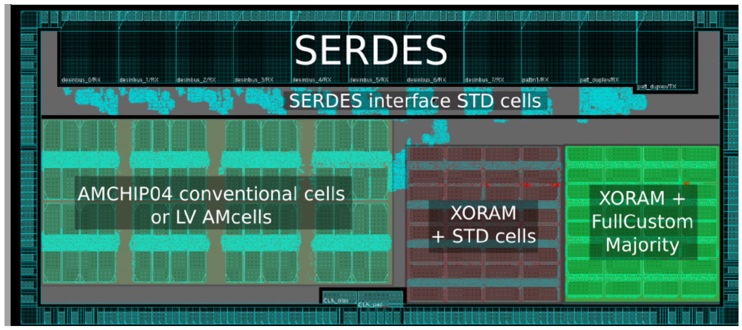

Figure 19: Floor plan of the AMchip05.

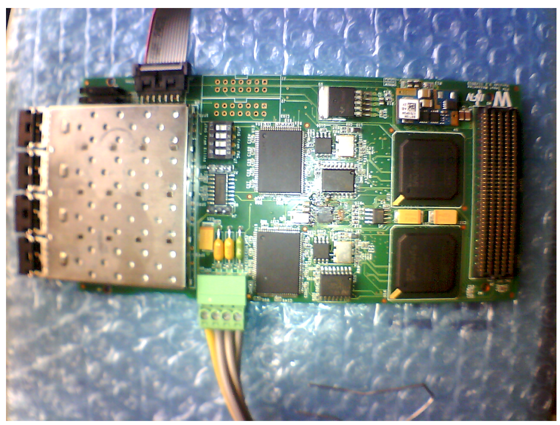

Figure 20: Final version of the FTK IM mezzanine board.

5 MicroMegas tests with cosmic rays

The ATLAS cosmic Ray Stand (CRS) is located in the Gran Sasso hall at LNF. It was originally designed for the test of the ATLAS muon chambers (MDT). A recent picture is shown in figure 21. A fully instrumented MDT chamber is hooked to a couple of rails that allow it to roll in and out. A second MDT, on top of the first one, could be instrumented and used to increase tracking precision. Below the lower MDT chamber, a table is free to roll on the rails to easy the detector posistioning. Plastic scintillators are used for triggering: three pairs (only one in the picture) are mounted below the table; four pairs are placed on ground, below 30 cm of iron used for screening from low-momentum muons. The MDT chamber has been calibrated reconstructing cosmic-ray tracks (figure 22). The spatial resolution is not yet optimal since sag correction is needed to center the anode wire inside the tube.

Figure 21: Left: Recent picture of the ATLAS CRS.

We are now putting into operation the ATLAS *rasnik* system needed to apply this correction.

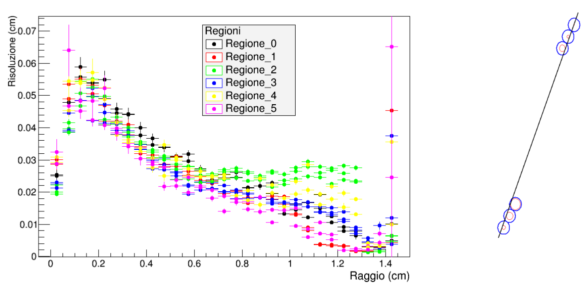

Figure 22: Left: Resolution measured for different region of the MDT chamber. Sag correction is needed to reach optimal resolution of about $100\mu m$. Right: Cosmic-ray track reconstructed in the MDT chamber.

Three $10 \times 10\text{cm}^2$ MicroMegas chambers have been mounted on a frame and tested with cosmic rays. The three chambers could be rotated in order to change the average impinging angle of cosmic rays. Several studies have been performed on efficiency, resolution and calibrations [18, 19].
The frame has been put below the MDT chamber for a combined data acquisition, as shown in the left panel of figure 23. In the left panel we show a reconstructed combined event. Six hit MDT-tubes are visible with the corresponding track. Three red circles show the clusters recosntructed in the MicroMegas. The blue boxes represent the hit scintillators.

6 MicorMegas tests with particle beams

In June 2013 we performed a test on MicroMegas chambers with an electron beam at Desy laboratory. The electron energies varied from 3 to 6 GeV at a

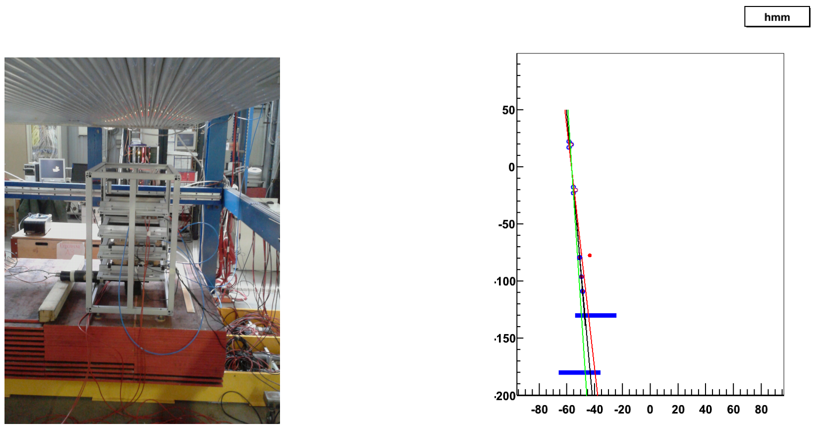

Figure 23: Left: CRS setup fo the combined run of MDT and three MicroMegas chambers. Right: Fully reconstructed event.

rate ranging from 10 to 30 Hz. The chambers were placed both in front and inside a magnet coil to allow momentum measurement. Several prototype

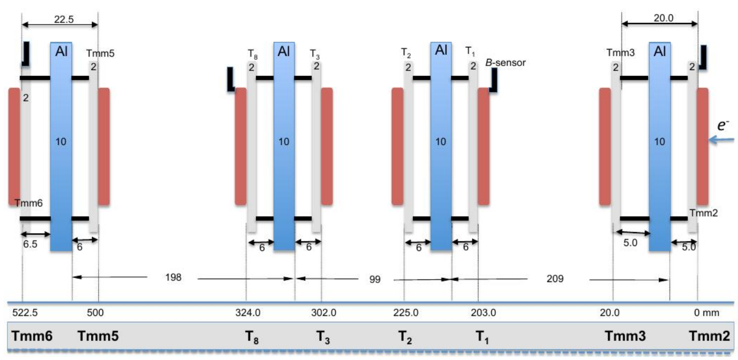

Figure 24: Test beam setup at Desy.

chambers were tested. These had an active area of about 10×10 cm^2 and strip pitches ranging from 250 to 400 μm. A gas mixture of 93% Ar and 7%CO_2 was used. The test beam setup is shown in figure 24. The chambers were mounted on a frame and were free to rotate around the vertical axis allowing the test of the tracking capabilities for non orthogonal tracks (μTPC mode). The readout was performed with an APV25 hybrid chip sampling the integrated charge on the strips every 25 ns. These prototypes showed an efficiency close to 100% and spatial resolution of about 70μm for orthogonal tracks.

7 Sandwich construction

Due to the high precision required in the MM detector, several mechanical tests have been conducted in order to verify the feasibility of building composite sandwich, an LHCb mold (Fig: 25) has been reused to work like a stiff-back and for producing panels of about 1.6x0.35 m^2. This solution as opposed to vaccum bag technique, ensure high precision and reproducibility of results.

LHCb mold

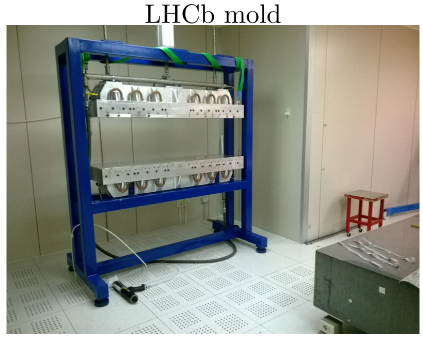

Some built panels

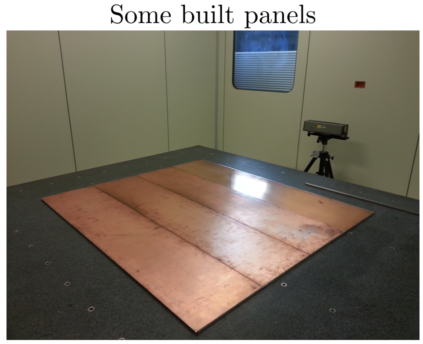

Figure 25: LHCb mold used for panel cosntruction

With the help of LNF aligment service, panels have been measured using a Laser Tracker, plots in figure 26 show results inside the specifications (less than 30μm RMS) and a good uniformity on panels shape

7.0.1 Thermoechanical Simulation

Considering the composite structure of the detector, Finite Element simulations (Figure 27) are needed in order to predict the behaviuor of prototypes and the final chamber and so, to help the designing of the whole detector. Position, thickness, shape of inner and outer frame, interconnection between panels, materials are important element to take into account, simulations will be performed to check the stability in operating conditions and morover during the assembly and construction

Surface plot of 3 jointed panels

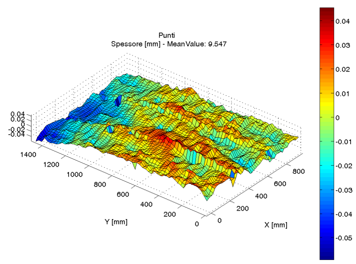

RMS: 0.018μm Mean value:9.547mm

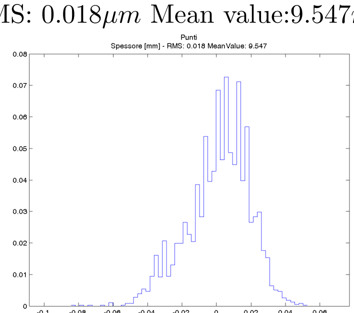

Figure 26: Panel measurements

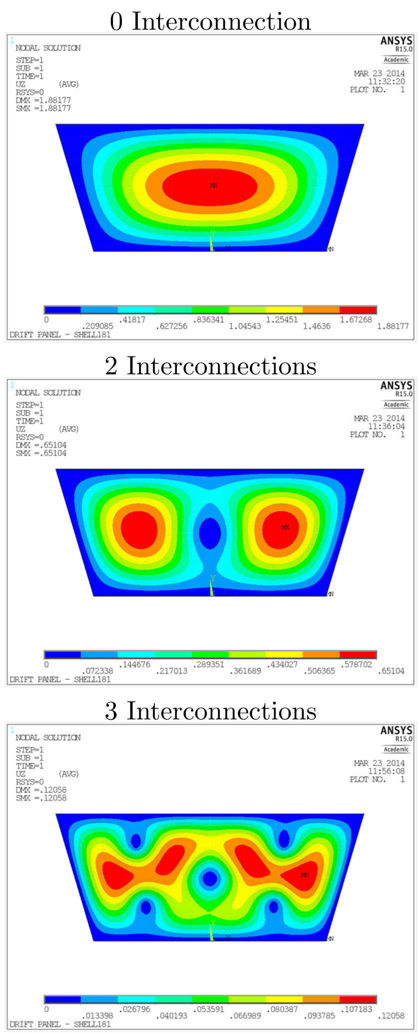

Figure 27: Direct comparison of different interconnection positions on M3 panel under $3mbar$ pressure

7.0.2 MM NSW Coordination acvtivity

A dedicated working group with the partecipation of several italian and foreign labs has been established with the aim of define final design of the detector. LNF is directly involved, playing a a role of direct responsability in design, mehcanical simulations and assembly procedures.

8 Working prototype

The first working quadruplet (Figure 28) is planned to being built in the first months of 2014

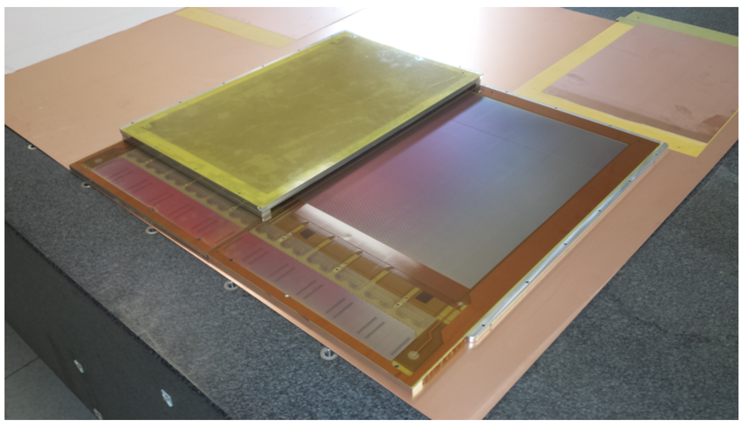

Figure 28: Working prototype first gap

Publications, internal documents and public presentations:

- R. Di Nardo,"Higgs combined results: mass, signal strengths, scalar couplings, spin and parity" , VI Workshop Italiano sulla Fisica p-p a LHC , Genova 8–10 Maggio 2013

- R. Di Nardo,“Individual and Combined Measurements of the Spin and Parity Properties of the Higgs boson using the ATLAS Detector”, PASCOS 2013 , November 20–26 2013
- R. Di Nardo,“A caccia della particella da Nobel”, INFN-Piano Triennale 2014-2016 , Napoli 17-18 Ottobre 2013
- R. Di Nardo,“Double Drell Yan process in the $Z^{*}Z^{*} \to 4l$ (e/μ) channel”, Poster, ATLAS SM Workshop, Harward 19-21 September 2013
- K. Prokofiev, “ Discovery and experimental studies of the Higgs boson at the LHC”, Invited seminar at the University of Puebla , November 23 2013.
- K. Prokofiev, “ Experimental Higgs boson studies in ATLAS”, Invited lecture at XIV Mexican Workshop on Particles and Fields, Oaxaca, Mexico , November 25-29 2013.
- K. Prokofiev, “ Higgs boson spin and parity measurements at the LHC”, Invited presentation at XIV Mexican Workshop on Particles and Fields, Oaxaca, Mexico , November 25-29 2013.
- K. Prokofiev, “ The Higgs boson and its properties: discovery, status, prospects”, Invited seminar at the University of Hong Kong , December 15 2013.
- G. Mancini, “Osservazione della nuova risonanza Higgs-like nel canale di decadimento $H \to ZZ^{*} \to 4\ell$ nell’esperimento ATLAS”, IFAE 2013, Cagliari 3-5 April 2013
- G. Mancini, “$ll + \mu\mu$ control regions for the $H \to ZZ^{*} \to 4\ell$ decay channel”, ATLAS HSG2 Rome Workshop, 16-19 April 2013
- “Evidence for the spin-0 nature of the Higgs boson using ATLAS data”, Phys. Lett. B 726 (2013), pp. 120-144
- “Measurements of Higgs boson production and couplings in diboson final states with the ATLAS detector at the LHC”, Phys. Lett. B 726 (2013), pp. 88-119
- “Study of the spin of the new boson with up to 25 fb1 of ATLAS data”, ATLAS-CONF-2013-040 (2013)
- “Measurements of the properties of the Higgs-like boson in the four lepton decay channel with the ATLAS detector using 25 fb-1 of proton-proton collision data”, ATLAS-CONF-2013-013 (2013)
- “Prospects for measurements of the HZZ vertex tensor structure in $H \to ZZ^{*} \to 4\ell$ decay channel with ATLAS”, ATL-PUB-2003-013 (2013).

- “Spin measurement in $H \to WW^* \to \ell\nu\ell\nu$ channel with 20 fb-1 of data collected with the ATLAS detector at sqrts=8 TeV”, ATL-COM-PHYS-2013-152
- “H to WW reanalysis of the 4.6 of sqrt(s) = 7 TeV data collected with the ATLAS detector in 2011”, ATL-COM-PHYS-2013-129
- ”Search for the Standard Model Higgs boson in the H-¿WW(*)-¿ leonine decay mode with 4.7 fb-1 of ATLAS data at sqrt(s) = 7 TeV” ATLAS-CONF-2012-012, 5 March 2012
- ”Search for the Standard Model Higgs boson in the H-¿WW(*)-¿lvlv decay mode using Multivariate Techniques with 4.7 fb-1 of ATLAS data at sqrts=7 TeV” ATLAS-CONF-2012-060, 6 June 2012
- Observation of an Excess of Events in the Search for the Standard Model Higgs Boson in the H -¿ WW -¿ l nu l nu Channel with the ATLAS Detector” ATLAS-CONF-2012-098, 18 July 2012
- ”Update of the H -¿ WW(*) -¿ e nu mu nu analysis with 13.0 fb1 of sqrts = 8 TeV data collected with the ATLAS detector” ATLAS-CONF-2012-158, 13 November 2012
- ”Measurements of the properties of the Higgs-like boson in the four lepton decay channel with the ATLAS detector using 25 fb-1 of proton-proton collision data”, ATLAS-CONF-2013-013
- ”Updated results and measurements of properties of the new Higgs-like particle in the four lepton decay channel with the ATLAS detector”. ATLAS-CONF-2012-169
- ”Observation of an excess of events in the search for the Standard Model Higgs boson in the H-¿ ZZ(*)-¿ 4l channel with the ATLAS detector”, ATLAS-CONF-2012-092
- ”Observation of a new particle in the search for the Standard Model Higgs boson with the ATLAS detector at the LHC”, Phys.Lett. B716 (2012) 1-29
- ”Observation of a new particle in the search for the Standard Model Higgs boson in the H ZZ()4 channel and its properties using 4.6 fb1 and 20.7 fb1 of proton-proton collisions at s = 7 TeV and 8 TeV, respectively, recorded with the ATLAS detector.”,ATL-COM-PHYS-2013-146
- ”Observation of a new particle in the search for the Standard Model Higgs boson in the H ZZ()4 channel : limits on the for VBF and VH production of the new particle and High mass search using 4.6 fb1 and 20.7 fb1 of proton-proton collisions at s = 7 TeV and 8 TeV, respectively, recorded with the ATLAS detector.”ATL-COM-PHYS-2013-145

- "Observation of a new particle in the search for the Standard Model Higgs boson in the H ZZ()4 channel : mass and signal strength measurement using 4.6 fb1 and 20.7 fb1 of proton-proton collisions at s = 7 TeV and 8 TeV, respectively, recorded with the ATLAS detector."ATL-COM-PHYS-2013-144
- "Observation of a new particle in the search for the Standard Model Higgs boson in the H ZZ()4 channel and measurements of its properties using 4.6 fb1 and 13.0 fb1 of proton-proton collisions at s = 7 TeV and 8 TeV, respectively, recorded with the ATLAS detector." ATL-COM-PHYS-2012-1483
- "Search for the Standard Model Higgs boson in the decay channel HZZ()4 with 5.8 fb1 of pp collision data at s=8 TeV with ATLAS", ATL-COM-PHYS-2012-835
- R. Di Nardo et al., Enabling data analysis la PROOF on the Italian ATLAS Tier-2s using PoD, J. Phys.: Conf. Ser. 396 (2012) 032043, [http://iopscience.iop.org/1742-6596/396/3/032043/]
- The EDRO board connected to the Associative Memory: a "Baby" FastTracker processor for the ATLAS experiment https://cdsweb.cern.ch/record/1382040/, doi:10.1016/j.phpro.2012.02.502, Physics Procedia, Vol 37, 2012, 1772-1780, ISSN 1875-3892
- The FastTrack Real Time Processor and Its Impact on Muon Isolation, Tau and b-Jet Online Selections at ATLAS, IEEE Trans. Nu cl. Sci. 59, 348. http://dx.doi.org/10.1109/TNS.2011.2179670
- "Associative Memory for L1 Track Triggering in LHC Environment", Real Time Conference (RT), 2012 18th IEEE-NPSS , vol., no., pp.1-6, 9-15 June 2012, doi: 10.1109/RTC.2012.6418193
- The AMchip04 and the processing unit prototype for the FastTracker, 2012 JINST 7 C08007

Thesis

- G. Mancini, "Study of the Higgs boson in $H \to ZZ^* \to 4\ell$ decay channel and its backgrounds determination with the ATLAS detector at LHC."

  Public presentations:

References

[1] "Measurements of Higgs boson production and couplings in diboson final states with the ATLAS detector at the LHC", Phys. Lett. B 726 (2013), pp. 88-119

[2] Gao, Y. et al.,"Spin determination of single-produced resonances at hadron colliders", Phys. Rev. , D81, 075022 (2010)

[3] LHC Higgs Cross Section Working Group and Heinemeyer, S. and Mariotti, C. and Passarino, G. and Tanaka (Eds.), R., "Handbook of LHC Higgs Cross Sections: 3. Higgs Properties", CERN-2013-004 (2013), arXiv hep-ph:1307.1347

[4] Bolognesi, S. et al., "On the spin and parity of a single-produced resonance at the LHC", Phys. Rev. D86 095031 (2012).

[5] Cowan G., Cranmer K., Gross E. and Vitells O. "Asymptotic formulae for likelihood-based tests of new physics", Eur. Phys. J. C71 1554 (2011)

[6] CMS Collaboration, "Updated results on the new boson discovered in the search for the standard model Higgs boson in the $H \to ZZ \to 4l$ channel in pp collisions at $\sqrt{s} = 7$ and 8 TeV," CMS-PAS-HIG-12-04 (2012)

[7] The ATLAS Collaboration " Prospects for measurements of the HZZ vertex tensor structure in $H \to ZZ^* \to 4\ell$ decay channel with ATLAS", ATL-PUB-2003-013 (2013).

[8] K. Grimm, E. Guido, F. Meloni, S. Pagan Griso, K. Prokofiev, M. Rudolph and A. Wildauer, "Methods to quantify the performance of the primary vertex reconstruction in the ATLAS experiment under high luminosity conditions," J. Phys. Conf. Ser. **396**, 022041 (2012).

[9] S. Hageböck and E. von Toerne "Medical Imaging Inspired Vertex Reconstruction at LHC," J. Phys. Conf. Ser. **396** 022021 (2012)

[10] ATLAS Collaboration, "Performance of missing transverse momentum reconstruction in proton-proton collisions at 7 TeV with ATLAS", EPJC 72 (2012), arXiv:1108.5602 [hep-ex]

[11] M.Cacciari and G.P.Salam, "PileUp subtraction using jet areas",Phys.Lett.B659 (2008) 119-126, arXiv:0707.1378 [hep-ph]

[12] ATLAS Collaboration, "Measurements of the properties of the Higgs-like boson in the $W \to l\nu l\nu$ decay channel with the ATLAS detector using 25 $\mathrm{fb}^{-}1$ of proton-proton collision data", ATLAS-CONF-2013-030

[13] : D. Barberis et al., "ATLAS computing activities and developments in the Italian Grid Cloud", J. Phys.: Conf. Ser. 396 (2012) 042052

[14] : R. Di Nardo et al., Enabling data analysis la PROOF on the Italian ATLAS Tier-2s using PoD, J. Phys.: Conf. Ser. 396 (2012) 032043, [http://iopscience.iop.org/1742-6596/396/3/032043/]

[15] M.Cacciari and G.P.Salam, "PileUp subtraction using jet areas",Phys.Lett.B659 (2008) 119-126, arXiv:0707.1378 [hep-ph]

[16] : D. Barberis et al., "ATLAS computing activities and developments in the Italian Grid Cloud", J. Phys.: Conf. Ser. 396 (2012) 042052

[17] : R. Di Nardo et al., Enabling data analysis la PROOF on the Italian ATLAS Tier-2s using PoD, J. Phys.: Conf. Ser. 396 (2012) 032043, [http://iopscience.iop.org/1742-6596/396/3/032043/]

[18] V.Santini Tesi di Laurea, "Preparazione di una stazione per raggi cosmici per il test delle camere MicroMegas per l'upgrade del rivelatore dell'esperimento ATLAS", Università "La Sapienza" AA 2012/2013 Relatori C.Bini e C.Gatti.

[19] F.Lucchesi Tesi di Laurea Triennale, "Studio di rivelatori a gas MicroMegas per l'applicazione allo spettrometro a muoni dell'esperimento ATLAS a LHC", Università "Tor Vergata" AA 2012/2013, Relatori A.Di Ciaccio e C.Gatti.

BABAR

R. de Sangro (Resp.), G. Finocchiaro, P. Patteri, S. Martellotti,
I. Peruzzi , M. Piccolo, M. Rama, A. Zallo

1 Introduction

The *BABAR* experiment has been running at the PEP-II asymmetric B factory of the SLAC National Laboratory (Stanford, USA) from 2000 to 2008, collecting a data sample corresponding to approximately $0.5\,\mathrm{ab}^{-1}$. Analysis of this large data set is still ongoing, and resulted in about thirty papers published in 2013.

Members of the LNF group have contributed to the writing of the "Physics of B Factories Book", a joint effort of the *BABAR* and Belle collaborations. The book is a comprehensive description of the B-factory experiments, of the data taking, the analysis techniques, and the physics results obtained. This endeavour has been completed at the end of 2013, and will shortly be available in print.

A PhD student member of the group has completed her doctoral thesis "Search for effects of an an Electric Dipole Moment of the τ lepton with the *BABAR* experiment", discussed in the following section.

2 Measurement of the τ lepton Electric Dipole Moment in the $e^+e^- \to \tau^+\tau^-$ production

A search for a CP violation signature arising from a non-vanishing electric dipole moment (EDM) of the τ lepton, d_τ, was performed in the $e^+e^- \to \tau^+\tau^-$ reaction with *BABAR* data. In 2013 a preliminary measurement of the τ EDM has been performed with 100 fb^{-1}.

A non-vanishing EDM would affect the $e^+e^- \to \tau^+\tau^-$ cross section in the $\tau^+\tau^-$ production vertex, modifying the Standard Model squared spin density matrix for the reaction as:

$$\mathcal{M}^2_{prod} = \mathcal{M}^2_{SM} + Re(d_\tau)\mathcal{M}^2_{Re} + Im(d_\tau)\mathcal{M}^2_{Im} + |d_\tau|^2\mathcal{M}^2_{d^2}.$$

Our EDM search is based on the method proposed by Atwood and Soni [1] of the so-called optimal observable, which maximize the sensitivity to d_τ. The optimal observables are defined as:

$$\mathcal{O}_{Re} = \frac{\mathcal{M}^2_{Re}}{\mathcal{M}^2_{SM}}, \quad \mathcal{O}_{Im} = \frac{\mathcal{M}^2_{Im}}{\mathcal{M}^2_{SM}}. \tag{1}$$

The matrix elements $\mathcal{M}^2_i = \mathcal{M}^2_i(\vec{k}, \vec{S}_\pm)$ depend on the τ^+ momentum $\vec{k}$ and on the τ^+ and τ^- spin vectors $\vec{S}_\pm$ in the τ-pair rest frame. Complete reconstruction of these quantities is impeded by the presence of undetectable neutrinos in the τ decay. We started the analysis selecting final states in which both τ leptons decay hadronically via $\tau^{\pm} \to \pi^{\pm}\nu$, since the double-body decay has only a twofold ambiguity in the τ momentum reconstruction. The $\tau^+\tau^- \to \pi^+\pi^-\nu_\tau\bar{\nu}_\tau$ event selection is performed with a cut-based procedure followed by a Multivariate Analysis with the Boosted Decision Tree (BDT) method. The purity of the final selected sample is of 47%.

Distributions of the real and imaginary optimal observables for selected data and Monte Carlo (MC) events are shown in Fig.1.

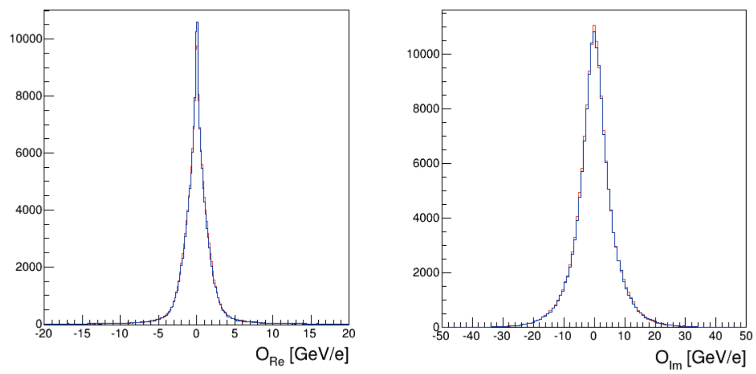

Figure 1: Distribution of the optimal observables for data (blue) and MC (red) selected events. Left: $\mathcal{O}_{Re}$; right: $\mathcal{O}_{Im}$.

The mean values of the $\langle\mathcal{O}_{Re}\rangle$ and $\langle\mathcal{O}_{Im}\rangle$ observables are linear functions of d_τ:

$$\langle\mathcal{O}_{Re}\rangle = a_{Re} \cdot Re(d_\tau) + b_{Re}, \quad \langle\mathcal{O}_{Im}\rangle = a_{Im} \cdot Im(d_\tau) + b_{Im}. \tag{2}$$

In order to extract the value of d_τ from the observable means measured on the data, we need the coefficients a_j and the offsets b_j. The slopes a_j represent the real and imaginary EDM sensitivity, the offsets b_j represent the $\langle\mathcal{O}_j\rangle$ values obtained with the MC when $d_\tau = 0$. The parameters a_j are extracted from the correlations between $\langle\mathcal{O}_{Re}\rangle$ ($\langle\mathcal{O}_{Im}\rangle$) and $Re(d_\tau)$ ($Im(d_\tau)$) obtained with the full MC simulation in which different EDM values are inserted.

The preliminary result for the the τ EDM is:

$$\begin{aligned} Re(d_\tau) &= (2.32 \pm 3.66) \times 10^{-17}\, e\,\mathrm{cm}, \\ Im(d_\tau) &= (0.61 \pm 1.12) \times 10^{-17}\, e\,\mathrm{cm}. \end{aligned} \tag{3}$$

The results are consistent with zero-EDM and show no evidence of *CP*-violation. Thanks to the large selection efficiency of the present analysis, the statistical sensitivity to the τ EDM in the $\pi^+\pi^-\nu_\tau\bar{\nu}_\tau$ final state is better compared to previous analyses. A complete evaluation of the systematic uncertainties is still underway.

References

1. D.Atwood, A.Soni, Phys.Rev. D45, 2405 (1992).

Conference Talks by LNF authors in 2013

1. **"Direct observation of time-reversal violation in B^0 decays"**
   G. Finocchiaro
   Time and Matter 2013 Conference – Venice Italy, March 2013.

2. **"$\sin 2\beta$ Measurements"**
   R. de Sangro
   Flavor Physics & *CP* Violation 2013 (FPCP 2013) – Buzios (Rio de Janeiro), May 2013.

3. **"γ from e^+e^- colliders"**
   M. Rama
   Flavor Physics & *CP* Violation 2013 (FPCP 2013) – Buzios (Rio de Janeiro), May 2013.

4. **"Recent *BABAR* results on dark matter and light Higgs searches and on *CP*- and *T*-violation"**
   I. Peruzzi.
   International Conference on New Frontiers in Physics 2013. Kolymbari, Crete, Aug. 2013

Conference papers by LNF authors in 2013

1. **"Mixing Induced T and CP Violation at *BABAR*"**
   R. de Sangro.
   PoS ICHEP **2012**, 328 (2013).

2. **"Recent *BABAR* results on dark matter and light Higgs searches and on *CP*- and *T*-violation"**
   I. Peruzzi.
   EPJ Web of Conferences vol. 71.

3. **"Direct observation of time-reversal violation in B^0 decays"**
   G. Finocchiaro.
   Proceedings of the Time and Matter 2013 Conference – Venice Italy, march 2013.

Papers published by *BABAR* in 2013

In 2013 the *BABAR* collaboration published 23 papers on Phys. Rev. D, two papers on Phys. Rev. Lett., and two papers on Nucl. Instrum. Meth. A. The complete list can be retrieved from the inspire database (http://inspirehep.net).

BESIII

M. Anelli (Tecn.), R. Baldini Ferroli (ass.), M. Bertani (Resp.), A. Calcaterra,
G. Felici, P. Patteri, A. Russo(Tecn.), Y. Wang (borsista), A. Zallo (ass.), X. Zhou(FAI fellowship),
K. Zhu (FAI fellowship) and in collaboration with: LNF Spas, S. Cerioni

1 The BESIII experiment

The BESIII experiment is taking data since 2009 at the Beijing Electron Positron Collider BEPC-II, at the Beijing Institute of High Energy Physics, IHEP. The BESIII detector is designed to study the τ-charm physics and so far BESIII collected the world largest samples of J/ψ, $\psi(3686)$, $\psi(3770)$ and $\psi(4040)$, $Y(4260)$, $Y(4360)$, the latter two having already led to a number of surprises (par 2). The actual maximum instantaneous value of the luminosity reached is 0.7×10^{33} cm^{-2} s^{-1} .

2 Five XYZ discoveries from BESIII in 2013

The quark model of charmonium, with a charm quark bound to an anticharm quark with a particular configuration of quantum numbers, has been very successful in describing the spectrum of the observed states below the $D\bar{D}$ threshold. At higher masses many new states seem to point beyond the simple $c\bar{c}$ picture, such states are ofter referred to as XYZ states and can open the window to new physics beyond the quark model. BESIII is in the unique position to provide direct production of Y(4026) and Y(4360) by simply tuning the BEPCII collider to these c.m. energies.

Between December 2012 and June 2013 BESIII collected $2.9 fb^{-1}$ of data in this energy region, mainly at $E_{cm} = 4.23, 4.26, 4.36$ GeV useful also for the production of "charged charmoniumlike states", the $Z_c(3900)$ and the $Z_c(4020)$ as well as radiative production of $X(3872)$.

2.1 The Charged $Z_c(3900)$

The $Y(4260)$ was originally discovered by BaBar [1)] and later confirmed by Belle [2)] in the initial state radiation (ISR) process $e^+e^-(\gamma_{ISR}) \rightarrow Y(4260) \rightarrow \pi^+\pi^- J/\psi$. BESIII directly produced it via $e^+e^- \rightarrow Y(4260)$ at E_{cm}=4.26GeV with $515pb^{-1}$ [22)] confirming the cross section for this process. More surprisingly, BESIII also found a charged charmoniumlike structure in the $\pi^\pm J/\psi$ subsystem. Fitting this structure, referred to as the $Z_c(3900)$, with a resonant line shape (upper left of fig.1) resulted in a mass and width of $(3899.0 \pm 3.6 \pm 4.9)$ MeV/c^2 and $(46 \pm 10 \pm 20)$ MeV, respectively. The observation of this state is remarkable because since the $Z_c(3900)$ contains $c\bar{c}$ but it is also charged, it must be composed of four quarks. It may be a tetra quark state (like $cu\bar{c}\bar{d}$) or a molecular state (such as $D^\pm \bar{D}^{o*}$). Only a few days later the $Z_c(3900)$ was confirmed by Belle [3)].

2.2 Structure in charged in $D\bar{D}^*$+c.c.

To investigate the interpretation of the $Z_c(3900)$ as a virtual $D\bar{D}^*$ molecular structure, BESIII analysed the process $e^+e^- \rightarrow \pi^- D^+ \bar{D}^{*o}$+$c.c.$ and $e^+e^- \rightarrow \pi^- \bar{D}^o D^{*+}$+$c.c.$ at $E_{cm} = 4.26$ GeV [13)]. Clear structure, referred to as the $Z_c(3885)$, in the mass spectrum of both $D^+\bar{D}^{*o}$ and $\bar{D}^o D^{*+}$ are found (middle left of fig.1). The measured mass and width are $(3883.9 \pm 1.5 \pm 4.2)$ MeV/c^2 and $(24.8 \pm 3.3 \pm 11.0)$ MeV respectively, being both slightly lower than those of the $Z_c(3900)$, and it is likely that the two structures are related to the same resonance.

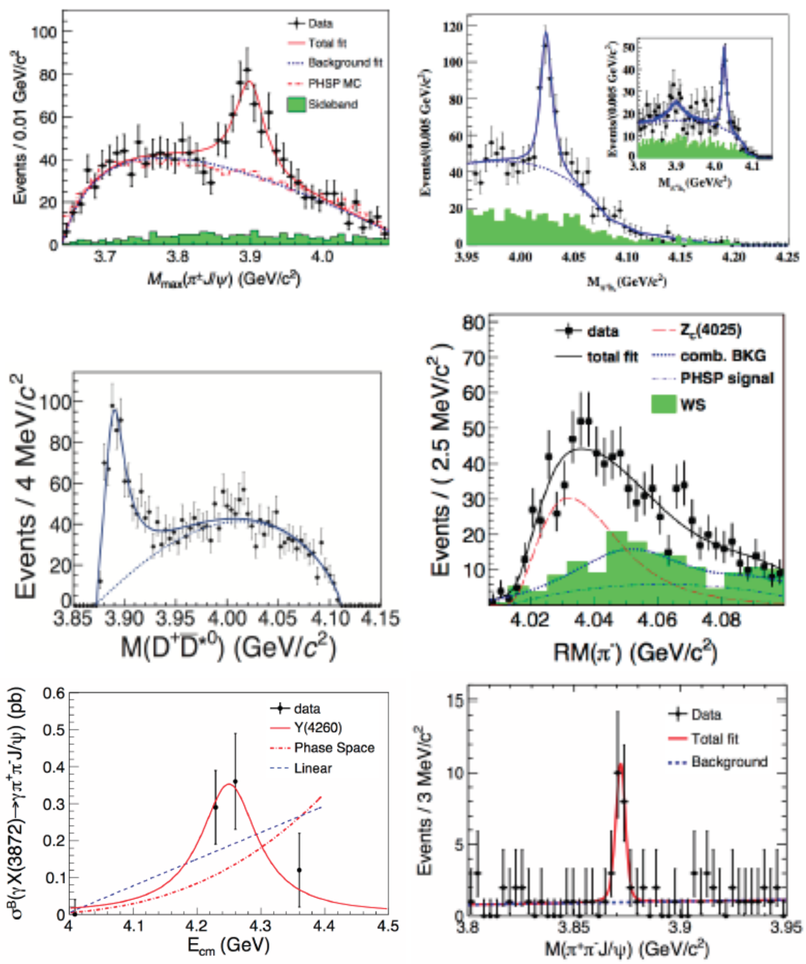

Figure 1: The five discoveries by BESIII in 2013 (see text for details): 1) Upper left: $Z_c(3900)$; 2) middle left: $Z_c(3885)$; 3) Upper right: $Z_c(4020)$; 4) middle right: $Z_c(4025)$; 5) bottom right: $X(3872)$ mass peak and bottom left: cross section for $e^+e^- \to \gamma X(3872)$ as a function of energy.

2.3 The Charged $Z_c(4020)$ in πh_c

BESIII studied also $e^+e^- \to \pi^+\pi^- h_c$ at 13 c.m. energies from 3.90 GeV to 4.42 GeV. It is found that the Born cross section is of the same order of $e^+e^- \to \pi^+\pi^- J/\psi$ but with different lineshape. More surprisingly, in the $\pi^\pm h_c$ mass spectrum, a distinct structure, the $Z_c(4020)$, is observed [14] at 4.02 GeV/c^2 (upper right of fig1). The mass and width of this structure are measured to be $(4022.9 \pm 0.8 \pm 2.7)$ MeV/c^2 and $(7.9 \pm 2.7 \pm 2.6)$ MeV. Like the $Z_c(3900)$, the $Z_c(4020)$ is charged and so must contain more quarks than just $c\bar{c}$.

2.4 Structure in charged $D^*\bar{D}^*$

Since the masses of $Z_c(3900)$ and $Z_c(4020)$ are slightly larger than the $D\bar{D}^*$ and $D^*\bar{D}^*$ mass threshold, a search for Z_c candidates via direct decay into $D^*\bar{D}^*$ has been performed at 4.26 GeV by BESIII. A structure decaying to $(D^*\bar{D}^*)^\pm$ in the process $e^+e^- \to \pi^\pm(D^*\bar{D}^*)^\pm$ has been found [15] (middle right plot of fig1). The mass and width of the structure, $(4026.3 \pm 2.6 \pm 3.7)$ MeV/c^2 and $(28.4 \pm 5.6 \pm 7.7)$ MeV respectively, are somewhat larger than those of the $Z_c(4020)$ but close enough to suggest a connection between the two.

2.5 Observation of the radiative production of X(3872)

One final surprise from the 2013 BESIII data is the observation for the first time of the X(3872) in the process $e^+e^- \to \gamma X(3872)$ with $X(3872) \to \pi^+\pi^- J/\psi$ (lower right plot of fig.1) [12]. This is a new way to access the X(3872) which is still one of the least understood of the XYZ states. The cross section of $e^+e^- \to \gamma X(3872)$ as a function of c.m. energies shown in the left bottom plot of fig.1, suggests the X(3872) is more consistent with a Y(4260) shape rather than phase space or a liner line shape.
The five discoveries of BESIII seen in e^+e^- collisions with c.m. energies near the mass of the Y(4260) suggest there is an intimate connection between Y(4260) and the $Z_c(3900)$, the $Z_c(4020)$ and the X(3872) and further studies are going on in BESIII.

3 Cylindrical GEMs study for the of the BESIII Inner Traker

The BESIII group applied at the end of 2012 for funding to the Italian Ministry of Foreign Affairs (MAE) in the cadre of a Program of Great Relevance between Italy and the People Republic of China. The proposition was for constructing a prototype layer of a Cylindrical GEM Inner Tracker, much similar to the one made in previous years at LNF by the KLOE-2 group.

This one layer is designed to be incorporated in a final, 3-layer complete detector to be installed in the year 2017 in BESIII, with the object to replace the inner part of the present BESIII drift chamber, that shows signs of degradating performance due to the high machine background.

The innovative part of the proposal consists in the strip readout, that in KLOE-2 is digital: we propose an analogic readout, to measure the particle impact points via weighted averages of charges developed on adjacent strips. This improvement on hit resolution is necessary because the magnetic field in BESIII, higher than in KLOE-2, has a greater dispersing effect on the charges migrating in the detector cells, resulting in wider clusters.

The proposition was approved by MAE in January 2013, and the group started intensive cooperation with the Chinese counterpart to discuss and clarify all details regarding construction, in view of final installation of this prototype in BESIII (once proved functional). In 2013 the MAE project was advanced by procurement of all materials and parts needed to build the first CGEM-IT prototype: molds, GEM and electrode foils, and all parts for the HV system. Preparation of the clean room at LNF where the prototype will be built has also been concluded.

The LNF-specific work was dedicated to refurbishment of the clean room used by the KLOE-2 physicist to produce their detectors, modifications to fixtures and apparata for lamination of planar electrodes into cylindrical ones, made necessary by the different dimensions of our detectors with respect to KLOE-2, and to the setup of a cosmic ray laboratory to investigate the behaviour of a small planar chamber that we built, but otherwise identical to the final cylindrical prototype.

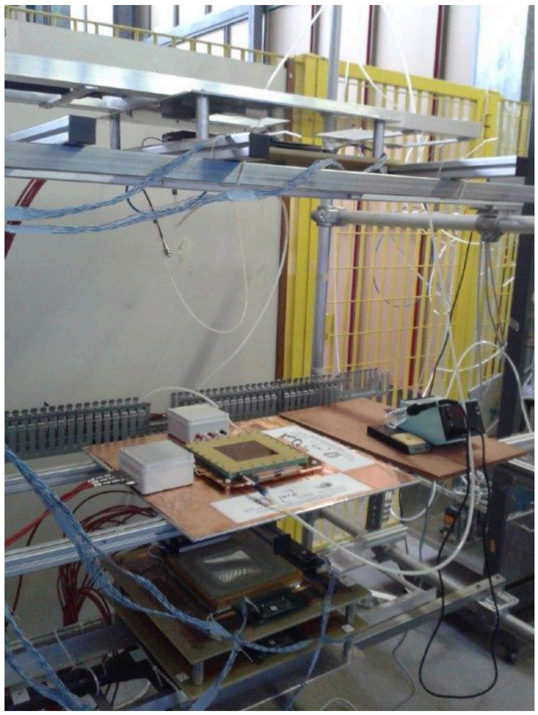

Figure 2: Picture of the cosmic ray setup test in LNF, see description in the text.

3.1 Cosmic Ray Test Setup

A cosmic ray setup has been implemented to test different gas mixtures and readout electrode geometries on a new 10x10cm^2 planar chamber with analog readout. The setup is composed of two 10x10cm^2 scintillators and three 10x10 cm^2 GEM tracking chambers of the KLOE-2 type, using 650μm wide XY strips.

The scintillators are used to generate the acquisition trigger, while the tracking chambers, instrumented with the GASTONE64 chip developed in Bari for digital readout, measure the impact point of cosmic rays with a single-hit resolution of about 200μm.

The hardware setup, shown in fig.2 , is built around a support structure for detectors, a 2-component (Argon/Isobutane) gas system, a system for HV distribution and associated slow controls, and a VME readout chain. It was implemented in late 2013, and the early 2014 cosmic ray activity will be mainly devoted to the development and crosscheck of the acquisition and tracking software.

4 Physics analysis

The relative phase between the J/ψ decay amplitudes, strong and electromagnetic one, is a hot topic and rised wide interests in the high energy physics community for many years. Knowledge of this fundamental parameter will help us to understand the decay mechanics and sub-structure of hadrons. Many studies have been done via J/ψ two body decays to 0^-0^-, 1^-0^-, 1^-1^-, and $N\bar{N}$ [4, 5, 7], also reported in the 2012 LNF Activity Report, and all of these results favour a nearly orthogonal relative phase angle between strong and electromagnetic amplitudes in the J/ψ decays. In contrast, this large phase angle has not been observed in $\psi(3686)$ decays so far. Within the experiment uncertainties, the relative phase angle is consistent with zero in 1^-0^- and 1^+0^- decays. Some suggestions are proposed to explain this marked difference between the phase angles in J/ψ and $\psi(3686)$ decays. However, none of these explanations has been widely accepted as a final answer to this question partially due to the lack of information also from experimental side. However no simple explanation has been put forward until now on why in the case of J/ψ decay there is this large phase angle.
In this regard, following the analysis reported last year on $J/\psi \to p\bar{p}$ and $n\bar{n}$ at BESIII, we have studied the relative phase between the amplitudes of strong and electromagnetic interactions at the J/ψ through an energy scan, it is a model independent method, and also we looked to $\psi(3686) \to p\bar{p}$ and $n\bar{n}$, as reported in the following two paragraphs.
On the basis of the results we got (no interference with the continuum for hadronic J/ψ decays), in order to explain them, we have developed a new quarkonium model. In short, following a suggestion by Freund and Nambu, it is assumed that quarkonium is a superposition of a very narrow state, coupled to leptons but not to hadrons, and a wide state, not coupled to leptons but coupled to hadrons (a glueball). In this way the 90 degrees phase is naturally achieved and the glueball can be wide enough do not contradict any experimental result, at least at the present level of accuracy. Remarkably enough the same model, applied to the OZI violating decay of the ϕ, predicts a 180 degrees phase, the coupling constant between narrow and wide state is the same as the J/ψ one, and the glueball is expected at about 1.34 GeV, 0.5 GeV wide, very consistent with an unexpected resonance found by BaBar, decaying into three pions.

Finally a measurement of $e^+e^- \to \Lambda\overline{\Lambda}$ cross section close to threshold has been performed, as reported in the third paragraph.

The analysis described in the following have been completed and preliminary results have been submitted to the Collaboration review therefore they cannot yet be listed here.

4.1 Study of the phase between J/ψ strong and electromagnetic decay amplitudes by means of a resonance scan

The J/ψ can decay into hadrons mainly via a strong or electromagnetic (EM) process, In pQCD, the J/ψ strong amplitude A_{3g} and the EM amplitude A_{EM} are predicted to be both real as expected for the non-resonant amplitude. According to QCD, the phase angle between A_{3g} and A_{EM} should be no more than $10°$. On the other side, experimental evidences point toward an unexpected $90°$ phase difference [4, 5, 7] which means A_{3g} is orthogonal to A_{EM}. All the imaginary amplitudes are mostly obtained by comparing decay processes, belonging to the same category, modelling the amplitudes by means of SU_3 and SU_3 breaking.

In this work, a model-independent way to measure the phase difference between the strong and EM amplitudes is used by searching for an interference in Q^2 behavior. With a serie of data samples scanning the J/ψ peak in 2012 by BESIII, the phase angle between A_{3g} and A_{EM} is measured in $\pi^+\pi^-\pi^+\pi^-\pi^0$ and $\pi^+\pi^-\pi^0$ channels. The full interference between the e.m. decays and the continuum ($A_{cont.}$) has been observed in $e^+e^- \to \mu^+\mu^-$ at SLC, BES and KEDR, which means A_{EM} and $A_{cont.}$ share one common phase. This is also verified in $\mu^+\mu^-$ and $\pi^+\pi^-\pi^+\pi^-$ in our work.

After having applied common track event selections and calculated the number of events N_{obs}, the cross section for each multi-channel process is calculated with $\sigma_{obs} = N_{obs}/L\epsilon_{obs}$, where L is the luminosity of each data sample and ϵ_{obs} is the efficiency of our event selections. The phase angles are obtained by fitting J/ψ lineshapes and taking into account initial state radiation (ISR) and beam energy spread. The fitting results on J/ψ lineshape from the channels analysed are shown in Fig. 3. We have started to analyse the $\mu^+\mu^-$ and $2\pi^+2\pi^-$ channels where full interference is expected between J/ψ e.m. decay and continuum, the preliminary results are shown in figs. 3(a) and (b).

An interference pattern in the $\mu^+\mu^-$ channel was identified and measured soon after the discovery of J/ψ at SLAC, the relative phase between the resonant and non-resonant amplitudes being in good agreement with the one expected. The J/ψ lineshape of $\mu^+\mu^-$ from BESIII improves the significance of previous results and is consistent with full interference between A_{EM} and $A_{cont.}$.

In $e^+e^- \to 2\pi^+2\pi^-$ no strong decay is allowed because of G-parity conservation and full inteference between the e.m. decay and the continuum is expected. The sign of the interference is not established a priori and should be an interesting byproduct.

From the analysis of the $\pi^+\pi^-\pi^+\pi^-$ channel in BESIII, the phase angle between A_{EM} and $A_{cont.}$ is verified to be consistent with $0°$ as expected. The interference in $2\pi^+2\pi^-$ has never been measured before.

Based on $\varphi_{EM,cont.} \sim 0°$, the phase angles between A_{3g} and A_{QED} are measured from $e^+e^- \to \pi^+\pi^-\pi^+\pi^-\pi^0$ and from $e^+e^- \to \pi^+\pi^-\pi^0$, the corresponding line shapes and fit results are shown in figs. 3(c) and (d). Preliminary results on the phase angle between A_{3g} and A_{EM} turn out to be about $105°$ both for $\pi^+\pi^-\pi^+\pi^-\pi^0$ and $\pi^+\pi^-\pi^0$, confirming other results from direct hadronic decays.

4.2 Study of $\psi(3686) \to p\bar{p}$ and $n\bar{n}$

As already stated, the measurement of $\psi(3686) \to p\bar{p}$ and $n\bar{n}$ can give information on the relative phase between the strong and electromagnetic amplitude. Moreover another interesting topic would be the angular distribution of the final $N\bar{N}$ states. As it is well known, the interaction rate for the decay of a neutral vector resonance V into a particle-antiparticle pair $h\bar{h}$ has a general structure $\mathrm{d}N/\mathrm{d}\cos\theta \propto 1 + \alpha\cos^2\theta$ derived from the helicity formalism, where θ is the polar angle which specifies the direction of motion of the produced h or $\bar{h}$ in the V rest-frame. In an original paper by Brodsky and Lepage [6], they predicted $\alpha = 1$ on the basis of the QCD helicity conservation rule. However, after a very small α value of $J/\psi \to p\bar{p}$ was reported MARK II (unpublished) data, later theoretical calculations suggested the α should be smaller than 1, i.e. 0.46, if the hadron mass effect had been considered. Since then, measurements and theoretical calculation on J/ψ decays favoured the small α value conclusion. For the measurements on the α in $\psi(3686)$ decays to proton and anti-proton pairs, several results have been reported, they all prefer to a value of α smaller than 1 with large uncertainty. But the information from $\psi(3686)$ decays to neutron and anti-neutron is still missing.

In our work, we measured the branching fractions and α value via the processes of $\psi(3686) \to p\bar{p}$ and $\psi(3686) \to n\bar{n}$. This analysis is based on a $\psi(3686)$ data sample of 1.06×10^8 events collected by BESIII.

The preliminary results show a $Br(\psi(3686) \to p\bar{p} \sim Br(\psi(3686) \to n\bar{n}$, α consistent with 1 and a phase angle around $50°$.

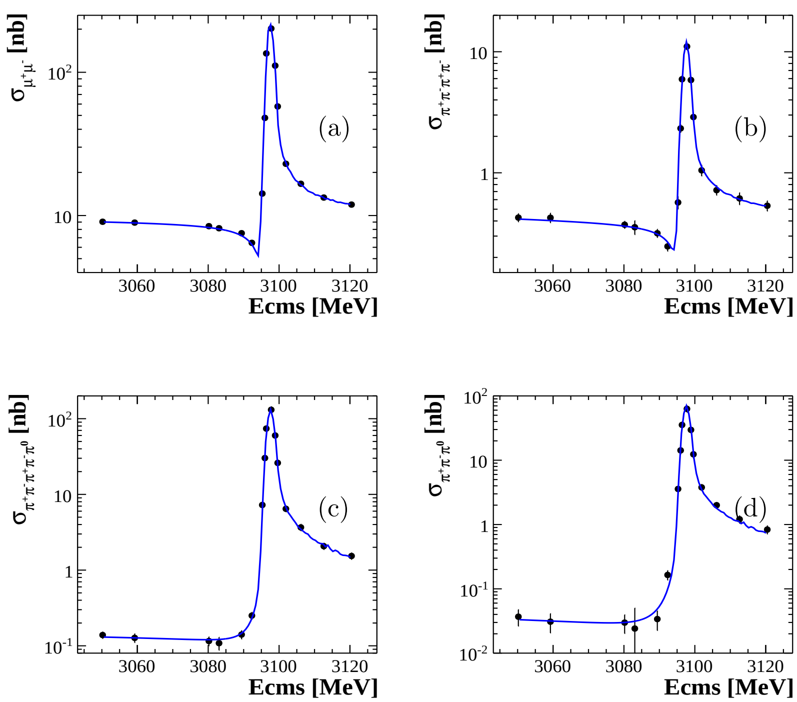

Figure 3: Fit results of J/ψ lineshape from $\mu^+\mu^-$ (a), $\pi^+\pi^-\pi^+\pi^-$ (b), where full interference is observed, $\pi^+\pi^-\pi^+\pi^-\pi^0$ (c), and $\pi^+\pi^-\pi^0$ (d) with no interference.

4.3 Study of $e^+e^- \to \Lambda\bar{\Lambda}$ close to threshold

The cross section for process $e^+e^- \to B\bar{B}$, where B is a spin-1/2 neutral baryon is expressed as follow:

$$\sigma_{B\bar{B}}(m) = \frac{4\pi\alpha^2\beta}{3m^2}[|G_M(m)^2 + \frac{1}{2\tau}|G_E(m)|^2] \qquad (1)$$

where $\beta = \sqrt{1 - 4m_B^2/m^2}$. It indicates that at threshold, cross section of neutral baryon pair production is expected to be almost 0. It could be a little larger than 0 due to the energy spread. However, the BABAR cross section [8] $\sigma = 204 \pm 60 \pm 20$ pb, which is an average value from threshold up to W = 2270 MeV, implies that there should be a spike close to threshold in the cross section. At BESIII, with 2.631 pb^{-1} data collected at 2.2324 GeV, the cross section for $e^+e^- \to \Lambda\bar{\Lambda}$ at threshold, where $\Lambda \to p\pi^-$ and $\bar{\Lambda} \to \bar{p}\pi^+$, has been measured to be (442 ± 67) pb [9].

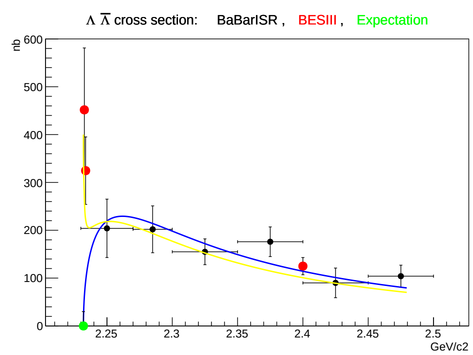

Figure 4: Comparison of the cross section for the BESIII preliminary results with BABAR results and theoretical expectation.

In this work with the 2.631 pb^{-1} data collected at 2.2324 GeV, process $e^+e^- \to \Lambda\bar{\Lambda}$ is studied. Instead of selecting the charged channel of $\Lambda \to p^+\pi^-$ and $\bar{\Lambda} \to \bar{p}\pi^+$, we only tag the $\bar{\Lambda}$ side with $\bar{\Lambda} \to \bar{n}\pi^0$. The smaller branching fraction of $\bar{\Lambda} \to \bar{n}\pi^0$ comparing to charged decay channel of Λ or $\bar{\Lambda}$ can be recovered by the semi-inclusive method. In the neutral channel of $\bar{\Lambda}$, $\bar{n}$ has information in EMC and the monoenergetic π^0 has a momentum of 105 MeV. Furthermore, $\bar{n}$ and π^0 has an angle larger than 140°. These information can be used to preliminarily select signals from data. A Boosted Decision Trees (BDT) based Multiply Variable Analysis is applied to classify signal events and hadronic background. The yields in data is obtained by fitting the π^0 momentum distribution. The cross section preliminary result is shown in fig. 4 together with BABAR results. At threshold, a cusp is observed which is much larger than the expectation in Eq. 1.

5 List of talks by LNF Authors in 2013

1. , Y. Wang, "Looking for the phase interference between strong and EM in J/ψ decays", Radio MontecarLow WG meeting: ECT* Trento, 10-12 April 2013

2. M. Bertani, "NNbar physics at BESIII" workshop "Scattering and annihilation electromagnetic processes" - ECT* Trento, 18-22 February 2013.

3. Y. Wang, " Baryon form factors at BESIII", International Workshop on e+e- collisions from Phi to Psi, 9-12 September 2013, Rome

References

1. B. Aubert *et al.* [BaBar Collaboration] Phys. Rev. Lett. **95** (2005) 142001

2. C.Z. Yuan *et al.* [Belle Collaboration] Phys. Rev. Lett. **99** (2007) 182004

3. Z.Q.. Liu *et al.* [Belle Collaboration] Phys. Rev. Lett. **110** (2013) 252002

4. G. Lopez Castro, J. L. Lucio M. and J. Pestieau, AIP Conf. Proc. **342**, 441 (1995) [hep-ph/9902300].

5. R. Baldini, M. Bertani, C. Bini, R. Calabrese, A. De Falco, M. L. Ferrer, P. Gauzzi and E. Luppi *et al.*, "Measurement of $J/\psi \to N\bar{N}$ branching ratios and estimate of the phase of the strong decay amplitude," Phys. Lett. B **444**, 111 (1998).

6. S. J. Brodsky and G. P. Lepage, Phys. Rev. D **24**, 2848 (1981).

7. M. Ablikim *et al.* [BESIII Collaboration], "Study of $J/\psi \to p\bar{p}$ and $J/\psi \to n\bar{n}$," Phys. Rev. D **86**, 032014 (2012) [arXiv:1205.1036 [hep-ex]].

8. B. Aubert, *et al*. [BaBar Collaboration], Phys. Rev. D **76**, 092006 (2007)

9. L. Yan, Report on BESIII Winter Collaboration Meeting 2013 "Lambda lambdabar at threshold".

6 Publications in 2013

10. M. Ablikim *et al.* [BESIII Collaboration], arXiv:1312.0374 [hep-ex].

11. M. Ablikim *et al.* [BESIII Collaboration], Phys. Rev. D **88** (2013) 112007

12. M. Ablikim *et al.* [BESIII Collaboration], "Observation of $e^+e^- \to \gamma X(3872)$ at BESIII," arXiv:1310.4101 [hep-ex].

13. M. Ablikim *et al.* [BESIII Collaboration], "Observation of a charged $(D\bar{D}^*)^\pm$ mass peak in $e+e- \to \pi(D\bar{D}^*)$ at $E_{cm} = 4.26GeV$,"

    [arXiv:1310.1163 [hep-ex]].

14. M. Ablikim *et al.* [BESIII Collaboration], "Observation of a charged charmoniumlike structure $Z_c(4020)$ and search for the $Z_c(3900)$ in $e^+e^- \to \pi^+\pi^-h_c$,"

    Phys. Rev. Lett. **111** (2013) 242001 [arXiv:1309.1896 [hep-ex]].

15. M. Ablikim *et al.* [BESIII Collaboration], "Observation of a charged charmoniumlike structure in e^+e^- to $(D^*\bar{D}^*)^\pm\pi^\mp$ at $\sqrt{s} = 4.26$GeV,"

    arXiv:1308.2760 [hep-ex].

16. M. Ablikim *et al.* [BESIII Collaboration], Phys. Rev. D **88** (2013) 091502

17. M. Ablikim *et al.* [BESIII Collaboration], Phys. Rev. D **87** (2013) 112011

18. M. Ablikim *et al.* [BESIII Collaboration], Phys. Rev. D **87** (2013) 112007

19. M. Ablikim *et al.* [BESIII Collaboration], Phys. Rev. D **88** (2013) 032010

20. M. Ablikim *et al.* [BESIII Collaboration], Phys. Rev. D **87** (2013) 9, 092011

21. M. Ablikim *et al.* [BESIII Collaboration], Phys. Rev. D **87** (2013) 092006

22. M. Ablikim *et al.* [BESIII Collaboration], "Observation of a charged charmoniumlike structure in $e+e-$ to pi^+pi^-J/ψ at $\sqrt{s}=4.26GeV$," Phys. Rev. Lett. **110** (2013) 252001

23. M. Ablikim *et al.* [BESIII Collaboration], Phys. Rev. D **87** (2013) 112004

24. M. Ablikim *et al.* [BESIII Collaboration], Phys. Rev. D **87** (2013) 5, 052005

25. M. Ablikim *et al.* [BESIII Collaboration], Phys. Rev. D **87** (2013) 9, 092009

26. M. Ablikim *et al.* [BESIII Collaboration], Phys. Rev. D **87** (2013) 032008

27. M. Ablikim *et al.* [BESIII Collaboration], Phys. Rev. D **87** (2013) 012007

28. M. Ablikim *et al.* [BESIII Collaboration], Phys. Rev. D **87** (2013) 5, 052007

29. M. Ablikim *et al.* [BESIII Collaboration], Phys. Rev. D **87** (2013) 3, 032006

30. M. Ablikim *et al.* [BESIII Collaboration], Phys. Rev. D **87** (2013) 3, 032007 [Erratum-ibid. D **87** (2013) 5, 059901]

31. M. Ablikim *et al.* [BESIII Collaboration], Phys. Rev. D **87** (2013) 012003

32. M. Ablikim *et al.* [BESIII Collaboration], Chin. Phys. C **37** (2013) 063001

33. M. Ablikim *et al.* [BESIII Collaboration], Phys. Rev. D **87** (2013) 012009

34. M. Ablikim *et al.* [BESIII Collaboration], Phys. Rev. D **87** (2013) 012002

35. M. Ablikim *et al.* [BESIII Collaboration], Phys. Rev. D **87** (2013) 3, 032003

36. M. Ablikim *et al.* [BESIII Collaboration], Phys. Rev. Lett. **110** (2013) 022001

CDF2

M. Cordelli (Resp.)

Not received

CMS

L. Benussi, S. Bianco, M.A. Caponero (Ass.) F.L. Fabbri (Ass.),
M. Parvis (Ass.), L. Passamonti (Tecn.), D. Piccolo (Resp.)
D. Pierluigi (Tecn.), G. Raffone, A. Russo (Tecn.), G. Saviano (Ass.), C. Franchi (Laureando.)

In collaboration with:
A.Cecchetti (SPECAS), D.Orecchini (SPECAS),

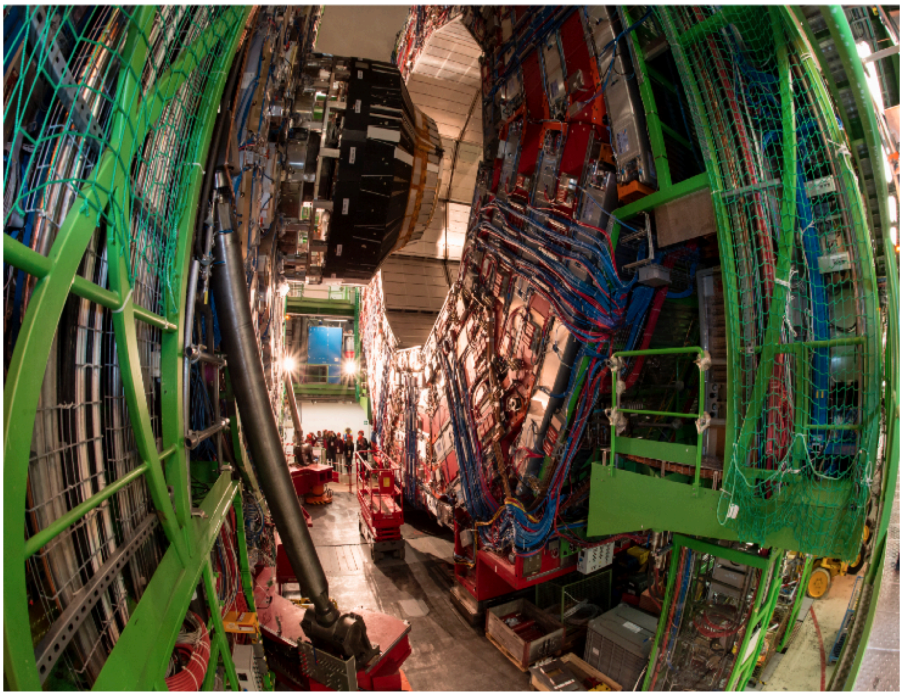

The Compact Muon Solenoid (CMS) experiment [1] [2], after the discovery of the Higgs Boson [3], is now profiting of the LHC shutdown period to consolidate the detector. In 2015 the experiment will start again ready to explore the new energy regime of 13 TeV collisions to improve the precision on the Higgs boson parameters and to search for physics above standard model. A key element of the CMS detector is a highly performing and redundant muon system. Drift tubes and Resistive Plate Chambers (RPC) in the Barrel and Cathode Strip Chambers and RPCs in the endcap are used for both triggering and tracking of muon particles. The activity of the CMS Frascati group is centered on various responsibilities in the construction, operations and monitoring of the RPC detector, as well as in the quality control of data and physical data analysis. In view of the high luminosity LHC upgrades of phaseII, the group is also highly involved in studies of longevity of the present system and in the development of GEM detectors for the completion of the muon system at high η.

1 Activity of the CMS Frascati group in 2013

The Frascati group is involved in the muon project of the CMS experiment since 2005. The group has been responsible of the construction and of the maintenance of the Gas Gain Monitor system and is well integrated in all the activities both during the running periods and during the last years shutdown efforts. Several responsibilities have been covered by members of the group during these years: In 2010 and 2011 the RPC DPG (Detector Performance Group) coordinator was a Frascati charge; In 2011 and 2012 the RPC Run coordination and since 2013 the CMS GEM hardware coordination were covered by Frascati; For the period 2013-14 a member of the group (Stefano Bianco) is the RPC national responsible.

In 2013 the main efforts of the group were devoted to the support to the shutdown activities of CMS and on studies and R&Ds for the future muon upgrades at high eta.

During the shutdown period the completion of the muon system has been planned [4] and a new station of RPC detectors is under installation in the endcap regions to improve the muon trigger performances.

In view of the PhaseII of LHC an extension of the muon system has been scheduled and GEM detectors have been proposed [5] in order to cope with the high background and hostile environment expected in the next years of LHC operations.

The Frascati group was also involved in 2013 in the analysis of the single top production with specific studies of trigger and selection for the s-channel cross section and on studies of the longevity of the present RPC system in view of the long life of LHC.

1.1 Long Shutdown 1 activities and RE4

A total number of 144 new RPC chambers will cover the outermost station of the muon endcap system (RE4) (see figure 1 for a schematic layout of the muon system with indications in the dashed box of future planned upgrades as well) in view of the LHC Run 2 operations. The positive endcap has been succesfully installed in december 2013 (fig. 2). Frascati physicists and technicians have been involved in the preparations of the RPC chambers at CERN before the installation and in the tests of the HV and readout system for this new set of chambers. This work will see the Frascati group involved also for the 2014 with contributions in terms of physicists and technicians both in installations and commissioning activities.

1.2 GEM chamber assembling at Frascati

CMS is planning an upgrade of the muon system with the installation of GEM detectors in the high eta region. These chambers will improve the muon trigger performance allowing to maintain low pt thresholds at Level 1 trigger level. Frascati will be one of the GEM assembling sites in view of the full production. The dimensions of these chambers will be 80 x 100 cm^2 a size very big with respect to previews experiences. During 2013 several activities started in order to set up the laboratory to assemble these large size GEM chambers and to prepare the tools for the quality control and tests of the gain with x-ray gun. After summer the first prototype has been successfully mounted in the lab. Figure 3 show the first prototype mounted in the Frascati clean room.

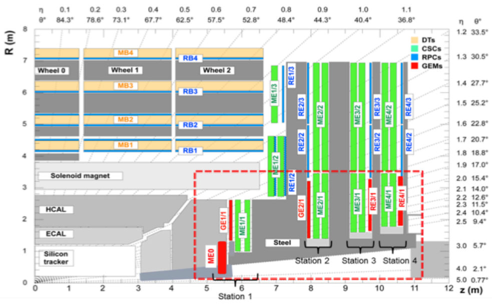

Figure 1: CMS muon system layout. In the dashed box are shown the upgrades proposed for the Muon system

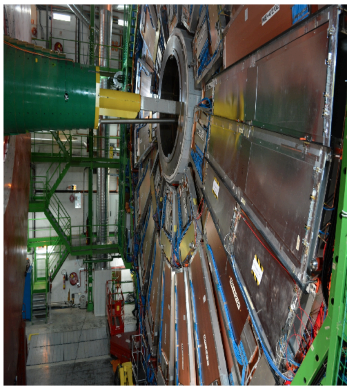

Figure 2: Completion of the first RE4 station installation.

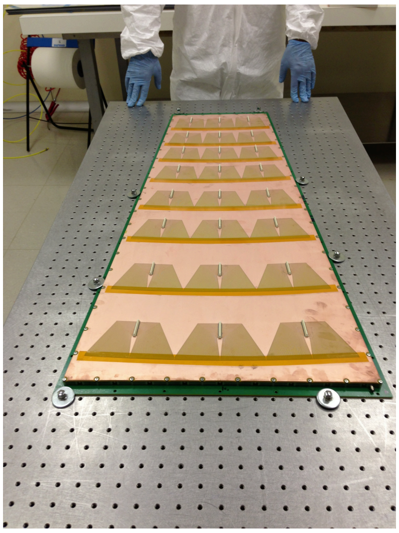

Figure 3: First prototype of CMS GEM chamber assembled in the Frascati clean room.

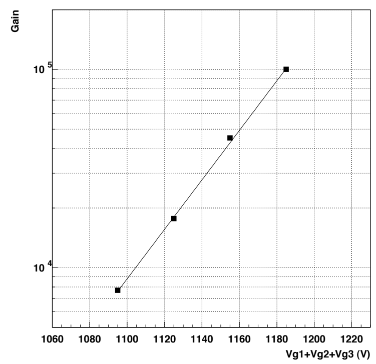

Figure 4: GEM gain vs applied Voltage measured in CMS Frascati laboratory with standard gas mixture.

1.3 GEM R&Ds

In view of the upgrade of CMS with GEM detectors, the Frascati group started an R&D program in order to study few critic issues important for the CMS GEM program: The R&D items, aimed to both the phase 2 Technical Proposal and the GE1/1 TDR and funded by INFN comprise studies on GEM gas mixtures studies, GEM materials analysis and stretching of the GEM foils. All these tasks address important challenges that need to be solved for the TDR.

1.3.1 GEM gas mixture R&D

The choice of the gas mixture is fundamental to keep an high detection efficiency in parallel to a time resolution of the order of ns. At moment the CMS GEM detectors have been operated with a mixture of $Ar/CO_2/CF_4$ in the ratios 45/15/40. With this gas mixture a time resolution of about 4-5 ns is reached, enough to maintain high efficiency detection inside the LHC time window of 25 ns. Nevertheless the European Community has prohibited the production and use of gas mixtures with Global Warming Power (GWF) above 150. Gas mixtures used by GEMs (and RPCs as well) contains CF_4 (and $C_2H_2F_4$ for RPCs) with GWF=5800 and 1430 respectively so an R&D to find new eco-friendly gas mixtures with same performance as the previews one is necessary. The Frascati group started the tests with a small 10x10 cm^2 GEM chamber and we were able to reproduce the results with the standard gas mixture (see fig 4). During 2014 new gas mixtures will be systematically tested to identify few candidates to be further tested at GIF for aging studies.

1.3.2 GEM foil tensioning R&D

The goal is to develop a simple, cost-effective, mass production tools to assess both planarity and parallelism of GEM foils within 100 μm over the 1 mm gap. This task addressed a specific question raised by the Apollinari review committee set-up by CMS in March 2013. Solution proposed is based on optical tools based on Moiré interferometry (Fig.5). Preliminary results show clear fringes with patterns sensible to 100 μm deviations from planarity. A factor of 5 improvement using phase-shift techniques is expected. The second goal is to discover if an *in situ* monitoring of stretching and planarity is possible. The solution being studied is based on the use of optical sensors installed on GEM films/frames. For both items the R&D started in 2013 and is expected to continue throughout the next years.

1.3.3 GEM materials aging R&D

In order to guarantee safe operation of a GEM detector made of composite materials over 20 years, in harsh high-radiation environment, a detailed programme aimed to the full characterization of materials pre- and post-irradiation was funded and started (kapton, glue, gas, etc). Initial studies on the deployment of eco-friendly gases to replace R134a and CF_4 were also initiated. Results (Fig.6) on first measurement of H_2O absorption in kapton and GEM films, and on measurement of tensile properties of dry/humid kapton/GEM films were presented at Siena 2013 Conference.

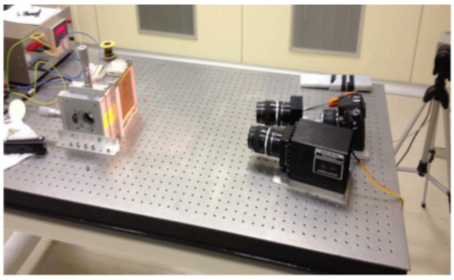

Figure 5: Moiree setup mounted in the Frascati Laboratory and under sted with a small 10 x 10 cm^2 gem foil

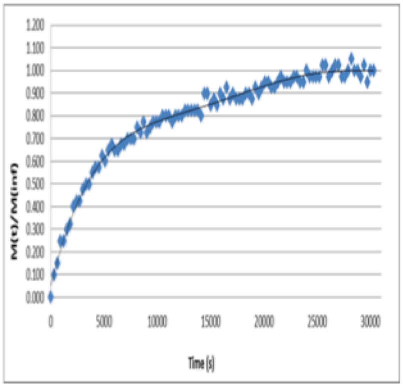

Figure 6: First results of H_2O absorption coefficient inside the GEM kapton foil, before irradiation at GIF. Measurements will be repeated in 2014 after full irradiation

1.4 GGM maintenance and data analysis

The Gas Gain Monitoring construction has been the first contribution of the Frascati group to the RPC collaboration. The system monitors the changes in working point due to gas variations, by means of monitoring of anodic charge in small RPC gaps in a cosmic ray telescope. During 2013 few hardware intervention have been necessary to fix a leaky chamber and some electronic channel. The full data sample collected during 2011 and 2012 has been analyzed offline and final results

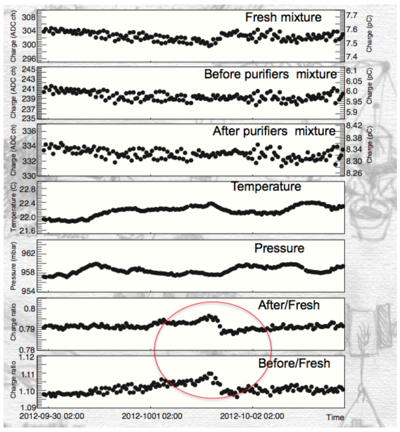

Figure 7: GGM performance during 2011 and 2012. Anodic charge collected in different chambers and ratio between charges coming from recirculated and fresh gas flowed RPCs. Clear sign of warning is spotted inside the circle due to a SF_6 gas flowmeter fault.

have been organized in view of the RPC 2014 conference where a poster has been dedicated to this work. Figure 7 shows anodic charge collected in different chambers of the GGM system and the ratios to factorize out environmental contributions. Signs of gas mixture variation, due to a SF_6 gas flowmeter fault, is clearly spotted in the trend and marked in the circle.

1.5 RPC longevity analysis

Studies of the present RPC system longevity in view of High Luminosity LHC (HL-LHC) operations have started in 2013 and are coordinated by Frascati member. The goal is to analyze the performance of the system from different point of view (detection efficiency, dark current, intrinsic noise) to correlate the results and to spot possible aging effects, background dependent, or weak points that could generate failures on the long term. Up to now no visible signs of aging have been identified but smaller effects are under study. In parallel the background rate on the RPCs have been systematically studied and clear extrapolations for the HL-LHC scenarios have been extracted . The conclusions of such studies will drive R&D programs to be carried out in the near future in local laboratories and at GIF++ at CERN.

1.6 Physics analysis: single top production

In LHC the top quark can be produced both in pairs or as a single top via Electroweak mechanism. The single top production is possible through three different diagrams: t-channel [6], tW channel [7] and s-channel, each of them sensible to different possible effects of new physics. The precise measurement of the cross section of the single top production is so an important standard model check and a window for new physics. The Frascati group joined in 2012 the group of Analysis of the single top and was mainly involved in two main activities: study of the hadronic cross-trigger efficiency and study of selection for the s-channel cross section measurement. In may 2013 the overview of the CMS results on single top analysis were presented by a member of Frascati group (D. Piccolo).

2 Activity planned for 2014

The 2014 will still see big efforts to complete the installation of the negative disk of the RPC endcap system (RE-4). Frascati group will support the activities with contribution of physicists and technicians in the commissioning and installation phases in P5. At the same time the GEM collaboration is progressing very fast to realize a system based on GEM detectors for the coverage of the high η region of the CMS muon system [5]. A technical design report is under preparation and should be ready for the summer. Frascati is involved in this effort with a several years plan of R&D activities started in 2012 and to be carried on in Frascati.

From the R&D point of view the Frascati group will finalize the tensioning studies of the GEM foils inside the CMS chambers and the studies of gas mixture. The layout that is under development in the Frascati lab will permit to plan a systematic study of several ecological gas mixtures in parallel on GEM and RPC detectors. The analysis of the materials used in the GEM chambers, after irradiation at GIF, will be completed and will be part of the TDR document under development.

A new and improved mechanical prototype of CMS GEM chamber has been ordered at cern and will be mounted and tested in Frascati to exercise and standardize the production and quality control capabilities of our laboratory in view of the large scale production.

Additional contributions of the group will cover the development of software tools for the monitoring of the RPC performance and for longevity studies that is a task under Frascati responsibility.

3 Status of the CMS experiment

During 2013, much visible progress has been made, as the LS1 programme approaches the halfway point. Several intervention took place both to consolidate the present system fixing hardware failures, and installing the fourth station of the muon system in the endcap composed by CSC and RPC chambers. The system has been also prepared for the tracker colder operations and for installation of pixels tracker in 2016-17. The successful completion of Long Shutdown 1 (LS1) activities has been the top priority of CMS, however, Technical Coordination intends to pursue, during 2014, a limited set of objectives in support of the work to develop a Technical Proposal for Phase 2.

From the physics analysis point of view more than 70 new analysis have been finalized by CMS during 2013. The Higgs analysis group produced several new results including the search for ttH with H decaying to ZZ, WW, $\tau\tau$+bb where an excess of 2.5σ is observed in the like-sign di-muon channel, and new searches for high-mass Higgs bosons. Search for invisible Higgs decays have also been performed both using the associated and the VBF production channels. A combined limit on the invisible decay branching fractions have been set to BR(H$\rightarrow$invisible) of $\leq$52% (at 95% confidence level). The final Run 1 VH(bb) search, which sees a 2.1σ excess consistent with the SM

Higgs boson has been submitted to a journal. The final Run 1 H(WW), H(ZZ), H($\tau\tau$) analyses have been approved and are in the final stages of preparing for journal submission. The SUSY seraches continued harvesting the 8 TeV dataset in the search for "natural" SUSY. New results include searches for sbottom and stop by gluino-induced production by using the razor variable and specific (1,2,3 leptons + b jet) topologies as well as searches for gluinos decaying to top-pairs and neutralinos. The lower limits on the gluino mass have been pushed up to 1350 GeV at a 95% CL. A new series of searches with Higgs in the final state have started to appear, such as searches for stop pair production or electroweak partner pair production with Higgs bosons in the decay chain. Chargino and neutralinos masses are probed up to about 200 GeV in the latter search.

One of the most prominent results of this year has been the first observation of the B0$\rightarrow \mu\mu$ decay by both the CMS and the LHCb collaborations after a 25-year-long relay race of different facilities to establish this rare decay. The measured decay rate by CMS experiment is (3.0 $\pm$ 1.0) $\times 10^{-9}$. The combination with LHCb gives a decay rate of (2.9 $\pm$ 0.7) $\times 10^{-9}$. In good agreement with SM predictions.

More results have been obtained in Exotica, Standard Model and QCD analysis.

4 Status of the RPC Muon system

In the second part of 2013 the two main activities of the RPC project are the reparation and maintenance of the present system and the construction and installation of the RE4 system. The RPC group took advantage of the long shutdown period to fix most of the hardware problems in the regions physically accessible on the detector. At the end of 2012 the number of inactive channels, due to problems of any kind, was about 2.5%. They are mainly determined by chambers disconnected because of HV connectors problems and to the failure of the electronic component used to set the discriminating threshold and causing very noisy channels that have to be masked. About 0.24% of the channels due to HV problems and about 0.87% for threshold problems have been fixed.

A big campaign to fix leaks in the RPC gas system has permitted to reduce the total leak of the system from 459 l/h to 232 l/h. The problem of these leaks has been identified in small "T" junctions used to distribute the gas inside the chamber.

In parallel to the consolidation plan the RPC group has been heavily involved in the installation of the new station (RE4) in the outermost region of the endcap muon system.

5 Conference Talks by LNF Authors

1. D. Piccolo et Al., "Single top quark production with CMS" talk at LHCP 2013 conference, Barcellona, Spain, May 2013.
2. G. Saviano et Al., "Study of materials for the GEM detector for the muon detector upgrades of CMS at LHC" talk at IPRD2103 conference, Siena, Italy, October 2013.

6 Papers

1. For the listing of CMS papers in 2013 see /www.slac.stanford.edu/spires/
2. L. Benussi, *et al.*, "The status of the GEM project for CMS high-η muon system" Nucl. Inst. Meth. A732 **2013** 203-207.

3. L. Benussi, *et al.*, “Development and performance of large scale triple GEM for CMS” JINST 8 **2013** C11017.

4. L. Benussi, *et al.*, “GEM based detector for future upgrade of the CMS forward muon system” Nucl. Inst. Meth. A718 **2013** 383-386.

5. G. Saviano, *et al.*, “Characterization of metallic gas purifiers used in Closed Loop gas systemof the CMS RPC detector” JINST 8 **2013** T08004.

6. CMS Collaboration, “The performance of the CMS muon detector in proton-proton collisions at sqrt(s)=7 TeV at the LHC” JINST 8 **2013** C11002.

7. L. Benussi, *et al.*, “Study of contaminants and interaction with materials in RPC closed loop system” arXiv:1302.5225[physics.ins-det] **2013**

8. D. Piccolo,*et al.*, “Simulation of the CMS Resistive Plate Chambers” JINST 8 **2013** P03001.

9. D. Piccolo for the CMS Collaboration, “Single top quark production with CMS” EPJ Web Conf. 60 **2013** 16010

References

1. CMS Collaboration home page is /cms.cern.ch/.

2. R. Adolphi *et al.*, “The CMS experiment at the CERN LHC,” JINST **3** (2008) S08004

3. S. Chatrchyan et al., “Observation of a new boson at a mass of 125 GeV with the CMS experiment at the LHC”, Phys. Lett. B 716 (2012) 30

4. M. Tytgat, *et al.*, “The Upgrade of the CMS RPC System during the First LHC Long Shutdown,” PoS RPC **2012** (2012) 063 [JINST **8** (2013) T02002] [arXiv:1209.1979 [physics.ins-det]].

5. D. Abbaneo, *et al.*, “A GEM Detector System for an Upgrade of the High-eta Muon Endcap Stations GE1/1 + ME1/1 in CMS,” arXiv:1211.1494

6. S. Chatrchyan et al., “Measurement of the single-top-quark t-channel cross section in pp collisions at $sqrts$ = 7 TeV “ Phys. Lett. B 716 (2012) 30

7. S. Chatrchhyan et al., “Evidence for associated production of a single top quark and W boson in pp collisions at sqrt(s) = 7 TeV “ Phys. Rev. Lett. **110** (2013) 022003

KLOE-2

The KLOE-2 Collaboration at the LNF

D. Babusci, G. Bencivenni, C. Bloise (Resp.), F. Bossi, G. Capon (Ass.), P. Ciambrone, E. Dané (Art. 23), E. De Lucia, P. de Simone, D. Domenici (Art. 23), G. Felici, G. Fortugno (Tecn.), S. Giovannella, F. Happacher, M. Iannarelli (Tecn.), J. Lee-Franzini (Ass), M. Martini (Ass)*, S. Miscetti, A. Palladino, G. Pileggi (Tecn.), B. Ponzio (Tecn.), R. Rosellini (Tecn.), P. Santangelo, A. Saputi (Tecn.), I. Sarra (Dott.), F. Sborzacchi (Tecn.), B. Sciascia, E. Turri (Tecn.), G. Venanzoni.

In Collaboration with "LNF-SEA"
A. Balla, G. Corradi, U. Denni, A. Frani, M. Gatta, C. Paglia, G. Papalino
and "LNF SPAS"
S. Cerioni

Also Dipartimento di Scienze e Tecnologie applicate, "Guglielmo Marconi" University, Rome, Italy

1 The detector upgrades

A major achievement of the KLOE Collaboration in year 2013 was the successful completion of the detector upgrades followed by the challenging phase of their installation on DAΦNE. The latter has been acknowledged as exemplary for the collaborative efforts taken by the KLOE and Accelerator Division members. The detector has been upgraded i) to improve vertex reconstruction near the beam interaction region, ii) to increase the acceptance for low polar angle photons, and iii) to reconstruct particles passing through the DAΦNE final focusing region. A cylindrical tracking chamber based on the Gaseous Electron Multiplier (GEM) technology [1] has been installed between the beam pipe and the big Drift Chamber to track particles closer to their origin; two small stations of LYSO calorimeters [2] have been placed on the beam pipe for the detection of low polar angle photons; the final focusing region has been instrumented with sampling calorimeters done by five layers of tungsten interleaved with scintillator tiles coupled to fibers that are readout on one side by silicon photomultipliers [3]. The inner tracker (IT), the first cylindrical 3-GEM detector ever built, is operative. First tests of the detector with circulating beams have shown the feasibility of the data taking and preliminary performance studies on cosmic muons demonstrate stable, efficient device operation. Precise localization of each strip on respect the drift chamber layers is being obtained and particle tracking using both DC and IT information is being finalized. The LYSO–crystals calorimeter CCALT, and the tungsten/scintillator–tiles calorimeter QCALT have been installed and all on–detector channels tested. For the operation on DAΦNE, the cooling system for the QCALT front–end electronics is being completed with the installation of an air–compressor, and the off–detector boards for CCALT are being tested. The work has been presented to several topical conferences on particle detector and read–out electronics, including those from Ref. [4, 5, 1, 6, 7, 8, 9, 10, 11].

2 Physics program and published results in year 2013

We worked on data analysis, publishing five papers on i) $\gamma\gamma$ physics [12], a topic that we intend to pursue with the KLOE-2 data taking, on ii) the precision measurement of the hadronic cross section [13], iii) on kaon [14] and η physics [15], and iv) searches for the U–boson [16].

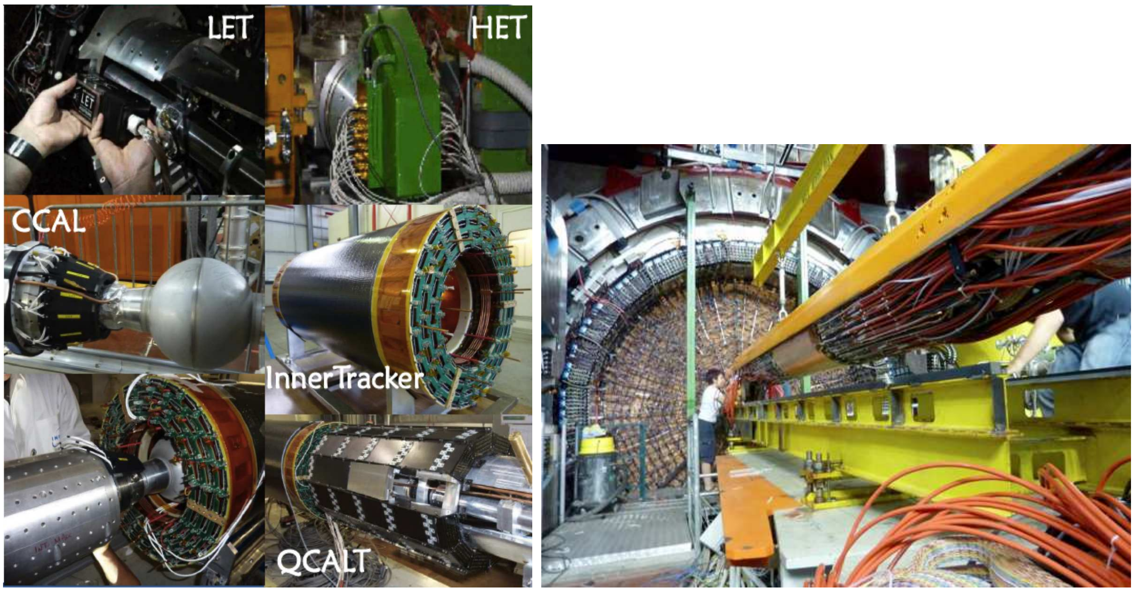

Figure 1: Detector upgrades. Left–Top: γ–γ taggers. Left-Center: LYSO–crystal calorimeter CCALT and IT. Left–Bottom: CCALT insertion inside IT, and QCALT on the beam pipe. Right: Upgrade installation on DAΦNE.

The γ–γ couplings and the partial widths of light mesons can be measured at the ϕ–factory through $e^+e^- \to e^+e^-\gamma^*\gamma^* \to e^+e^-X$ interactions. The study of the η production is based on an integrated luminosity of 240 pb^{-1}, taken in year 2006 at the center of mass energy of 1 GeV, outside the ϕ peak to suppress backgrounds from ϕ decays, without any tag from e^+/e^- in the final state. The most precise measurement of the cross section for η production, with two independent analyses selecting $\eta \to \pi^+\pi^-\pi^0$ and $\eta \to \pi^0\pi^0\pi^0$, has been used to obtain the $\Gamma(\eta \to \gamma\gamma)$ partial width at 5% precision level, $\Gamma(\eta \to \gamma\gamma) = (520 \pm 20_{\rm stat} \pm 13_{\rm syst})$ eV.

Two different kinds of γ–γ taggers have been recently installed on DAΦNE for the detection of e^+/e^- from $e^+e^- \to e^+e^-X$, crucial for the identification of such processes while running at the ϕ resonance. The two (e^+ and e^-) stations for the detection of particles in the 160-230 MeV energy range are constituted by LYSO calorimeters [17] installed 1.5 m from the IP; the other two are scintillator strips [18] installed 11 m from the IP, in a Roman pot placed on the $DA\Phi NE$ first bending dipole, to detect electrons with $E_{e^\pm} > 400$ MeV.

Most of the physics program with the detector upgrades for the new run at $DA\Phi NE$ is discussed in Ref. [19]. In particular, with the forthcoming data taking in year 2014–2015 and the operation of the tagger stations we expect to obtain, among other measurements, the $\Gamma(\pi^0 \to \gamma\gamma)$ width at 1% precision level, and the transition form factors at low q^2 with 5-6% per-bin accuracy [20].

The measurements of the muon magnetic anomaly performed at the Brookhaven Laboratory have reached a fractional accuracy of 0.54 10^{-6}. The final result differs from the Standard Model prediction by 3.2–3.6 standard deviations. Main uncertainty on the theoretical evaluations is due to hadronic loop contributions which, at low energy, are not calculable in perturbative QCD and are obtained from a dispersion integral over the measured hadronic cross section. KLOE was the first to exploit Initial State Radiation (ISR) processes for the precision measurement of the hadronic cross section below 1 GeV, that accounts for most (75%) of the hadronic contribution to the muon anomaly. In 2005 and 2008 KLOE published two measurements of the $e^+e^- \to \pi\pi\gamma$ cross section, with the ISR photon at small angle [21, 22]. An independent measurement with the photon emitted at large angle, to reach the dipion production threshold at $s = 0.1\,\mathrm{GeV}^2$, was published in year 2011 [23]. The three measurements of $\sigma(e^+e^- \to \pi^+\pi^-)$ cover the interval $[0.1 < M^2_{\pi\pi} < 0.95]\,\mathrm{GeV}^2$, with consistent results and a combined fractional uncertainty of about 1%. The new analysis of KLOE data [13] directly derives the pion form factor from the bin–by–bin ratio of $e^+e^- \to \pi\pi\gamma$ to $e^+e^- \to \mu\mu\gamma$ cross sections, giving the two-pion contribution to muon anomaly in the interval $0.35 < M^2_{\pi\pi} < 0.95\,\mathrm{GeV}^2$, $\Delta^{\pi\pi}a_\mu = (385.1 \pm 1.1_{\mathrm{stat}} \pm 2.6_{\mathrm{exp}} \pm 0.8_{\mathrm{th}}) \times 10^{-10}$, that is consistent with our previous measurements. It has a comparable total experimental uncertainty and a theoretical error reduced by about 70%, and confirms the discrepancy between the SM prediction and the experimental value of a_μ.

Some models of physics beyond the SM predict the existence of light neutral vector particles (called U–bosons) mediator of new gauge interactions under which ordinary matter is uncharged [24]. Motivated by astrophysical arguments, their mass, M_U, is expected to be of order of 1 GeV or lighter [25, 26]. Coupling of SM particles with the U is possible via kinetic mixing between the U and the ordinary photon, regulated by a dimensionless parameter ϵ, expected to be of order $\epsilon \sim 10^{-3}$ or lower. High-luminosity e^+e^- colliders at the GeV scale have been recognized to be an ideal environment to search for the U–boson in the Dark Force sector. These new particles can be observed as sharp resonances at M_U in the invariant mass distribution of charged lepton or pion pairs in reactions of the type $e^+e^- \to l^+l^-\gamma$ or $V \to Pl^+l^-$, where V (P) stands for any vector (pseudoscalar) meson, and $l^\pm$ can be muons, electrons or charged pions. KLOE has searched for U boson production in both modes, using $\phi \to \eta e^+e^-$ (a), and $e^+e^- \to \mu^+\mu^-\gamma$ events (b). As for reactions (a), a first paper has been published [27] in which the presence of the η meson was tagged using its $\pi^+\pi^-\pi^0$ decays; a second paper has been issued in year 2013 [16] in which also the $3\pi^0$ decay channel of the η was used. We set an upper limit at 90% C.L. on the ratio between the U boson coupling constant and the fine structure constant of $\epsilon^2 < 1.7 \times 10^{-5}$ for $30 < M_U < 400\,\mathrm{MeV}$ and $\epsilon^2 < 8 \times 10^{-6}$ for the sub- region $50 < M_U < 210\,\mathrm{MeV}$. The analysis of sample (b) is in progress; the preliminary results set upper limits on ϵ^2 from 4×10^{-7} to 5×10^{-6} in the mass region $570 < M_U < 980\,\mathrm{MeV}$.

Working issues in hadronic physics are on the π^0 and η coupling to photons. Meson to photon couplings and the transition form factors, TFFs, are fundamental measurements in hadron physics, of interest for the effective Lagrangians based on ChPT [28, 29] and for their extensions to the transition regime from soft, non-perturbative QCD, to hard interactions, described by pQCD. The transition form factors for π^0 and η in the time-like region are provided by the measurements of i) the Dalitz decays (e.g. $\eta \to \gamma e^+e^-$), ii) $V \to P\gamma^*$ transitions ($\phi \to \eta e^+e^-$, $\phi \to \pi^0 e^+e^-$, $\omega \to \pi^0 e^+e^-$, ...), while iii) meson production in γ–γ interactions ($e^+e^- \to e^+e^-\gamma^*\gamma^* \to e^+e^-\eta(\pi^0, ...)$) gives the coupling to space-like photons, of interest also for the evaluation of light–by–light contribution to the anomalous magnetic moment of the muon [30]. The $\phi \to \eta e^+e^-$ process has been analyzed using both, $\eta \to \pi^+\pi^-\pi^0$, and $\eta \to \pi^0\pi^0\pi^0$ decays. Pure samples, of about 13,000 and 30,000 events in the charged and neutral mode, respectively, with background contamination at the level of 2-3%, have been obtained. The branching fraction is $BR(\phi \to \eta e^+e^-) = (1.131 \pm 0.007^{+0.011}_{-0.006} \pm 0.031_{norm}) \times 10^{-4}$, where the fourth term is the uncertainty on the normalization to the total cross section, $\sigma(e^+e^- \to \phi) \cdot BR(\eta \to 3\pi^0)$. From M_{ee} distribution we obtain the slope parameter $b_{\phi\eta} = (1.17 \pm 0.10^{+0.09}_{-0.08})\ \mathrm{GeV}^{-2}$. The results completely superseded previous measurements [31] and are in agreement with expectations from the VMD model [32]. We are also studying on a sample of 14,000 events the $\phi \to \pi^0 e^+e^-$ decay for which no data on the transition form factor were available.

References

1. A. Balla et al., Acta Phys.Polon.Supp. **6**(4), 1053 (2013)
2. F. Happacher, M. Martini, S. Miscetti, I. Sarra, Nucl.Phys.Proc.Suppl. **197**, 215 (2009), `0906.1157`
3. M. Cordelli, G. Corradi, F. Happacher et al., Nucl.Instrum.Meth. **A617**, 105 (2010)
4. A. Balla, G. Bencivenni, P. Branchini, A. Budano, S. Cerioni et al., Nucl.Instrum.Meth. **A732**, 523 (2013)
5. A. Balla, G. Bencivenni, P. Branchini, A. Budano, M. Capodiferro et al., Nucl.Instrum.Meth. **A732**, 221 (2013)
6. A. Balla, G. Bencivenni, P. Branchini, A. Budano, M. Capodiferro et al., Nucl.Instrum.Meth. **A718**, 416 (2013)
7. A. Balla, P. Ciambrone, G. Corradi, M. Martini, C. Paglia et al., Nucl.Instrum.Meth. **A718**, 95 (2013)
8. M. Cordelli, E. Dane, S. Giovannella, M. Gatta, F. Happacher et al., Nucl.Instrum.Meth. **A718**, 81 (2013)
9. P. Branchini, A. Budano, A. Balla, M. Beretta, P. Ciambrone et al., JINST **8**, T04004 (2013)
10. D. Babusci, F. Gonnella, L. Iafolla, M. Iannarelli, M. Mascolo et al., Nucl.Instrum.Meth. **A718**, 577 (2013), `1206.0680`
11. L. Iafolla, A. Balla, M. Beretta, P. Ciambrone, M. Gatta et al., Nucl.Instrum.Meth. **A718**, 213 (2013), `1205.6663`
12. D. Babusci et al. (KLOE Collaboration), Phys.Lett. **B718**, 910 (2013), `1209.4611`
13. D. Babusci et al. (KLOE Collaboration), Phys.Lett. **B720**, 336 (2013), `1212.4524`
14. D. Babusci et al. (KLOE Collaboration), Phys.Lett. **B723**, 54 (2013), `1301.7623`
15. D. Babusci et al. (KLOE-2 Collaboration), JHEP **1301**, 119 (2013), `1211.1845`
16. D. Babusci et al. (KLOE-2 Collaboration), Phys.Lett. **B720**, 111 (2013), `1210.3927`
17. D. Babusci, C. Bini, P. Ciambrone et al., Nucl.Instrum.Meth. **A617**, 81 (2010), `0906.0875`
18. F. Archilli, D. Babusci et al., Nucl.Instrum.Meth. **A617**, 266 (2010)
19. G. Amelino-Camelia, F. Archilli, D. Babusci et al., EPJ **C68**, 619 (2010)
20. D. Babusci, H. Czyz, F. Gonnella, S. Ivashyn, M. Mascolo et al., Eur.Phys.J. **C72**, 1917 (2012)
21. A. Aloisio et al. (KLOE Collaboration), Phys.Lett. **B606**, 12 (2005), `hep-ex/0407048`
22. F. Ambrosino et al. (KLOE Collaboration), Phys.Lett. **B670**, 285 (2009), `0809.3950`
23. F. Ambrosino et al. (KLOE Collaboration), Phys.Lett. **B700**, 102 (2011), `1006.5313`

24. P. Fayet, Phys. Lett. **B95**, 285 (1980)

25. N. Arkani-Hamed, N. Weiner, JHEP **12**, 104 (2008), 0810.0714

26. M. Pospelov, A. Ritz, M.B. Voloshin, Phys. Lett. **B662**, 53 (2008), 0711.4866

27. F. Archilli et al., Phys.Lett. **B706**, 251 (2012), 1110.0411

28. C. Terschlusen, S. Leupold, Prog.Part.Nucl.Phys. **67**, 401 (2012), 1111.4907

29. S.P. Schneider, B. Kubis, F. Niecknig, Phys.Rev. **D86**, 054013 (2012), 1206.3098

30. F. Jegerlehner, A. Nyffeler, Phys.Rept. **477**, 1 (2009), 0902.3360

31. M.N. Achasov et al., Phys. Lett. **B504**, 275 (2001)

32. L.G. Landsberg, Phys. Rept. **128**, 301 (1985)

LHCb/LNF 2013

M. Anelli (Tecn.), F.Archilli (Ass. Ric.), G. Bencivenni, P. Campana ,
P. Ciambrone, P. De Simone, G. Felici, G. Lanfranchi,
F. Murtas, M. Palutan (Resp.), M. Rama, R. Rosellini (Tecn.),
A. Saputi (Tecn.), A. Sarti (Ass.), B.Sciascia,
F. Soomro (Bors. PD), R. Vazquez Gomez (Bors. PD)

In collaboration with "LNF-SEA"
A. Balla, M. Carletti, G. Corradi, M. Gatta

1 Introduction

The LHCb experiment data taking campaign in years 2011 and 2012 was very succesful, with ~ 1 fb^{-1} and ~ 2 fb^{-1} of pp collisions integrated at $\sqrt{s} = 7$ and $\sqrt{s} = 8$ TeV, respectively. This was possible thanks to the performance of the LHC, to the luminosity leveling technique, consisting of taking data at constant instantaneous luminosity of 4×10^{32} cm^{-2} s^{-1} , and to the excellent run of the detector, which was capable to work at full efficiency far beyond its design parameters. The acquired data represent an unprecedented sample of b and c decays which considerably increased our sensitivity in the search of physics beyond the Standard Model (SM) in the flavor sector. This allowed to publish during 2013 several "world record" measurements in the core physics channels. Among these, most relevant is the evidence for a $B_s^0 \to \mu^+\mu^-$ signal with $3.5\,\sigma$ significance, which is the result of the joint analysis of 2011 data and half of the 2012 data. This eagerly awaited result, published beginning of 2013 in Physical Review Letters, [1] resulted to be the 2013 top-cited hep-ex paper (220 citations). The LNF team contributed substantially to this achievement, partecipating in all of the aspects of the analysis, and coordinating the effort of the international analysis working group (with G. Lanfranchi and M. Palutan serving as convenors of the "Rare Decays" and "$B_s^0 \to \mu^+\mu^-$ analysis" working groups, respectively). During 2013, the analysis of the full 2012 dataset was performed with the same strategy, and the results were presented at EPS conference last summer (by F. Archilli of the LNF team), and published in Ref [2]. This publication yields a $4.0\,\sigma$ significance of $B_s^0 \to \mu^+\mu^-$ signal, thus confirming what was found with 70% of the available statistics. After decades of experimental efforts, the above results represent a major achievement of the LHC. However, the current precision on the decay rate is not sufficient to exclude contributions from new physics processes. In particular, even if strong enhancements from scalar Higgs have been already ruled out, we start to experimentally probe only now possible new physics contributions from the semileptonic operators. Moreover, it is now of primary interest to experimentally measure the ratio of $B^0 \to \mu^+\mu^-$ to $B_s^0 \to \mu^+\mu^-$ decay rates, which would allow to further constrain the flavor structure underlying any new physics model. To reach this physics goal in the near future, a substantial effort was put by the LNF group in the last months of 2013 in the improvement of background rejection.

In parallel, a brand new analysis activity was carried on by the LNF team in the search for lepton-flavour violating B decays with purely leptonic final states. This effort lead during 2013 to the publication of world best upper limits on $B_s^0 \to e^\pm\mu^\mp$ and $B^0 \to e^\pm\mu^\mp$ decays, [3] and to set lower bounds on leptoquark masses, which are a factor of two higher than the previous bounds.

Last but not least, a member of the LNF group, M. Rama, obtained important results in establishing the impact of the $D-\overline{D}$ mixing in the extraction of CKM angle γ from $B^- \to D^0K^-$ and $B^- \to D^0\pi^-$ decays. [4] This work lead to an appreciable correction to the γ determination from the combination of $B \to Dh$ analyses at LHCb, published in Ref [5].

Besides the above analysis activities, considerable efforts have been spent by the team on the muon system, and namely on detector maintenance and performance assessment. On the latter aspect, we have since the early times of LHCb operation a great expertise in the calibration of the offline muon identification performances, covering both aspects of muon efficiency and hadron misidentification probability. This matter has been recently reviewed in a performance paper fully dedicated to muon indentification at LHCb. [6] The high degree of competence reached in this field has been recognized by the LHCb Collaboration at the end of 2013, by appointing two members of LNF team, B. Sciascia and R. Vazquez Gomez, to the roles of LHCb PID coordinator and Muon Identification co-convener, respectively.

Even though the physics harvest is now in full flow, the LHCb Collaboration is already planning for an upgrade of the experiment, intended to collect ~ 50 fb^{-1} starting in 2019, after the long shutdown 2 of LHC. This very large sample should allow to determine several SM variables in the flavor sector to a precision comparable with the ultimate theoretical uncertainty. The LNF team will guarantee the full operation of the muon system readout in the upgrade conditions, the production of the needed spare muon chambers, and the production (if needed) of new chambers based on GEM technology, on which the group has a leadership position. Detailed studies on the detector hardware performances in special high luminosity runs have been performed at LNF. The results of these studies, together with projected performances of the muon identification algorithm, are part of the Particle Identification Upgrade TDR, which has been presented in November 2013 and recently endorsed by the LHCC. [7]

As demonstrated above, the LHCb LNF group has a leadeship role in many aspects, and this has been fully recognized by appointing Pierluigi Campana as spokeperson of the LHCb collaboration, with a three years mandate starting June 2011.

2 List of Talks by LNF Authors in Year 2013

1. F. Archilli, "Searches for very rare decays to purely leptonic final states at LHC", EPS-HEP 2013 European Physical Society Conference on High Energy Physics, Stockholm, Sweden, 18 - 24 Jul 2013.
2. P. Campana, "Heavy Flavor Physics and New Phenomena at hadron colliders", 25th Rencontres de Blois on "Particle Physics and Cosmology", Chateau de Blois, Blois, France, 26 - 31 May 2013.
3. P. De Simone, "b and c spectroscopy at LHCb", 13th International Conference on Meson-Nucleon Physics and the Structure of the Nucleon, Rome, Italy, 30 Sep - 4 Oct 2013.
4. G. Lanfranchi, "LHCb physics highlights", riunione CSN1/INFN, Milano, 25 - 26 Marzo 2013.
5. A. Sarti, "Latest results on $B^0_{(s)} \to \mu^+\mu^-$ and other very rare decays", 48th Rencontres de Moriond on Electroweak Interactions and Unified Theories, La Thuile, Italy, 2 - 9 Mar 2013.
6. B. Sciascia, "Summary on K physics", 14th International Conference on B-Physics at Hadron Machines, Bologna, Italy, 8 12 Apr 2013.
7. F. Soomro, "Rare decays at LHCb", 25th Rencontres de Blois on "Particle Physics and Cosmology", Chateau de Blois, Blois, France, 26 - 31 May 2013.
8. F. Soomro, "Charged lepton flavor violation searches at LHCb", CERN-LHC Seminar: Searches for lepton flavor violation at LHCb, CERN, Switzerland, 25 Jun 2013.
9. R. Vazquez Gomez,"Searches for very rare B, D and τ decays at LHCb", 19th International Symposium on Particles, Strings and Cosmology , Taipei, Taiwan, 20 - 26 Nov 2013.
10. R. Vazquez Gomez,"Rare decays at LHCb", Implications of LHCb measurements and future prospects, CERN, Switzerland, 14 - 16 Oct 2013.

3 Publications

References

1. R. Aaij *et al.*, The LHCb Collaboration, "First evidence for the decay $B^0_s \to \mu^+\mu^-$", Phys. Rev. Lett. 110 (2013) 021801.

2. R. Aaij *et al.*, The LHCb Collaboration, “Measurement of the $B_s^0 \to \mu^+\mu^-$ branching fraction and search for $B^0 \to \mu^+\mu^-$ decays at the LHCb experiment”, Phys. Rev. Lett. 111 (2013) 101805.

3. R. Aaij *et al.*, The LHCb Collaboration, “Search for the lepton-flavour violating decays $B_s^0 \to e^\pm\mu^\mp$ and $B^0 \to e^\pm\mu^\mp$”, Phys.Rev.Lett. 111 (2013) 141801.

4. M. Rama, “Effect of $D-\overline{D}$ mixing in the etraction of γ with $B^- \to D^0K^-$ and $B^- \to D^0\pi^-$ decays”, Phys.Rev. D89 (2014) 014021.

5. R. Aaij *et al.*, The LHCb Collaboration, “Measurement of the CKM angle gamma from a combination of $B \to Dh$ analyses”, Phys. Lett. B726 (2013) 151.

6. F. Archilli *et al.*, “Performance of the Muon Identfication at LHCb”, JINST 8 (2013) P10020

7. The LHCb Collaboration, “LHCb Particle Identification Upgrade TDR”, CERN/LHCC 2013-022, LHCb TDR 14, 28 November 2013.

NA62

A. Antonelli (Resp.), V. Fascianelli (Laur.), F. Gonnella (AR),
V. Kozhuharov (Bors.), M. Moulson, M. Raggi (Art. 23),
T. Spadaro

In collaboration with
E. Capitolo, R. Lenci, V. Russo,
S.Valeri, T. Vassilieva;

the Servizio di Progettazione Apparati Sperimentali (SPAS):
C. Capoccia, A. Cecchetti;

the Servizio di Sviluppo e Costruzione Rivelatori (SSCR):
G. Bisogni, A. Franceschi

the Divisione Acceleratori, Servizio di Vuoto:
R. Di Raddo, V. Lollo;

and the Servizio di Elettronica:
G. Corradi, D. Tagnani.

1 The NA62 Experiment

The branching ratio (BR) for the decay $K^+ \to \pi^+\nu\bar{\nu}$ can be related to the value of the CKM matrix element V_{td} with minimal theoretical uncertainty, providing a sensitive probe of the flavor sector of the Standard Model. The goal of the NA62 experiment at the CERN SPS is to detect $\sim$100 $K^+ \to \pi^+\nu\bar{\nu}$ decays with a S/B ratio of 10:1. The experimental layout is illustrated in Fig. 1.

The experiment will make use of a 75 GeV unseparated positive secondary beam. The total beam rate is 800 MHz, providing $\sim$50 MHz of K^+'s. The decay volume begins 102 m downstream of the production target. 5 MHz of kaon decays are observed in the 65-m long fiducial vacuum decay region. Ring-shaped large-angle photon vetoes (LAVs) are placed at 12 stations along the decay region and provide full coverage for decay photons with 8.5 mrad $< \theta <$ 50 mrad. The last 35 m of the decay region hosts a dipole spectrometer with four straw-tracker stations operated in vacuum. The NA48 liquid krypton calorimeter is used to veto high-energy photons at small angle. Additional detectors further downstream extend the coverage of the photon veto system (e.g. for particles traveling in the beam pipe).

In 2013, the main responsibilities of the LNF NA62 group were the following:

- Construction and installation of the LAV stations.
- Construction and installation of the front-end electronics (FEE) for the LAV stations. The LAV FEE boards use the time-over-threshold technique to obtain both hit times and energies

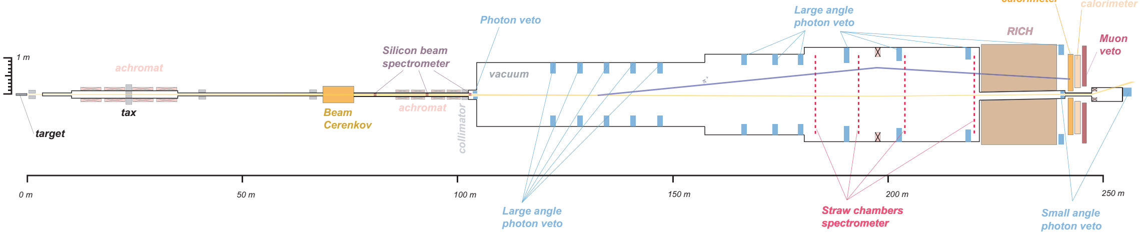

Figure 1: *The NA62 experimental layout.*

from time measurements alone. This FEE board was developed at LNF and has been adapted for use with various other NA62 detectors.

- Development of level-zero trigger firmware for the LAV system.
- Construction and installation of the small-angle vetoes (IRC and SAC) and development of the associated readout systems.
- Commissioning of the above detector systems.
- Development of software and analysis tools for the above detector systems.
- Assistance with the development of a small, dedicated calorimeter system to veto charged pions leaving the acceptance through the beam pipe (HAC)
- Coordination of the NA62 Photon Veto working group.

The principal involvement of the LNF NA62 group is in the design and construction of the LAV system.

NA62 running will commence in mid-October 2014. In view of the approaching run, 2013 was a critical year for the Frascati NA62 group.

2 Large-Angle Photon Vetoes

Development and commissioning of the LAV system was the most important commitment of the group in 2013. The group's activity on the LAV detectors can be divided into the following areas: construction and installation; electronics; commissioning and testing.

2.1 Construction and installation

In 2013, LAV stations A9 and A10 were constructed at Frascati and transported to CERN, bringing the total number of completed stations to 11, of 12 total. Stations A9 and A10 will be operated in the vicinity of the NA62 spectrometer magnet. They were assembled at a later time than stations A1–A8 and A11, since the vacuum vessels in which they are housed must be constructed from high-quality, non-magnetic stainless steel.

Also in 2013, LAV station A9 was installed into the NA62 vacuum tank, bringing the total number of installed stations to 9, of 12 total. Sections of the vacuum tank needed for the installation of stations A10 and A11 do not yet exist. The NA62 photon veto group has assumed responsibility for supplying these missing sections. With the coordination of the Frascati group and the SPAS, a contract for the missing sections was awarded to Fantini SpA (the manufacturer of the LAV vessels) and the sections are currently under construction.

The design of the A12 station is different from that of the other 11 stations in many important respects: it is operated in air rather than in vacuum, it is modular rather than monolithic because of its large size, and its installation into the closed space at the downstream end of the beamline will require a delicate insertion procedure. By the end of 2012, the basic design of the A12 station had been defined. In 2013, the construction drawings were finalized and offers were received for the external fabrication of the large mechanical components. Fabrication of the smaller components was organized at the Frascati central machine shop and at INFN Pisa. The lead-glass blocks for A12 were prepared for installation. Construction of A12 is now underway.

2.2 Readout, trigger, and detector control systems

The first NA62 technical run was carried out in November 2012. The goal of this run was to test the full readout chain and data acquisition system. During the technical run, three complete LAV stations were powered up with the definitive HV systems and data were acquired with the final acquisition chain with muon and kaon beams. The entire readout chain was tested, with data recorded in the L1 PC farm. The data collected during the technical run were comprehensively analyzed by group members in 2013.

One problem to emerge from the 2012 run was noise on some channels of the FEE boards designed at Frascati for use with the LAV detectors. This noise was traced to the crates in which these boards are housed. The NA62 group carried out extensive measurements of the noise as a function of applied threshold. In collaboration with CERN and Wiener (the manufacturer of the crates), members of the group and the LNF Electronics Service identified a technical solution (installation of line filters in the crates).

Additionally, data from the 2012 run showed that the amplification factor at the input stage of the FEE boards was too small to allow the effective discrimination thresholds to be set as low as required for the experiment. In collaboration with the LNF Electronics Service, the Frascati group tested boards with input gain increased from 3 (as in the previous version) to 5, 6, and 11. These tests were conducted in the laboratory and, with cosmic rays, on detectors already in the NA62 experimental area at CERN, with two different readout schemes. A gain of 6 was chosen and all boards from early production with gains of 3 were modified. As a result, the minimum set value of the effective threshold was decreased from 10 mV to 6 mV for all channels.

Mass production of the FEE boards was started and completed in 2013. Each FEE board ready to be installed was individually tested and characterized. A new, more accurate test procedure was developed to calibrate the effective threshold setting as a function of the nominal setting for each board. In addition, the firmware for the FEE boards was extensively tested and a new version, with increased stability and reliability, was released. The FEE boards were successfully integrated into the NA62 detector control system.

During the July 2013, the group participated in a exercise at CERN to test the integration with the experiment's trigger and data-acquisition systems. Using LAV stations A1 and A2, which were fully cabled, we performed intensive tests of the firmware developed at Pisa for the collaboration's standard TEL62 digital readout board. We identified some substantial limitations, in particular in the DDR memory manager, which led to a rewrite of some of the code sections.

3 Forward vetoes: IRC and SAC

The Small-Angle Calorimeter (SAC) and Intermediate-Ring Calorimeter (IRC) complete the coverage of the NA62 photon veto system for particles that would otherwise escape down the beam pipe. Both detectors are of the shashlyk type, with alternating layers of lead and scintillator traversed perpendicularly by a dense matrix of wavelength-shifting (WLS) fibers, which are read out by photomultiplier tubes (PMTs). The development of these detector systems is currently the responsibility of the Frascati group. During 2013, the following milestones were reached.

3.1 Detector construction

In data from the 2012 technical run, the signals from the SAC were measured to be more than 30 ns FWHM in duration. Moreover, the photoelectron yield obtained with the FEU-85 PMTs used for the SAC prototype and during the technical run was found to be too low at the nominal operating voltage of the tubes. The PMTs were therefore changed with Hamamatsu R6427 tubes, which have a rise time of $\sim$1.7 ns. Changes to the mechanics of the PMT assembly were also required.

The scintillator geometry for the IRC was finalized and a supplier for the plastic scintillator was selected. An order for 300 square tiles 1.5-mm thick, of area 150×150 mm^2, was placed and the material was delivered to CERN, as were the WLS fibers. The scintillator was painted with a reflective white paint to provide better light collection, and then sent to IHEP Protvino for drilling and cutting. A series of measurements were undertaken to confirm that it was possible to match the holes in the lead with the holes in the original matrix and to produce a precise map of the 570 holes. After the scintillator is cut and drilled, final assembly will take place at Frascati.

3.2 SAC tests at the Frascati Beam-Test Facility (BTF)

After replacement of the PMTs, the SAC was tested at the BTF. A single-electron beam with an energy of 600 MeV was used for the test. The SAC was read out using two different types of waveform digitizer. Clear peaks in the distribution of deposited energy were observed for electron multiplicities from 1 to up to 8 electrons. The linearity and the energy resolution were measured, as well as the inefficiency of the detector for 600 MeV electrons, which was found to be lower than 5×10^{-3}. After the BTF test run the SAC was transported back to CERN and is ready for reinstallation.

3.3 Detector readout

In 2013, the data chain and readout model for the IRC and SAC was defined. These detectors are very near the beam. Because of the high expected rate and the need to be able to distinguish between beam halo muons (which occur randomly) and low energy electrons and positrons from photon conversions (which are in time with the event), a continuous waveform digitizer must be used.

After investigating various commercial solutions, we decided to use the GANDALF framework, which provides 8 channels of 500 MS/s and an optical interface board able to sustain transfer rates of 3.1 GB/s. A readout system similar to that intended for use was obtained on loan in June and was tested with the SAC both at the BTF test run and at the NA62 dry run. With new firmware, the readout was able to sustain a rate up to about 1 MHz of NA62 triggers.

4 Conference talks by NA62 LNF members

- V. Kozhuharov: Les Rencontres de Physique de la Vallée d'Aoste (La Thuile 2013).
  La Thuile (AO), Italy, 24 February–2 March 2013.
  Talk: "Rare kaon decays : Present and perspectives with NA62".

- M. Moulson: 2013 Kaon Physics International Conference (KAON13).
  Ann Arbor MI, USA, 29 April–1 May 2013.
  Talk: "Forbidden pion and kaon decays in NA62". Poster: "The NA62 Large-Angle Veto System".

- M. Raggi: 2013 Kaon Physics International Conference (KAON13).
  Ann Arbor MI, USA, 29 April–1 May 2013.
  Talk: "High precision measurement of the form factors of the semileptonic decays $K^\pm \to \pi^0 \ell^\pm \nu$ ($K_{\ell 3}$) at NA48/2".

- M. Moulson: Meeting of the American Physical Society Division of Particles and Fields (DPF13).

Santa Cruz CA, USA, 13–17 August 2013.
Talk: "Searches for rare and forbidden decays with the NA62 experiment at CERN".

- V. Kozhuharov: International Workshop on e^+e^- collisions from Phi to Psi (PHIPSI13).
  Rome, Italy, 9–12 September 2013.
  Talk: "Measurement of the ratio of charged kaon leptonic decay rates at NA62".

- M. Raggi: International Workshop on e^+e^- collisions from Phi to Psi (PHIPSI13).
  Rome, Italy, 9–12 September 2013.
  Talk: "Study of the rare decay $K^\pm \to \pi^\pm\gamma\gamma$ and high precision measurement of the form factors of the semileptonic decays $K \to \pi^0\ell\nu$".
  Poster: "Tests of chiral perturbation theory with $K^\pm_{e4}$ and K^{00}_{e4} decays at the CERN NA48/2 experiment".

- M. Moulson: 19th International Symposium on Particles, Strings, and Cosmology (2013 PASCOS).
  Taipei, Taiwan, 20–26 November 2013.
  Talk: "Searches for rare and forbidden decays with the NA62 experiment at CERN".

Super$B$

M. Beretta, R. de Sangro, G. Felici, G. Finocchiaro (Resp.),
P. Patteri, I. Peruzzi (Ass.), M. Piccolo, M. Rama, E. Vilucchi

1 The Conclusion of Super$B$

The ambitious project of building a high-luminosity e^+e^- asymmetric energy flavour factory (Super$B$) in the Tor Vergata University area was unfortunately canceled at the end of 2012 as a consequence of a more realistic cost estimate of the project, and of the unavailability of funds due to the global economic crisis.

During 2013 the Super$B$ community, who had been committed to the project for several years, continued the work to conclude unfinished commitments. In particular, we strove for completing the Detector *Technical Design Report*, whose preparation was already quite advanced at the time of the cancelation of the project. This decision was taken both to keep trace of the hard work of the group, and to provide documentation of the technical achievements for future scientific enterprises.

The book has been completed and published [1)] at the beginning of 2013. The LNF group, involved since the beginning of Super$B$ in the project of the Super$B$ Drift Chamber (DCH) and of the whole detector with major responsibilities, carried out the task of writing the chapters related to the DCH. Here we discuss the challenges, and the technical solutions devised, to design an ultra-light tracking detector capable of matching - in several respects exceeding - the excellent performances of the *BABAR* drift chamber, while at the same time sustaining the Super$B$ background rates.

During 2013 the LNF group also continued the R&D activity on the *cluster counting* technique, which we undertook to possibly improve the energy loss performances of the tracking detector. Results obtained with a full-length drift chamber Prototype showing how the ionisazion loss measurement in a drift chamber can be improved by counting the ionization clusters, have been published in [2)].

References

1. M. Baszczyk et al., the Super$B$ Collaboration: *SuperB Technical Design Report.* arXiv:1306.5655 [physics.ins-det].

2. J.F. Caron, C. Hearty, P. Lu, R. So, R. Cheaib, J.P. Martin, W. Faszer, A. Beaulieu, S. de Jong, M. Roney, R. de Sangro, G. Felici, G. Finocchiaro, M. Piccolo: *Improved Particle Identification Using Cluster Counting in a Full-Length Drift Chamber Prototype.* Nucl. Instr. and Meth. in Phys. Res. A 735 (2014) 169-183.

The MU2E project

M. Anelli, M. Cordelli, G. Corradi, U. Denni, A. Frani, G. Fuga, S. Giovannella,
F. Happacher, A. Lucà (Dott.), M. Martini (Ass.), S. Miscetti (Resp.), B. Ponzio,
G. Pileggi, R. Rosellini, A. Saputi, I. Sarra, V. Stomaci (Laur.), G. Venanzoni

1 Introduction

The Mu2e experiment, proposed at Fermilab, aims to search for the neutrinoless, coherent conversion of a negative muon into an electron in the Coulomb field of a nucleus [1]. The measurement will be expressed by the ratio of the muon-to-electron conversion rate relative to the ordinary muon capture rate on an aluminum nucleus:

$$R_{\mu e} = \frac{\Gamma(\mu^- + Al \to e^- + Al)}{\Gamma(\mu^- + Al \to \nu_\mu + Mg)}\,. \tag{1}$$

The process of muon to electron conversion is an example of Charged Lepton Flavor Violation (CLFV). While it is strongly suppressed in the Standard Model (SM), (BR($\mu \to e$) $\approx 10^{-54}$), many scenarios of physics beyond the SM, predict enhanced BRs close to the reaches of current or near future experiments. Therefore, any signal is a compelling evidence of New Physics. If no events are seen in the signal window, the experiment is designed to set an upper limit of $R_{\mu e} \leq 6 \times 10^{-17}$ at 90% C.L. in three years of running. This value represents an improvement of four orders of magnitude over the current best experimental limit $R_{\mu e}(Au) < 7 \times 10^{-13}$, from the SINDRUM II experiment [2]. The conversion of a muon to an electron in the field of a nucleus occurs coherently, resulting in a monoenergetic electron with an energy equal to the muon rest mass, apart from corrections for the nuclear recoil and the K-shell binding energy of the muon ($E_e = 104.97$ MeV). This distinctive signature has several experimental advantages, including the near-absence of background from accidentals and the suppression of background electrons near the conversion energy from muon decays.

The overall design of Mu2e is driven by the need to suppress potential backgrounds and to produce a high intensity, low energy muon beam that should provide around 10^{18} stopped muons on target. The desired Mu2e muon beam will be produced using the Fermilab accelerator complex, which will deliver 8 GeV protons into the *Mu2e beamline*. A pulsed structure of beam and a veto gate allow prompt beam background to die down during 750 ns, after which the detector is activated to look for μ-atom decays. The Mu2e beamline consists in an evacuated inner bore (to 10^{-4} Torr) of a series of superconducting solenoids which form a graded magnetic field. Pions produced by target interactions and the muons into which they decay are captured. The muon stopping target composed of a set of thin aluminum foils and has a graded magnetic field. The graded field increases the acceptance for conversion electrons and plays a key role in rejecting certain backgrounds. The downstream section of the DS has a nearly uniform field (< 1% non-uniformity) in the region occupied by the Tracker and the Calorimeter that accurately analyze electrons emerging from the stopping foils.

The LNF group, together with INFN groups of Pisa and Udine is in charge of the construction of the calorimeter.

2 Characterization of LYSO crystals

The Mu2e calorimeter is composed by ~ 2000 crystals. The choice of the crystal composition is still in progress. Possible alternatives are BaF_2, pure CsI and LYSO. Extensive studies has been

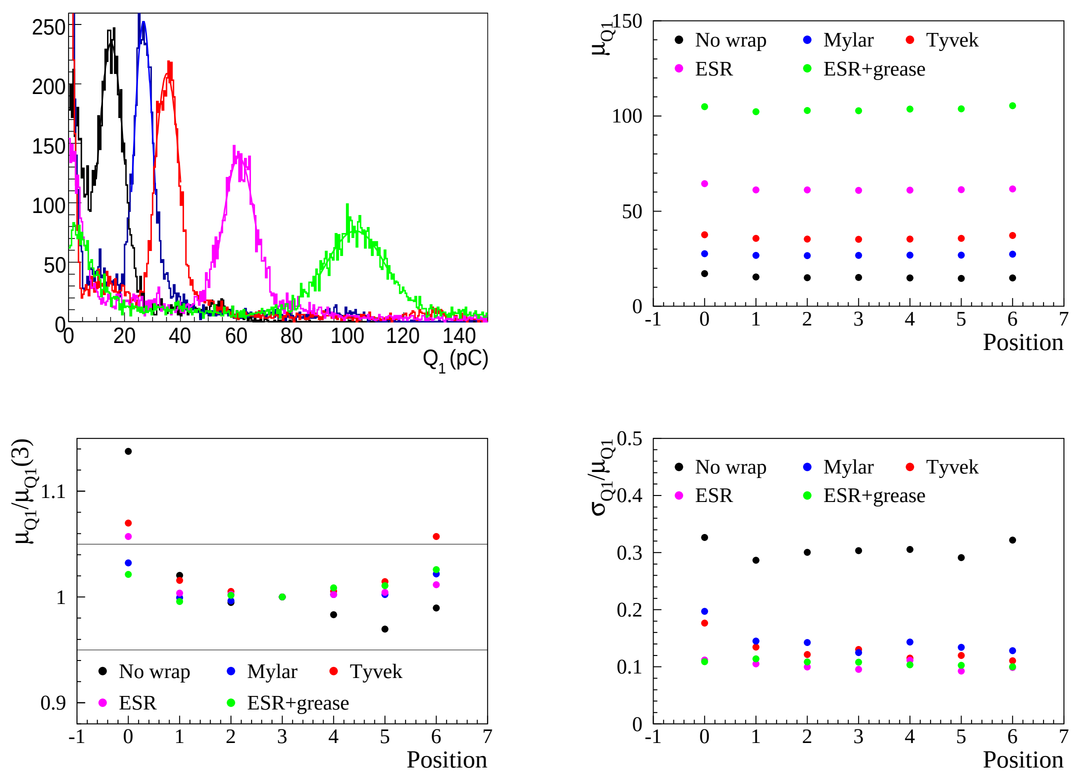

Figure 1: *Top-left: charge spectrum for a LYSO crystal, with* ^{22}*Na source placed in the middle of the crystal along the longitudinal position, for different kind of wrapping: without any wrap (black), mylar (blue), tyvek (red) and ESR (magenta). The green distribution is obtained with ESR wrapping and optical grease. Light yield (top-right), linearity (bottom-left) and resolution (bottom-right) obtained from the* ^{22}*Na scan of the same crystal along its length, for all configurations.*

done for sixteen $(3 \times 3 \times 13)$ cm^3 LYSO crystals. used to build a small calorimeter prototype (Sec. 2.2). For all of them, light yield, longitudinal uniformity, emission spectra and transmission quality have been measured.

2.1 Test results with ^{22}Na source

Light yields and longitudinal uniformity for LYSO crystals have been measured using a collimated ^{22}Na source that illuminates the crystals in a region of few mm^2. One of the two 511 keV photons produced by this source is tagged by means of a small monitor system constituted by a LYSO crystal, $(3 \times 3 \times 10)$ mm^3, readout by a (3×3) mm^2 MPPC. The second photon is used to calibrate the crystals, that is readout by means of a 1 inch bi-alkali Hamamatsu photomultiplier (PMT). Tag and test signals are both acquired by means of a CAEN DT5751 digitizer system at 1 Gsample.

Crystals have been tested both undressed and fully wrapped with different materials: mylar, tyvek and Enhanced Specular Reflector (ESR) from 3M. In this last configuration the effect of optical grease has also been studied. The longitudinal scan has been done in seven points, with 2

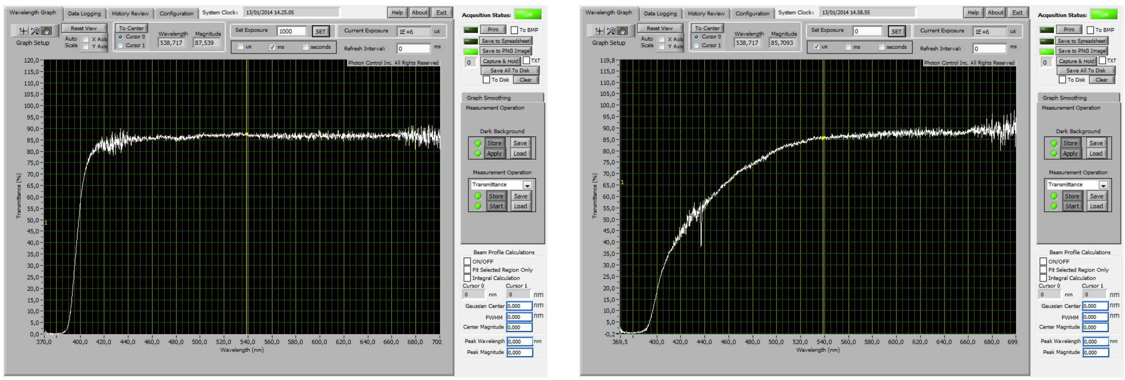

Figure 2: *Longitudinal transmittance (%) as a function of the wavelength in nm for a good (left) and a bad (right) transmitting crystal.*

cm steps, using both crystal orientation. In Fig. 1 light yield, linearity and resolution for one LYSO crystal with different types of wrapping are shown. The best yield is obtained with ESR wrapping, that increase the light output by a factor of 4. With the usage of optical grease a further 1.5 increase is obtained. After wrapping crystals, a resolution below 20% and a response uniformity better than $-1 \div 5\%$ are obtained.

2.2 Test results with spectrophotometer

A transmission station, LATTER (Longitudinal and Transverse Transmission Emission Response), has been designed and assembled during 2013 at LNF, tuned in the range 350-900 nm. A light source uniformly illuminates the back of the crystal while a spectrophotometer with a special focusing optics, is able to read light transmitted in a narrow ellipse of 1.5, 2 mm radii. The crystal can be positioned in front of the spectrophotometer by means of a dedicated crystal movement arm and can then be translated longitudinally, adjusted vertically or rotated around its axis by precise step-motors. The whole measurement of transmittance takes 5 sec/point. This setup allows to measure transmission and uniformity in both longitudinal and transverse directions. The emission spectra of the crystal can be also tested by firing a UV Led (350 nm) over its surface. All $(3 \times 3 \times 13)$ cm^3 LYSO crystals have been tested and qualified for longitudinal transmission by acquiring 8 points/crystal. Only one crystal was found with a bad longitudinal transmission, while all the others are above 75% at 420 nm and 80% at 440 nm. Examples of an acceptable and a not acceptable spectra are shown in Fig.1.2-left, 1.2-right respectively.

New Prototype construction

During the year 2013 we have designed and realized a new larger prototype for the crystal calorimeter. This matrix is composed of 5x5 LYSO crystals of $(3 \times 3 \times 13)$ cm^3 dimension. Each crystal is read out by a (10×10) mm Hamamatsu APD and the signal is processed through a custom made voltage amplifier. We have also designed a custom board to provide HV to the APD and LV to the buffer/amplifier card. The analog signals are then digitized using VME CAEN V1720 modules. A light distribution system prototype has also been assembled. It consists of a 0.5 microJ/pulse green emitting laser (530 nm) synchronized with an external trigger followed by a 2 inch diffusing sphere from ThorLab and a bundle of 50 LEONI fused silica fibers. The fibers are inserted by means of

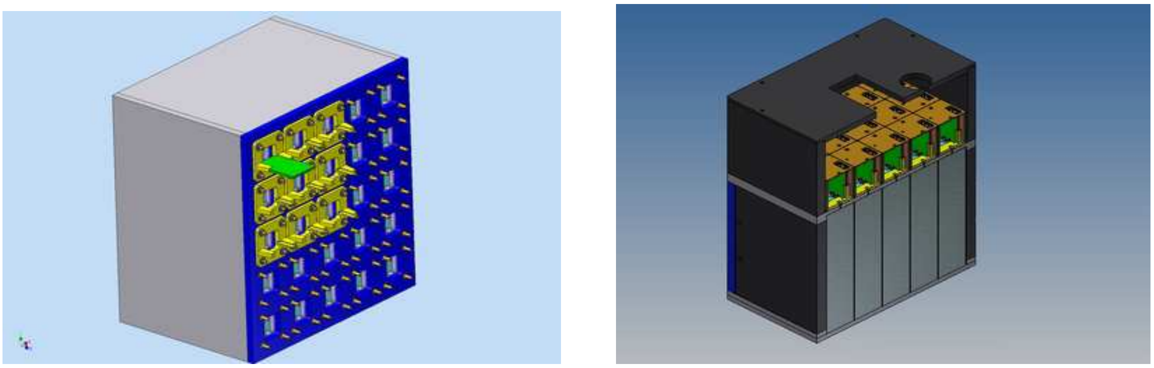

Figure 3: *Drawings of the crystal matrix prototype.*

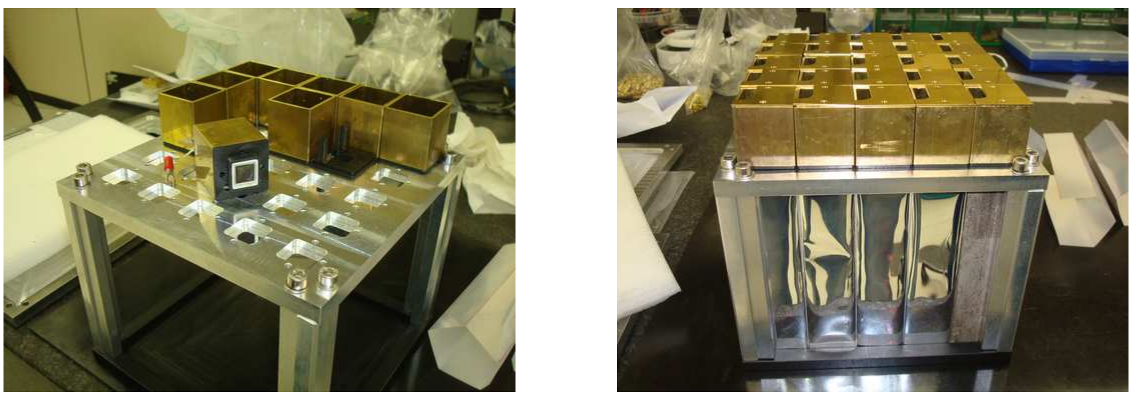

Figure 4: *Realization of the crystal matrix prototype.*

a dedicated connector close to the APD holders thus illuminating the crystal. By reflection and diffusion they allow to calibrate and monitor the APD gains.

In Fig. 3 the CAD drawings of the matrix layout are shown; the APD and the FEE boards are housed in holders that are obtained using PVC 3D printing. All LYSO crystals are wrapped in a 3M ESR film. The APD holders are inserted in a copper case with Faraday cage functionality to avoid noise pick up. The matrix is now fully assembled (see Fig. 4) and we will undertake a test beam campaign at the BTF facility in Frascati and with a tagged photon beam at the Mainz Microtron. For the moment we are calibrating the prototype with cosmic rays and laser pulses.

Acknowledgments

The authors are grateful to many people for the successful realization of the matrix. In particular, we thank all the LNF mechanical shop for the realization of the support, especially G. Bisogni, U. Martini and A. De Paolis. We also thank the SEA electronic department for the realization of the preamplifiers and for the design and control of the crystal test station.

3 List of Conference Talks by LNF Authors in Year 2013

1. F. Happacher, “A Crystal calorimetert for the Mu2e experiment”, CHEF2013 - Calorimetry for High Energy Frontier 20-25 April 2013, Paris, France

4 List of Papers/Proceedings

1. G. Pezzullo *et al.*, ”Cosmic Background rejection by means of the calorimeter in the Mu2e experiment at Fermilab”, proceedings of CLFV-2013, Lecce, to appear on Nuclear Physics B Proceedings Supplement.
2. D. Brown for the Mu2e Collaboration, ”Mu2e: A Muon to Electron Conversion Experiment”, proceedings of CLFV-2013, Lecce, to appear on Nuclear Physics B Proceedings Supplement.
3. G. Pezzullo *et al.*, ”The LYSO crystal calorimeter for the Mu2e experiment”, proceedings of IPRD 2013, Siena, to appear on Nuclear Physics B.
4. F. Happacher *et al.*, ”A LYSO crystal calorimeter for the Mu2e experiment”, proceeding of CHEF 2013, Parigi.

References

1. The Mu2e Collaboration, R. M. Carey *et al.*, http://mu2e-docdb.fnal.gov, document 388-v1.
2. W. Bertl *et al.*, Eur. Phys. J. C **47**, 337 (2006).

UA9

S. Dabagov (Resp.)

Not received

ICARUS_DTZ

A. Bilokon (Resp.)

Not received

JEM-EUSO-RD

A. Franceschi, A. Marini (Assoc.), G. Modestino, T. Napolitano, M. Ricci (Resp. Naz.), F. Ronga (Assoc.)

The JEM-EUSO experiment (Extreme Universe Space Observatory at the Japanese Experiment Module of the International Space Station), is a planned space mission devoted to the observation and study of cosmic rays at the highest energies (UHECRs, UltraHigh Energy Cosmic Rays) above 10^{20} eV.
JEM-EUSO is a new type of observatory, based on a large UV telescope, which uses the whole Earth as detector. It will observe, from an altitude of ~ 400 km, the fluorescence tracks produced at (330÷400) nm by Extensive Air Showers (EAS) originated by UHE primaries which traverse the Earth's atmosphere at ultra-relativistic speed.
The main scientific objectives, the instrument and the observational principle of JEM-EUSO have been described in detail in previous reports.
The LNF JEM-EUSO group is responsible (in collaboration with the SPCM LNF Service) of the design of the Focal Surface (FS) mechanical structure and of the 137 PDMs (Photo Detector Modules) which cover the entire FS where about 5000 multi anode Photomultipliers Hamamatsu M64 are accommodated.
Engineering studies have been carried out, including 3D CAD design of the structure, finite element model calculations, vibration mode studies related to the launch vehicle parameters. First assembled prototypes of PDMs have been produced for testing and for both pathfinders EUSO-TA (the test on ground at Telescope Array site in Utah) and EUSO-Balloon (the precursor flight on stratospheric balloon managed by CNES, France, to be launched in 2014). Members of the LNF group are involved in the JEM-EUSO Editor's Team of the Technical Reports and Design Reviews and in the JEM-EUSO Speaker's Bureau which manages and organizes the activities related to publications and conferences. The group participates and contributes to the definition and assessment of the scientific objectives of the mission. In 2013, the activity has been be mainly dedicated to the continuation and implementation of the engineering project of the FS structure according to possible new launch vehicle configurations, to the production of more PDMs, in an updated version as far as the front end, the DAQ and the power supply electronic boards design is consolidated, in view of reaching the successive Technical Readiness Levels required by a Space mission. Scientific contributions to some of the exploratory objectives of the mission, like the search for nuclearites and Strange Quark Matter (SQM) have been given by the Frascati group at the International Cosmic Ray Conference (ICRC 2013, Rio de Janeiro) and will be published in a dedicated paper.

Recent publications

1. "An Evaluation of the Exposure in Nadir Observation of the JEM-EUSO Mission"; The JEM-EUSO Collaboration: J.H. Adams *et al*., Astrop. Phys. **44**, 76 (2013);
2. “Nuclearites observations with JEM-EUSO”: M. Bertaina, A. Cellino, F. Ronga (for the JEM-EUSO Collaboration); Proc. ICRC 2013, Rio de Janeiro (in press, also in arXiv:1307.7071 [astro-ph.IM]);
3. “Status of the JEM-EUSO mission and studies of the instrument’s performance”; M. Bertaina et al. Nucl. Phys. B (Proc. Suppl.) **239,** 225 (2013);
4. Euso-Balloon: A pathfinder mission for the JEM-EUSO experiment: G. Osteria, V. Scotti *et al*. NIM A, **732,** 320 (2013).

NEMO (km3 from January 2013)

Orlando Ciaffoni, Marco Cordelli, Agnese Martini (Resp.), Luciano Trasatti (Ass.), Roberto Habel (Ospite)

The NEMO collaboration, in the framework of the KM3Net initiative, aims at building a km^3 scale Cerenkov neutrino detector in the Mediterranean Sea.
On February 2013 the collaboration has deployed NEMO Phase II, an 8 floor tower, at the final site, 100 km SE of Capo Passero, taking advantage of the electrooptical cable already deployed from the site to the counting room in Portopalo.
Four PORFIDO probes have been installed in four Optical Modules of the NEMO Phase II apparatus, and they are now working correctly at a depth of 3500m, transmitting to shore on request a temperature reading. In the mean time the KM3Net collaboration is developing the DOM (Digital Optical Module), a 17" glass sphere containing 31 small PMTs. The LNF group, as a consequence, has developed PORFIDOM, a version of PORFIDO that can be fitted in the new DOM.
In 2013 the LNF group has continued the development of the PORFIDO probes adding a 24 bit ADC with 2 NTC temperature probes, that is read by the WISP and provides two temperature measurements with an accuracy of 0.001 ˚C. A prototype is working in the lab. In addition we are developing a salinity monitor that can be connected to the same ADC with a resolution of about 1 ppm.
These new developments will be installed on the Phase 3 towers, where 12 PORFIDO probes have been approved by the collaboration.

Publications

1. S. Aiello et al.: The optical modules of the phase-2 of the NEMO project
Published in JINST 8 (2013) P07001, Erratum-ibid. 8 (2013)
2. KM3NeT Collaboration (S. Adrian-Martinez (Valencia, Polytechnic U.) et al.).:
Expansion cone for the 3-inch PMTs of the KM3NeT optical modules.
Published in JINST 8 (2013) T03006

MoonLIGHT-2

G. Bellettini (Ass.), G. Bianco (Ass.), A. Boni (AR), C. Cantone (AR),
E. Ciocci (Bors.), S. Dell'Agnello, G.O. Delle Monache, N. Intaglietta (Tecn.),
C. Lops (AR), M. Maiello (Ass.), R. March (Ass.), M. Martini (PhD), C. Mondaini (Bors.), G. Patrizi (AR),
L. Salvatori (Bors.), R. Tauraso (Ass.),M. Tibuzzi (Tecn.), R. Vittori (Ass.)

1 Introduction

Lunar Laser Ranging (LLR) experiment, performed since 1969 with retro-reflector arrays deployed by Apollo 11, 14 and 15, is the only Apollo experiment, designed by a team led by C. O. Alley, D. Currie, P. Bender and Faller et al [4], still taking data today. In the past 40 years, laser ranging to these arrays has provided most of the definitive tests of the many parameters describing General Relativity [5, 7]. In addition, the analysis of the LLR data, has greatly enhanced our understanding of the interior structure of the Moon [6, 7, 8, 9]. Initially, the Apollo arrays contributed a negligible portion of the LLR error budget. Nowadays, the ranging accuracy of ground stations has improved by more than two orders of magnitude: the new APOLLO station at Apache Point, USA, is capable of mm-level range measurements [1]; MRLO, at the ASI Space Geodesy Center in Matera, Italy, has re-started LR operations. Now, because of lunar librations, the Apollo arrays dominate the LLR error budget, which is a few cm. The University of Maryland, Principal Investigator for the Apollo arrays, and INFN-LNF are proposing an innovative CCR array design that will reduce the error contribution of LLR payloads by more than two orders of magnitude, down to tens of microns. This is the goal of the MoonLIGHT-2 (Moon Laser Instrumentation for General relativity High-Accuracy Tests for the ILN)[2], a technological experiment of INFN and of the SCF, the CCR space test facility at LNF.

2 Science Objectives of MoonLIGHT-2

Lunar Laser Ranging (LLR) has for decades provided the very best tests of a wide variety of gravitational phenomena, probing the validity of Einstein's theory of General Relativity. The lunar orbit is obviously influenced by the gravity fields of the Earth and Sun, but also is sensitive to the presence of many other solar system bodies. This makes the dynamics of the lunar orbit complex, but the system is relatively pure in that non-gravitational influences (solar radiation pressure, solar wind, drag) are negligible. This makes the Earth-Moon distance a useful tool for testing the nature of gravity, constraining potential deviations from general relativity[3]. LLR currently provides the best constraints on tab.1.

The equivalence principle states that any mass, independent of composition, will react (accelerate) in precisely the same way when placed in a gravitational field. This is the same as saying that the inertial mass and gravitational mass of any object are precisely the same. The equivalence principle is fundamental to GR, allowing gravity to be treated as an aspect of the geometry of spacetime. In general, scalar additions to general relativity – motivated by string theories or quantum gravity – produce a violation of the equivalence principle and also lead to secular changes in the fundamental constants. Scalar fields are also frequently invoked to account for the apparent acceleration of the expansion of the universe. Thus tests of the equivalence principle are a vital part of understanding the interface between gravity and quantum mechanics, and in probing our cosmological fate.

The equivalence principle comes in two flavors. The WEP relates to the composition of an object, in effect probing electromagnetic, strong nuclear, and weak nuclear energy contributions. The SEP extends to include gravity itself. The Earth-Moon system allows a test of the SEP in a way that laboratory tests cannot, in that the contribution of gravitational self-energy to the total

Gravity Science Measurement	Timescale	LLR Measurement Accuracy		
		Current (cm)	1 mm	0.1 mm
Weak Equivalence Principle (WEP)	Few years	$\lvert\Delta a/a\rvert<1.3\times10^{-13}$	10^{-14}	10^{-15}
Strong Equivalence Principle (SEP)	Few years	$\lvert\eta\rvert<4.4\times10^{-4}$	3×10^{-5}	3×10^{-6}
Time Variation of Gravitational Constant	~5 years	$\lvert\dot{G}/G\rvert<9\times10^{-13}\mathrm{yr}^{-1}$	5×10^{-14}	5×10^{-15}
Inverse Square Law (ISL)	~10 years	$\lvert\alpha\rvert<3\times10^{-11}$	10^{-12}	10^{-13}
Parameterized Post-Newtonian (PPN) β	Few years	$\lvert\beta-1\rvert<1.1\times10^{-4}$	10^{-5}	10^{-6}

Figure 1: The expected improvements on the GR measurements with MoonLIGHT are shown in table, together with their measurement time scale.

mass-energy budget is 5×10^{-10} for the earth, but only 10×10^{-27} for typical laboratory masses. LLR allows us to ask the questions: "Do the Earth and Moon fall at the same rate toward the sun? Does the gravitational self-energy of the Earth fall toward the Sun at the same rate as the less gravity-burdened Moon? Does gravity pull on gravity in the same way it pulls on ordinary matter?". The Earth-Moon system is currently the best laboratory for answering these questions. If the SEP were to utterly fail – that is, gravitational self-energy failed to gravitate – the Moon's orbit would be shifted by 13 meters. Current LLR constrains this shift to be less than 5 mm, constituting a 4×10^{-4} constraint on violation of the SEP.

LLR can also constrain new theoretical paradigms. An example is an idea to account for the apparent acceleration of the universe by allowing gravitons to leak off of our 4-dimensional spacetime "brane" into another bulk dimension, thus weakening gravity over cosmological scales. Though small, such a process would have an impact on the lunar orbit, causing it to precess by effectively invalidating the $1/r^2$ force law of gravity. LLR needs to see a factor of 15 improvement to reach this level of sensitivity to new physics.

Furthermore much of our knowledge of the interior of the Moon is the product of LLR [8, 9, 10, 11], often in collaboration with other modalities of observation. These physical attributes of the lunar interior include Love number of the crust, the existence of a liquid core, the Q of the Moon, the physical and free librations of the Moon and other aspects of lunar science.

3 2nd Generation of Lunar Laser Ranging

The general concept of the second generation of LLR is to consider a number (notionally eight) large single Cube Corner Retroreflectors (CCRs). Each of these will have a return that, with a single photoelectron detection system such as current APOLLO system located at the Apache Point Observatory, can be used to determine the range to the limit determined by the librational effects of the current arrays and the laser pulse length. By using single CCRs, the return is unaffected by the libration. That is, there is no increased spread of the FWHM due to the CCR and the librational effects. We plan to use eight such single reflectors spread over tens of meters. The return from each of the CCRs will be registered separately and can be identified by comparison with the nominal lunar orbit and earth rotational parameters. This is shown schematically in Fig.1.

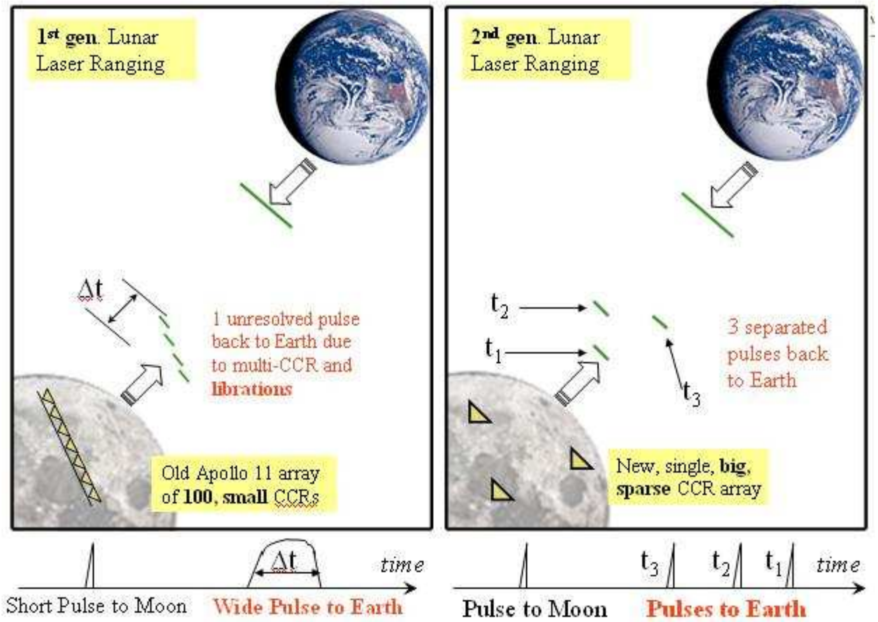

Figure 2: *Concept of the 2nd generation of Lunar Laser Ranging*

4 The New Maryland/Frascati Payload

We currently envision the use of 100 mm CCRs composed of T19 SupraSil I. This is the same material used in LLRA 20^{th} and both LAGEOS satellites. This will be mounted in an aluminum holder that is thermally shielded from the Moon surface, in order to maintain a relatively constant temperature through the lunar day and night. It is also isolated from the CCR, by two coassial "gold cans", so the CCR receives relatively little thermal input due to the high temperature of the lunar day and the low temperature of the lunar night. The mounting of the CCR inside the housing is shown in Fig.2. KEL-F could be used for this mounting (its used in LAGEOS) due to its good insulating, low out-gassing and non-hygroscopic properties.

5 Technical challenges of the MoonLIGHT CCR

The primary technical objectives of the LLRRA-21 are to provide adequate laser return to Earth ground stations and to be stable over long term, decades, with respect to the center of mass of the Moon. The major technical/engineering challenges that follow from the technical objective are then:

- Fabricate a large CCR with adequate homogeneity and that meet the required tolerances, mentioned in the previous section.
- Thermal control to reduce thermal gradients inside the CCR to acceptable levels. Thermal gradients produce index of refraction gradients, which cause beam spread and low return.
- Emplacement goal of long-term stability of $10\mu m$ with respect to the Center of Mass of the Moon.

The large diameter of the CCR introduces a great challenge in its fabrication, the availability of such material of the required homogeneity, the fabrication and polishing procedures and the

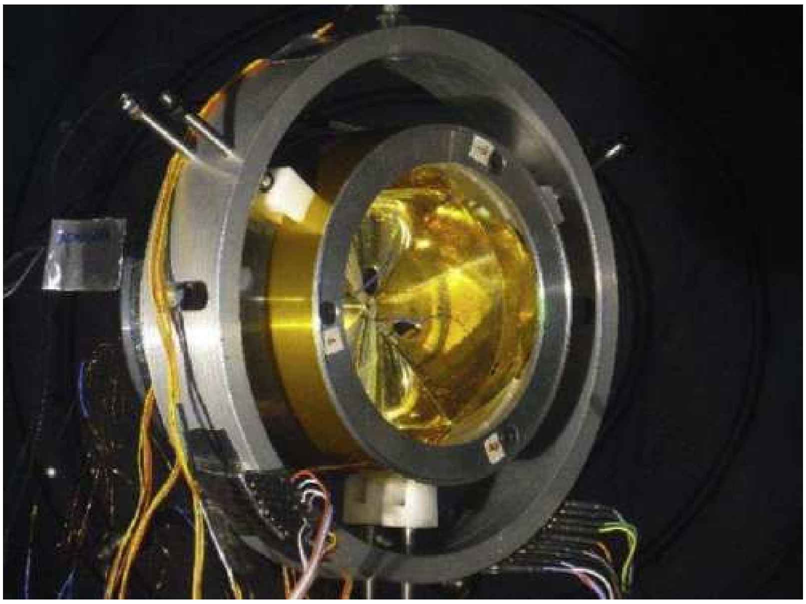

Figure 3: Views of current design of the MoonLIGHT/LLRRA21 CCR (fully assembled).

measurement methods. The angle between the three back reflecting faces, which govern the shape of the pattern, have a more challenging tolerance of ± 0.2 arcsec; this is more restrictive by a factor of 2.5 than the current state of the art for SLR CCR fabrication. The material choice is primarily driven by three requirements:

- extremely uniform index of refraction (very good homogeneity)
- resistance to darkening by cosmic radiation
- low solar radiation absorption

To satisfy these requirements, this CCR has been fabricated with SupraSil 1. For the next generation of CCRs, LLRRA-21, we plan to use SupraSil 311 which has even better homogeneity.

The optical performance of the CCR is determined by its Far Field Diffraction Pattern (FFDP), which represents the intensity of the laser beam reflected back to the ground by the CCR. Figure 4 is a simulation of the FFDP of the LLRRA-21 (performed with the software CodeV) according to its dimensions and angle specifications; at the correct velocity aberration the intensity (calculated in optical cross section) should have a value which guarantees that enough photons come back to the ground station. Optical cross section is an intrinsic characteristic of CCRs or LRAs, and its defined as follows:

$$\sigma_{CCR} = I_{CCR/MIRR} \left(\theta_x, \theta y\right) 4\pi \left(\frac{A_{CCR}}{\lambda}\right)^2 \tag{1}$$

Where $I_{CCR/MIRR}$ is the intensity of the FFDP of the CCR, at a certain point of the (θx, θy) plane, referred to a perfect mirror of the same aperture as the CCR, λ is the laser wavelength. One of the most critical challenges of this new model is the issue of the thermal gradient. Since

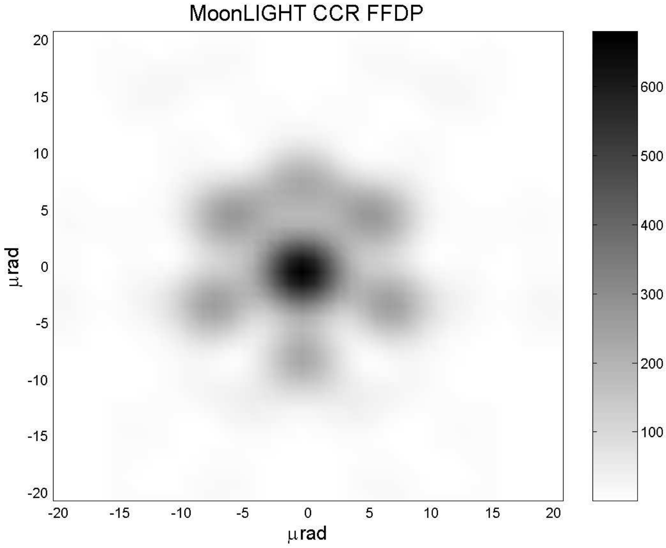

Figure 4: *FFDP of LLRRA-21 under its design specification of offset angles (0.0" 0.0" 0.0"). Grid is in angular dimensions (μrad)*

the index of refraction of the fused silica depends upon temperature, a thermal gradient inside the CCR will cause the index of refraction to vary within the CCR and thus modifying the FFDP. In Figure 6, is represented the average intensity over the velocity aberration for the LLRRA-21 at Standard Temperature and Pressure (STP). At the velocity aberration for the Moon, $\sim 4\mu rad$, we will test thermal perturbations and, if needed, develop an optimized design to control the drop of FFDP intensity to an acceptable level. For this reason we need to understand in detail how the external factors heat the CCR and in what magnitude, either on the Moon or on a satellite. This is accomplished using dedicated programs developed in parallel at LNF and UMD. To perform these simulations we use Thermal Desktop, a software package of C&R Technologies of Boulder CO. Then using IDL and CodeV we translate these thermal gradients into the effects on the FFDP of the CCR. There are three primary sources of heat that causes thermal gradients; here we briefly describe their effect:

- *Absorption of solar radiation within the CCR*: during a lunar day, the solar radiation enters the CCR and portions of this energy are absorbed by the fused silica. Since the different wavelengths in the solar radiation are absorbed with different intensity, according to fused silica absorptivity characteristic, the heat is deposited in different parts of the CCR.

- *Heat flux flowing through the mechanical mounting tabs*: if the CCR is at a temperature that is different than the housing temperature there will be a flux of heat passing into (or out of) the CCR through the holding tabs. Conductivity of the mounting rings should be reduced.

- *Radiation exchange between the CCR and the surrounding pocket*: in the case of the Apollo LRAs, the back surfaces of the CCRs view the aluminum that makes up the housing, machined with a relative high emissivity/absorptivity. If the temperatures of the CCR and the aluminum are different there is a radiation exchange of thermal energy, which in turn causes a flux in the CCR as the heat exits out of the front face to cold space. In the Apollo array this is not been a serious issue, but the bigger dimensions of the LLRRA-21 complicate things,

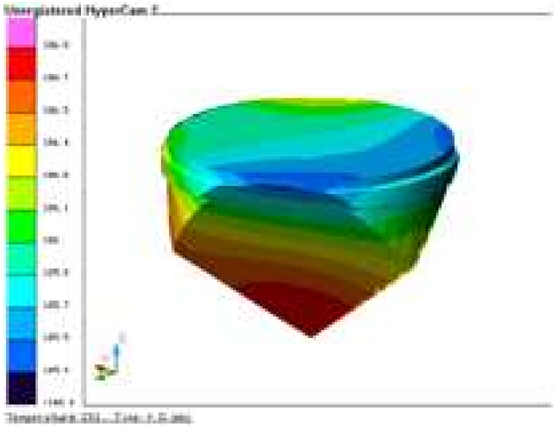

Figure 5: *Typical distribution of temperature inside the CCR for a given set of conditions.*

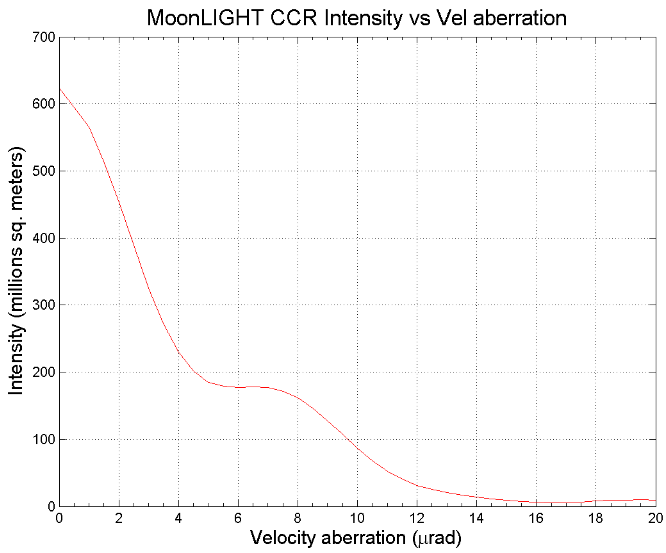

Figure 6: *Average intensity over velocity aberration of an unperturbed MoonLIGHT CCR*

and we need to reduce this effect. Thus we enclose the CCR into two thermal shields, with a very low emissivity (2%), that should prevent this radiative heat flow.

Thermal simulations performed on the current configuration show that currently the variation of the ΔT between the front face and the tip of the CCR is within 1K. We are still proceeding to optimize this further, both with optical design procedures and with thermal stabilization of the overall housing.

As mentioned earlier, to achieve the desired accuracy in the LLR, a long term stability is needed with respect the center of mass of the Moon; to attain this we must understand and simulate the temperature distribution in the regolith (and its motion), the effects of a thermal blanket that will be spread about the CCR and the effects of heat conduction in the INVAR supporting rod. A locking depth is chosen such that the thermal motion effects are small ($\sim 1m$). The placement of the thermal blanket further reduces the thermal effects and also reduces the effects of conduction in the supporting rod. This simulation cycles through the lunation and annual cycles.

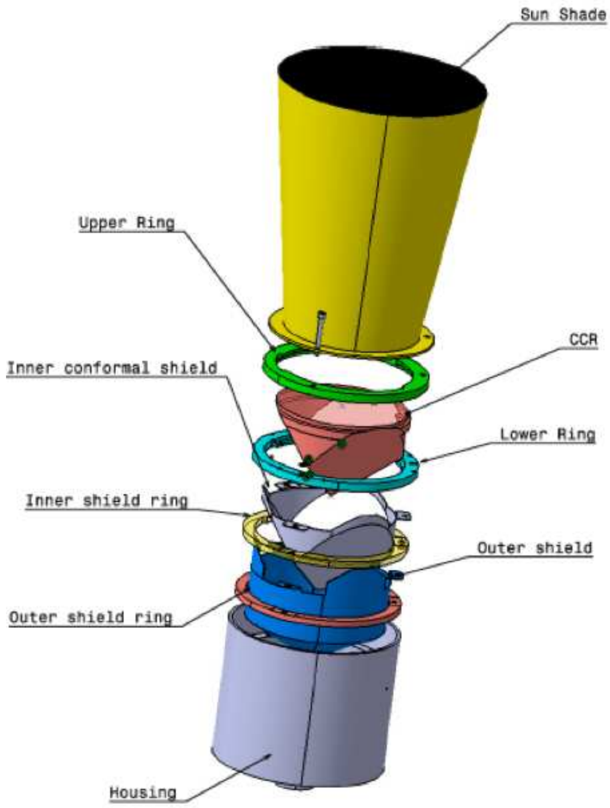

Figure 7: *Design concept.*

6 LLRRA-21 Background

However, over the past four decades, the ground station technology has improved by a factor of over 200, such that the Apollo lunar arrays are now a significant contributor to the ranging errors. Currently, the University of Maryland leads a program to design and validate LLRRAs that are composed of a single 100 mm solid CCRs (a.k.a. LLRRA-21) to be robotically deployed on the moon. These are expected to improve the accuracy that will be supported by the lunar emplacement by two orders of magnitude and should support ranging down to the level of tens of microns. This is a collaboration between University of Maryland and Frascati National Laboratory (LNF) of the National Institute for Nuclear Physics (INFN) of Italy. This joint effort is addressing the design, analysis, thermal and optical simulation, fabrication and thermal vacuum testing of our concept for the lunar array.

6.1 Current LLRRA-21 Design Concept

The figures 8,9 illustrate the current design concept. The thermal shields, shown in gold, isolate the CCR from the pocket or housing. This, reduces the radiative transfer between the pocket and the CCR. The interior of the inner shield is silver coated and shaped like the rear surfaces of the CCR. This, reflects most of the solar radiation that passes through the CCR and enters the housing. In the center, there is the prototype of the LLRRA-21 showing the stepped Sun/Dust Shade. This, improves the thermal behavior to maintain the signal level and protect the CCR from lofted dust and secondary ejecta. On the right, the image of the package that has been used in the thermal vacuum chamber tests.

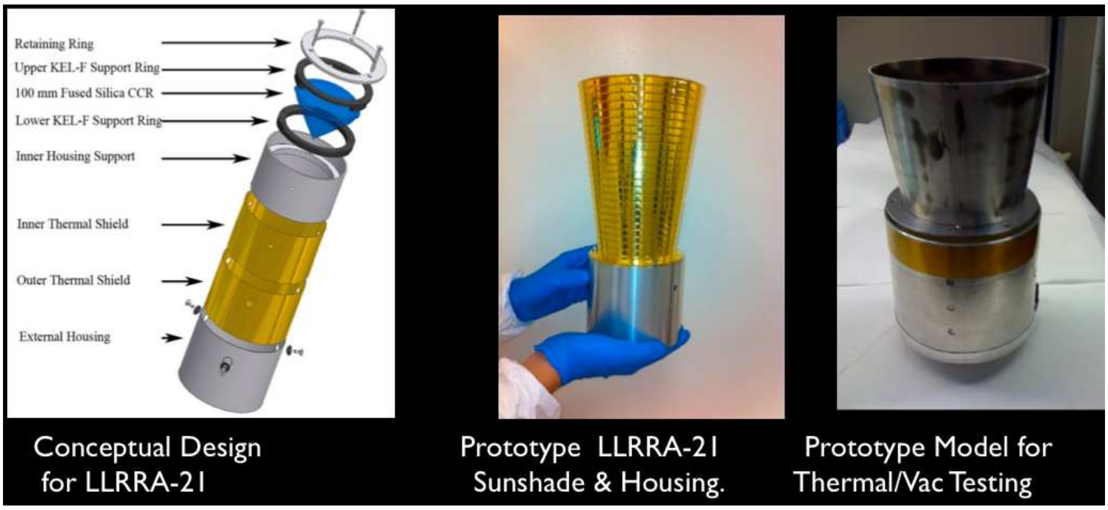

Figure 8: *Current design concept.*

6.2 LLRRA-21 Science Objectives

- General Relativity: many of the most accurate tests of GR are currently derived from LLR to the Apollo arrays. In particular, these results show that the variation of G is less than 1% since the Big Bang, that Gravitational energy has inertial properties. We expect to improve the current accuracy of these tests up to a factor of 100. This will address the validity of General Relativity at a new level of accuracy, especially as one confronts the possible temporal and spatial variation of G, cosmic acceleration and the conflict between the current formulations of General Relativity and Quantum Mechanics.

- Lunar Science: lunar Laser Ranging (LLR) discovered the existence, size and shape of the moons liquid core. Thus, much of our knowledge of the interior of the moon is the product

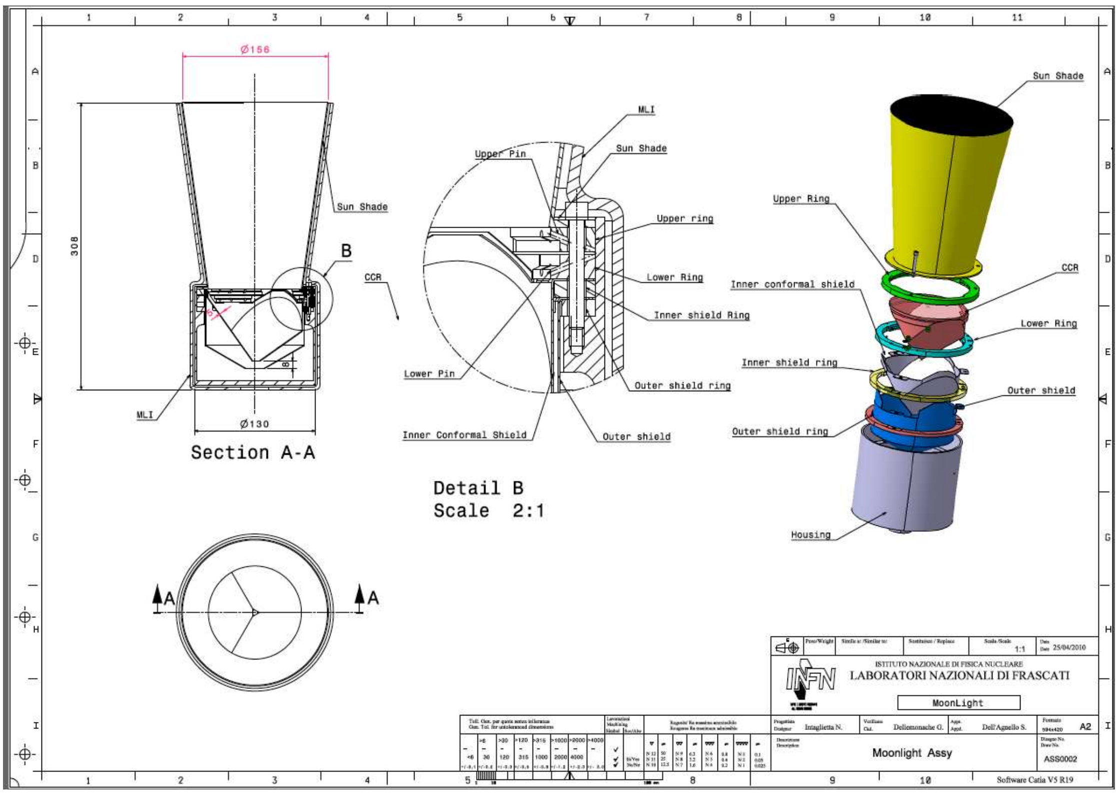

Figure 9: *Current chart concept.*

of the forty years of Lunar Laser Ranging to the Apollo arrays. Hence, we seek to further parameterize the liquid core, search for an inner solid core, obtain better knowledge of Love numbers and address other effects related to the librations and the Q of the lunar motion. This understanding of the deep interior will be coordinated with the knowledge of the upper interior that has been determined by the GRAIL mission.

6.3 Issues for Thermal Design

The Issues Related to Thermal Design Consist of:

- Thermal Gradients in the CCR cause Gradients in the Index of Refraction:
  - Gradients in Index of Refraction Degrade the Diffraction Limit of CCR.
  - This results in a much reduced signal back at the Observatory on Earth.
- Variety of Thermal Inputs and Outputs of LLRRA-21 Package, the largest are:
  - Solar Energy Input to CCR, Sunshade and Housing.
  - Thermal Emission from Regolith to Housing and Sunshade.
  - Thermal Emission from CCR to Cold Space.
  - Internal Conduction of Energy among LLRR-21 Package Components.
  - Resultant Expected Lifetime.

6.4 Thermal Simulation Programs Addressing LLRRA-21 Design

Structure of the Various Components of the Simulation Programs are:

- Solar Input to Cube Corner Reflector (CCR) and Interior of Sunshade through a Lunation:
  - Using the AMO2 Solar Spectrum and Divide the Spectrum into 1 nm bands.
  - Using Absorption of SiO2 and Inner Coating of Sunshade.
  - Using Beers Law for each band on each of 1000 Rays passing through the CCR for Heat Loads.
  - Performed for ach Sun Angle during a Lunation.
  - This task is Performed by a University of Maryland developed IDL program.
- Solar Inputs, Radiation to Space, Internal Conduction through a Lunation:
  - Using Variation of Sun Angle through Lunation for the Heat Loads on exterior of package.
  - Computing Energy Exchange between Housing, Sunshade and Regolith.
  - Addressing Conduction Effects of Various Heat Loads and Radiation Effects.
  - Computing Resultant 4D Temperature Distributions in the CCR throughout a Lunation.
  - This task is performed by Thermal Desktop, a commercial Program by CR Technologies.
- Obtain the Effect of TIR Phase Delays and Back Angle Offsets:
  - Back angles are offset to correct for velocity aberration.

    - Total Internal Reflection (TIR) produces anomalous phase shifts.
    - Create a phase error map due to these effects.
    - This task is Performed by a Code V.

- Conversion from the 4D Temperature Distributions to Signal Return at Earth Observatory:
    - Conversion of 4D Temperature Distributions into 4D Index of Refraction Distributions.
    - Computation of Integrated Phase Delays for each of 1000 Rays through the CCR.
    - Creation of 2D+Time Phase Error Maps .
    - Evaluation of Far Field Diffraction Pattern.
    - Evaluation of Signal level at Velocity Aberration Earth Observatory Through a Lunation.
    - This task is Performed by a University of Maryland developed IDL program.

7 Conclusion

We have created a unique facility and a new industry-standard laboratory test to validate the thermal and optical behavior of CCR in space. The experimental apparatus and the test procedures are described in great detail in DellAgnello et al. (2011) and ETRUSCO (2011). The MoonLIGHT-2 experiment is the result of collaboration between two teams: LLRRA21 and the INFN-LNF. With Moon- LIGHT we are exploring improvements in both instrumentation and the modeling of CCR. For the SCF-Test, we can conclude that the intensity of the FFDP decreases during no orthogonal lighting of the CCR, in particular when the Sun enters in the housing cavity during the test. We have obtained a measurement of geodetic precession that is consistent with the prediction of GR with a competitive uncertainty. This is an interesting and promising preliminary study.

References

1. Murphy T., Battat J., et al., *"The Apache Point Observatory Lunar Laser-Ranging Operation (APOLLO): two years of Millimeter-Precision Measurements of the Earth-Moon Range"*, PASP 121, 29 (2009).

2. D.G.Currie, S. Dell'Agnello, *"A Lunar Laser Ranging Retroreflector Array for the 21st Century"*, AMOS 2009.

3. J.G.Williams, S.G.Turyshev, D.H.Boggs, *"Progress in Lunar Laser Ranging Test of Relativistic Gravity"*, Phys.Rev.Lett.93:261101,2004.

4. Bender P. L., et al, *"The Lunar Laser Ranging Experiment"*, Science, Volume 182, Issue 4109, pp. 229-238, 1973.

5. Williams J. G., Turyshev S. G., Boggs D. H., Ratcliff J. T., *"Lunar Laser Ranging Science: Gravitational Physics and Lunar Interior and Geodesy"*, 35th COSPAR Scientific Assembly, July 18-24, 2004.

6. Williams J. G., Boggs D. H., Ratcliff J. T., *"A larger lunar core?"*, 40th Lunar and Planetary Science Conference, March 23-27, 2009.

7. Williams J. G., Turyshev S. G., Boggs D. H., *"Lunar Laser Ranging Test of the Equivalence Principle with the Earth and Moon"*, International Journal of Modern Physics D, Volume 18, 1129-1175, 2009.

8. Rambaux N., Williams J. G., Boggs D. H., *"A Dynamically Active Moon-Lunar Free Librations and Excitation Mechanisms"*, 39th Lunar and Planetary Science Conference, March 10-14, 2008.

9. Williams J. G., Boggs D. H., Ratcliff J. T., *"Lunar Tides, Fluid Core and Core/Mantle Boundary"*, 39th Lunar and Planetary Science Conference, March 10-14, 2008.

10. Nordtvedt K., *"Lunar Laser Ranging: a comprehensive probe of post-Newtonian gravity"*, Gravitation: from the Hubble length to the Planck length, edited by Ciufolini I., Coccia E., Gorini V., Peron R., Vittorio N., ISBN 07503 0948, published by Institute of Physics Publishing, the Institute of Physics, London, 2005, p.97.

11. Murphy T. W., Adelberger E. G., Strasburg J. D., Stubbs C. W., Nordtvedt K., *"Testing Gravity via Next Generation Lunar Laser-Ranging"*, Nuclear Physics B Proceedings Supplements, Volume 134, 155-162.

12. Nordtvedt K., *"Testing the Equivalence Principle with laser ranging to the Moon"*, Adv. in Space Research, Volume 32, Issue 7, 1311-1320.

13. Dvali G., Gruzinov A., Zaldarriaga M., *"The Accelerated Universe and the Moon"*, Physical Review D, Vol. 68, Issue 2, id. 024012.

14. Currie D. G., et al., *"A Lunar Laser Ranging Retro-Reflector Array for NASA's Manned Landings, the International Lunar Network, and the Proposed ASI Lunar Mission MAGIA"*, 16th International Workshop on Laser Ranging Instrumentation, October 13-17, 2008.

15. Prete F., *"Contact structural analysis of the MoonLIGHT Laser Retro-reflector Assembly with ANSYS"*, Bachelor thesis (unpublished), Dipartimento di Meccanica e Aeronautica, University of Rome "La Sapienza".

16. Minghiglioni A., *"Modal analysis of the MoonLIGHT Laser Retro-reflector Assembly with ANSYS"*, Bachelor thesis (unpublished), Dipartimento di Meccanica e Aeronautica, University of Rome "La Sapienza".

17. `http://ilrs.nasa.gov/docs/retroreflectorspecification070416.pdf`

18. Pearlman M. R., Degnan J. J., Bosworth J. M., *"The International Laser Ranging Service"*, Adv. in Space Research, Vol. 30, No. 2, 135-143, 2002.

19. Urschl C., Beutler G., Gutner W., Hugentobler U., Schaer S., *"Contribution of SLR tracking data to GNSS orbit determination"*, Adv. in Space Research, 39(10), 1515-1523, 2007.

20. Urschl C., Beutler G., Gutner W., Hugentobler U., Ploner M., *"Orbit determination for GIOVE-A using SLR tracking data"*, ILRS Workshop, 2006.

21. `http://ilrs.nasa.gov/docs/ILRSRetroreflectorStandards200812.pdf`

22. Neubert R., Neubert J., Munder J., Grunwaldt L., *"Proposed Single Open Reflector for the GALILEO Mission"*, International Technical Laser Workshop on SLR Tracking of GNSS Constellations, 2009.

The NESSiE experiment proposal

A. Longhin, A. Paoloni
in collaboration with
LNF-SPAS (Div. Ric.): A. Cecchetti, D. Orecchini

1 Introduction

Several experimental results provide indications for the existence of additional neutrinos beyond the three known states which couple via the electro-weak force (sterile neutrinos): a deficit of $\bar{\nu}_e$ from nuclear reactors measured at distances of $\mathcal{O}$(10-100 m) from the core [2], a deficit of ν_e from MCi ^{51}Cr and ^{37}Ar calibration sources at $\mathcal{O}$(m) distances (SAGE, GALLEX [3]), an excess of ν_e and $\bar{\nu}_e$ in artificial ν_μ and $\bar{\nu}_\mu$ at distances of $\mathcal{O}$(km) (LSND [4], MiniBooNE [5]). Furthermore, current cosmological fits based on CMB data show a moderate preference for extra neutrino states [6]. All these inputs triggered the community towards an experimental effort with the goal of, either disproving with large significance the existing indications, or leading to a ground-breaking discovery.

The ICARUS-NESSiE experiment (SPSC–P–347 [1]) is a joint proposal for the search for sterile neutrinos with a short-baseline neutrino beam based at CERN. The experiment concepts consists in exposing two almost identical detectors at two distances (640 and 1600 m) from a $\nu_\mu/\bar{\nu}_\mu$ neutrino source with a peak energy of about 2 GeV. The existence of extra neutrinos with a squared mass difference with respect to the three known states of $\mathcal{O}$(eV^2) is expected to manifest itself both with an energy-dependent disappearance of the ν_μ and/or appearance of ν_e above the instrinsic beam contamination. Each setup is composed of a liquid-Argon Time Projection Chamber (LAr-TPC) which is optimal for the reconstruction of the electronic component followed by a magnetic spectrometer for a complete reconstruction of muonic final states (Fig.2). A substantial part of the far-site LAr-TPC will consist of the ICARUS detector which will be transported from the LNGS underground laboratories. The muon spectrometers at the far and near sites will be build by the NESSiE (Neutrino Experiment with SpectrometerS in Europe) Collaboration which is currently composed by groups from Bari, Bologna, Lecce, LNF, Roma-1 and Padova.

In order to measure with high precision the charge and the momentum of muons produced by neutrino interactions in the LAr target and those interacting in the spectrometer itself, two complementary spectrometers will be installed: an air-core magnet (ACM), followed by an iron-core magnet (ICM). The ICM is dedicated to the precise reconstruction of high-energy muons (up to 30 GeV) and to reach few % precision, through range measurement, on the momentum of muons with energy lower than 3 GeV while the ACM covers the low momentum region where it ensures high momentum resolution and charge discrimination (allowing to separetely study the ν and $\bar{\nu}$ components).

2 Activities of the LNF group

The LNF OPERA group, in sinergy with the SPAS service, is actively involved in the proposal since the beginning of the project and is playing a crucial role thanks to the recognised expertise

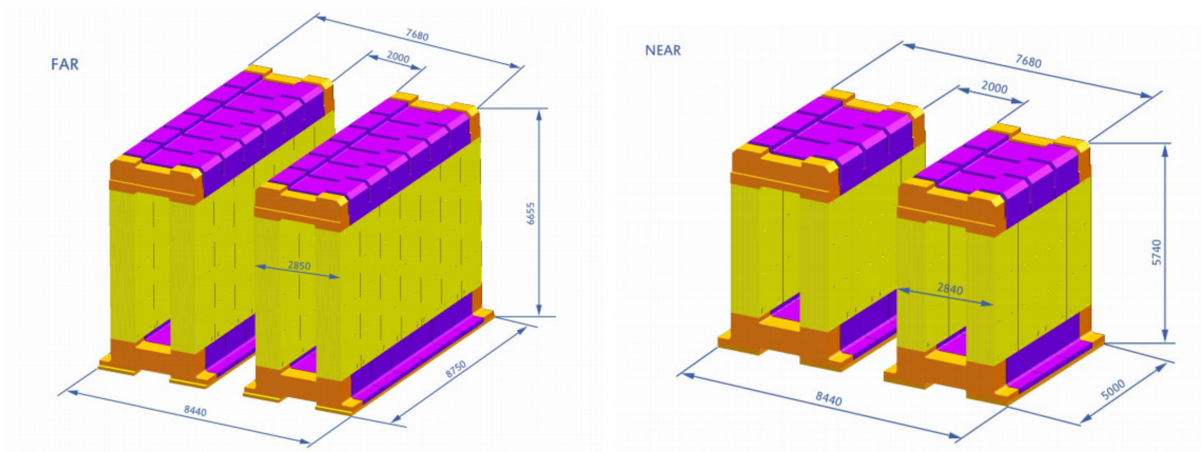

Figure 1: Mechanical model of the far ICM (left), near ICM (right) from the SPAS.

gained during the design and construction of the OPERA ICM spectrometers (mechanics and RPC detectors). The schedule of the project in its present form is naturally connected with the dismantling of the OPERA detector, activity in which the group is naturally committed (definition of the schedule, costing, optimization). The present layout of the ICMs is show in Fig. 2 (SPAS technical drawings). The about 1000 resistive plate chambers installed in the OPERA spectrometers are sufficient to instrument both the near and far site spectrometers. The RPC gas system, two power supplies and the refrigerating system for the magnet coils of the OPERA spectrometers can also be recovered.

Figure 2: A phase of the installation of the OPERA top yokes for the OPERA spectrometers in 2004 (right).

During 2013 the decision making process has progressed and the CENF (CErn Neutrino Facility) is currently envisaged more as a test-area for innovative detectors for future neutrino

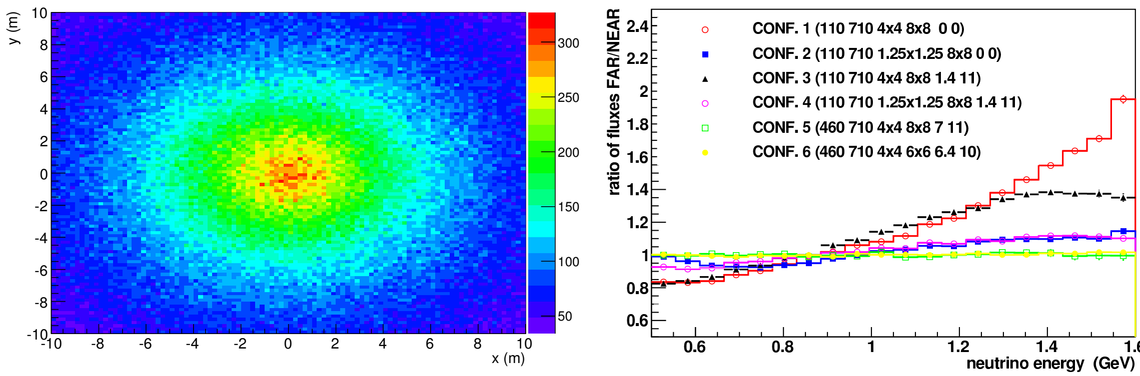

Figure 3: Left: Beam profile at 110m from the target. Right. Far-to-near ratios for several considered experimental layouts.

experiments using charged beam from the SPS extraction lines. The layout of beam-lines and the civil engineering is still kept compatible with a neutrino beam in case the scenario would change in the future. NESSiE and ICARUS have joined this effort and are identified as WA-104 group. The aim is to further develop and test techniques for muon reconstruction complementing a LAr detector eventually extending the current design (iron and air-core spectrometers) with new techniques based on superconducting solenoids allowing a magnetisation of large LAr volumes. A technical design report has been recently submitted to the SPSC committee. The LNF group has proposed the re-usage of a mock-up of the OPERA muon spectrometer which is currently stored at the LNGS to test the integration and performances of an iron spectrometer coupled to an iron-core magnet in a dedicated test-beam experiment.

A second line of activity has been developed more recently based on the idea of applying the concept of a dual ICM spectrometer experiment at the Booster Neutrino Beam, existing at the Fermilab laboratory (Illinois, USA). An experimental proposal is currently in an advanced phase. The LNF group has been actively involved in the beam simulation, the evaluation of beam systematics and their impact in the choice of the most favourable sites in terms of Physics reach. As an example we show in Fig. 3 the expected neutrino beam profile at the near spectrometer and the ratio of the expected neutrino spectra at the near and far sites for different possible choices of the geometry and baselines. Preliminary studies indicate that this scenario could allow extending the exclusion region of ν_μ disappearance at short baseline by about one order of magnitude in the mixing angle. The FNAL proposal would benefit from using an existing neutrino beam and from the favourable coincidence with the need for dismantling the OPERA spectrometers starting from 2015.

References

1. P. Bernardini *et al.* (NESSiE Coll.) SPSC–P–343, arXiv:1111.2242v1 (2011). M. Antonello *et al.* (ICARUS-NESSiE Coll.), SPSC–P–347 (2012), arXiv:1203.3432 (2012), arXiv:1208.0862v2 (2012).

2. G. Mention, *et al.*, Phys. Rev. D**83** 073006 (2011).

3. J.N. Abdurashitov *et. al* (SAGE Coll.) Phys. Rev. C**73**, 045805 (2006). M.A. Acero, C. Giunti, M. Laveder, arXiv:0711.4222 (2007). C. Giunti, M. Laveder, arXiv:1006.3244 (2010).

4. A. Aguilar *et al.* (LSND Collaboration), Phys. Rev. D 64, 112007 (2001).

5. A. A. Aguilar-Arevalo (MiniBooNE Coll.), Phys. Rev. Lett. 102, 101802 (2009). A. A. Aguilar-Arevalo *et al.* (MiniBooNE Coll.), arXiv:1007.1150. F. Mills, ICHEP 2010, Paris, France. R. Van de Water, Neutrino 2010, Athens, Greece. E.D. Zimmerman, PANIC 2011, Cambridge, U.S.A.. A. A. Aguilar-Arevalo (MiniBooNE Coll.), arXiv:1207.4809.

6. E. Komatsu *et al.*, Astrophys. Jour. Suppl. 192:18, (2011). J. Dunkley *et al.*, Astrophys. Jour. 749 90 (2012). J. Hamann *et al.*, Phys. Rev. Lett. 105:181301, (2010). Y. I. Izotov, T. X. Thuan, Astrophys. Jour. Lett. 710 (2010).

The OPERA experiment

V. Chiarella, F. Grianti (Ass.), A. Gambarara (Tecn., Ass.),
N. Intaglietta (Tecn., art.15), A. Mengucci (Tecn.), A. Paoloni (Resp.),
M. Spinetti, F. Terranova, T. Tonto (Tecn.), M. Ventura (Tecn.), L. Votano

in collaboration with

LNF-SEA (Div. Ric.): U. Denni, G. Papalino
LNF-SPAS (Div. Ric.): A. Cecchetti, D. Orecchini

1 The experiment

OPERA [1] has been designed to provide a very straightforward evidence for $\nu_\mu \rightarrow \nu_\tau$ oscillations in the parameter region indicated by Super-Kamiokande as the explanation of the zenith dependence of the atmospheric neutrino deficit. It is a long baseline experiment located at the Gran Sasso Laboratory (LNGS) and exploiting the CNGS neutrino beam from the CERN SPS. The detector [2] is based on a massive lead/nuclear emulsion target. The target is made up of emulsion sheets interleaved with 1 mm lead plates and packed into removable "bricks" (56 plates per brick). Each brick is equipped with a detachable emulsion doublet ("Changeable Sheet", CS), which is scanned before the full development of the brick emulsions. The bricks are located in a vertical support structure making up a "wall". These bricks were produced in situ by a "brick assembly machine" (BAM) located near the OPERA experimental Hall; they are inserted into the wall support structure by a dedicated robot (BMS). Nuclear emulsions are used as high resolution tracking devices for the direct observation of the decay of the τ leptons produced in ν_τ charged current interactions. Electronic detectors positioned after each wall locate the events in the emulsions. They are made up of extruded plastic scintillator strips read out by wavelength-shifting fibers coupled with photodetectors at both ends. Magnetized iron spectrometers measure charge and momentum of muons. Each spectrometer consists of a dipole magnet made of two iron walls interleaved with pairs of precision trackers. The particle trajectories are measured by these trackers, consisting of vertical drift tube planes. Resistive Plate Chambers (RPC) with inclined strips, called XPC, are combined with the precision trackers to provide unambiguous track reconstruction in space. Moreover, planes of RPC are inserted between the magnet iron plates. They allow for a coarse tracking inside the magnet to identify muons and ease track matching between the precision trackers. They also provide a measurement of the tail of the hadronic energy leaking from the target and of the range of muons which stop in the iron. A block of 31 walls+scintillator planes, followed by one magnetic spectrometer constitutes a "super-module". OPERA is made up of two super-modules (SM) located in the Hall C of LNGS (see Fig. 1). Since 2008 all bricks have been inserted, for a total of 150036 bricks, corresponding to a target mass of 1.25 kton, now decreased to 1.15 kton after the extraction of the bricks analyzed so far.

OPERA is able to observe the ν_τ signal with an impressively low background level. The

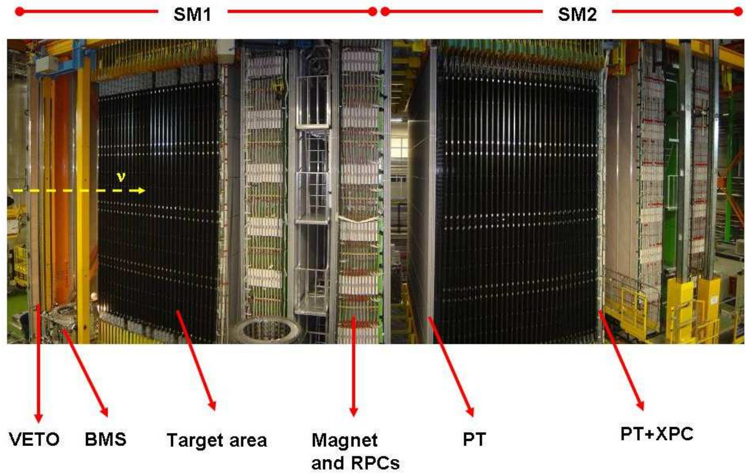

Figure 1: *A fish-eye view of the OPERA experiment. The upper red horizontal lines indicate the position of the two identical super-modules (SM1 and SM2). The "target area" is made up of planes of walls filled with lead-emulsion bricks interleaved with planes of plastic scintillators (TT): the black covers visible in the photograph are the end-caps of the TT. Arrows show also the position of the VETO planes, the drift tubes (PT) followed by the XPC, the magnets and the RPC installed among the magnet slabs. The Brick Manipulator System (BMS) is also visible. The direction of incoming neutrinos from CERN is indicated by the yellow arrow.*

direct and unambiguous observation of $\nu_\mu \to \nu_\tau$ appearance will constitute a milestone in the study of neutrino oscillations. Moreover, OPERA has some sensitivity to the sub-dominant $\nu_\mu \to \nu_e$ oscillations [3]. The potential of the experiment for the research of oscillations into sterile neutrinos and non standard interactions has also been investigated [4, 5].

Opera is an international collaboration (Belgium, Croatia, France, Germany, Israel, Italy, Japan, Russia, Switzerland and Turkey) and the INFN groups involved are Bari, Bologna, LNF, LNGS (Gran Sasso), Naples, Padova, Rome and Salerno. The Technical Coordinator (A. Paoloni) is a LNF researcher.

2 Overview of the OPERA activities in 2013

The CNGS complex ended its operation after the 2012 run, collecting, 2008 to 2012, a total of 17.97×10^{19} proton-on-target (about 80% of the statistics considered in the OPERA proposal), corresponding to 19505 events inside the OPERA bricks. To speed up the research of tau candidates in the exposed bricks, the collaboration decided to postpone the analysis of those events in which the neutrino vertex is not localized in the first scanned brick and to give priority to events without muons or with muons of momentum lower than 15 GeV. Up to the end of 2013, about 10000 bricks have been scanned and more than 6000 events located.

During last year, the collaboration reported the observation of the third observed tau candidate in the muon decay channel, whose picture is shown in Fig.2, The expected number of ν_μ

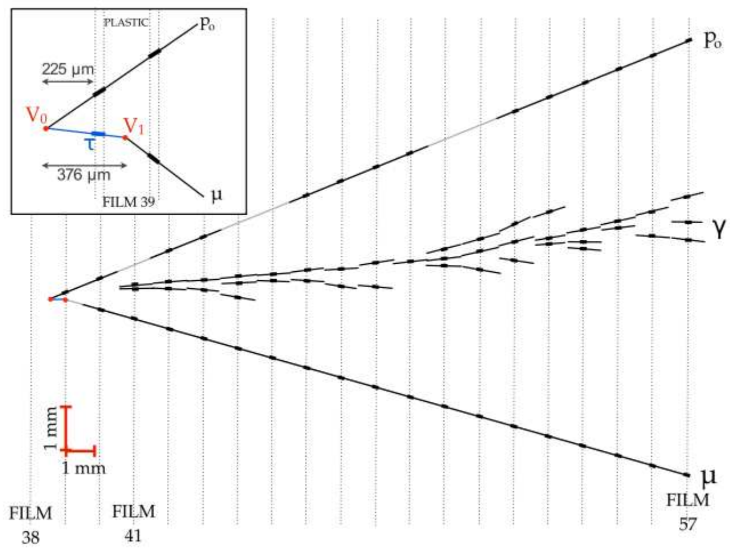

Figure 2: *The third OPERA τ candidate event.*

into ν_τ oscillations is 1.7 (assuming full mixing and $\Delta m^2_{32} = 2.32\ 10^{-3}\ eV^2$) with 0.18 background events.

The extraction of bricks with neutrino interactions will continue in 2014, while a small queue of data analysis is exptected also in 2015.

3 Activities of the LNF group

The Frascati group has been responsible for the design and the construction of the dipole magnets and the general support structure of the sub-detectors. It shared responsibility with INFN Padova and LNGS for the construction and running of the bakelite RPC planes. Frascati and Naples also designed and prototyped the wall support structures housing the lead/emulsion bricks and LNF was responsible for their production and installation. The Frascati group has been also involved, with the University of Hamburg, in the trigger of the drift tubes, performed by the Resistive Plate Chambers.

On the emulsion side, LNF was highly involved in the construction and operation of the Brick Assembly Machine (BAM) and, since 2008, contributes to the emulsion scanning with one dedicated microscope located in Frascati. Finally, since 2007 LNF follows the brick handling of OPERA, with the management of the X-ray marking facilities and the automation of the temperature control of the development tanks.

At present with the help of the SPAS, we are involved in the preparation of the detector de-commissioning, that will start in 2015. The group is contributing also to data analysis, with particular interest in electronic detectors (cosmic ray studies and RPC data quality checks), in the study of the third τ candidate (charge measurement and precise background estimation), in the statistical significance assessment of the observed ν_μ into ν_τ oscillations as well as in the research

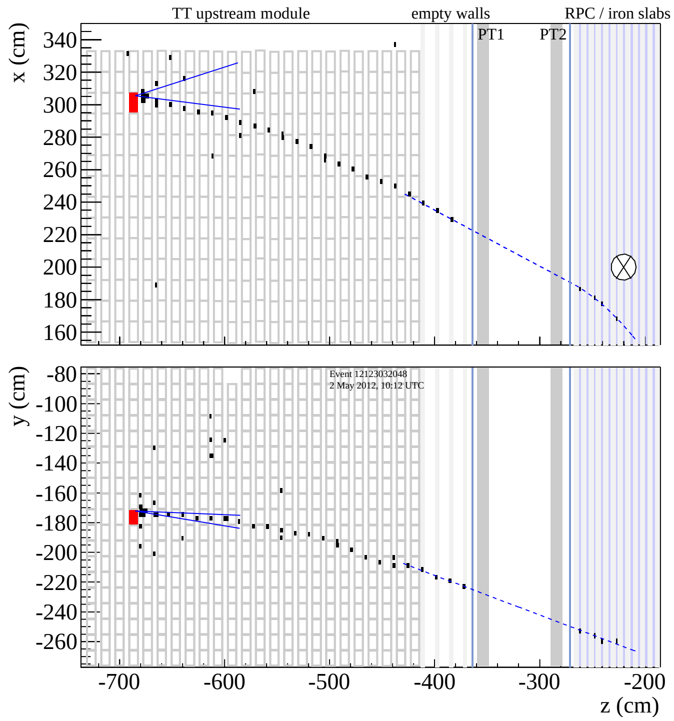

Figure 3: *The third OPERA τ candidate event, electronic detector display. The dashed blue lines show the fit of the most downstream hits according to the model* $x(z) = p_{0x} + p_{1x}(z - z_0) + p_{2x}(z - z_0)^2$ *with* $z_0 = -267.826$ *cm. The quadratic term is* $p_{2x} = (-0.00389 \pm 0.00069)$ cm^{-1} *and the* χ^2/ndf *of the fit is 2.6/4.*

of new physics beyond the standard three neutrino scenario.

3.1 Analysis of the third τ candidate

The electronic detector display of the third OPERA τ candidate is shown in Fig.3.

The particle coming from the decay of the τ candidate is recorded in 24 planes of the TT and crosses six RPC planes before stopping inside the first arm of the spectrometer. This range corresponds to 1650 g/cm^2 of material and the particle is therefore classified as a muon. Its momentum is estimated from the range to be (2.8 ± 0.2) GeV/c while its charge is measured with a fit on TT and RPC hits using a simple analytical model consisting of a straight line in the field-free region matched to a parabola in the magnetized region. The fitted parabola bends toward smaller x values, as shown in Fig.3, corresponding to a negative charge with the quadratic parameter different from zero at 5.6 σ significance.

The charge mis-identification probability has been estimated by means of a GEANT4 based MC simulation of muons entering the spectrometer with the same direction of the candidate and stopping in the same iron layer. The resulting distributions of the quadratic term for positive and negative muons is shown in Fig.4, together with the value measured on the candidate event. The

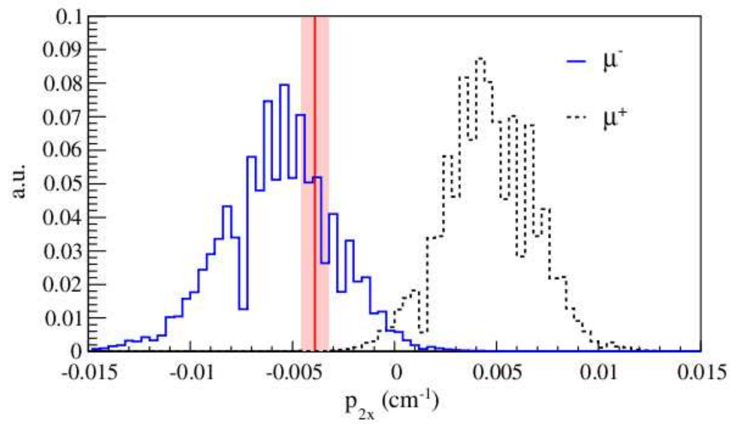

Figure 4: *Distributions of p_{2x} for a MC sample of positive and negative muons. The vertical solid line represents the values measured for the candidate, while the vertical band corresponds to 1 σ confidence interval.*

fraction of μ^+ with a bending reconstructed as negative, and therefore mimicking a μ^-, is 2.5%, but only 0.063% of the μ^+ has a bending more negative than the observed one.

3.2 Analysis of the OPERA emulsion detectors at the LNF scanning station

The OPERA brick is based on the Emulsion Cloud Chamber (ECC) detector concept, fulfilling the requirements of high granularity and micrometric resolution necessary to distinguish the τ decay vertex from the primary ν_τ interaction. Each ECC can act as a standalone detector that can be selectively removed from the target, developed and analyzed after the interaction took place.

A detailed description of the automatic microscopes developed for the analysis of OPERA ECCs can be found in Ref. [7]. The ECC (or "brick") dimensions and length are optimized to contain the primary as well the decay vertex and to provide particle identification and kinematical reconstruction. The use of passive material, combined with high accuracy tracking devices, allows for momentum measurement of charged particles via multiple Coulomb scattering (MCS) and for electromagnetic shower identification [8].

The bricks selected by the electronic detectors as containing a neutrino interaction vertex are extracted from the OPERA target and equally shared between Japan and Europe for the scanning. The CS doublet acts as a confirmation of the trigger provided by the Target Tracker: the brick is developed only if the prediction is confirmed, otherwise the CS is replaced and the brick is put back in the target. For events assigned to the European community the CS doublets are analyzed at the LNGS scanning station and the scanning load is shared among a group of specialised shifters. Since 2008 the LNF group contributes to the CS doublets scanning performing shifts at the LNGS station, in addition to the work load at the home scanning laboratory. The LNF scanning station [10] is part of the network of italian scanning groups including Bari, Bologna, LNGS, Napoli, Padova and Roma1 to which the emulsions developed at LNGS are sent for the final analysis.

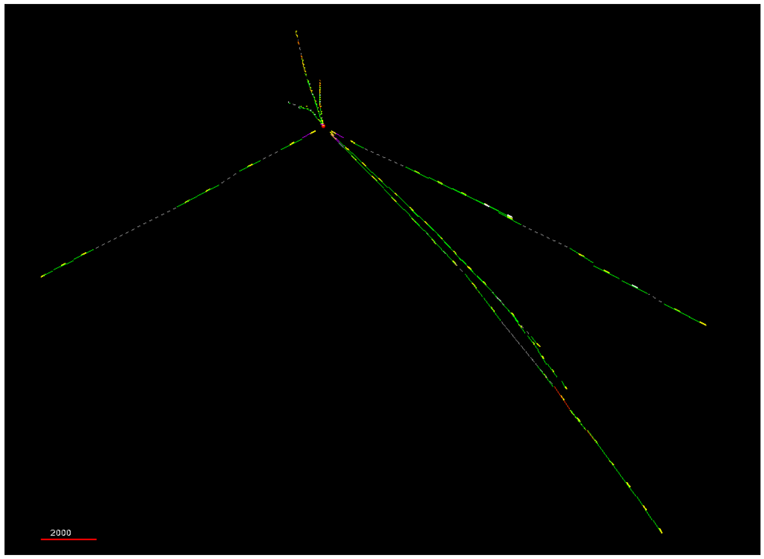

Figure 5: *A neutrino interaction in an OPERA brick found at the LNF scanning station.*

The LNF emulsion scanning station (Building 29) is hosted in a climatised environment to ensure good conditions for emulsion storage. The station is equipped with a motorized optical microscope instrumented with a system for the emulsion plates loading on the microscope stage (Plate Changer). The whole chain for brick scanning at LNF is fully operational since 2008. It consists of three phases: the brick scanning, the event reconstruction and the data publication on the central database.

During 2013 the laboratory has continued the coordinated activity of event location and reconstruction of the assigned samples with a special focus on Neutral-current like events. In particular we have defined and applied an improved procedure for the location of events with a clear shower-like signature in the CS films but having low "location" efficiency using standard procedures. The event display an event identified with the LNF microscope during the 2013 campaign is shown in Fig. 5. The scanning and analysis flow is smoothly running in parallel with the brick assignment. The LNF scanning laboratory shows good performances with a 75% location efficiency, in agreement with expectations.

Besides the scanning activity we are also deeply involved in the development of the simulation and the global analysis of the emulsion data in view of upcoming publications.

4 Publications

1. T. Adam *et al.* [OPERA Collaboration], "Measurement of the neutrino velocity with the OPERA detector in the CNGS beam using the 2012 dedicated data", JHEP **1**, 153 (2013).

2. N. Agafonova *et al.* [OPERA Collaboration], "Search for $\nu_\mu \Rightarrow \nu_e$ oscillations with the OPERA experiment in the CNGS beam", JHEP **07**, 004 (2013).

3. N. Agafonova *et al.* [OPERA Collaboration], "New results on $\nu_\mu \Rightarrow \nu_\tau$ appearance with

the OPERA experiment in the CNGS beam", JHEP **11**, 036 (2013).

References

1. M. Guler *et al.*, OPERA proposal, CERN/SPSC 2000-028, SPSC/P318, LNGS P25/2000.
2. R. Acquafredda *et al.*, JINST **4**, P04018 (2009).
3. M. Komatsu, P. Migliozzi, F. Terranova, J. Phys. **G29**, 443 (2003); P. Migliozzi, F. Terranova, Phys. Lett. **B563**, 73 (2003).
4. A. Donini, M. Maltoni, D. Meloni, P. Migliozzi and F. Terranova, JHEP **0712**, 013 (2007).
5. M. Blennow, D. Meloni, T. Ohlsson, F. Terranova and M. Westerberg, Eur. Phys. J. **C56**, 529 (2008).
6. See "LNF 2009 Annual Report", D. Babusci ed., LNF-10/15 (IR), p.97, "LNF 2008 Annual Report", D. Babusci ed., LNF-09/04 (IR), p.99, "LNF 2007 Annual Report", M. Antonelli ed., LNF-08/20 (IR), p.103; "LNF 2006 Annual Report", M. Antonelli ed., LNF-07/10 (IR), p.87; "LNF 2005 Annual report", E. Nardi ed., LNF-06/10 (IR), p.78; "LNF 2004 Annual Report", E. Nardi ed., LNF-05/5 (IR), p.70; "LNF 2003 Annual Report", S. Dell'Agnello ed., LNF-04/08 (IR), p.64.
7. N. Armenise *et al.*, Nucl. Instrum. Meth. **A551**, 261 (2005).
8. L. Arrabito *et al.*, JINST **2**, P05004 (2007).
9. A. Anokhina et al. [OPERA Coll.], JINST **3**, P07005 (2008).
10. LNF scanning station.
    `http://www.lnf.infn.it/esperimenti/opera/scanning.html`,
    `http://www.lnf.infn.it/esperimenti/opera/scanning/figs/animation_54105.gif`

ROG

G. Giordano (Resp.), M. Iannarelli (Tecn.), R. Lenci (Tecn.),
A. Marini (Ass.), G.P. Murtas (Ass.), G. Pizzella (Ass.),
F. Ronga (Ass.), E. Turri (Tecn.)

ROG Collaboration includes groups at :
University of Rome La Sapienza and INFN Roma 1,
University of Rome Tor Vergata and INFN Roma 2

1 Introduction

The ROG group is currently operating the cryogenic gravitational wave (GW) bar detector NAUTILUS, hosted in Frascati National Laboratory. The other detector that was operated by the ROG group, EXPLORER at CERN, ceased its operation on June 2010, by decision of INFN. The main goal of this search is the direct detection of the GW's that could be emitted by astrophysical sources (such as Supernovae or Coalescent Binaries). Such detection would be of enormous interest for general relativity and astrophysics.

The LNF group has major responsibilities in the maintenance and running of NAUTILUS (including the production of liquid Helium), in the maintenance, upgrading and running of the cosmic ray detectors, in the data acquisition and in many items of data analysis.

Both EXPLORER and NAUTILUS have been kept in continuous observational mode since 2003, with a duty cycle between 80 and 90%, mainly limited by the necessary periodic cryogenic operations.

2 NAUTILUS and EXPLORER

Both the NAUTILUS and EXPLORER detectors consist of an aluminum cylindrical bar having a mass of $\simeq 2.3$ tons, with a capacitive resonant transducer mounted on one of the bar faces. They are contained in a vacuum cryostat, cooled at cryogenic temperatures (at present $\simeq 3$ K, but a temperature as low as 0.1 K can be reached) to reduce thermal noise, and isolated from seismic and acoustic disturbances.

The capacitive transducer is coupled to a very low noise superconducting amplifier (d.c. SQUID) whose output is acquired by a VME ADC board, sampled at 5 kHz.

A GW signal would excite the mechanical resonant modes of the bar-transducer system. When searching for impulsive signals, the data are filtered with an adaptive filter matched to a delta-like signal. This search for bursts is suitable for any transient GW which shows a nearly flat Fourier spectrum at the two resonance frequencies of the detector.

Both detectors are equipped a cosmic ray detector to detect cosmic ray showers : in NAUTILUS it is based on a streamer tube assembly, while in EXPLORER on a set of long plastic scintillators.

NAUTILUS is operating at the INFN Frascati National Laboratory since December 1995. The present data taking started in 2003, with a new bar tuned at 935 Hz, where a pulsar, remnant of the SN1987A, is supposed to emit GW's, with a more sensitive readout chain (the same as for EXPLORER), and a new suspension cable, to provide a more stable position setting. At present, the temperature of the bar is 3.5 K and the resulting strain noise (the minimum detectable spectral density) is $\tilde{h} \simeq 1 \cdot 10^{-21}\ /\sqrt{Hz}$ around 935 Hz, and $\tilde{h} \leq 10^{-20}\ /\sqrt{Hz}$ over about 50 Hz. The noise temperature is about 1 mK, corresponding to an adimensional amplitude of GW bursts $h \simeq 2.4 \cdot 10^{-19}$.

The EXPLORER antenna was located at CERN and was very similar to NAUTILUS. Also its duty cycle was very high (of the order of 90%), its noise temperature was about 2 mK, with a strain sensitivity $\tilde{h} \simeq 2 \div 3 \cdot 10^{-21}$ $/\sqrt{Hz}$ around the two resonances at 904 Hz and 927 Hz, and $\tilde{h} \leq 10^{-20}$ $/\sqrt{Hz}$ over about 30 Hz.

The read-out systems installed in 2001 on EXPLORER and in 2003 on NAUTILUS, obtained a larger bandwidth and consequently improved the time resolution (a few ms), as it is also been checked with the events due to cosmic ray showers.

In the last years a continuos effort has been paid in improving the data analysis system already present and in testing independent algorithms and new methods. As a result of these, still going, efforts we were able to improve the accuracy in the reconstruction of both the amplitude and time characteristic of the signals. At the same time, we performed detailed studies of the detectors response to other class of signals than the simple delta-like burst previously considered. All this was done also with a particular eye on the perspective of performing joint analyses with the interferometric type of GW detectors, which do have a much better sensitivity than the resonant bar detectors, but up to now have suffered from very long interruptions in their operation. At present, both the US interferometers (LIGO) and the french-italian one (VIRGO) are down for a major upgrade that will return operative in 2015-2016, up to then leaving the INFN bar detectors (AURIGA and NAUTILUS) the only continually operational GW detectors.

3 Analysis of EXPLORER-NAUTILUS data

We continued to study all possible wide-band noises that can result in a candidate event and also, through simulations and software injections of signals, to find the event characteristics (e.g. length vs. amplitude) that an event due to a real excitation must have. All this was used to reduce the number of candidate events by putting vetos on periods or single events with understood instrumental noise excess, in addition to the usual vetos on events triggered by cosmic rays showers.

We have finished the analysis of the last period of NAUTILUS- EXPLORER overlapping operations, from April 2007 to June 2010 [1]. The analysis of this period of data, about 3 years long, was performed improving the methods used in the past, including a detailed study of the efficiencies of both detectors through the use of software injections. The search for coincidences of possible delta-like excitations, at the level of 0.1 accidentals expected in the whole period, produced a null result. We produced upper limits on the rate of GW short signals impinging on the Earth, also in this case with more refined techniques, including optimization procedures at each amplitude. The computed upper limits, at least in the high-amplitude range, are the lowest ever produced, and in all ranges improved the results previously published by resonant detectors.

The gravitational wave resonant detectors can be used as detectors of quark nuggets, like nuclearites (nuclear matter with a strange quark). The bar excitation mechanism is based on the so called thermo-acoustic effect, studied on dedicated experiments that use particle beams. This mechanism predicts that vibrations of bars are induced by the heat deposited in the bar from the particle. The geometrical acceptance of the bar detectors is 19.5 $m^2 sr$, that is smaller than that of other detectors used for similar searches. However, the detection mechanism is completely different and is more straightforward than in other detectors. We have presented to the ICRC2013 cosmic ray conference (Rio de Janeiro) the results of ten years of data from NAUTILUS (2003-2012) and 7 years from EXPLORER (2003-2009) [2]. The experimental limits we obtain are of interest because, for nuclearites of mass less than 10^{-4} grams, we find a flux smaller than the one predicted considering nuclearites as dark matter candidates (see Fig.1).

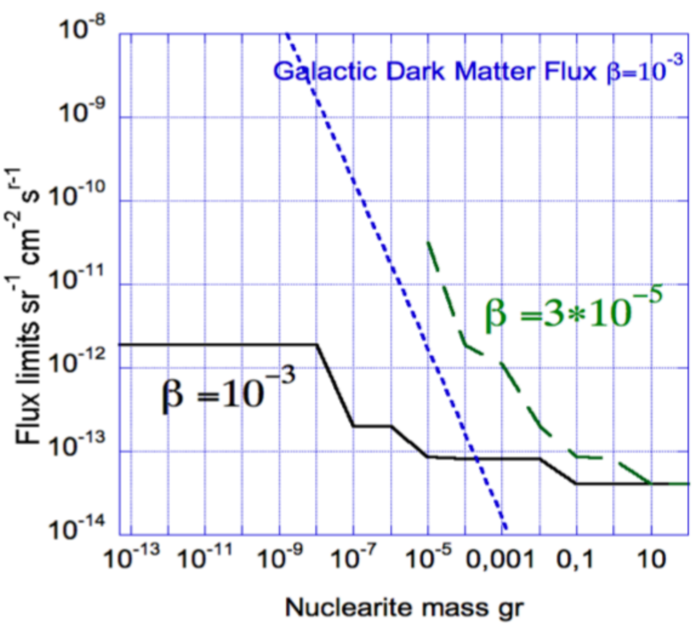

Figure 1: Flux upper limits for $\beta = 10^{-3}$ and $\beta = 3 \cdot 10^{-5}$ as a function of mass.

4 Astrowatch

Since the large interferometric GW detectors (LIGO, Virgo) have suspended operations for major upgrades, in the next 3-4 years the only continually operating GW detectors will be NAUTILUS and AURIGA, at Legnaro National Laboratory. The two groups have reached an agreement to be in a coordinated "astrowatch operation". The intent is to be ready for a common data analysis in case an important astrophysical event (that is an event thought to be a source of GW radiation) would happen. This would lead to at least the establishment of an upper limit on the amount of GW delivered by the event, or, in the most optimistic case, if the data would show a clear behavior above any reasonable possibility of a noise fluctuation and in agreement with the expectations for that event, to a claim for detection.

In 2012, the interferometric detector GEO (Hannover, Germany) has joined this agreement for astrowatch operation. GEO operations is not continuos, being on mainly on weekends and nights, since its main operation is devoted to upgrade and operational studies.

Up to now, no such astrophysical triggers showed up.

References

1. P. Astone *et al* "Analysis of 3 years of data from the gravitational wave detectors EXPLORER and NAUTILUS" Phys. Rev. D **87**, 082002 (2013).

2. P. Astone *et al* "Quark nuggets search using 2350 Kg gravitational waves aluminum bar detectors" 33rd Internation Cosmic Ray Conference, Rio de Janeiro 2-9 July 2013, arXiv:1306.5164 [astro-ph.HE].

WIZARD/PAMELA

G.Basini, M.Martucci (Dott.), G. Pizzella (Assoc.), M.Ricci (Resp.)

The space mission PAMELA is running and taking data since 2006 and will operate until the end of 2015 according to recent agreements between INFN, ASI and the Russian Space Agency Roscosmos. The instrument, the main scientific goals and the results of the experiment have been described in detail in the previous reports.
The LNF PAMELA group has continued in 2013 the regular activity in the analysis, running and quick-look control of the mission. In particular, it is fully involved in the study and analysis of solar events (Solar Flares, SEP, Forbush decrease) in collaboration with Universities and Institutions (including NASA) in USA, Germany and South Africa.
Significant results have been obtained and published on the spectrum of positrons, electrons antiprotons and He nuclei. In 2013, in particular, the analysis has been mostly focused to refine and better understand, with more statistical data, the unexpected difference in the shape of proton and He spectra between 30 GV and 1.2 TV of Rigidity.
Presentations on the most recent results of the experiment have been given in several Conferences, in particular at the biennial International Cosmic Ray Conference (ICRC 2013, Rio de Janeiro).
It is worth to note that, since 2013, under the agreement between INFN, ASI and Telespazio, a dedicated database for PAMELA has been created and is in operation in the ASI Science Data Center as a data archive with open access through web interface to the scientific community.

Recent publications

1. "Cosmic-Ray Positron Energy Spectrum Measured by PAMELA"; O. Adriani *et al.*, Phys. Rev. Lett. **111**, 081102 (2013);
2. "Measurement of the isotopic composition of Hydrogen and Helium nuclei in Cosmic Rays with the PAMELA experiment"; O. Adriani *et al.*, *ApJ* **770**, 2 (2013);
3. " Time dependence of the proton flux measured by PAMELA during the 2006 July – 2009 December Solar Minimum"; O. Adriani *et al*, Astrop. J., **765**, 91 (2013);
4. "Study on 2012 March 7 Solar Particle Event and Forbush decrease with the PAMELA experiment"; M. Ricci (for the PAMELA Collaboration), Proc. ICRC 2013, Rio de Janeiro;
5. "Solar modulation of galactic hydrogen and helium over the 23rd solar minimum with the PAMELA experiment"; M.Ricci and V. Di Felice (for the PAMELA Collaboration), Proc. ICRC 2013, Rio de Janeiro.

ALICE

N. Bianchi, G.P. Capitani (Ass.), A. Casanova Diaz (Ass.), L. Cunqueiro,
P. Di Nezza (Resp. Loc.), A. Fantoni, P. Gianotti, S.Liuti (Ass.), A. Moregula (Ass.), V. Muccifora,
A. Orlandi (Tecn.), A.R. Reolon, F. Ronchetti, S. Sakai, A. Viticchié (Tecn.)

1 Introduction

ALICE is an experiment at CERN which involves about 1300 physicists from more than 100 Institutions from several Countries. Italy participates with 12 groups and about 200 physicists. The Frascati group is deeply involved in the electromagnetic calorimeter (EMCal), both on the hardware and software side, while for the data analysis side the group is focused on the physics of the jets from both light and heavy flavors. The choice of these specific analyses comes from the fact that the EMCal enables ALICE, like no other experiment before, to explore the physics of jet quenching, i.e. the interaction of energetic partons with the QCD hot and dense medium, over the large kinematic range provided by the LHC. The EMCal provides both fast triggers (level 0 and 1) for photons, electrons, and jets and a High Level Trigger (HLT) as well. The EMCal also measures the neutral energy component of jets, enabling full jet reconstruction in all collision systems, from proton-proton to Pb–Pb, passing through the p–Pb collisions. The combination of the EMCal+DCal calorimeters, the excellent ALICE charged tracking capabilities, and the modest ALICE magnetic field strength, is a preferred configuration for jet reconstruction in the high background environment of heavy-ion collisions, allowing detailed optimization of background rejection while preserving the crucial jet quenching signals down to very low transverse momenta. The majority of the INFN groups in ALICE decided to participate to the major upgrade of the spectrometer by constructing a new generation Inner Tracking System (ITS) based on hybrid silicon pixel detectors or Monolithic Active Pixel Sensors (MAPS), with greatly improved features in terms of: determination of the distance of closest approach (DCA) to the primary vertex, standalone tracking efficiency at low p_t , momentum resolution and readout rate capabilities. The new detector will replace the existing ITS and will be installed during the LHC Long Shutdown 2. The Frascati group is involved, before, in the R&D for the electronic testing station, and then will be the hub for the final assembly and test of the modules (staves) ready to be installed in the ALICE spectrometer. ALICE data open the frontiers to rare events, to very high transverse momentum jets and give new tools for investigating the QCD and the Quark Gluon Plasma physics.

2 EMCal and DCal

The 10 full-size super-modules of the EMCal detector has been fully operational during the data taking, in particular during the heavy-ion run, 19 nb^{-1} of rare γ and jet events have been collected at the Level-1 trigger. The detector has been very stable running with an average dead time of 270 μs, a performance obtained using the two-branch Readout Control Unit based on the GTL bus arbitration. On the other hand the 2, 1/3-size, EMCal super-modules have been equipped with a new point-to-point readout units able to push the readout data rate up to 50 kHz. The firmware of such units was still under commissioning during the 2013 p–Pb run, so they where not included in the data taking for stability reasons. The point-to-point readout unit (SRU, Scalable Readout Unit) links to the single front end cards via ordinary (shielded) Ethernet cables and RJ45 connectors. The direct control of the front end, in the absence of the noisy and obsolete GTL-bus arbitration grants higher rates (up to 50 kHz Pb–Pb, which is already the promised LHC RUN3 performance) and more stability via market standard connections. The SRU readout is common to the DCal (EMCal back-to-back extension) and now also to the PHOS calorimeter. In practice,

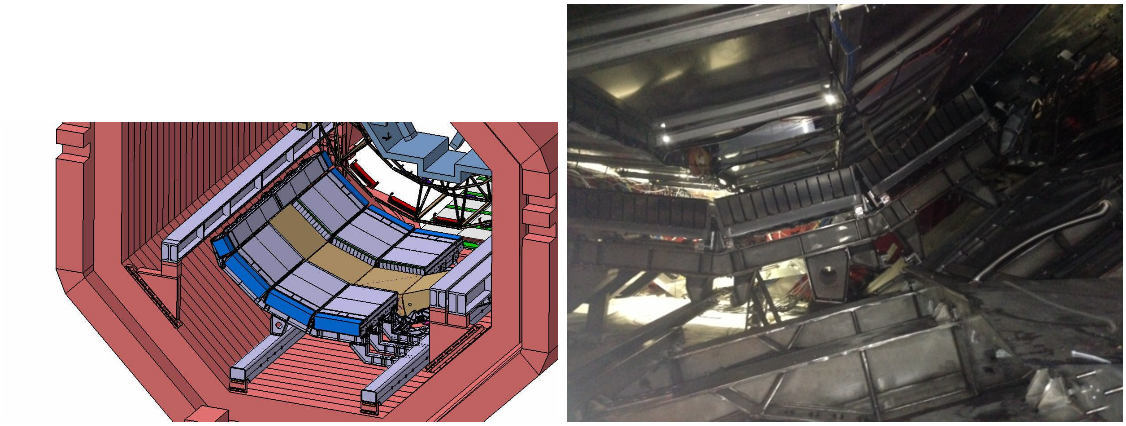

Figure 1: *Left panel: Rendering of 6 DCal (in blue) super-modules plus the 2 with reduced length (1/3) together with the PHOS super-modules (in violet) in between. Right panel: View of the DCal C-side super-modules installed in October 2013.*

already for RUN2 the DCal and PHOS modules will act as a single calorimeter back-to-back with the EMCal, allowing a substantial increased yield of γ-jet, h-jet and jet-jet events.

During the Long Shutdown 1, the EMCal has been fully upgraded to the SRU readout, by removing all the RCU units and equipping each front-end card with a mezzanine card used for the direct DTC (Data Trigger and Control) communication with the SRU. The present SRU firmware was finalized and a first performance boost was observed with a readout rate of 20 kHz and less noise induced on the trigger units which was mainly generated by the GTL-bus commands, now gone. The present readout rate is adequate to cope with the rates foreseen for RUN2 for rare triggers in *pp* (500 kHz of interaction rate) and Pb–Pb (8 kHz, equivalent to 700 kHz of *pp* track rates). The EMCal/DCal slow control system is being migrated to winCC (the new platform which replaced the PVSS framework) and further developments have been done to reduce the configuration times at Start of Run and to implement an on-the-fly recovering procedures to clear out front-end hick ups (which are expected to be extremely rare in the new setup).

The DCal expands the physics capabilities of the EMCal by enabling back-to-back correlation measurements, which are impossible with the EMCal alone, essential to obtain a complete picture of the physics addressed by the EMCal. Together, DCal, PHOS and EMCal form a two-arm electromagnetic calorimeter. The EMCal subtends 110° and the DCal+PHOS subtends 60° in the azimuthal angle ϕ, with the detectors covering $|\eta| <0.7$, thereby providing good acceptance for di-jets with radii R<0.4 up to transverse momenta $p_T \sim 150$ GeV/c.

The LNF group has the responsibility of coordinating the construction/assembly of the detector in the European-Asiatic zone and provided all WLS fibers for 1.5 DCal super-modules and for the two reduced length super-modules, for a total of 62000 fibers, grouped in 1700 bundles.

All the calorimeter super-modules have been completed and calibrated in 2013 in Grenoble, and tested with the new readout on surface at P2 at CERN before their installation. As scheduled, the DCal support structure and rails have been inserted in the L3 magnet in July-August 2013. In October, two DCal extension, with reduced length, have been placed inside and immediately after 3 DCal C-side supermodules have been installed.

In Fig. 1 is shown a schematic view of the DCal and PHOS super-modules (left panel) and a picture of the "C" side super-modules installed in 2013 (right panel). The DCal installation is expected to be completed in October 2014, just after the insertion of the four PHOS modules and before the closure of the L3 magnet.

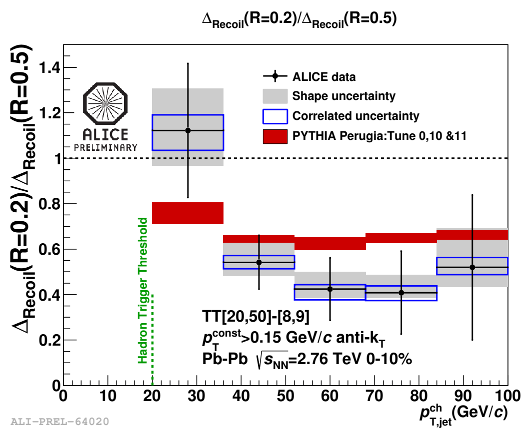

Figure 2: Indirect measurement of the jet shape via the ratio of recoil yields measured with different resolution parameter R.

3 Physics results

3.1 Jet quenching via intra-jet studies

During 2013 the group worked on the exploration of intra-jet broadening in central Pb–Pb at 2.76 TeV collisions using the 2011 data set. Our approach was to select a subsample of minimally biased jets and to study the transverse energy profile, comparing it to a pp vacuum reference. To select and measure a minimally biased jet subsample in heavy-ion collisions, a new technique for combinatorial background removal was applied. This technique consists on measuring the difference of the jet yields recoiling from two exclusive hadron trigger p_T windows (in this case [20,50]-[8,9] GeV). This differential observable, Δ_{Recoil}, is free of fake jet contribution and can be corrected to particle level by unfolding detector effects and residual background fluctuations. The measurement can be performed with arbitrarily large jet resolution R and down to low jet p_T, never reached before at the LHC. The ratio of Δ_{Recoil} at different R is an indirect measurement of the jet shape. In Fig.2 we show their ratio corresponding to $R = 0.2$ and $R = 0.5$, and its comparison to a Pythia calculation. The results show no significant energy redistribution within R=0.5, contributing to the LHC heavy-ion jet puzzle, where jet yields are significantly suppressed compared to vacuum, while intra-jet broadening is compatible with zero.

3.2 Heavy-flavour decay electron R_{AA}

Heavy quarks, i.e. charm and beauty, are produced primarily in the initial, hard partonic scatterings in hadron collisions. Their production in pp collisions is well described by perturbative QCD while, in the hot and dense matter (QGP), measurements of heavy-flavour production provide relevant information on the early stage of the collisions and parton-medium interaction. In our analysis, we measure electrons from heavy-flavour decays at mid rapidity ($|\eta|$ <0.6) in Pb–Pb collisions at $\sqrt{s_{\rm NN}} = 2.76$ TeV. Electrons are identified using the Time Projection Chamber (TPC) and the Electro-Magnetic Calorimeter (EMCal) that provided a trigger to measure high $p_{\rm T}$ electrons, and allowed to measure electrons up to 18 GeV/c in most central collisions (0-10%). The main background consists of electrons from photon conversion and neutral meson decays. The background is measured by calculating an invariant mass of the e$^+$e$^-$ pair, and it is statistically subtracted to obtain the signal from heavy-flavour decays. The nuclear modification factor is defined as:

$$R_{\mathrm{AA}}^{\mathrm{HF}} = \frac{dN_{\mathrm{AA}}^{\mathrm{HF}}/dp_{\mathrm{T}}}{\langle T_{\mathrm{AA}}\rangle d\sigma_{\mathrm{pp}}^{\mathrm{HF}}/dp_{\mathrm{T}}}, \tag{1}$$

where $\langle T_{\mathrm{AA}}\rangle$ is the nuclear overlap function for Pb–Pb collisions obtained via Glauber MC calculations, $dN_{\mathrm{AA}}/dp_{\mathrm{T}}$ is the differential yield in Pb–Pb collisions and $d\sigma_{\mathrm{pp}}/dp_{\mathrm{T}}$ is the differential cross section in pp collisions. In the following, $d\sigma_{\mathrm{pp}}/dp_{\mathrm{T}}$ was obtained by scaling the cross-sections measured at $\sqrt{s} = 7$ TeV down to 2.76 TeV according to the $\sqrt{s}$ dependence predicted by FONLL calculation. Figure 3 shows the nuclear modification factor of heavy-flavour decay electrons in 0-10% (left) and 40-50% (right) central collisions. If R_{AA} is less than unity, it indicates that production of heavy-flavour in Pb–Pb collisions is suppressed by the energy loss in the QCD matter. We observed a strong suppression of heavy-flavour decay electrons up to 18 GeV/c in 0-10% central collisions, and a smaller suppression in the 40-50% central collisions. The results clearly indicate an energy loss of charm and beauty quarks in the QGP.

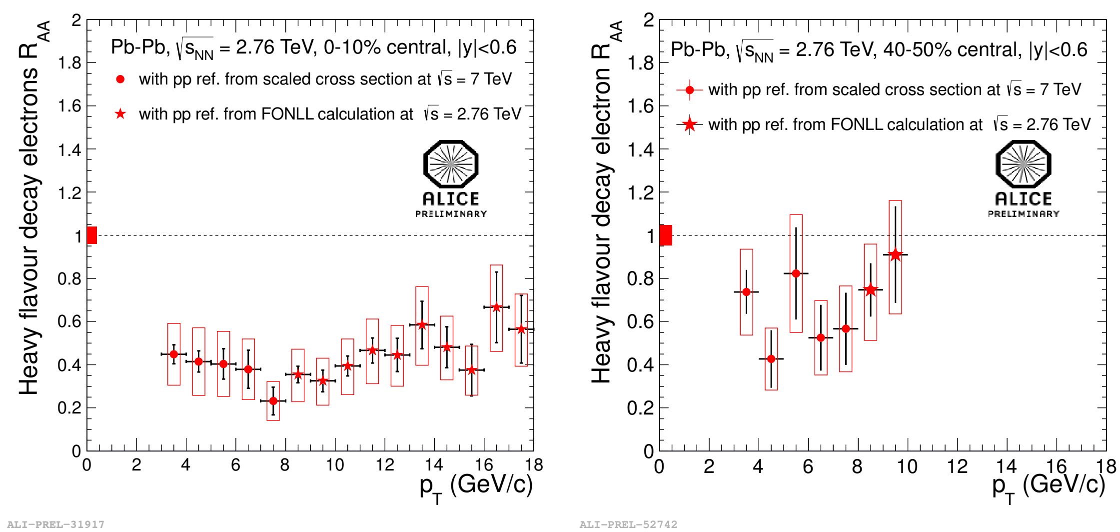

Figure 3: Nuclear modification factor of heavy-flavour decay electrons as a function of p_T for central 0-10% (left) and 40-50% (right) Pb–Pb collisions.

3.3 Λ^0 and $\bar{\Lambda}^0$ transverse polarization analysis

There are still several fundamental questions related to the spin structure of the nucleon which remain unanswered and the Λ^0 hyperon polarization is a potentially powerful way of probing polarized distributions inside the nucleon. Its decay into a proton and a pion in a parity violating weak decay enables the determination of the Λ^0 hyperon polarization by measuring the angular distribution of its decay products. Particularly, the study of the transverse polarization of Λ^0 and $\bar{\Lambda}^0$ hyperon in ALICE would allow to access distributions that measure the transverse spin functions of quarks inside an unpolarised hadron, in a kinematic regime never studied before.

The first step carried out was the reconstruction of these particles via the V0 candidates found at the reconstruction level making use of the properties of their weak decay topology from pp collisions at $\sqrt{s} = 2.76$, 7 and 8 TeV. The calculated invariant mass is in agreement with the PDG value in the full kinematic range which goes from 0.150 GeV to 16 GeV, unique among the LHC experiments. A not negligible signal of transverse asymmetry has been found.

4 Inner Tracking System and test station preparation

The main activity has been focused on the development of the sensor test, mainly from the point of view of the beam test of the prototype sensors. During the months of November, a beam test has taken place at the BTF (Beam Test Facility) of the laboratory. The sensors M22THRa1 and M22THRb, developed by the Strasbourg group (IPHC) in the framework of the ITS sensors development, have been exposed to a 500 MeV electron beam to study their characteristics. A simple two layers reference telescope made of two M18 pixel sensors, each composed by 512x512 pixels matrix with a pitch of 10 micrometers and thinned down to 50 micrometer thickness, have been used. The test system setup has been developed on purpose starting from a preexisting one used in a previous activity for the study of the fragmentation of the carbon-ions for hadrontherapy treatment plan optimization. The data acquisition software, based on a Linux machine, the FPGA firmware for the VME V1495 Caen board to produce the control signals and to readout the outputs have been developed for the two mentioned specific sensors. Moreover, an acquisition program to readout only the ZS (Zero Suppressed) data coming from the two M18 analog sensors readout by a VME sampling ADC module has been implemented to reduce the amount of data to be written on disk.

Preliminary results show the charge distribution per pixel of the two analog sensors in the telescope and the level of occupancy (i.e. the number of pixel over threshold, per event) in the M22THRb versus the event number. The electron beam used is produced as a secondary one obtained from a copper target. The impinging primary beam produced by the Daphne linac is alternately composed by electrons or positrons, with intensity lower roughly by one order of magnitude in the latter. We clearly see the primary beam changing from positron to electron around the event number from two hundred to four hundred.

5 Activity in the Seventh Framework Programme of HadronPhysics3: a dijet electromagnetic calorimeter for jet quenching studies

Part of the activities of the LNF group described in the present report, have been performed within the HadronPhysics3 in the Seventh Framework European Programme. In particular, a Joint Research Activity has been developed in collaboration with the Centre National de la Recherche Scientifique CNRS/IN2P3 and the Universidad de Santiago de Compostela, with the aim to expand the physics capabilities of the ALICE Electromagnetic Calorimeter (EMCal) by enabling back-to-back correlation measurements.

The completion of the installation of DCal supermodules during the Long Shutdown 1 of the LHC allows to start an extensive program of combined inclusive and correlation measurements. To this aim jet trigger development, jet reconstruction and new theoretical formalism have been implemented in the framework of the project and a new clustering algorithms for High Level Trigger (HLT) have been developed to optimize the cluster reconstruction in the electromagnetic calorimeter for different type of collisions. The performances of these algorithms have been checked by offline reconstruction efficiencies during the LHC run data taking. The online HLT chain, capable of producing trigger decision based on a full event reconstruction has been developed and tested on the LHC *pp* and Pb–Pb runs. Relevant triggers as neutral cluster trigger, electron trigger and jet trigger have been implemented too.

A new theoretical formalism and Monte Carlo modelization for the jet quenching has been developed unveiling a new picture of the jet quenching: for medium-induced gluon radiation, a jet is composed of a set of colored emitters, which may not correspond to the actual number of partons in the shower. This new picture provides a more consistent understanding of the present data on reconstructed jet observables and constitutes the basis for future developments.

Publications

The ALICE Collaboration has published 28 papers in 2013. The publications are accessible at the link: http://aliceinfo.cern.ch/ArtSubmission/publications;

1. N. Armesto, L. Apolinario, L. Cunqueiro, *An analysis of the influence of background subtraction and quenching on jet observables in heavy ion collisions*, JHEP **1302** (2013) 022.

Conference Talks

1. V.Muccifora, *Status of the Di-Jet Electromagnetic Calorimeter for Jet Quenching Study*, I3HP Hadron Physics 3 Workshop Frascati, 27-28 May 2013;
2. L. Cunqueiro, *Measurement of inclusive and recoil jets in central PbPb collisions with ALICE at the LHC*, INPC 2013 - International Nuclear Physics Conference - Firenze, Italy - 2 - 7 June 2013;
3. P. Di Nezza, *Jet Physics at the LHC*, International Conference on New Frontiers in Physics, Crete (Greece) 28 Aug. - 5 Sep. 2013 (invited talk);
4. S.Sakai *Heavy Flavour production in ALICE*, International Conference on the Initial Stages in High-Enegy Nuclear Collisions (IS2013), Galicia (Spain) 8-14 Sep. 2013, (invited talk);
5. L. Cunqueiro, *Measurment of jet production in central Pb–Pb collisions at* $\sqrt{s_{NN}} = 2.76$ *TeV using semi-inclusive hadron-jet distributions*, Hard Probes 2013, South Africa, 4-8 Nov. 2013.

Conferences Organization

1. INPC 2013 - International Nuclear Physics Conference - Firenze, Italy - 2 - 7 June 2013;

Proceeding and Notes

1. P. Di Nezza, Editor Proceedings *INPC 2013 - International Nuclear Physics Conference*, EPJ Web of Conferences;
2. P. Di Nezza, *Jet Physics at the LHC*, European Physical Journal Web of Conferences, vol. 71;
3. L. Cunqueiro, *Jet structure in 2.76 TeV Pb–Pb collisions at ALICE*, Nuclear Physics A 904 : 728C-731C May 2 2013;
4. P. Di Nezza, *Probing the medium with jets in ALICE*; International Conference on Heavy-Ion Collisions in the LHC Era, 422: Art. No. 012010 2013, IOP Publishing LTD.

Activity Report 2012 - JLAB12

M. Aghasyan (Art. 23), A. Courtoy (Ass. from Liege Universite'),
S. Anefalos Pereira (Ass. from Sao Paulo University), E. De Sanctis (Ass.), D. Hasch,
M. Hoek (Ass. from Glasgow University), V. Lucherini, M. Mirazita (Resp.) ,
R. Montgomery (PostDoc INFN), D. Orecchini (Tech.), A. Orlandi (Tech.),
J. Phillips (Ass. from Glasgow University), S. Pisano (Ass.),
P. Rossi, L. Trevisan (Borsista INFN), A. Viticchié (Tech.)

1 Introduction

The Frascati JLAB12 group participates into the physics program carried on by the CLAS collaboration in the Hall B of the Jefferson Laboratory (JLab). The physics program of the group is focused on the precision study of the three-dimensional structure of the nucleon and its internal dynamics. This is achieved through the determination of new three-dimensional parton distribution functions: the Transverse Momentum Dependent parton distribution (TMD) and the Generalized Parton Distribution (GPD) functions. The former describe the quarks and gluons inside the nucleon in the 3D momentum space and are accessible in Semi-Inclusive Deep Inelastic Scattering (SIDIS) measurements. The latter describe longitudinal momentum distributions at a given transverse spatial point and are measured in exclusive reactions. The structure functions containing the TMDs and GPDs enter in the Fourier components of the cross section of the process and they are accessed through the measurement of single or double spin asymmetries.

The operation of the JLab electron accelerator has been shout down in May 2012 to increase the maximum beam energy up to 12 GeV, to upgrade the three exististing experimental halls and to build a fourth new hall. In Hall B, the new CLAS12 spectrometer is now under construction. To improve the particle identification capabilities of this new detector also to the kaons, the Frascati group is involved in the construction of a RICH detector.

In the period covered by this report, the group has continued to work to the analysis of already available experimental data and in the completion of many $R\&D$ activities for the RICH.

2 Data analysis activity

We report here the analysis ongoing with data taken in the past years of operation with the 6 GeV JLab electron beam and the CLAS detector in Hall B.

2.1 GPD measurements

The simplest way to access GPDs is to study the Deeply Virtual Compton Scattering (DVCS) exclusive process, in which a hard photon is produced in the final state. Data have been collected with 5.5 GeV energy polarized electron beam and a longitudinally polarized proton target. This allowed to measure at the same time Single Beam and Target Spin Asymmetries (BSA and TSA) as well as Double Spin Asymmetries (DSA). All the three final state particles (the scattered electron, the recoil proton and the hard photon) are clearly identified in CLAS so that the kinematics of the process can be fully reconstructed. The asymmetries are extracted as a function of Q^2, x_B and t. Significant effects have been measured in the whole kinematic plane explored. As an example, in Fig. 1, we show the $-t$ dependece of the BSA, TSA and DSA asymmetries at Q^2=2 GeV^2 and x_B=0.26.

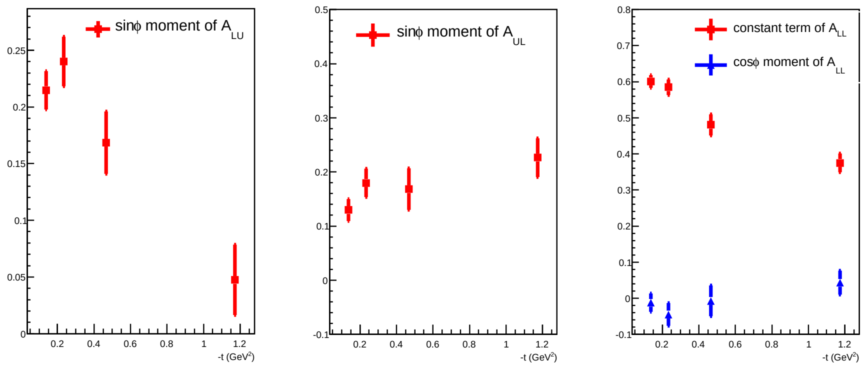

Figure 1: *DVCS amplitudes measured in the BSA (left), TSA (center) and DSA (right) measured at* Q^2*=2* GeV^2 *and* x_B*=0.26 as a function of -t.*

The measurement of the asymmetries from the experimental data has been completed, the analysis is now under the Collaboratioin review and will be released soon. The extraction from the experimental of the so-called Compton Form Factors, that are the observables containing the GPD, is currently underway.

2.2 TMD measurements

The TMDs, 3D extension of the collinear Pardon Distribution Functions (PDFs), are in general measured in SIDIS experiments with a meson (pion or kaon) in the final state. In these processes, the TMDs enter in convolution integrals with the Fragmentation Functions, thus sophisticated algorithms for their extraction are required. In recent years, the calculation of the Bessel-weightd asymmetries has been proposed as a convenient extraction method. This approach has been tested by the Frascati group with simulated data, using a dedicated Monte Carlo event generator in which the kinematic correlations between the parton and hadron momenta have been introduced. Systematics uncertainties in the extraction of the TMDs from the data in this new approach have been evaluated for a number of reference channels. Results of this analysis have been presented in International Conferences (2 and 12 in the list).

An alternative way to the TMDs is provided by the DiHadron SIDIS processes (DiSIDIS), in which two mesons (for example two pions) are produced in the final state. In this case, the cross section takes a much simpler form, with TMDs and DiHadron Fragmentation Functions entering as products instead of convolution integrals. In the collinear limit, the DiSIDIS allows the access to the higher-twist PDF e, g_T and h_L, that, together with the leading twist unpolarized f_1, helicity g_1 and transversity h_1, complete the collinear desctiption of the nucleon structure up to *twist-3*. Measurement of DiSIDIS asymmetries with a charged pion pair has been performed with both unpolarized as well as longitudinally polarized hydrogen target as a function of the relevant kinematic variables. As an example, in Fig. 2, we show the amplitudes extracted in the BSA, TSA and DSA as a function of the bjorken-x variable. The analysis with unpolarized target has been completed and submitted to the Collaboration review, while that with the polarized target is under completion. Results of this analysis have been presented in International Conferences (5, 11 and 13 in the list).

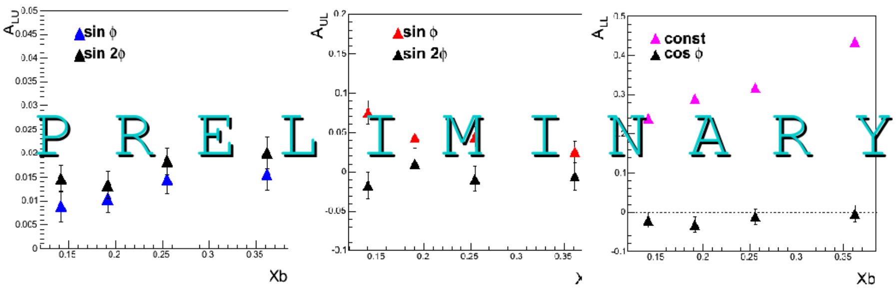

Figure 2: *Fourier amplitudes in the BSA (left), TSA (center) and DSA (right) measured in the* $ep \to e'\pi^+\pi^- X$ *process as a function of* x_B.

3 The CLAS12 Rich for the Hall B of JLab

The new CLAS12 detector under construction for the Hall B will have unique features (luminosity, resolution and large acceptance) to allow substantial progresses in the nucleon structure studies. In its baseline configuration, CLAS12 allows the identification of particles with the combination of time-of-flight and Cherenkov detectors in six azimuthal independent sectors. While these detectors are adequate for the identification of electrons, pions and protons, they don't allow clean identification of kaons. Nevertheless, SIDIS experiments with kaons in the final state are a key ingredient in the understanding of the nucleon structure. The physics case connected with the strangeness in the studies of the nucleon structure has been extensively discussed in two workshops organized at Frascati, the second of which in November 2013 [1].

In order to extend the capabilities of CLAS12 to detect kaons in the momentum range from 3 to 8 GeV/c, the Frascati group proposed in 2010 to replace one of the Cherenkov counters with a Ring Imaging CHerenkov (RICH) detector. This project now involves other INFN groups (Fe, Roma1/ISS, Ge, Ba) as well as International institutions: besides JLab, also the University of Glasgow (UK), the Gutenberg Universitat of Mainz (Germany), the UTFSM in Valparaiso (Chile), the Argonne Laboratory and the Universities of Duquesne and of Connecticut (USA) and the Kyungpook National University (Korea).

After an intense activity of *R&D* over the last years, a document describing the layout of the detector and tests of the various components has been released [2]. Then, in the second part of 2013 the RICH project made two major steps forward. During summer, the CLAS12-RICH project has been reviewed by two JLab committees and finally approved and started. The goal of the project, led by the INFN, is the construction of the first RICH sector and its installation in CLAS12 by the end of 2016, ready for the start of physics operation. In september, the CLAS-MED project has been approved by the Italian Ministry of the Scientific Research and awarded with the *premiali* funds. The main goal of CLAS-MED is the construction of a second RICH sector, necessary for the data taking with a transversed polarized target.

A sketch of the layout of the detector is shown in Fig. 3. The large dimensions (several squared meters) of the RICH suggested a hybrid proximity and mirror-focusing configuration, that uses aerogel as radiator material and multi-anode photomultipliers. In order to reduce the instrumented area of the detector to about 1 m^2 per sector and limit the costs, focalizing mirrors will be used to direct the light produced from particles at large angles into the light-detection region.

For forward scattered particles ($\theta < 13^o$), a proximity imaging method with thin (2 cm)

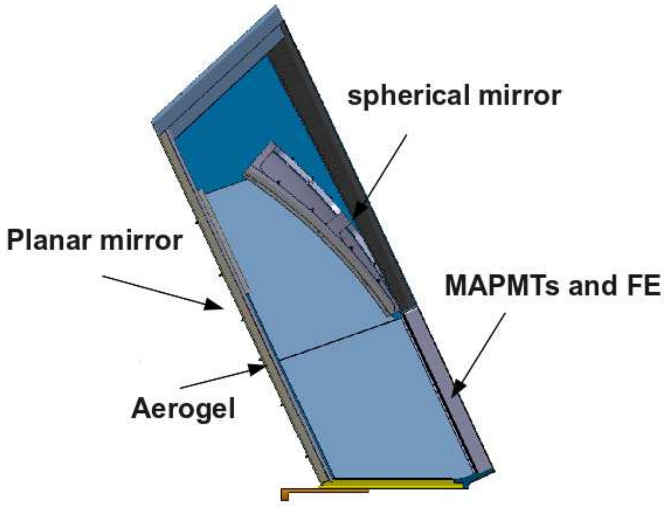

Figure 3: *Schematic lateral view of one RICH sector*

aerogel and direct Cherenkov light detection will be used. For larger incident particle angles of ($13^o < \theta < 25^o$), the Cherenkov light will be focused by a spherical mirror, undergo two further passes through the thin radiator material and a reflection from planar mirrors before detection. The longer path of light and the focusing mirror allows the use of a thick (6 cm) aerogel to compensate yield losses into the thin radiator. The Cherenkov photons are detected by an array of Multi-Anode PhotoMultiplier Tubes (MAPMTs) Hamamatsu H8500, a matrix of 8x8 pixels of 6x6 mm^2 size.

During 2013, the analysis of the large amount of data collected in laboratory and beam tests has been completed. These analyses include laboratory test of MAPMTs and of the Front-End electronics as well as the test beam, performed at the LNF Beam Test Facility and at the T9 beam line of CERN, of a large scale RICH prototype projected and build in Frascati. The results have been presented in International Conferences (1, 6 and 10 in the Conference list).

The project has started in 2013 the construction phase, and the Frascati group is responsible for the mechanic design of the external frame, of the panel hosting the MAPMTs and the electronics and of the mirror system. Preliminary designs have been developed and discussed with the responsibles of the CLAS12 detector design [3)].

4 List of Conference Talks

1. R. Montgomery, *A Ring Imaging Cherenkov Detector for CLAS12* - 13th Vienna Conference on Instrumentation - February 11-13 2013, Vienna, Austria

2. M. Aghasyan, *Studies of TMDs with CLAS* - XXI International Workshop on Deep-Inelastic Scattering and related subjects - April 22-26 2013, Marseille, France

3. M. Mirazita, *Studies of the transverse structure of the nucleon at Jefferson Laboratory* - International Nuclear Physics Conference - June 2-7 2013, Firenze, Italy

4. D. Hasch, *3D structure of nucleons from an EIC* - Workshop on the Structure of Nucleons and Nuclei, June 10-14 2013, Como, Italy

5. S. Anefalos Pereira, *Dihadron production at JLab* - Workshop on the Structure of Nucleons and Nuclei, June 10-14 2013, Como, Italy

6. R. Montgomery, *A Ring Imaging Cherenkov Detector for CLAS12* - International Conference on the Structure of Baryons, June 24-28 2013, Glasgow, UK

7. P. Rossi, *Jefferson Lab at 12 GeV: New Opportunities in Hadronic Physics* - 5^{th} Workshop on Hadron Physics in China and Opportunities in US, July 2-6, 2013, Huangshan, Anhui (China)

8. P. Rossi, *Jefferson Lab: New Opportunities in Hadronic Physics* - XXXVI Brazilian Meeting on Nuclear Physics, September 1-5, 2013, Maresia, SP (Brazil)

9. P. Rossi, *Jefferson Lab: a journay from quarks to matter and beyond* - SIF XCIX Congresso Nazionale, September 23-27, 2013, Trieste, Italy

10. M. Mirazita, *The CLAS12 Rich project* - 2nd Workshop on Probing Strangeness in Hard Processes, November 11-13, 2013, Frascati, Italy

11. S. Pisano, *JLab news on TMD observables* - 2nd Workshop on Probing Strangeness in Hard Processes, November 11-13, 2013, Frascati, Italy

12. M. Aghasyan, *Monte Carlo for TMDs* - 2nd Workshop on Probing Strangeness in Hard Processes, November 11-13, 2013, Frascati, Italy

13. A. Courtoy, *Analysis of di-hadron observables* - 2nd Workshop on Probing Strangeness in Hard Processes, November 11-13, 2013, Frascati, Italy

14. P. Rossi, *CLAS12 baseline equipment and status of the project* - 2nd Workshop on Probing Strangeness in Hard Processes, November 11-13, 2013, Frascati, Italy

5 Publications

1. CLAS Collaboration, Demonstration of a novel technique to measure two-photon exchange effects in elastic e(+/-)p scattering, Phys. Rev. C 88, 025210 (2013)

2. CLAS Collaboration, First Observation of the Line Shape of the $\Lambda(1405)$ in Electroproduction, Phys. Rev. C 88, 045202 (2013)

3. CLAS Collaboration, ϕ-meson photoproduction on Hydrogen in the neutral decay mode H. Seraydaryan et al. Submitted PRC

4. CLAS Collaboration, Differential Photoproduction Cross Sections for the $\Sigma^0(1385)$, $\Lambda(1405)$, and $\Lambda(1520)$, Phys Rev C 88, 045201 (2013)

5. CLAS Collaboration, Cross sections for the γ p $K^{*+}\Lambda$ and $K^{*+}\Sigma^0$ reactions measured at CLAS, PRC 87, 065204 (2013)

6. CLAS Collaboration, Transverse Polarization of $\Sigma^+(1189)$ in Photoproduction on a Hydrogen Target, PRC 87, 045206 (2013)

7. CLAS Collaboration, Measurement of the $\Sigma\pi$ Photoproduction Line Shapes Near the $\Lambda(1405)$, PRC 87, 035206 (2013)

8. CLAS Collaboration, Measurement of Transparency Ratios for Protons from Short-Range Correlated Pairs, PLB 722, 63 (2013)

9. CLAS Collaboration, Separated Structure Functions for Exclusive K+ Λ and K+ Σ^0 Electroproduction at 5.5 GeV with CLAS, PRC 87, 025204 (2013)
10. CLAS Collaboration, Hard Two-body Photodisintegration of 3He, PRL 110, 242301 (2013)
11. CLAS Collaboration, Beam asymmetry Σ for π^+ and π^0 photoproduction on the proton for photon energies from 1.102 to 1.862 GeV, Phys. Rev. C 88, 065203 (2013)
12. CLAS Collaboration, Deep exclusive π^+ electroproduction off the proton at CLAS, Eur. Phys. J. A 49 (2013) 16.
13. CLAS Collaboration, Near Threshold Neutral Pion Electroproduction at High Momentum Transfers and Generalized Form Factors, PRC 87, 045205 (2013)

References

1. http://www.lnf.infn.it/conference/2013/PSHP2013/
2. http://www.lnf.infn.it/ mirazita/RICH/RICH_TDR.pdf
3. https://clasweb.jlab.org/wiki/index.php/Clas12_RICH/Meetings

KAONNIS

M. Bazzi (Art. 23), C. Berucci (Ass.), M. Bragadireanu (Bors. UE), A. Clozza,
C. Curceanu (Resp. Naz.), A. D'Uffizi (Ass. Ric.),
C. Guaraldo, M. Iliescu (Art. 23), P. Levi Sandri, F. Lucibello (Tecn.),
S. Okada (Art. 23), D. Pietreanu (Ass.), K. Piscicchia (Bors.),
M. Poli Lener (Art. 23), E. Sbardella (Bors.),
A. Scordo (Ass. Ric.), H. Shi (Ass.),
D. Sirghi (Art. 23), F. Sirghi (Bors. UE),H. Tatsuno (Post. Doc.)
I. Tucakovic (Bors.), O.Vazquez Doce (Ass.)

1 The KAONNIS scientific program

KAONNIS represents an integrated initiative in the field of the low-energy kaon-nucleon/nuclei interaction studies. Under KAONNIS the following activities are performed:

- the study of kaonic atoms by the SIDDHARTA and SIDDHARTA-2 experiments
- the study of kaon-nuclei interaction at low energies in the framework of AMADEUS.

We present in what follows these scientific lines, together with the 2013 activities and the plans for 2014. The KAONNIS scientific program and its realization are partially financed within the FP7 HadronPhysics2 and HadronPhysics3 EU programs.

2 The SIDDHARTA and SIDDHARTA-2 experiments

The objective of the SIDDHARTA (Silicon Drift Detector for Hadronic Atom Research by Timing Application) experiment and of its successor, SIDDHARTA-2, is to perform high precision measurements of X-ray transitions in exotic (kaonic) atoms at DAΦNE.

The precise measurement of the shift and width of the 1s level with respect to the purely electromagnetic calculated values, in kaonic hydrogen and kaonic deuterium, generated by the presence of the strong interaction, through the measurement of the X-ray transitions to this level, will allow the first precise experimental extraction of the isospin dependent antikaon-nucleon scattering lengths, fundamental quantities in understanding low-energy QCD in strangeness sector.

The accurate determination of these scattering lengths will place strong constraints on the low-energy $K^{-}N$ dynamics, which, in turn, constraints the SU(3) description of chiral symmetry breaking in systems containing the strange quark. The implications go from particle and nuclear physics to astrophysics.

SIDDHARTA performed the most precise measurement of kaonic hydrogen and the first exploratory one of kaonic deuterium. Moreover, the kaonic helium 4 and 3 transitions to the 2p level were measured, for the first time in gas in He4 and for the first time ever in He3. Presently, a major upgrade of SIDDHARTA, namely SIDDHARTA-2, is under way, with the aim to measure kaonic deuterium and other types of kaonic atoms in the coming years.

2.1 The SIDDHARTA setup

SIDDHARTA represented a new phase in the study of kaonic atoms at DAΦNE. The previous DEAR experiment's precision was limited by a signal/background ratio of about 1/70 for the kaonic hydrogen measurement. To significantly improve this ratio, a breakthrough was necessary.

An accurate study of the background sources present at DAΦNE was redone. The background includes two main sources:

- synchronous background: coming together with the kaons -related to K^- interactions in the setup materials and also to the ϕ-decay processes; it can be defined as hadronic background;
- asynchronous background: final products of electromagnetic showers in the machine pipe and in the setup materials originating from particles lost from primary circulating beams either due to the interaction of particles in the same bunch (Touschek effect) or due to the interaction with the residual gas.

Accurate studies performed by DEAR showed that the main background source in DAΦNE is of the second type, which shows the way to reduce it. A fast trigger correlated to a kaon entering into the target would cut the main part of the asynchronous background. X rays were detected by DEAR using CCDs (Charge-Coupled Devices), which are excellent X-ray detectors, with very good energy resolution (about 140 eV FWHM at 6 keV), but having the drawback of being non-triggerable devices (since the read-out time per device is at the level of 10 s). A new device, which preserves all good features of CCDs (energy resolution, stability and linearity), but additionally is triggerable - i.e. fast (at the level of 1μs), was implemented. The new detector was a large area Silicon Drift Detector (SDD), specially designed for spectroscopic application. The development of the new 1 cm^2 SDD device, together with its readout electronics and very stable power supplies, was partially performed under the Joint Research Activity JRA10 of the I3 project"Study of strongly interacting matter (HadronPhysics)" within FP6 of the EU.

The trigger in SIDDHARTA was given by a system of scintillators which recognized a kaon entering the target making use of the back-to-back production mechanism of the charged kaons at DAΦNE from ϕ decay: of the type:

$$\phi \to K^+K^-. \tag{1}$$

The SIDDHARTA setup contained 144 SDD chips, 1 cm^2 each, placed around a cylindrical target, containing high density cryogenic gaseous hydrogen (deuterium or helium). The target was made of kapton, 75μm thick, reinforced with aluminium grid.

The SIDDHARTA setup was installed on DAΦNE in late summer 2008, see Figure 1 - and the period till the end of 2008 was used to debug and optimize the setup performances (degrader optimization included). The kaonic atoms (hydrogen, deuterium, helium4 and 3) measurements were done in 2009 and data analysis followed in the coming years.

2.2 SIDDHARTA activities in 2013

SIDDHARTA was in data taking until 9 November 2009. In 2013 the group activity was dedicated to the kaonic low-Z and helium atoms analysis and to the upgrade of the setup, SIDDHARTA-2, to perform in the future the kaonic deuterium and other precision kaonic atoms measurements. For the results of SIDDHARTA analyses in 2013 see the publication list.

2.3 *SIDDHARTA-2*

In 2010 the proposal for the SIDDHARTA upgrade was put forward. The upgrade of SIDDHARTA to SIDDHARTA-2 is based on five main modifications:

- Trigger geometry and target density: By placing the upper kaon-trigger detector close in front of the target entrance window, the probability that a triggered kaon really enters the gas and is stopped there is much improved. Making the detector smaller than the entry area gives away some signal, but suppresses efficiently the kaonic lines from "wall-stops" (kaons

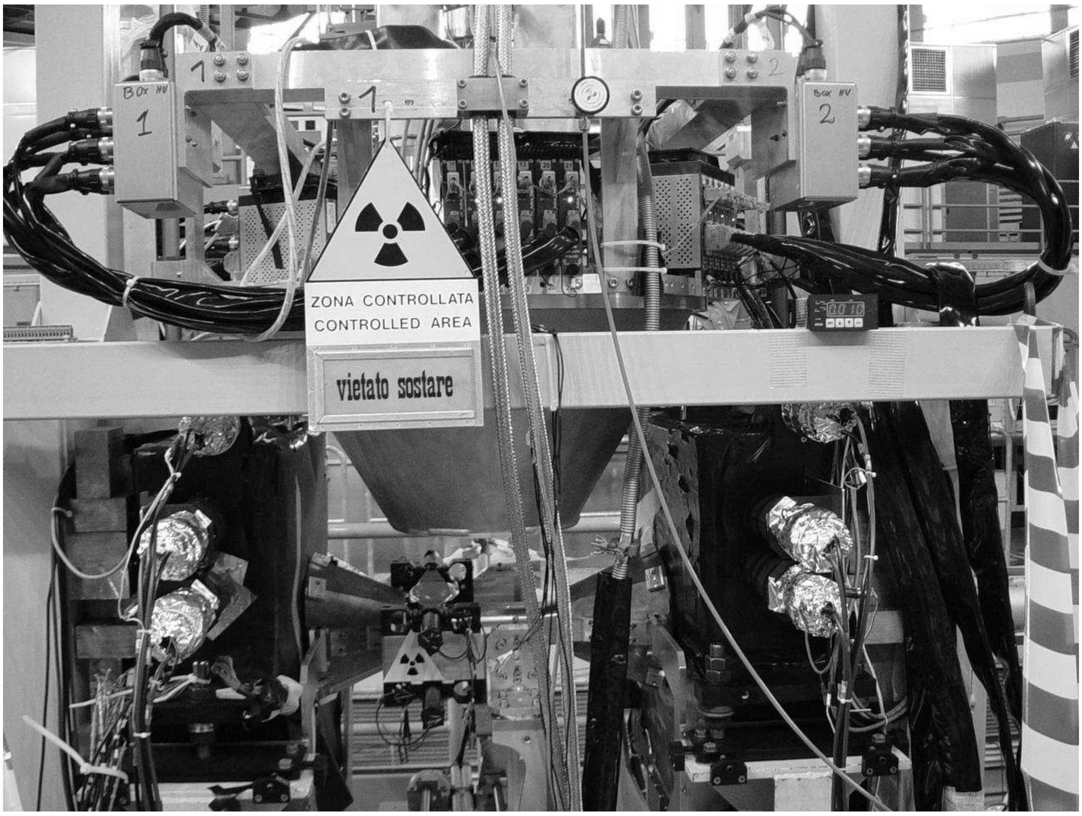

Figure 1: The SIDDHARTA setup installed at DAΦNE

entering the gas volume, but passing from the inside of the target to the cylindrical walls). The number "signal per trigger" goes up, which also reduces the accidental background coming along with every trigger. We plan as well to double the gas density which enhances the gas stops and further reduces the wall-stops.

- K^+ discrimination to suppress kaon decay background: A "kaon stopper"scintillator is placed directly below the lower kaon trigger scintillator. When a $K^-$is stopped there, only one (large) signal from pileup of stopping and kaon-absorption secondaries is seen, whereas when a K^+ is stopped, the kaon-decay particles are seen after the signal from the stopping (mean K^+ lifetime 12.8 ns). Using a flash-ADC we will be able to efficiently distinguish the 2 cases. In addition, we will use scintillators surrounding the target to measure K^- absorption secondaries pions). The time window for gas stops is about 4 ns wide. By this condition we also suppress stops in the entry window.

- Active shielding: The scintillators surrounding the target will also be used in prompt anti-coincidence if the spatial correlation of SDD and scintillator hits indicates that it originated from a pion ("charged particle veto"). An anticoincidence covering the SDD time window of about 600 ns (with the exception of the 4 ns of the gas stopping time) will reduce the accidental background. Although the scintillators have only low efficiency for gammas, the abundance of secondaries from the electromagnetic showers allows a relevant reduction of accidental ("beam") background. The upper trigger scintillator has 2 functions, it is also used as an anticoincidence counter: after the kaon and eventual prompt kaon-absorption secondaries pass, it vetos beam background.

- Use of new SDD detectors, produced by FBK, having a much better active/total surface ratio.

- Operating SDDs at a lower temperature: tests indicate that an improvement of the timing resolution by a factor of 1.5 is feasible by more cooling. The signal enhancement by a factor 2 to 3 is due to moving the target cell closer to the IP, by changing its shape, by a better solid angle of the SDDs and by the higher gas density. In such conditions, with an integrated luminosity of 800 pb^-1 a precision of about 70 eV for the shift, and 160 eV for the width are attainable, resulting in a relative precision similar to that obtained for kaonic hydrogen.

In 2013 various tests on prototypes were performed, together with Monte Carlo simulations to optimize the setup.

More details can be found in the various presentations to the LNF International Scientific Committee on the LNF-INFN web-site.

2.4 Activities in 2014

The LNF group main activities in SIDDHARTA and SIDDHARTA-2 for 2014 are the following ones:

- Monte Carlo simulations for the SIDDHARTA-2 setup and physics;
- construction and tests of the SIDDHARTA-2 setup components: target, veto counters, new trigger, new cryogenic systems;
- definition of the strategy for SIDDHARTA-2 measurements (including interaction region definition and construction).

The SIDDHARTA scientific program is an important part of the Network LEANNIS (WP9) in the framework of the EU FP7 HadronPhysics3 program.

3 The AMADEUS proposal and the 2013 activities

The low-energy ($<$ 100 MeV/c) kaon-nuclei interaction studies represents the main aim of the AMADEUS experiment. In order to do these type of measurements, in a most complete way, by detecting all charged and neutral particles coming from the K^- interactions in various targets with an almost 4π acceptance, the AMADEUS collaboration plans to implement the existent KLOE detector in the internal region of the Drift Chamber with a dedicated setup (see Figure 2). The dedicated setup contains the target which can be either solid or a gaseous cryogenic one, a trigger (TPC-GEM) and a tracker system (scintillating fibers read by SiPM detectors).

The negatively charged kaons can stop inside the target or interact at low energies, giving birth of a series of processes we plan to study. Among these, a key-role is played by the generation of $\Lambda(1405)$ which can decay into $\Sigma^0\pi^0$, $\Sigma^+\pi^-$ or $\Sigma^-\pi^+$. We plan to study all these three channels in the same data taking. Another important item is represented by the debated case of the “kaonic nuclear clusters”, especially the K^-pp, and K^- -ppn cases. We can study these channels by measuring, for example, their decays to Λp and to Λd. In the same time, many other kaon-nuclei processes will be investigated, either for the first time, or in order to obtain more accurate results than those actually reported in literature. Cross sections, branching ratios, rare hyperon decay processes will be investigated, taking advantage of the unique kaon-beam quality delivered by DAΦNE and of the unique characteristics of the KLOE detector.

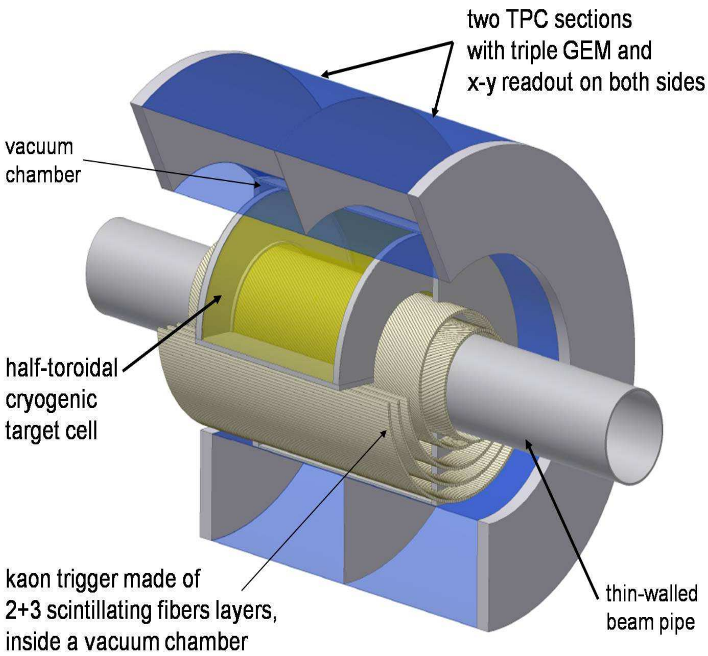

Figure 2: The AMADEUS dedicated setup implemented in the Drift Chamber of the KLOE detector. In this situation a cryogenic gaseous target is used.

As targets to be employed, we plan to use gaseous ones, like d, ^{3}He or ^{4}He and solid ones as C, Be or Li. In the summer of 2012 a first dedicated target, half cylinder done in pure carbon was realized and installed inside the Drift Chamber of KLOE as a first setup towards the realization of AMADEUS (see Figure 3). The target thickness was optimized such as to have a maximum of stopped kaons (about 24% of the generated ones) without degrading too much the energy of resulting charged particles inside the target material. In the period of data taking a total integrated luminosity of about 80 pb^{-1} was achieved. The analysis of these data will provide new insights in the low-energy interactions of charged kaons in the nuclear matter. For the future, other targets are planned to be used compatible with the beam assignment.

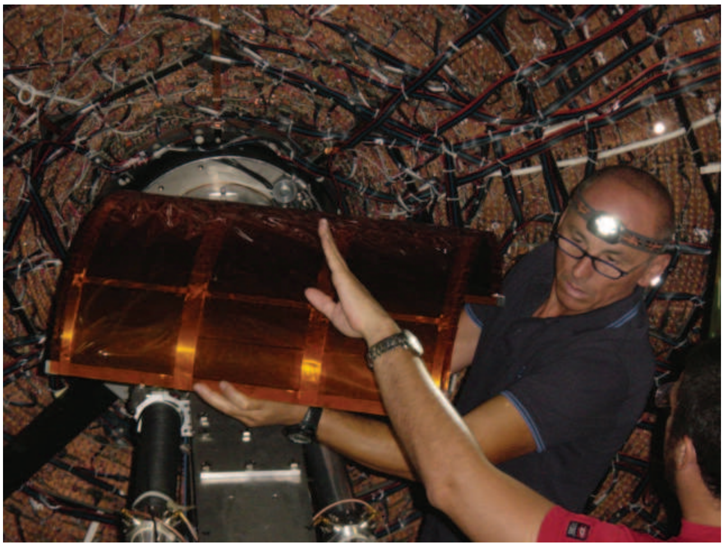

Figure 3: The AMADEUS carbon target (half cylinder) installed inside the Dift Chamber of KLOE detector.

Activities done in 2013:

- analysis of 2002-2005 KLOE data.
- analysis of the 2012 Carbon target data.
- R&D for the trigger system: a prototype based on scintillating fibers read by Silicon Photo-Multipliers (see Fig. 4).
- R&D for the inner tracker - a small TPC-GEM prototype, Fig. 5, for traking performance.
- Monte Carlo simulations.

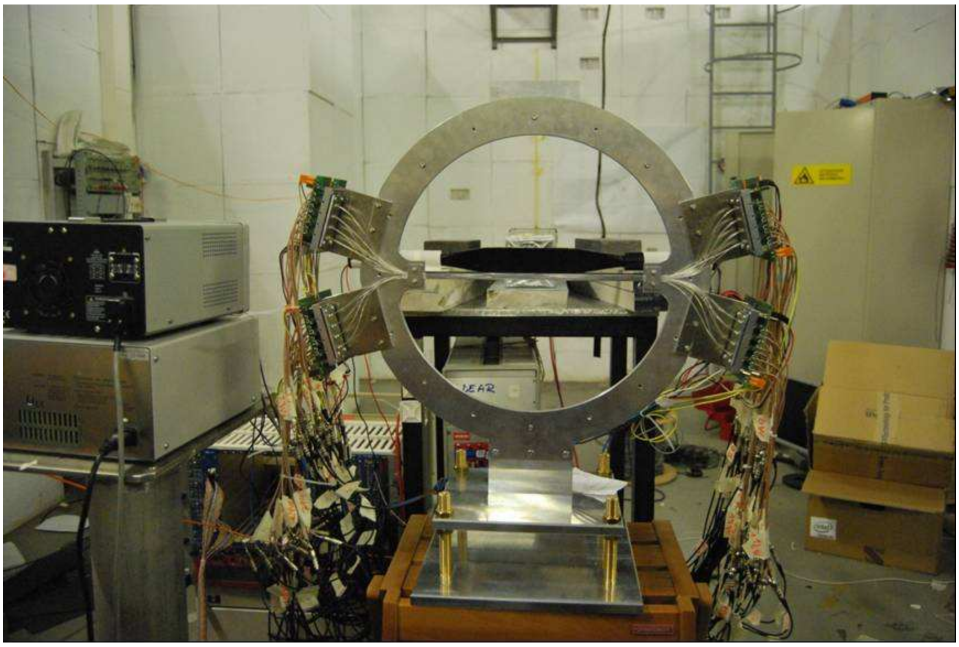

Figure 4: The AMADEUS trigger ptototype, based on scintillating fibers read at both ends by SiPM

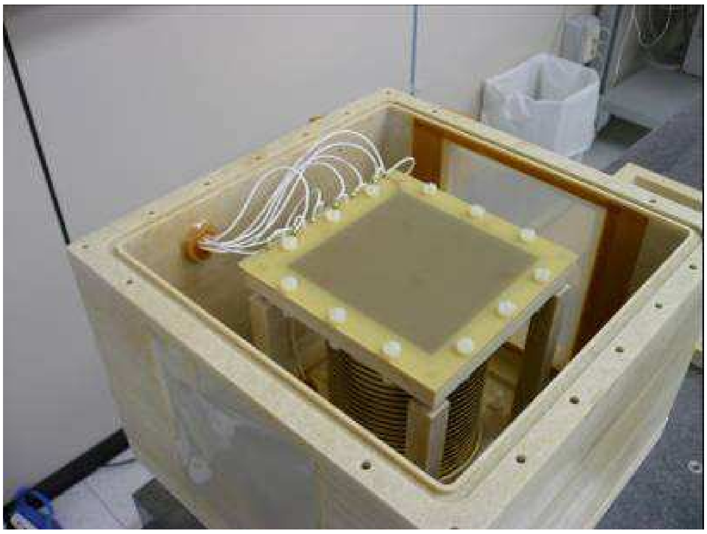

Figure 5: The TPC-GEM prototype

3.1 AMADEUS activities in 2014

The main activities of AMADEUS in 2014 will be:

- continuation of the R&D for the trigger system: tests of the prototype and readout electronics at BTF-LNF and PSI.
- continuation of the R&D for the inner tracker: tests of the prototype at BTF-LNF and PSI
- Monte Carlo simulations.
- finalization of the KLOE 2002-2005 data analyses searching for low-Z kaons interaction in the materials of the KLOE setup.
- continuation of the analyses of data with carbon target
- definition of the experiment strategy

To be mentioned that the AMADEUS activities are supported in the framework of the EU FP7 HadronPhysics3, as WP24 (GEM), WP28 (SiPM) and WP9 (Network on kaon-nuclei interaction studies at low energies) programs.

Acknowledgements
The support from HadronPhysics3 FP7 project is acknowledged.

4 Publications in 2014

1. M. Bazzi, C. Berucci, C. Curceanu, A. d'Uffizi, M. Iliescu, E. Sbardella, A. Scordo and H. Shi *et al.*, Characterization of the SIDDHARTA-2 second level trigger detector prototype based on scintillators coupled to a prism reflector light guide, JINST **8** (2013) T11003.
2. S. Ajimura, G. Beer, H. Bhang, M. Bragadireanu, P. Buehler, L. Busso, M. Cargnelli and S. Choi *et al.*, A search for deeply-bound kaonic nuclear state at the J-PARC E15 experiment, Nucl. Phys. A **914** (2013) 315.
3. T. Ishiwatari *et al.* [SIDDHARTA Collaboration], Strong-interaction shifts and widths of kaonic helium isotopes, Nucl. Phys. A **914** (2013) 305.
4. C. Curceanu, M. Bazzi, G. Beer, C. Berucci, L. Bombelli, A. M. Bragadireanu, M. Cargnelli and A. Clozza *et al.*, Unlocking the secrets of the kaon-nucleon/nuclei interactions at low-energies: The SIDDHARTA(-2) and the AMADEUS experiments at the DAΦNE collider, Nucl. Phys. A **914** (2013) 251.
5. S. Ajimura, G. Beer, H. Bhang, M. Bragadireanu, P. Buehler, L. Busso, M. Cargnelli and S. Choi *et al.*, A Search for Deeply Bound Kaonic Nuclear States at J-PARC, Few Body Syst. **54** (2013) 1195.

6. M. Iliescu, M. Bazzi, G. Beer, L. Bombelli, A. M. Bragadireanu, M. Cargnelli, C. Curceanu (Petrascu) and A. Duffizi *et al.*, Kaon-Nucleon Strong Interaction in Kaonic Atoms: The SIDDHARTA Program, Few Body Syst. **54** (2013) 1123.

7. D. Alesini, M. Alessandroni, M. P. Anania, S. Andreas, M. Angelone, A. Arcovito, F. Arnesano and M. Artioli *et al.*, IRIDE White Book, An Interdisciplinary Research Infrastructure based on Dual Electron linacs and lasers, arXiv:1307.7967 [physics.ins-det].

8. V. V. Barmin *et al.* [DIANA Collaboration], Observation of a narrow baryon resonance with positive strangeness formed in K^+Xe collisions, arXiv:1307.1653 [nucl-ex].

9. M. Bazzi *et al.* [SIDDHARTA Collaboration], X-ray transition yields of low-Z kaonic atoms produced in Kapton, Nucl. Phys. A **916** (2013) 30

10. K. Piscicchia *et al.* [AMADEUS Collaboration], Low energy kaon-nuclei interaction studies through the $\Sigma^0\pi^0$ channel with the KLOE detector, PoS Bormio **2013** (2013) 034

11. A. Scordo *et al.* [AMADEUS Collaboration], Study of $\Sigma^+\pi^-$ Invariant Mass spectrum with the KLOE detector; preliminary results and possible hints for $\Sigma^+ n$ internal conversion, PoS Bormio **2013** (2013) 011

12. M. Poli Lener, M. Bazzi, G. Corradi, C. Curceanu, A. D'Uffizi, C. Paglia, E. Sbardella and A. Scordo *et al.*, A GEM-based Time Projection Chamber for the AMADEUS experiment, PoS Bormio **2013** (2013) 037

13. K. Piscicchia *et al.* [AMADEUS Collaboration], Kaon-nuclei interaction studies at low energies (the AMADEUS project), Nuovo Cim. C **36** (2013)

14. M. Poli Lener, M. Bazzi, G. Corradi, C. Curceanu, A. D'Uffizi, C. Paglia, A. Romero Vidal and E. Sbardella *et al.*, Performances of a GEM-based Time Projection Chamber prototype for the AMADEUS experiment, arXiv:1302.3054 [physics.ins-det].

15. A. Scordo, M. Bazzi, C. Berucci, C. Curceanu, A. D'Uffizi, K. Piscicchia, M. Poli Lener and A. Romero Vidal *et al.*, Characterization of a scintillating fibers read by MPPC detectors trigger prototype for the AMADEUS experiment, JINST **8** (2013) T05006

16. M. Bazzi *et al.* [SIDDHARTA Collaboration], Preliminary study of kaonic deuterium X-rays by the SIDDHARTA experiment at DAFNE, Nucl. Phys. A **907** (2013) 69

MAMBO

D. Babusci, P. Levi Sandri (R), D. Pietreanu and A. Saputi.

1 Introduction

MAMBO groups together three complementary INFN activities in Germany: the experimental activity with the MAMI-C microtron in Mainz, the development of MRPC counters and the preliminary measurements towards a full proposal to measure the electric dipole moments (EDM) of proton and deuteron, and the new BGO-OD experiment at Bonn-ELSA. LNF are involved in the last two activities.

2 BGO-OD experiment

The BGO-OD esperiment is performed in collaboration between INFN sections of Roma2, LNF, Messina, Pavia, ISS-Roma1 and Torino, the University of Bonn, Physikalisches Institut, ELSA department, the University of Bonn, Helmholtz Institut für Strahlen- und Kernphysik, the University of Edinburgh, the National Science Center Kharkov Institute of Physics and Technology, the University of Moscow, Russia, the Petersburg Nuclear Physics Institute (PNPI), Gatchina and the University of Basel. More that 70 physicists participate to this experimental program foreseen to last until 2017 with possible extention.

The INFN contribution consist in the *Rugby Ball* calorimeter and associated detectors previously used at GRAAL, the target system, the cylindrical tracking chambers and the MRPC detector.

3 Activity in 2013

During the year 2013 the installation of the detector in the S-Beamline at ELSA was continued and the debugging of the experiment was started. The *Rugby Ball* calorimeter was completely installed with its new electronic based on S-ADC's that allows to obtain time information with 3 ns resolution. A good energy resolution was readily obtained in the invariant mass reconstruction (on-line results in Fig. 1).

Also the Barrel was installed and tested. Extra shielding to the residual magnetic field of the dipole is needed for the forward and upper part of the calorimeter. Dedicated simulation were performed an a satisfactory solution was found.

All the forward tracking detectors were installed and tested. Tracks are reconstructed and particles are identified (Fig. 2)

The linear beam polarization was obtained via coherent Bremsstrahlung and measured with the Stonhenge technique.

The experimental program was discussed in the joint ELSA-MAMI Physics Advisory Committee and all the proposals by the collaboration were accepted with good or very good ratings.

The experiment was presented at various international conferences (NSTAR, BARYONS, MENU).

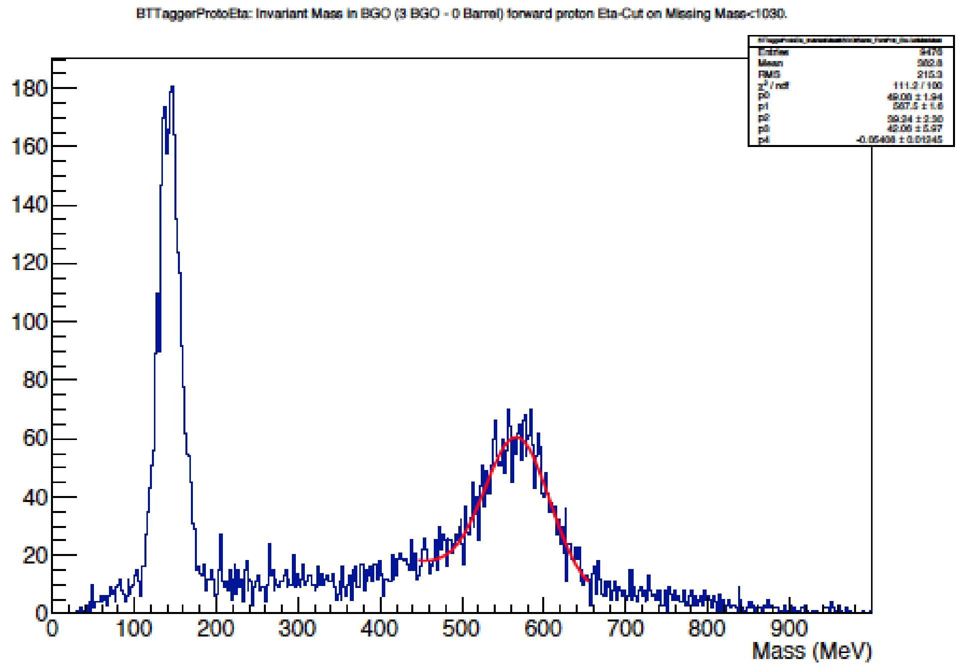

Figure 1: *On-line invariant mass reconstruction of $\gamma\gamma$ events from the Rugby Ball calorimeter.*

4 Planned activity in 2014

Two detectors must be installed to complete the apparatus. The MWPC cylindrical chambers are installed already and the front-end electronics is being connected. The MRPC chambers are being completed and will be installe before summer.

After the completion af the experimental apparatus, tha data taking will start in May 2014, with hydrogen target. Later on, the deuterium target will be installed as well and the experiment will be fully operational. Also a dedicated run with carbon target (η mesic nuclei) will be performed.

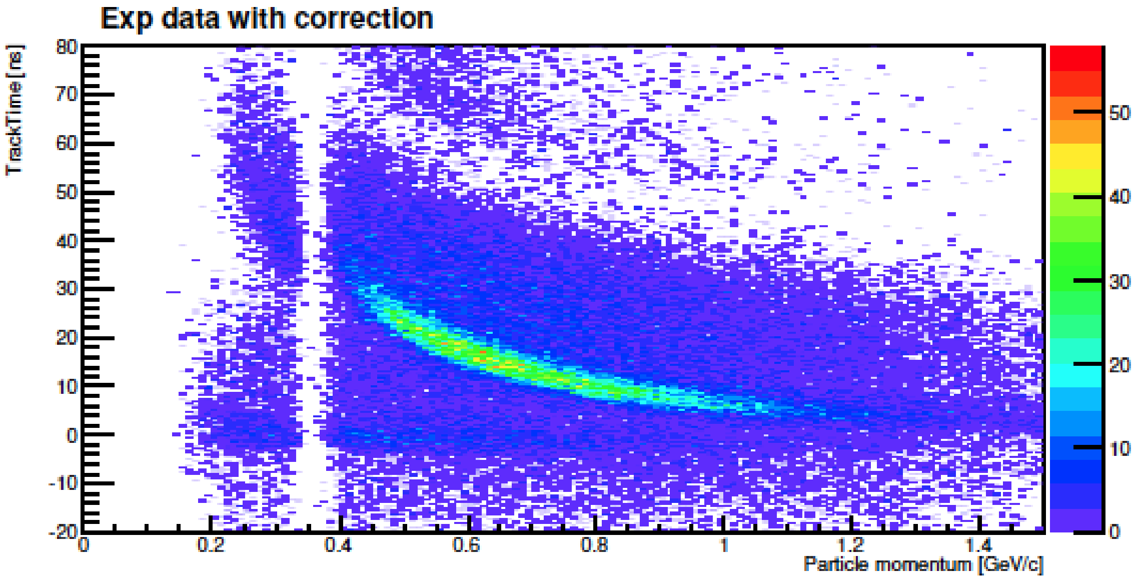

Figure 2: *Reconstructed particle momentum vs. arrival time in the Open Dipole spectrometer.*

$\overline{\text{P}}$ANDA - $\bar{\text{p}}$ Annihilation at Darmstadt

N. Bianchi, A. M. Bragadireanu (Ass.), P. Dorel (Ass.), P. Gianotti (Resp. Naz.),
C. Guaraldo (Ass.), V. Lucherini, E. Pace, D. Orecchini (Tec.).,
L. Passamonti (Tec.), D. Piergluigi (Tec.), A. Russo (Tec.)

1 Introduction

$\overline{\text{P}}$ANDA is one of the biggest experiments of hadron and nuclear physics that will be carried out at the new Facility for Antiproton and Ion Research (FAIR) at Darmstadt, Germany. It is dedicated to the study of the annihilations of antiprotons on nucleons and nuclei up to a maximum center-of-mass energy in $\bar{\text{p}}$p of 5.5 GeV.

The $\overline{\text{P}}$ANDA collaboration consists of more than 500 physicists from 18 countries spread all over the world. The Italian groups involved are: Torino, University, Politecnico and INFN, Trieste, University and INFN, Genova INFN, Pavia, University and INFN, Ferrara, University and INFN, Legnaro INFN laboratory and Frascati INFN laboratory. The LNF group is involved in the design and construction of the central straw tube tracker of the $\overline{\text{P}}$ANDA detector.

2 $\overline{\text{P}}$ANDA experiment

The construction in Germany of the new FAIR accelerator complex started in January 2013. It consists of a major upgrade of the presently running GSI accelerator complex of Darmstadt [1). Figure 1 shows a view of the construction site. The actual schedule of the project foresees the first

Figure 1: *Aerial view of the FAIR construction site.*

beams in year 2019.

An intense, high momentum resolution antiproton beam, with momenta between 1.5 and 15 GeV/c, will be available at the High Energy Storage Ring (HESR), and the experimental activity will be carried out using a general purpose detector $\overline{\text{P}}$ANDA that will be build surrounding an internal target station installed in one of the two straight sections of the storage ring. Figure 2 shows a schematic drawing of the $\overline{\text{P}}$ANDA apparatus. It is designed as a large acceptance multi-purpose detector consisting of two distinct parts: a solenoidal spectrometer, surrounding the interaction target region, and a forward spectrometer to cover the solid angle between 5 and

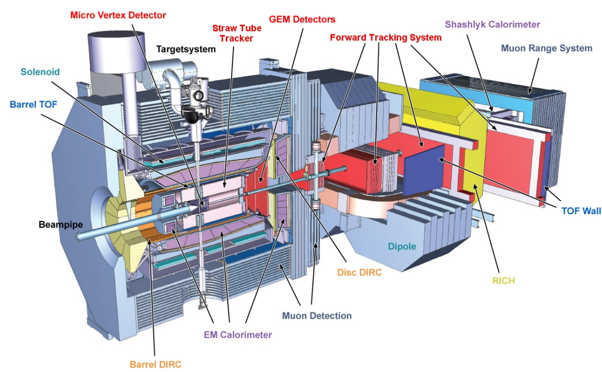

Figure 2: *A schematic view of the $\overline{\rm P}$ANDA apparatus.*

22 degrees. It will allow the detection and the identification of either the neutral and the charge particles emitted following $\bar{p}$ annihilation.

3 The $\overline{\rm P}$ANDA Central Tracker

For tracking charge particles in the target spectrometer, $\overline{\rm P}$ANDA will use different detectors: a silicon Micro Vertex Detector (MVD) a Straw Tube Tracker (STT) and a set of forward GEM chambers [3]. Figure 3 shows the layout of the Target Spectrometer tracking system.

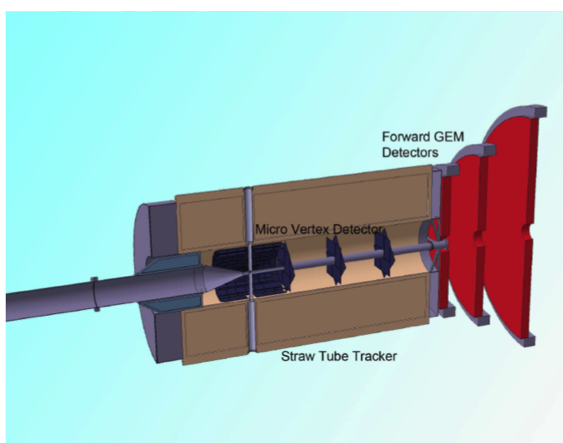

Figure 3: *The $\overline{\rm P}$ANDA tracking system of the Target Spectrometer. It consists of three detectors: Micro Vertex Detector, Straw Tube Tracker, Forward GEM.*

The requirements for this system are:

- almost full solid angle coverage;
- momentum resolution $\delta p/p \sim 1.5\%$;

- low material budget $X/X_0 \sim$ few %;
- good spatial resolution $\sigma_{r,\phi} = 150$, μm, $\sigma_z =$ few mm.

The Technical Design Report (TDR) of the STT has been completed in April 2012 and it has been positively evaluated by the FAIR technical committee (ECE).

The LNF $\overline{\mathrm{P}}$ANDA group is deeply involved in the STT realization and has the responsibility of the mechanics of the whole tracking system.

3.1 Layout of the straw tube detector

The $\overline{\mathrm{P}}$ANDA STT will consist of two identical chambers separated by the beam-target cross-pipe that is cutting the x, y plane in two halves (see fig. 4). Each chamber is made of aluminized mylar straw tubes, diameter 10 mm, length 1500 mm, thickness 30 μm, arranged in planar double layers.

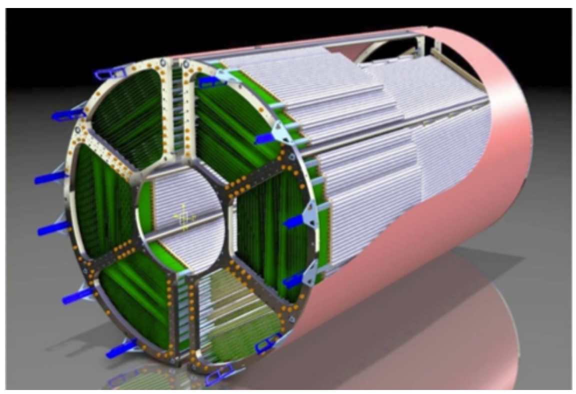

Figure 4: *CAD drawing of the $\overline{\mathrm{P}}$ANDA Straw Tube Tracker*

Inside a double layer the tubes are glued together and operated with an Ar+CO_2 (90+10) gas mixture with an over-pressure of 1 bar. This solution has been chosen to avoid strong support structures and to keep the detector design modular and simple. To measure also particle z coordinate, some layers will be mounted with a skew angle $\pm 3^o$ with respect to the beam axis.

4 Activity of the LNF $\overline{\mathrm{P}}$ANDA group

The STT mechanical structure has to support also the beam-target cross-pipe and the MVD. This frame, has to be extremely light and has to allow the movements of the whole block of detectors during the installation procedure or the maintenance operations.

Figure 5 shows the prototype of the mechanical structure of the whole $\overline{\mathrm{P}}$ANDA Central Tracking (CT). It has been designed by LNF SPAS and realised with the cooperation of the Torino INFN mechanical workshop.

The activity of the LNF $\overline{\mathrm{P}}$ANDA group during 2013 has been devoted to the following tasks:

- test of straw tubes prototypes in oder to determine the detector performances;
- development, together with the Torino INFN group, of the mechanical structure for the CT;

Figure 5: *The prototype of the Central Tracker mechanics hold by the insertion support system.*

Concerning the first item, LNF $\overline{\rm P}$ANDA group has collected data with radioactive sources, cosmic rays and has participated to test beam measurements at the Jülich Forschungscentrum.

Since the TDR of the STT has been approved, we can consider almost completed the R&D phase for this system. At present, the tracking group is defining the protocols for the straw tube construction and the module's assembly. Quality tests and quality assurance procedures are being defined in order to start soon the mass production that will be the main activity during 2014.

5 List of Conference Talks presented by LNF group members in Year 2013

1. P. Gianotti, "Future plans an perspectives for hadronic physics at the INFN Frascati National Laboratory", invited talk at the *Excited QCD 2013 Conference*, Bjelasnica Mountain, Sarajevo, Bosnia-Herzegovina, 3-9 February, 2013.

2. P. Gianotti, "$\overline{\rm P}$ANDA: Hadron Physics with antiprotons", invited talk at the *International SFAIR and Swedish Nuclear Physicists Meeting*, Stockholm, Sweeden, 4-6 November, 2013.

6 Publications

1. P. Gianotti, A. Kashchuk, O. Levitskaya, L. Passamonti, D. Pierluigi, A. Russo, M.Savriè, "Measurement of the absolute gas gain and gain variations study in straw-tube detectors", JINST 8 (2013) T08001.

2. P. Gianotti *et al.* , "The Straw Tube Trackers of the PANDA Experiment", IEEE Xplore publication 2013.

3. W. Erni *et al.* ,"Technical design report for the PANDA (AntiProton Annihilations at Darmstadt) Straw Tube Tracker ", Eur. Phys. J. A49 (2013) 25.

References

1. http://www.fair-center.com/.

2. http://www-panda.gsi.de/.

3. W. Erni *et al.*, Eur. Phys. J. A49 (2013) 25.

VIP

S. Bartalucci, M. Bazzi (Art. 23), A. Clozza, C. Curceanu (Resp. Naz.),
C. Guaraldo, M. Iliescu (Art. 23), F. Lucibello (Tecn.), S. Okada (Art. 23),
D. Pietreanu (Bors. UE), K. Piscicchia (Ass.), A. Scordo (Ass. Ric), H. Shi (Ric. Str.),
D. Sirghi (Art. 23), F. Sirghi (Bors. UE), L. Sperandio (Ass.), O. Vazquez Doce (Bors. UE)

1 The VIP scientific case and the experimental method

The Pauli Exclusion Principle (PEP) plays a fundamental role in our understanding of many physical and chemical phenomena, from the periodic table of elements, to the electric conductivity in metals and to the degeneracy pressure which makes white dwarfs and neutron stars stable and is a consequence of the spin-statistics connection. Although the principle has been spectacularly confirmed by the huge number and accuracy of its predictions, its foundation lies deep in the structure of quantum field theory and has defied all attempts to produce a simple proof. Given its basic standing in quantum theory, it seems appropriate to carry out precise tests of the PEP validity and, indeed, mainly in the last 20 years, several experiments have been performed to search for possible small violations. Many (if not all) of these experiments are using methods which are not obeying to the so-called Messiah-Greenberg superselection rule. The indistinguishability and the symmetrization (or antisymmetrization) of the wave-function should be checked independently for each particle, and accurate tests were and are being done.

The VIP (VIolation of the Pauli Exclusion Principle) experiment, an international Collaboration among 6 Institutions of 7 countries, has the goal to improve the limit on the probability of the violation of the PEP for electrons, (P $< 1.7 \times 10^{-26}$ established by E. Ramberg e G. A. Snow: *Experimental limit on a small violation of the Pauli principle*, Phys. Lett. **B 238** (1990) 438) by three-four orders of magnitude (P $<10^{-29 \div -30}$), exploring a region where new theories could allow for a possible PEP violation.

The experimental method consists in the introduction of electrons into a copper strip, by circulating a current, and in the search for X-rays resulting from the forbidden radiative transition that occurs if one of the new electrons is captured by a copper atom and cascades down to the 1s state already filled by two electrons with opposite spins. The energy of this transition would differ from the normal K_α transition by about 300 eV (7.729 keV instead of 8.040 keV) providing an unambiguous signal of the PEP violation. The measurement alternates periods without current in the copper strip, in order to evaluate the X-ray background in conditions where no PEP violating transitions are expected to occur, with periods in which current flows in the conductor, thus providing "fresh" electrons, which might violate PEP. The rather straightforward analysis consists in the evaluation of the statistical significance of the normalized subtraction of the two spectra in the region of interest.

The experiment is being performed at the LNGS underground Laboratories, where the X-ray background, generated by cosmic rays, is reduced.

2 The VIP experimental setups

The first VIP setup was realized in 2005, starting from the DEAR setup, reutilizing the CCD (Charge Coupled Devices) as X-ray detectors, and consisted of a copper cylinder, 4.5 cm in radius, 50 μm thick, 8.8 cm high, surrounded by 16 equally spaced CCDs of type 55.

The CCDs were at a distance of 2.3 cm from the copper cylinder, grouped in units of two chips vertically positioned. The setup was enclosed in a vacuum chamber, and the CCDs cooled to about 165 K by the use of a cryogenic system. The setup was surrounded by layers of copper

Figure 1: The VIP setup at the LNGS laboratory during installation.

and lead (as seen in the picture) to shield the setup against the residual background present inside the LNGS laboratory, see Fig. 1.

The DAQ alternated periods in which a 40 A current was circulated inside the copper target with periods without current, referred as background.

VIP was installed at the LNGS Laboratory in Spring 2006 and was taking data in this configuration until Summer 2010. In 2011 we started to work on a new version of the setup in order to gain a factor 100 in the probability of violation.

3 Activities in 2013

3.1 Present VIP limit on PEP violation

Until summer 2010 the VIP experiment was in data taking, alternating periods of "signal" (I=40 A) with periods without signal (I=0 A). Data analyses were performed (energy calibration, sum of spectra, subtraction of background) and the probability of violation of PEP for electrons obtained after a new refined analysis in 2013 is:

$$\frac{\beta^2}{2} < 2.8 \times 10^{-29} \tag{1}$$

We are attempting an interpretation of our results in the framework of quon-theory, which turned out to be a consistent theory of *small* violations of PEP. The basic idea of quon theory is that (anti)commutators, are replaced by weighted sums

$$\frac{1-q}{2}\left[a_i, a_j^+\right]_+ + \frac{1+q}{2}\left[a_i, a_j^+\right]_- = a_i a_j^+ - q a_j^+ a_i = \delta_{i,j} \tag{2}$$

where $q = -1$ ($q = 1$) gives back the usual fermion (boson) commutators. The statistical mixture in equation (2) also shows that the PEP violation probability is just $(1 + q)/2$ and thus our best experimental bound on q is

$$\frac{1+q}{2} < 2.8 \times 10^{-29} \tag{3}$$

3.2 VIP2 - a new high sensitivity experiment

In order to achieve the signal/background increase which will allow a gain of two orders of magnitude for the probability of PEP violation for electrons, we built a new setup with a new target, a new cryogenic system and using new detectors with timing capability and an active veto system. As x-ray detectors we use SDDs which were employed in the SIDDHARTA experiment on kaonic atoms at the DAΦNE electron-positron collider of Laboratori Nazionali di Frascati. SDDs have an even better energy resolution than CCDs but additionally provide timing capability which allow to use anti-coincidence operation with scintillators and therefore active shielding. The VIP2 system will provide:

1. signal increase with a more compact system with higher acceptance and higher current flow in the new copper strip target;

2. background reduction by decreasing the x-ray detector surface, more compact shielding (active veto system and passive), nitrogen filled box for radon radiation reduction.

In the table 1 the numerical values for the improvements in VIP2 are given which will lead to an expected overall improvement of a factor higher than ~120.

Figures 2 shows the main elements for the proposed setup in the VIP2 experiment. The copper strip target is 30 mm long, 10 mm wide and is about 40μm thick, and is installed in the center of the setup. The copper strip is cooled at ~90K by the use of an external cryogenic system using liquid argon as the cooling medium. The current connection lines made of copper wires with a cross-section area of 1.5 cm^2, allow a current flow of (at least) 100 A.

The current lines exhibit a temperature gradient from inside the vacuum chamber to the outside connectors of about 180 K. Monte Carlo simulations were performed to study the effect of the active shielding in various configurations of the setup and models of the background radiation. The background profiles measured at LNGS were used as input parameters in the simulations. As the veto counters, 2 pieces of 10 cm thick plastic scintillators are found to be optimal. During 2013 the setup was assembled and tested at LNF-INFN.

4 Activities in 2014

In 2014 we plan to finalize the tests of the VIP upgraded setup at LNF-INFN and transport, install, debug and test it at LNGS and start the data taking. We are, as well, considering to extend the scientific program towards a feasibility study of limits on parameters of the collapse model (as a solution of the measurement problem, put initially forward by Ghirardi, Rimini and Weber) by measurements of X rays spontaneously emitted in the continuous spontaneous localization (CSL) model.

Acknowledgements

The VIP Collaboration wishes to thank all the LNGS laboratory staff for the precious help and assistance during all phases of preparation, installation and data taking. The support from Museo Storico della Fisica e Centro Studi e Ricerche Enrico Fermi, Roma, the HadronPhysics

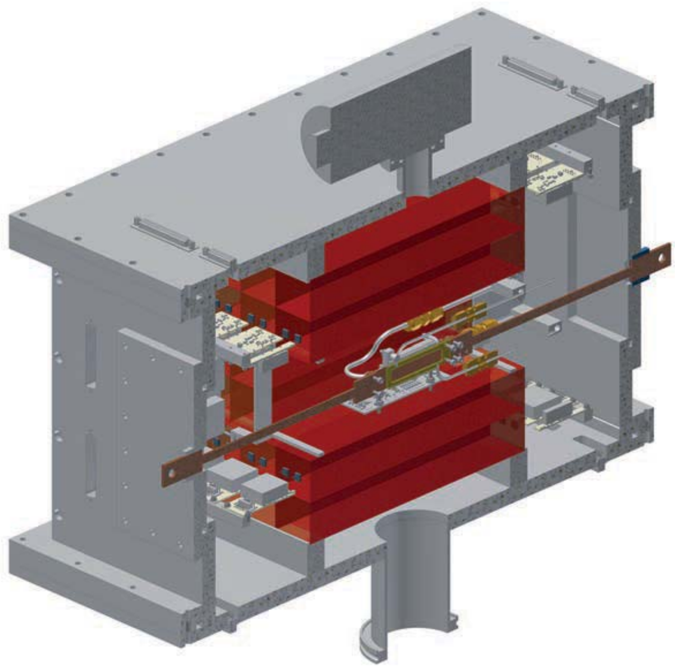

Figure 2: An artist view of the VIP2 experimental setup. In the middle the copper target and the x-ray detectors are installed. Plastic scintillators with solid state photodetector readout acting as active shielding are surrounding the inner part.

Table 1: List of numerical values of the changes in VIP2 in comparison to the VIP features (given in the brackets)

Changes in VIP2	value VIP2(VIP)	expected gain
acceptance	12%	12
increase current	100A (50A)	2
reduced length	3 cm (8.8 cm)	1/3
total linear factor		8
energy resolution	170 eV(340 eV)	4
reduced active area	6 cm^2(114 cm^2)	20
better shielding and veto		5-10
higher SDD efficiency		1/2
background reduction		200-400
overall implementation		$\sim$120

FP6, HadronPhysics2 and HadronPhysics3 FP7 and from the EU COST 1006 Action projects is acknowledged.

5 Publicationsin 2013

1. C. Curceanu (Petrascu) *et al.* Evaluation of the X-ray transition energies for the Pauli-Principle-violating atomic transitions in several elements by using the Dirac-Fock method, LNF preprint, INFN-13-21/LNF, 21-11-2013.

2. S. Di Matteo, L. Sperandio *et al.* Evaluation of the anomalous X-ray energy in VIP experiment: some values from Dirac-Fock method, LNF preprint, INFN-13-20/LNF, 21-11-2013.

3. S. Di Matteo, L. Sperandio *et al.* Evaluation of the Anomalous X-ray energy in VIP Experiment, LNF preprint, INFN-13-19/LNF, 21-11-2013.

4. S. Donadi, A. Bassi, L. Ferialdi and C. Curceanu, The Effect of Spontaneous Collapses on Neutrino Oscillations, Found. Phys. **43**, (2013) 1066.

5. M. Bahrami, S. Donadi, L. Ferialdi, A. Bassi, C. Curceanu, A. Di Domenico and B. C. Hiesmayr, Are collapse models testable with quantum oscillating systems? The case of neutrinos, kaons, chiral molecules, Sci. Rep. **3**, (2013) 1953.

6. J. Marton, S. Bartalucci, S. Bertolucci, C. Berucci, M. Bragadireanu,M. Cargnelli, C. Curceanu (Petrascu) and S. Di Matteo *et al.* Testing the Pauli Exclusion Principle for Electrons, J. Phys. Conf. Ser. **447** (2013) 012070

7. S. Donadi, A. Bassi, C. Curceanu, A. Di Domenico and B. C. Hiesmayr, Are Collapse Models Testable via Flavor Oscillations?, Found. Phys. **43** (2013) 813.

FA51: Fisica Astroparticellare

C. S. Fong (Bors.), A. Meroni (Ass.), E. Nardi (Resp.), E. Peinado (Bors.)

Description of the main scientific achievements during the year 2013.

i. We consider a major achievement of a line of researches that we started a couple of years ago, the paper ref. [1], in which we prove that the complete pattern of quark Yukawa couplings (quark masses, CKM mixing angles, and the CKM CP violating phase) can be obtained as a consequence breaking spontaneously the $SU(3)^3$ quark-flavour symmetry. A further interesting idea was put forth in ref. [2], that is that spontaneous flavour symmetry breaking could automatically avoid the strong CP problem. In spite of the fact that we have later found a subtle reason why the mechanism proposed in ref. [2] does not imply the vanishing of the QCD CP violating θ angle, there are good reasons to believe that the initial idea might still be correct. Ongoing studies in this direction seem to indicate that spontaneous flavour symmetry breaking can indeed have something to do with the fact that, as is experimentally observed, strong interactions do not violate CP.

ii. The general theory of leptogenesis, with special attention to its most striking phenomenological consequences, and including all the most recent refinements, was one of the main research topic of the group during the past few years. During 2013 we have focussed in particular on new mechanisms for low scale leptogenesis. In some cases the theoretical realizations that we have put forth imply the possibility of detecting direct signatures in collider experiments refs. [3,4].

References

1. **"Quark masses, mixings, and CP violation from spontaneous breaking of flavor $SU(3)^3$,"**
   C. S. Fong and E. Nardi,
   Phys. Rev. D **89**, 036008 (2014), [arXiv:1307.4412 [hep-ph]].

2. **"Spontaneous breaking of the flavor symmetry avoids the strong CP problem,"**
   C. S. Fong and E. Nardi,
   Phys. Rev. Lett. **111**, 061601 (2013), [arXiv:1305.1627 [hep-ph]].

3. **"New ways to TeV scale leptogenesis,"**
   C. S. Fong, M. C. Gonzalez-Garcia, E. Nardi and E. Peinado,
   JHEP **1308**, 104 (2013), [arXiv:1305.6312 [hep-ph]].

4. **"Cloistered Baryogenesis,"**
   D. Aristizabal Sierra, C. S. Fong, E. Nardi and E. Peinado,
   JCAP **1402**, 013 (2014), [arXiv:1309.4770 [hep-ph]].

LF21: PHENOMENOLOGY OF ELEMENTARY PARTICLE INTERACTIONS AT COLLIDERS

G. Corcella, V. Del Duca, G. Isidori (Resp.), G. Pancheri (Ass. senior)

The research topics investigated within this project can be divided into two main areas:

- Flavour physics, precision tests and physics beyond the Standard Model (G. Isidori);
- Theoretical and phenomenological aspects of QCD and collider phyiscs (G. Corcella, V. Del Duca, G. Pancheri).

Some of the most significant projects (and corresponding publications) completed in 2013 in these two research areas are listed below.

I. *Flavour physics, precision tests, and physics beyond the Standard Model*

1. *Neutrino Mixing and Masses from a Minimum Principle*,
   by R. Alonso, M. B. Gavela, G. Isidori and L. Maiani, JHEP **1311** (2013) 187 [arXiv:1306.5927].

2. *Higgs form factors in Associated Production*,
   by G. Isidori and M. Trott, JHEP **1402** (2014) 082 [arXiv:1307.405].

3. *Probing the nature of the Higgs-like Boson via $h \to V\mathcal{F}$ decays*,
   by G. Isidori, A. V. Manohar and M. Trott, Phys. Lett. B **728** (2014) 131 [arXiv:1305.0663].

4. *BR($B_s \to \mu^+\mu^-$) as an electroweak precision test*,
   by D. Guadagnoli and G. Isidori, Phys. Lett. B **724** (2013) [arXiv:1302.3909].

II. *Theoretical and phenomenological aspects of QCD and collider phyiscs*

1. *The BFKL equation, Mueller-Navelet jets and single-valued harmonic polylogarithms*,
   by V. Del Duca, L. J. Dixon, C. Duhr and J. Pennington, JHEP **1402** (2014) 086 [arXiv:1309.6647].

2. *Integration of collinear-type doubly unresolved counterterms in NNLO jet cross sections*,
   by V. Del Duca, G. Somogyi and Z. Trocsanyi, JHEP **1306** (2013) 079 [arXiv:1301.3504].

3. *Elastic pp scattering from the optical point to past the dip: an empirical parametrization from ISR to LHC*,
   by D. A. Fagundes, A. Grau, S. Pacetti, G. Pancheri and Y. N. Srivastava, Phys. Rev. D **88** (2013) 094019 [arXiv:1306.0452].

LF61: Low-dimensional strongly correlated electron systems, spin-Hall effect and nanoscale science and technology

S. Bellucci (Resp. Naz.), M. Benfatto, S.Bistarelli (Laur.), A. Cataldo (Bors.), M. Cini (Ass.), G. Giannini (Osp.), K. Hatada (Borsista PD), K. Hayakawa (Borsista PD), F. Micciulla (Osp.), C. Natoli (Ass.), F. Palumbo (Ass.), G. Stefanucci (Ass.), B.N. Tiwari (bors.)

External collaborating Institutions:

IHEP-Protvino, Russia
Belarus State Univ. Minsk,
Department of Physics, Yerevan State University, Armenia
Department of Physics, Univ. Roma Tor Vergata, Italy
Institute of Solid State Physics, University of Latvia, Kengaraga Str. 8, 1063 Riga, Latvia
Instituto de Ciencia de Materiales de Aragon, CSIC-Universidad de Zaragoza, 50009 Zaragoza, Spain.
ICB, UMR 5209 Universite' de Bourgogne - CNRS, BP 47870, F-21078 Dijon, France
Institut de Physique de Rennes, UMR UR1-CNRS 6251, Campus de Beaulieu, Universite' de Rennes, 35042 Rennes-cedex, France

Research Activity

Our theoretical study in collaboration focused on:

- Electron spectroscopy of magnetic systems,
- The fundamental properties of carbon nanotbes and graphene interconnects
- Energy functional of ensemble density functional theory (DFT) in systems with attractive interactions
- Scissors modes in crystals.
- Multiple scattering expansions.
- Magnetic properties of quantum rings

List of Conference Talks

M. Cini, Magnetic moments, pumping and spin polarization in ballistic nanoscopic circuits, International workshop on Nanoscience and nanotechnology 2013, Laboratori Nazionali di Frascati, 30 September-4 October 2013

S. Bistarelli et al., AFM characterization and cytotoxic effects induced by multiwalled carbon nanotubes on human breast adenocarcinoma cell line, International workshop on Nanoscience and nanotechnology 2013, Laboratori Nazionali di Frascati, 30 September-4 October 2013.

S. Bellucci, “Electromagnetic properties of epoxy nanocomposites”, Nanoscience & Nanotechnology 2013, Laboratori Nazionali di Frascati, 30 September-4 October 2013.

Publications by LNF Authors in the Year 2013

[1] Correlation functions in one-dimensional spin lattices with Ising and Heisenberg bonds
S Bellucci, V Ohanyan, The European Physical Journal B 86 (11), 1-12
[2] Magnetic moments, pumping and spin polarization in ballistic nanoscopic circuits, Cini M and Bellucci S, ICEAA: 2013 Int. Conf. on Electromagnetics in Advanced Applications (Torino, Italy, Sept. 2013) pp 699–702 Print ISBN: 9781467357050, doi:10.1109/ICEAA.2013.6632335
[3] Pumping through a Luttinger liquid ring threaded by a time-varying magnetic field, Perfetto E, Cini M and Bellucci S 2013 Phys. Rev. B 87 035412
[4] Formation of linear Ni nanochains inside carbon nanotubes: Prediction from density functional theory, J Kazerovskis, S Piskunov, YF Zhukovskii, PN D'yachkov, S Bellucci, Chemical Physics Letters 577, 92-95
[5] A new target design for laser shock-compression studies of carbon reflectivity in the megabar regime, S Paleari, et al., The European Physical Journal D 67 (7), 1-8
[6] In Vivo Targeting of Intratumor Regulatory T Cells Using PEG-Modified Single-Walled Carbon Nanotubes, C Sacchetti, et al., Bioconjugate chemistry 24 (6), 852-858
[7] Electromagnetic Properties of CNTs and GNRs Based Nanostructures for Nanosensor Systems
Yu N Shunin, VI Gopeyenko, N Yu Burlutskaya, TD Lobanova-Shunina, S Bellucci, Physics, Chemistry and Applications of Nanostructures-Proceedings of the International Conference Nanomeeting-2013. Edited by Borisenko Victor E et al. Published by World Scientific Publishing Co. Pte. Ltd., 2013. ISBN# 9789814460187, pp. 250-253
[8] Incorporation of Ni Nanofilament Inside Carbon Nanotubes:. DFT Calculations, S Piskunov, J Kazerovskis, Yu F Zhukovskii, PN D'Yachkov, S Bellucci, Physics, Chemistry and Applications of Nanostructures-Proceedings of the International Conference Nanomeeting-2013. Edited by Borisenko Victor E et al. Published by World Scientific Publishing Co. Pte. Ltd., 2013. ISBN# 9789814460187, pp. 139-142
[9] Intrinsic geometric analysis of the network reliability and voltage stability, N Gupta, BN Tiwari, S Bellucci, International Journal of Electrical Power & Energy Systems 44 (1), 872-879.
[10 Fermionic current from topology and boundaries with applications to higher-dimensional models and nanophysics, S Bellucci, AA Saharian, Physical Review D 87 (2), 025005
[11] Multi-walled Carbon Nanotubes/Unsaturated Polyester Composites: Mechanical and Thermal Properties Study, MSI Makki, MY Abdelaal, S Bellucci, MA Salam, Fullerenes, Nanotubes and Carbon Nanostructures
[12] Improved understanding of self-sustained, sub-micrometric multi-composition surface Constantan wires interacting with H2 at high temperatures: experimental evidence of Anomalous Heat Effects
F Celani, et al., Chemistry and Materials Research 3 (12), 21-32
[13] Deflection of 100 MeV positron beam by repeated reflections in thin crystals
S Bellucci, YA Chesnokov, PN Chirkov, M Cosic, G Giannini, VA Maisheev, S Petrovic, IA Yazynin, JETP Lett. 98 (11-12), 739
[14] Experimental Results on Sub-Micro Structured Cu-Ni Alloys under High Temperature Hydrogen/Deuterium Interaction, F Celani, et al., Chemistry and Materials Research 3 (3), 27-56
[15] Geometrical Methods for Power Network Analysis, S Bellucci, BN Tiwari, N Gupta, SpringerBriefs in Electrical and Computer Engineering ISBN: 978-3-642-33343-9 (Print) 978-3-642-33344-6 (Online).
[16] Image charge effects in the nonequilibrium Anderson-Holstein model, E Perfetto, G Stefanucci Physical Review B 88 (24), 245437
[17] Kondo effect in the Kohn–Sham conductance of multiple-level quantum dots, G Stefanucci, S

Kurth, physica status solidi (b) 250 (11), 2378-2385
[18] Dynamical correction to linear Kohn-Sham conductances from static density functional theory S Kurth, G Stefanucci, Physical Review Letters 111 (3), 030601
[19] Equilibrium and nonequilibrium many-body perturbation theory: a unified framework based on the Martin-Schwinger hierarchy, R van Leeuwen, G Stefanucci, Journal of Physics: Conference Series 427 (1), 012001
[20] Time-dependent Landauer–Büttiker formula for transient dynamics, R Tuovinen, R van Leeuwen, E Perfetto, G Stefanucci, Journal of Physics: Conference Series 427 (1), 012014
[21] Nonequilibrium Many-Body Theory of Quantum Systems: A Modern Introduction, G Stefanucci, R van Leeuwen, Cambridge University Press
[22] Monitoring antiferromagnetism via angle-resolved Auger photoelectron coincidence spectroscopy: The case of NiO/Ag (001), R Gotter, et al., Physical Review B 88 (9), 094403
[23] Theory of the APECS spectra of antiferromagnetic transition metal oxides, M Cini, E Perfetto Journal of Electron Spectroscopy and Related Phenomena 189, 61-64
[24] Dynamical Formation and Manipulation of Majorana Fermions in Driven Quantum Wires in Contact with a Superconductor, E Perfetto, Physical review letters 110 (8), 087001
[25] Origin of incommensurate satellite reflections on TbMnO3 by resonant x-ray scattering, V. Cuartero, J. García, G. Subías, J. Herrero-Martín, J. Blasco, C. R. Natoli, Journal of Physics Conference Series 04/2013; 430(1):2101
[26] X-ray absorption spectroscopic investigation of the electronic structure differences in solution and crystalline oxyhemoglobin, Samuel A. Wilson et al., Proceedings of the National Academy of Sciences of the United States of America, PNAS, vol. 110 no. 41, 16333–16338, doi: 10.1073/pnas.1315734110
[27] IRIDE: Interdisciplinary research infrastructure based on dual electron linacs and lasers, M.Ferrario et al., Nuclear Instruments and Methods in Physics Research Section A: Accelerators, Spectrometers, Detectors and Associated Equipment, Volume 740, 11 March 2014, Pages 138–146
[28] Graphene-based wireless communications systems: Analysis of the EM-quantum transport of coupled nano-patch antennas, Pierantoni L., Mencarelli D., Coccetti F., Wireless Power Transfer (WPT 2013) IEEE, 15-16 May 2013, Perugia (Italy), Page(s): 66 – 68, Print ISBN: 978--14673-5008-2
[29] Advanced modeling of graphene nanodevices: Metal-carbon transition and patch antennas, Pierantoni L., Mencarelli D., Coccetti F., Antennas and Propagation (EuCAP), 2013 7th European Conference on, 8-12 April 2013, Gothenburg, Page(s): 712 – 715, E-ISBN : 978-88-907018-1-8, Print ISBN: 978-1-4673-2187-7
[30] Design of a coplanar graphene-based nano-patch antenna for microwave application, Mencarelli, D et al., Microwave Symposium Digest (IMS), 2013 IEEE MTT-S International, 2-7 June 2013, Page(s): 1 – 4, Seattle, WA, ISSN : 0149-645X, Print ISBN: 978-1-4673-6177-4, Digital Object Identifier : 10.1109/MWSYM.2013.6697800
[31] Scissors modes: The elusive breathing overtone, Keisuke Hatada, Kuniko Hayakawa, and Fabrizio Palumbo, Phys. Rev. C 88, 014305

MI12: Gauge and String Theories

S. Bellucci (Resp.), S. Ferrara (Ass.), S. Krivonos (Osp.), A. Sutulin (Bors. PD), B.N. Tiwari (Bors. PD), V. Yeghikyan (Bors. PD), A. Yeranyan (Bors. Fermi Institute)

Research Activity

Our main topic is supergravity, a concept that connects different fields of investigation - from physics to mathematics - and has enriched them with a lot of elegant ideas. Chronologically, supergravity was found to be a part of another impressive theory- superstring theory. Superstring theory is known to introduce a series of stunning concepts which, being discovered directly or indirectly at LHC, will make a real revolution in our world-view. Being born exclusively as a physical theory, it incredibly enriched as well modern mathematics - be it algebra or geometry- and even gave rise to new trends. On the other hand, the well established theories, such as quantum field theory, possess a lot of powerful techniques, such as those of statistical physics. In this way supergravity theory obtained considerable input from both superstring and quantum field theory. This fact allowed us to investigate of the properties of fundamental objects of supergravity - black holes. One of the main characteristic of black holes – entropy can be calculated using statistical physics methods to count black hole states along with a purely algebraic construction - Calabi-Yau manifold. The concept of entropy is quite interdisciplinary and, as well as a (super)symmetry, takes one of the principal places in the research.
The black holes are important tools for testing high energy theories and our research refers to construction and investigation of equations and solutions for black holes in supergravity and superstring theories.
The problems posed in this project are a natural continuation of our previous results obtained in recent years also within the framework of the ERC grant "SUPERFIELDS"(N.226455, 2009-2014) and in collaboration with groups from Torino University, Padua University, JINR-Dubna, Yerevan State University and CERN.

List of Conference Talks

S. Bellucci, On the road to N=2 supersymmetric Born-Infeld theory, Workshop on Breaking of supersymmetry and Ultraviolet Divergences in extended Supergravity (BUDS 2013), INFN-LNF March 25-28, 2013

S. Ferrara, Duality, Ehlers and form cosets, Workshop on Breaking of supersymmetry and Ultraviolet Divergences in extended Supergravity (BUDS 2013), INFN-LNF March 25-28, 2013

S. Bellucci, Coset approach and partial breaking of global Supersymmetry, Supersymmetry in Integrable Systems - SIS'13 International Workshop, 28-30 December 2013, Hannover, Germany

Publications by LNF Authors in the Year 2013

[1] Supersymmetric component actions via coset approach, S Bellucci, S Krivonos, A Sutulin, Physics Letters B 726 (1), 497-504
[2] Electromagnetic two-point functions and the Casimir effect in Friedmann-Robertson-Walker cosmologies, S Bellucci, AA Saharian, Physical Review D 88 (6), 064034

[3] The Coulomb problem on a 3-sphere and Heun polynomials, S Bellucci, V Yeghikyan, Journal of Mathematical Physics 54 (8), 082103
[4] Scalar and fermionic vacuum currents in de Sitter spacetime with compact dimensions, S Bellucci, AA Saharian, HA Nersisyan, Physical Review D 88 (2), 024028
[5] Symmetries of N= 4 supersymmetric CP(n) mechanics, S Bellucci, N Kozyrev, S Krivonos, A Sutulin, Journal of Physics A: Mathematical and Theoretical 46 (27), 275305
[6] On the road to N= 2 supersymmetric Born–Infeld action, S Bellucci, S Krivonos, A Shcherbakov, A Sutulin, Physics Letters B 721 (4), 353-357
[7] Isospin particle systems on quaternionic projective spaces, S Bellucci, S Krivonos, A Nersessian, V Yeghikyan, Physical Review D 87 (4), 045005
[8] Dual multiplets in N= 4 superconformal mechanics, S Bellucci, S Krivonos, A Sutulin
Journal of Physics A: Mathematical and Theoretical 46 (3), 035401
[9] Black Objects in Supergravity. S Bellucci, Springer Proceedings in Physics (Book 144), ISBN 9783319002149; 9783319002156
[10] Multi-centered first order formalism, Sergio Ferrara, Alessio Marrani, Andrey Shcherbakov and Armen Yeranyan, JHEP05 (2013) 127
[11] Minimal supergravity models of inflation, S Ferrara, R Kallosh, A Linde, M Porrati - Physical Review D, 2013
[12] Higher order corrections in minimal supergravity models of inflation, S Ferrara, R Kallosh, A Linde, M. Porrati - Journal of Cosmology and Astroparticle Physics, 2013
[13] Conjecture on hidden superconformal symmetry of N= 4 supergravity, S Ferrara, R Kallosh, A Van Proeyen - Physical Review D, 2013
[14] Vacuum structure in a chiral R+ Rn modification of pure supergravity, S Ferrara, A Kehagias, M Porrati, Physics Letters B, Volume 727, Issues 1–3, 25 November 2013, Pages 314–318
[15] On the supersymmetric completion of R+ R 2 gravity and cosmology, S Ferrara, R Kallosh, A Van Proeyen, 2013 Journal of High Energy Physics November 2013, 2013:134
[16] Freudenthal dual lagrangians, L Borsten, MJ Duff, S Ferrara, A.Marrani - Classical and Quantum Gravity, 2013

PI11: Quark Gluon Plasma, and strong dynamics Beyond the Standard Model

Maria Paola Lombardo and 2013 Co-authors :

Elisabetta Pallante, Gert Aarts, Kohtaroh Miura, Edwin Laermann, Sinead Ryan, Chris Allton, Tiago Nunes da Silva, Jon-Ivar Skullerud, Michael Mueller-Preussker, Erst-Michael Ilgenfritz, Florian Burger,Seyong Kim, Don Sinclair, Florian Meyer, Owe Philipsen, Carsten Urbach

We have studied the properties of bottomonia state in the Quark Gluon Plasma (QGP) and their suppression pattern and found them to be consistent with the observations of CMS at the LHC. Further we have computed the Equation of State – a fist step towards trasport coefficients – including a new important theoretical ingredient which was previously overlooked and should become important for temperature of about 300 MeV, to be explored in the upcoming LHC runs with heavy ions. Finally we have investigated strongly interactive preconformal dynamics which might help building non-standard models of electroweak symmetry breaking and mass generation (i.e. models alternative to supersymmetry perhaps more familiar to the LNF colleagues) – and we have shown how such exotic dynamics smoothly merges with the Quark Gluon Plasma thus uncovering a perhaps unexpected bridge across different fields.

Publications and Proceedings

1. **"Quark-Gluon Plasma: from lattice simulations to experimental results"**
G. Aarts, C. Allton, A. Kelly, J. -I. Skullerud, S. Kim, T. Harris, S. M. Ryan and M. P. Lombardo.
arXiv:1403.5183 [hep-lat]

2. **"The bottomonium spectrum at finite temperature from $N_f = 2 + 1$ lattice QCD"**
G. Aarts, C. Allton, T. Harris, S. Kim, M. P. Lombardo, S. a. M. Ryan and J. -I. Skullerud.
arXiv:1402.6210 [hep-lat]

3. **"Bottomonium spectrum at finite temperature"**
T. Harris, S. a. M. Ryan, G. Aarts, C. Allton, S. Kim, M. P. Lombardo and J. -I. Skullerud.
arXiv:1311.3208 [hep-lat]

4. **"Towards thermodynamics with $N_f = 2 + 1 + 1$ twisted mass quarks"**
F. Burger, G. Hotzel, M. Mller-Preussker, E. -M. Ilgenfritz and M. P. Lombardo.
arXiv:1311.1631 [hep-lat]

5. **"P wave bottomonium spectral functions in the QGP from lattice NRQCD"**
G. Aarts, C. Allton, S. Kim, M. -P. Lombardo, S. M. Ryan and J. -I. Skullerud.
arXiv:1311.0994 [hep-lat]

6. **"Melting of P wave bottomonium states in the quark-gluon plasma from lattice NRQCD"**
G. Aarts, C. Allton, S. Kim, M. P. Lombardo, S. M. Ryan and J. -I. Skullerud.
arXiv:1310.5467 [hep-lat]
10.1007/JHEP12(2013)064
JHEP **1312**, 064 (2013)

7. **"Quark-gluon plasma phenomenology from the lattice"**
C. Allton, G. Aarts, A. Amato, W. Evans, P. Giudice, S. Hands, A. Kelly and S. Kim *et al.*.
arXiv:1310.5135 [hep-lat]

8. **"Making the most of Taylor expansion and imaginary μ"**
E. Laermann, F. Meyer and M. P. Lombardo.
10.1088/1742-6596/432/1/012016
J. Phys. Conf. Ser. **432**, 012016 (2013).

9. **"Making the most of Taylor expansion and imaginary chemical potential"**
E. Laermann, F. Meyer and M. P. Lombardo.
arXiv:1304.3247 [hep-lat]

10. **"Phases of many flavors QCD : Lattice results"**
A. Deuzeman, M. P. Lombardo, K. Miura, T. Nunes da Silva and E. Pallante.
arXiv:1304.3245 [hep-lat]
PoS ConfinementX , 274 (2012)

11. **"Bottomonium from lattice QCD as a probe of the Quark-Gluon Plasma"**
G. Aarts, C. Allton, A. Kelly, J. I. Skullerud, S. Kim, T. Harris, S. M. Ryan and M. P. Lombardo *et al.*.
arXiv:1212.4368 [hep-lat]
10.1088/1742-6596/432/1/012014
J. Phys. Conf. Ser. **432**, 012014 (2013)

12. **"Lattice Monte-Carlo study of pre-conformal dynamics in strongly flavoured QCD in the light of the chiral phase transition at finite temperature"**
K. Miura and M. P. Lombardo.
arXiv:1212.0955 [hep-lat]
10.1016/j.nuclphysb.2013.02.008
Nuclear Physics B **871**, , pp. 52 (2013), [Nucl. Phys. B **871**, 52 (2013)]

13. **"S wave bottomonium states moving in a quark-gluon plasma from lattice NRQCD"**
G. Aarts, C. Allton, S. Kim, M. P. Lombardo, M. B. Oktay, S. M. Ryan, D. K. Sinclair and J. -I. Skullerud.
arXiv:1210.2903 [hep-lat]
10.1007/JHEP03(2013)084
JHEP **1303**, 084 (2013)

14. **"The bulk transition of QCD with twelve flavors and the role of improvement"**
A. Deuzeman, M. P. Lombardo, T. Nunes Da Silva and E. Pallante.
arXiv:1209.5720 [hep-lat]
10.1016/j.physletb.2013.02.030
Phys. Lett. B **720**, 358 (2013)

15. **"Thermal QCD transition with two flavors of twisted mass fermions"**
F. Burger *et al.* [tmfT Collaboration].
arXiv:1102.4530 [hep-lat]
10.1103/PhysRevD.87.074508
Phys. Rev. D **87**, no. 7, 074508 (2013)

!CHAOS

A. Stecchi (Resp.)

Not received

3L_2D

(Time Resolved e+/e- Light in 2-Dimension)

Alessandro Drago (Nat. Resp.), Augusto Marcelli, Mariangela Cestelli Guidi (art. 23), Emanuele Pace (ass.)

The 3L_2D experiment, funded by the 5-th National Scientific Commission of INFN for the years 2013-2014, is building an innovative 2D diagnostic tool to study bunch-by-bunch transverse instabilities using the mid-infrared light emitted by synchrotron acceleration from bending magnets in DAFNE. Main focus of the experiment is to collect 2D data from bunched positron beams in storage rings to study the beam behavior induced by parasitic e-cloud or by other instabilities, mostly correlated to bunch enlargement effects in the vertical plane.

The 3L_2D experiment is composed by multiple steps: first of all, during the year 2013, design, fabrication and assembly of the detector system has been carried on producing an infrared very compact camera that can acquire analog signals from eight or sixteen pixels with a bandwidth close to 1 GHz. An experimental array detector working in mid-infrared (~10 micron) and fabricated by the VIGO System company is the base of the detector. The array is made by a HgCdTe semiconductor grown on a GaAs substrate and consists of 2x32 pixels operating at room temperature. Each element has a size of ~50x50 micron^2 and a signal rise time <1 ns, so it can monitor each DAFNE bunch (2.7 ns) in longitudinal and in transverse dimensions. The array chip has been assembled in the accelerator division electronics laboratory together with four analog boards designed at LNF. The modules include three stages of amplifiers giving a total of ~52 dB gain for each pixel. Efforts have been dedicated to characterize a detector with the capability to monitor the bunch-by-bunch transverse (mainly vertical) and, at the same time, longitudinal behavior of the e+ beam.

In parallel, a modular digital multichannel data acquisition system has been designed and built: the system, sampling at 368 MHz and based on powerful FPGA's, is able to acquire beam signals by14-bit analog to digital converters and to record bunch-by-bunch and turn-by-turn data for each pixel. A precise timing system, calibrated for each pixel, is necessary to acquire correctly all the beam signals with the goal to extract an image of each bunch. Laboratory tests has shown 2.4 ps r.m.s. jitter for each of LVDS outputs. A final assembly of the digital apparatus is still in progress.

Goal of the experiment is to use the tool for making bunch-by-bunch transverse diagnostics of the e+ and e- DAFNE bunches at IR wavelengths. In the last part of 2013 two analog detectors, both single pixel and multi-pixels, have been tested and used for imaging at SINBAD-IR beam line from the electron DAFNE main ring. Still during the few possible acquisition periods, the signal-to-noise ratio has been too poor and some corrections to the detector have been implemented in the laboratory during the DAFNE winter shutdown. More complete beam data are expected for the 2014 year with the new DAFNE runs. Also the 3+L infrared beam line from a bending magnet of the positron ring has been aligned and tested during the last part of 2013 using the light coming from DAFNE positron beam. Now the system is aligned and ready to take data starting with a single pixel infrared detector.

BEAM4FUSION

F. Murtas (Resp.)

Not received

ETRUSCO-GMES (Activity Report 2013)

Cantone C. (1), Dell'Agnello S. (1), Boni A. (1), Delle Monache G. O. (1), Ciocci E. (1), Contessa S. (1), Lops C. (1), Martini M. (1), Palandra L. (1), Patrizi G. (1), Salvatori L. (1), Tibuzzi M. (1), Vittori R.(3,1), Bianco G. (4), Capotorto G.(1,2), Marra M. (1,2), Piergentili F. (1,2), Maiello M. (1), Porcelli L. (1), Mondaini C. (1), Tuscano P. (1)

(1)Laboratori Nazionali di Frascati (LNF) dell'INFN, Frascati (Rome), Italy
(2)University of Rome "Tor Vergata" , Italy
(3)Aeronautica Militare Italiana (AMI) and Italian Ministry of Foreign Affairs, Embassy of Italy, 300 Whiteheaven St. NW, Washington, DC 20008
(4)ASI, Centro di Geodesia Spaziale "G. Colombo" (CGS), Matera, Italy

1 Introduction

The SCF_Lab is a specialized infrastructure operational at INFN-LNF . It consists of two innovative OGSE (Optical Ground Support Equipment) facilities: SCF and SCF-G, for the SCF-Test. They were developed by INFN-LNF and are in use by NASA, ESA, ASI, ISRO (Indian Space Research Organization) and the Italian Ministry of Defence. They characterize an innovative industrial thermal-optical-vacuum test procedure to characterize and model the detailed thermal behavior and optical performance of cube corner laser retroreflectors (CCRs) for the Satellite Laser Ranging (SLR) to GNSS (Global Navigation Satellite System), i.e. it is composed of specialized instruments capable of measuring and modeling optical Far Field Diffraction Pattern (FFDP), Wavefront Fizeau Interferogram (WFI) and temperature distribution of Laser Retroreflector Arrays (LRAs) of CCRs under space conditions accurately simulated in the laboratory and also produced with close-match solar simulators. LRAs/CCRs are passive, maintenance-free instruments, which provide absolute positioning in space with respect to the Earth center of mass (geocenter), which is metrologically defined with SLR to LAGEOS I and II and to other ILRS reference satellites. SLR, with almost uniquely VLBI (and other geodesy techniques), also defines the absolute scale of length in space because the improvement of GNSS orbits will increase the accuracy, stability, and distribution of the ITRF (International Terrestrial Reference Frame), to provide a better definition of the geocenter (origin) and the scale (length unit). We will describe the SCF_Lab capabilities to design, construct and characterize LRAs for earth observation (EO) satellites and GNSS constellations paying particular attention to the project ETRUSCO-GMES (Extra Terrestrial Ranging to Unified Satellite Constellation-Global Monitoring for Environment & Security) whose main goal is the development and characterization of GNSS Retroreflector Arrays (GRA), targeted to Galileo and GPS-3, but open to other GNSS satellite constellations.

GMES is one of the two European Union flagship programmes in space that will provide data to help deal with a range of disparate issues including climate change and border surveillance. Land, sea and atmosphere - each will be observed through GMES, helping to make our lives safer. The project acronym underlines the importance of the integration (unification) between GNSS (Global Navigation Satellite System) and SLR positioning techniques. This project is aimed at optimizing the space segment and integrating GNSS with SLR geodesy techniques. Furthermore, its primary goal was to design an optimized GRA to propose for the deploying on Galileo and GPS-3 constellations, able to maximize ranging efficiency and improve signal intensity. Other purposes of ETRUSCO-GMES project are:

1. general relativity tests performance
2. space geodesy studies
3. improvement of GNSS orbits accuracy
4. enhancement of stability and distribution of ITFR to provide a more precise definition of its origin and scale.
5. geology

It is important for the development of LRAs with Formation Flying Functionality (LRA-3F) capabilities which is possible thanks to the framework of the R&D activities of the INFN National Scientific Committee n. 5 (INFN-CSN5) and the national contracts with public Entities which even encouraged the development an orbit-realistic SCF-Test for GNSS that we applied to Galileo IOV (In- Orbit Validation).
ETRUSCO-GMES is composed of:

- ETRUSCO-IOV: SCF-Test for Galileo IOV
- ETRUSCO-IRNSS : SCF-Test for 'Indian Galileo' (GNSS)
- G-CALIMES: Unification of Galileo and Italian constellations for radar mapping of Earth surface

In view of the HORIZON 2020 program, GMES has been renamed "Copernicus".

2 SCF_Lab

SCF_Lab (Satellite/lunar/GNSS laser ranging and altimetry Characterization Facility LABoratory) is a new ISO 7 Clean Room of about 85 m2 located inside the Frascati National Laboratories of the INFN. Unique worldwide, it is dedicated to design, characterization and modeling of the space segment of Satellite Laser Ranging (SLR), Lunar Laser Ranging (LLR) and Planetary Laser Ranging and Altimetry (PLRA) for industrial and scientific applications and endorsed by the International Laser Ranging Service (ILRS). Built to develop and characterize laser retroreflector arrays for GNSS, EGNOS-V2 and inter-satellite laser links, by means of specialized thermal-optical-vacuum test procedures and specialized instrumentation, it was originally constructed for the existing SCF (INFN property, Fig. 1, 2 and 3) which is very versatile for its large number of measurement ports (side and back), capability of long LRA horizontal translations and customization for LLR, PLRA and CubeSatsand. Afterwards, on the basis of the experience matured with it, in 2012 we developed a new version of this facility, optimized for Galileo and GPS-3: the SCF-G (Satellite/lunar laser ranging Characterization Facility optimized for Galileo and the GPS-3,property of INFN and of the Italian Space Agency, ASI, Fig. 4), a new cryostat which doubles and optimizes our metrology capabilities for GNSS LRAs. Its structure is innovative respect to SCF because of a back gate and an amplified diameter aperture. The SCF . SCF and SCF-G complement each other.

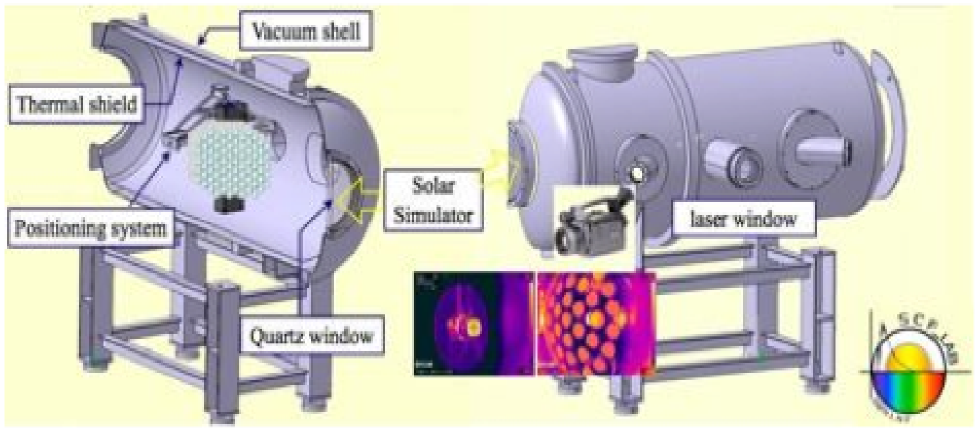

Fig. 2.1: Schematic view of SCF cryostat with: IR pictures of the LAGEOS Sector LRA and of a Galileo IOV CCR under test, IR camera and SCF_Lab logo

The success of doubling the metrology capabilities has been achieved also thanks to the optical instrumentation mounted on the three optical tables (in order to acquire Far Field Diffraction Patterns) and the new Solar Simulator (SS), installed to simulates the solar flux, both the intensity and the spectrum, outside the atmosphere according with the standard AM0 (Air Mass zero). Many solar simulators are usually implied in solar panel testing, it means that the part of the spectrum at short wavelength is the most important, while this solar simulator is customized right for the SCF-Test. In effect, even though the main part of the solar spectrum is made by high energy photons (with short wavelengths), it is the final part of the spectrum (at long wavelengths) that mostly warms up the reflectors when they are exposed to the sun in space or to the simulated solar beam inside the Laboratory. Hence, there is a close correspondence at long wavelengths between the spectrum of the new SS and the standard AM0 spectrum.
In the SCF_Lab we have SCF-Tested CCR of the following satellites: GNSS (GPS, GLONASS, GIOVE, Galileo IOV), LAGEOS, Apollo, new generation lunar and hollow CCRs. We are now testing an LRA of IRNSS (Indian Regional Navigation Satellite System).

3 WORK ACCOMPLISHED WITH ASI- INFN R&D FOR GALILEO AND GPS-3

We describe some key products of the INFN project of technological development ETRUSCO-GMES

- Definition of an improved and enhanced test procedure SCF-Test/Revision-ETRUSCO-GMES: implementation of advanced and innovative operational procedures for the test of the what we call the “GNSS Critical Orbit” (GCO), developed for Galileo IOV

- Full-size prototype GNSS Retroreflector Array (GRA) for Galileo & GPS-3: inherited from LAGEOS, it is composed of 55 CCRs of solid uncoated CCRs. GRA SCF-Test and modeling has been very successful.

- We studied the improved test of the gravitational redshift (GRS) predicted by General Relativity combining Galileo H-maser clocks with SLR stations equipped with H-maser clocks & collocated with respect to the ITRF through SLR & GNSS: the contribution of typical SLR positioning accuracy (cm level) on the GRS error budget is negligible compared to clock instrumental and calibration errors. The latter are the limiting contributions. The capability of performing the absolute calibration of the clock frequency of Galileo satellites is unique to SLR . Thanks to SLR data we evaluated the gravitational potential difference between Galileo and Earth. Supposing fixed the Earth gravitational potential, the GRS variation depends from the Galileo potential variation. Studying the perigee-apogee periodic Galileo potential variation along its orbit, we found that the GRS measurement must be done on orbit segments of about 1 hour. These data are also used for the validation of orbits fit with GNSS data.

4 SCF-TEST OF GALILEO IOV RETROREFLECTORS

The GRA has been characterized with the SCF-G, with the procedures which include

1. GCO SCF-Test under exposure to the new solar simulator
2. Measurement of CCR optical performance (FFDPs and WFIs)
3. Thermal behavior (IR thermometry and contact probes)

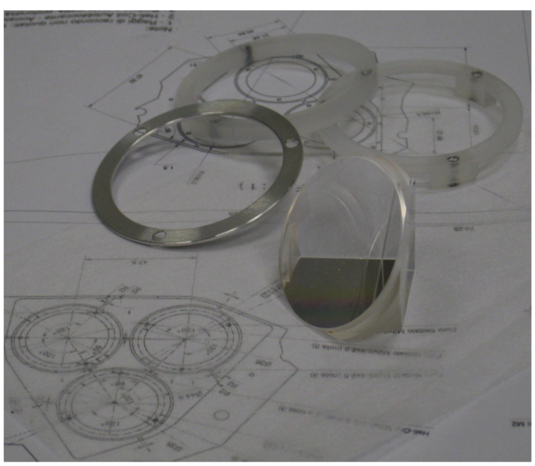

(a) Bare CCR with the Al ring and two KEL-F rings

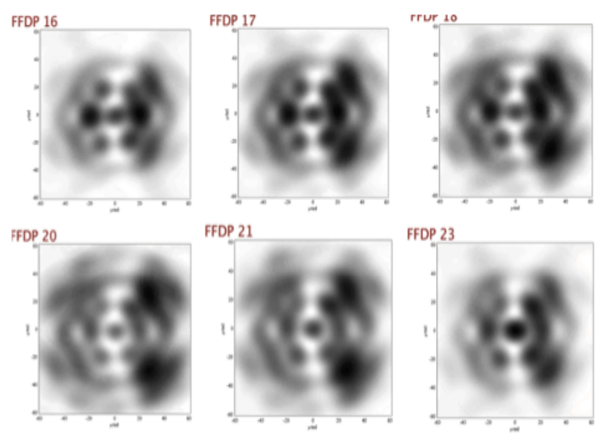

(b) IOV CCR: FFDP relative intensity during the GCO. FFDP scales are [-60,+60] μrad(right)

We performed an extensive SCF-Test on a prototype Galileo IOV retroreflector which is a fused silica uncoated CCR, deployed in planar arrays of 84 units on Galileo IOV satellites. This is very important for further SCF-Testing to expand the characterization of IOV LRAs, which have a better performance compared to old generation Al-coated GNSS CCRs (GPS, GLONASS, GIOVE). The SCF-Test consists in integrated and concurrent thermal and optical measurements performed either on single CCRs or on LRA breadboards, prototypes or flight payloads. The CCR/LRA is held at a fixed temperature, TM, starting from the expected average temperature, TAVG, of the payload in space. In Earth orbits the default LRA temperature is TAVG = 300 K. TAVG, the expected variation range of TM and the conditions of the LRA to spacecraft interface are inputs of the test. With SCF data and analysis we evaluate the CCR FFDPs under simulated space conditions and we compare them with the FFDPs measured in air conditions; the laser beam has a default linear polarization and an adjustable incidence angle with respect to the normal to the CCR face (the default laser angle is 0°). CCR surface temperature and its thermal relaxation time τCCR are measured during the test; we also measure the temperature and evaluate the thermal relaxation times of the other components of the LRA. The above procedure is repeated several times changing TM from TAVG to different temperatures inside the expected range of variation. This overall procedure is also performed for different SS illumination conditions. The Test evolved adding new items such as the thermal-optical conditions experienced by retroreflectors during a GNSS Critical half-Orbit and the retroreflector Wavefront Interferogram (WI) in space conditions. The GCO test has been developed with ETRUSCO for the IOVs.

4.1 GNSS Critical Orbit (GCO) SCF-TEST

The GNSS Critical Orbit is the orbit with its nodal line parallel to the Sun-Earth joining line. The test protocol, with the aim to reproduce an half GCO, has contemplated a three-hour period during which the payload has been rotated with 5 minute steps from the shroud towards the solar window (through which the emitted beam has been irradiated from the solar simulator) followed by a one hour period of shadow (during which the solar simulator was overshadowed by a shutter and the payload has been rotated towards the optical window to acquire FFDP, interferograms and ir photos) to finish with a three-hour period during which the payload has been rotated with 5 minute steps from the solar window towards the optical window.

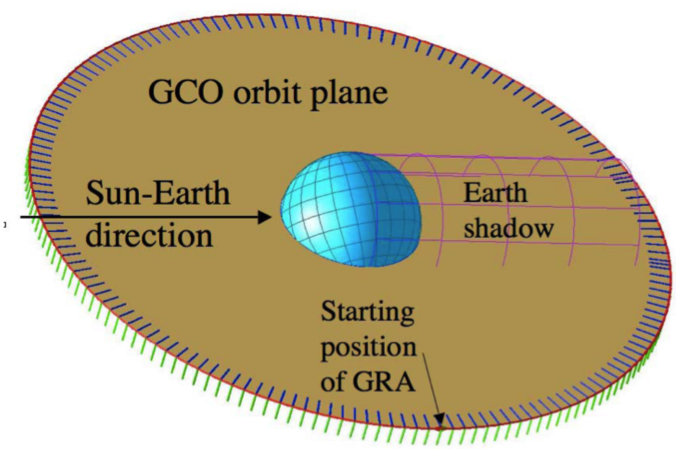

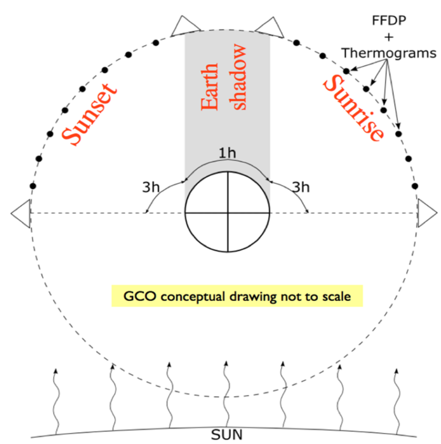

Fig. 4.1: GCO in space(left); GCO SCF-Test concept(right)

In order to evaluate the CCRs optical response, an optical circuit , outside of the cryostat, has been set up to reveal the horizontal and vertical Far Field Diffraction Patterns, subsequently integrated together in the analysis phase in order to obtain the total response of the retroreflector in exam. In addition to FFDP obtained by a 532 nm laser beam, the interferograms with a 633nm laser beam have been also made through the AccuFiz interferometer. Regarding the thermal response of all CCRs, it was possible to plot the thermal trend of the CCRs themselves thanks to an Infrared Camera.

5 THERMAL-OPTICAL SIMULATION OF THE GRA

Another considerable activity of the project is the development of a software procedure to integrate thermal and optical simulations of LRAs performance. ThermaOptiSim was an ETRUSCO-2 work package developed to realize this integration and better analyze CCRs behavior in a simulated orbit. The SCF-Test is fundamental to thoroughly investigate retroreflectors performance, but limited just to the simple GCO case.
The procedure of the simulation is divides into:

1. Definition of a finite element model of the GRA using the simulation software ANSYS® to then simulate it on a GCO orbit with the program Thermal Desktop considering no perturbations from high harmonics of the gravity field to simplify the problem. The program calculated the temperature distribution inside each CCR of the arrays for every step .

2. Development of an optical model of the GRA with the software CODEV to simulate the effects of a temperature distribution inside the CCRs which must be converted into an index of refraction distribution because we are dealing with optical characteristics.

3. Final analysis of the results using MATLAB, producing the FFDP of the whole array at each time step and the variation of the average intensity at the VA of Galileo, ~24μrad, during the GCO half orbit.

4. To make things simpler, the laser beam was considered orthogonal to the front face of the CCRs, even if in real laser ranging measurements this condition is not typical . For the simulations we used the measured intensity profile of the SCF-G laser.

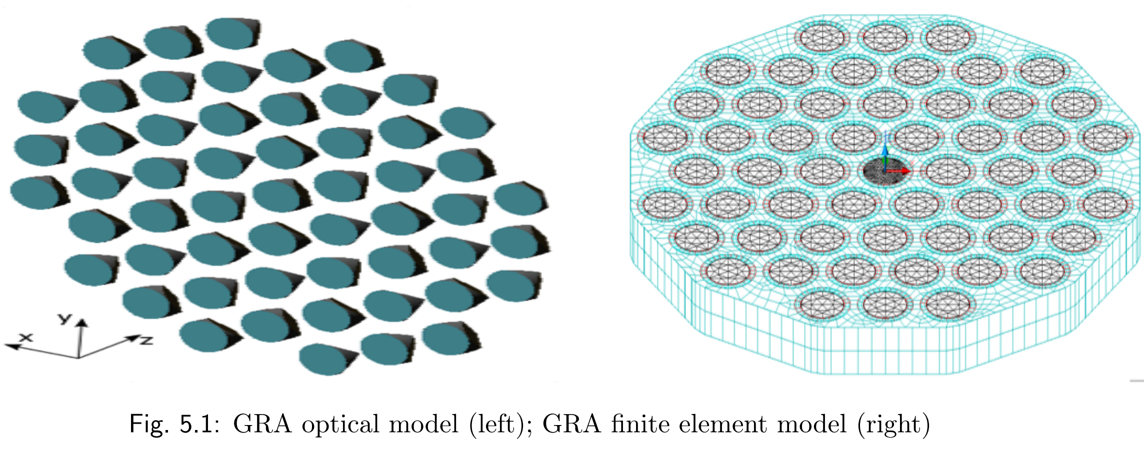

Fig. 5.1: GRA optical model (left); GRA finite element model (right)

6 RESULTS

These tests in the SCF_Lab will allow us to provide pre-launch validation of retroreflector performance under space conditions accurately simulated in the laboratory (in terms of pressure and temperature), as well as to characterize 'as-built' payloads, in order to optimize payload designs, to maximize ranging efficiency, to improve signal-to-noise conditions in daylight.
The GRA is an array made of 55 solid uncoated retroreflector, made of Suprasil 1. Five of these CCRs were realized with a different material, Suprasil 311, and two of the eight tested CCRs were made of this material. However, any particular difference between the two materials did not come out from the measurements.
Figures 6.1 shows the temperature variation of two of the CCRs tested, as results of the GCO measurement:

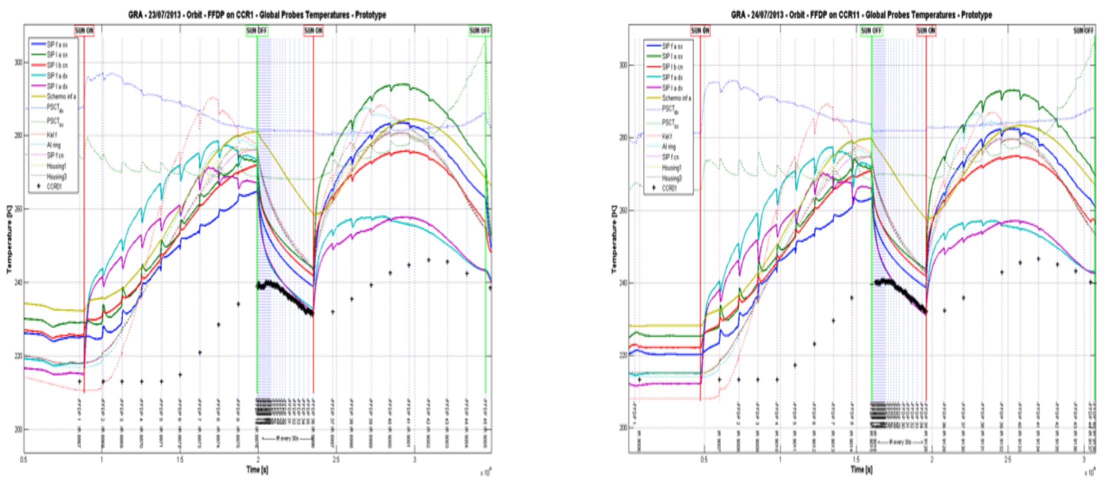

Fig. 6.1: Results of the ETRUSCO-GMES SCF-Test of 2 different CCRs

The CCR front face temperature measurements taken with InfraRed camera are marked with black crosses; they are all in the range between 213 K and 246 K even though their trends show some differences due to the different position of the single tested CCR. The other elements of the assembly are in the range between 200 K and 300 K.
Thermal and optical results show a good performance of the array in this realistic condition, representing a significant improvement from previous measured retroreflectors (Dell'Agnello 2011).
GRA SCF-Test and modeling has been very successful.
Regarding Thermal-Optical simulations, we used the measured intensity profile of the SCF-G laser. Results are in the following figures.

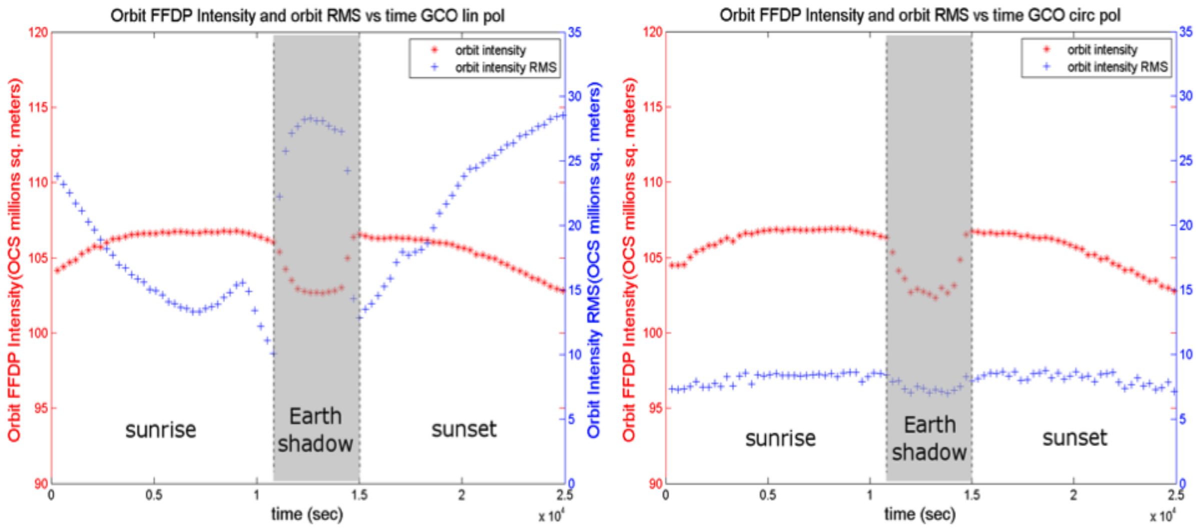

(a) Simulated GRA FFDP average intensity (red) and FFDP intensity RMS (blue), laser linearly polarized

(b) Simulated GRA FFDP average intensity (red) and FFDP intensity RMS (blue), laser circularly polarized

The intensity distribution of a CCR is however deeply influenced by the polarization of the laser. In Figure 6.2 a we simulated a linearly polarized beam, but, since recently there has been a wide discussion in the global laser ranging community regarding the use of a circular polarization (Kirchner 2012, Davis 2012), we analyzed the case of a circular polarization (Figure 6.2 b), in order to make a comparison to check for changes in performance. Comparing red ‘stars’ plots of the two Figures, displaying average intensity variations, there is not an appreciable difference, but it is looking at the intensity fluctuations at 24 μrad that the differences come out. We quantified those by calculating the RMS of the intensity at 24 μrad for each orbit position, blue ‘plus’ plots in the two Figures. A circular polarized laser determines more contained fluctuations at the Galileo VA; this means that a ground SLR station moving in the FFDP plane would experience a much smaller fluctuation of intensity, using a circular polarized laser beam instead of a linear one.

7 APPLICATIONS TO LRA-3F (CURRENT WORK AND FUTURE PROSPECTS)

With a shared 50%-50% collaboration between INFN and the Italian Ministry of Defense we are developing LRA-3F payloads for EO and GNSS missions of national and European interest, as well as customized, ad-hoc SCF-Test procedures for these missions. This effort includes design, construction, as well as characterization and study activities. We will apply all capabilities and instrumentations of the SCF_Lab to LRA-3F, including the SCF-Test/Revision-IR at 1064 nm laser wavelength is being developed for PLRA missions and for Satellite Formation Flying Missions and Technologies (SFFMT, including EO and GNSS). This is performed with a third movable table for optical FFDP measurements. The SCF-Test/Revision-IR capability is in addition to the SCF-Testing capabilities at 532 nm and 633 nm previously described. The 532 nm and 633 nm wavelengths have been used over the years by ILRS for SLR and LLR missions. The 1064 nm one is typically used for PLRA missions (including Mars Global Surveyor, Lunar Reconnaissance Orbiter and MESSENGER). Results from the current (first) Phase of the Defense-INFN contract must be consigned by 2014, with the publication of non-confidential content at the end of Phase 1 after the unanimous approval.

8 CONCLUSIONS

Inside the SCF_Lab we have developed unique procedures for the characterization of the performance of LRAs for several GNSS and lunar laser ranging missions and for LAGEOS, that is a reference of the standard ILRS payload. These are based on specialized instrumentation , on the measurement of the optical and temperature standard ILRS observable LRAs and on reference and/or representative orbit configurations (Default 'Earth-eclipse' SCF-Test, GCO SCF-Test, lunar day tests). Results in Figures 6.2 (a,b) show really good performance of the array in orbit with a contained average intensity variation. Experimental thermal results of the GRA test campaign have been shown and they underline the very good optical performance of the GRA. Moreover we showed that a shift from a linearly polarized laser beam to a circularly polarized one could bring a benefit in terms of intensity fluctuations, RMS, at the VA of the satellites. The work is proceeding to apply the SCF_Lab work program to LRA-3F for EO and GNSS missions. Current preliminary results and specifications are not released for publication. This work is the continuation and evolution of INFN and ASI work on laser ranging of GNSS, Moon and LAGEOS, in the framework of ILRS activities (see http://ilrs.gsfc.nasa.gov and http://www.lnf.infn.it/conference/laser2012/).

9 ACKNOWLEDGEMENTS

We thank the Italian INFN-CSN5, which is supporting the SCF_Lab since 2005 (with funds for the interdisciplinary experiments ETRUSCO, MoonLIGHT-ILN and ETRUSCO-GMES), and the Italian Ministry of Defense, which is co-funding SCF_Lab R&D activities under Defense-INFN Contract n. 10263. We also thank ASI for co-funding SCF_Lab R&D activities related to Galileo and GPS under ASI-INFN Contract n. I/077/09/0 (ETRUSCO-2 project).

10 REFERENCES

[1] Dell'Agnello, S., et al, Creation of the new industry-standard space test of laser retroreflectors for the GNSS and LAGEOS, J. Adv. Space Res. 47 (2011) 822–842. Galileo Special Issue on Scientific Applications of Galileo and other Global Navigation Satellite Systems – II, March 1, 2011, pub. Proc. of "2rd International Colloquium – Scientific and Fundamental Aspects of the Galileo Programme", Padua, September 2009.

See also: http://ilrs.gsfc.nasa.gov/about/reports/other_publications.html.

[2] S. Dell'Agnello et al., MoonLIGHT: A USA–Italy lunar laser ranging retroreflector array for the 21st century, Planetary and Space Science 74 (2012) 276–282.

[3] Dell'Agnello, S., et al, "Creation of the new industry-standard space test of laser retroreflectors for GNSS and LAGEOS", J. Adv. Space Res. 47 (2011) 822–842. This paper is linked at the ILRS web page of "Special Reports", as the reference on the SCF-Test:

http://ilrs.gsfc.nasa.gov/reports/special_reports/index.html. Results reported here are world-first measurements on Al-coated CCRRs deployed on the first generation of GNSS (GLONASS, GPS, GIOVE) and on an uncoated CCRR of LAGEOS.

[4] A. Boni et al, "Optical Far Field Diffraction Pattern characterization of Laser Retroreflectors for Satellite and Lunar Laser Ranging", INFN-LNF Internal Report, LNF– 08/26 (IR) November 24, 2008.

[5] Dell'Agnello, S., et al, "ETRUSCO-2: an ASI-INFN project of technological development and SCF-Test of GNSS laser retroreflector arrays", in ESA Proc. 3rd International Colloquium – Scientific and Fundamental Aspects of the Galileo Programme, Copenhagen, Denmark, 2011 (http://www.congrex.nl/11a12/). This paper is linked at the ILRS web page on Galileo, where, at the tab "Retroreflector Info:

http://ilrs.gsfc.nasa.gov/satellite_missions/list_of_satellites/gali_reflector.html, 3 documents are reported: 1) ESA's request for laser tracking of Galileo IOV-1 and IOV-2 satellites that were launched on Oct. 21, 2011; 2) ESA's IOV retroreflector info; 3) INFN's world-first SCF-Test activity for the CCR of Galileo IOVs. IOVs, the first 4 satellites of Galileo, have uncoated CCRs like IRNSS, COMPASS and QZSS CCRs.

[6] S. Dell'Agnello et al, "Isothermal FFDP-Test and SCF-Test of Flight-quality Uncoated Cube Corner Laser Retroreflectors", in Proc. 17th International Workshop on Laser Ranging, Bad Kötzting, Germany, May 2011. [RD-5] Boni, A., et al, "World-first SCF-Test of the NASA-GSFC LAGEOS Sector and Hollow Retroreflector", in Proc. 17th International Workshop on Laser Ranging, Bad Kötzting, Germany, May 2011.

[7] D. Currie, S. Dell'Agnello, G. Delle Monache, "A Lunar Laser Ranging Retroreflector Array for the 21st Century", Acta Astron. 68, 667– 680 (2011).

LIST OF ACRONYMS

BIPR = Background Intellectual Property Right
CCR = Cube Corner Retroreflector
COSMO-SkyMed = COnstellation of small Satellites for the Mediterranean basin Observation
CSG = COSMO Second Generation
CSNV = Commissione Scientifica Nazionale V, INFN National Scientific Committee V
CSK = COSMO-SkyMed
DAO = Dihedral Angle Offset
ESA = European Space Agency
ETRUSCO = Extra Terrestrial Ranging to Unified Satellite COnstellations, an INFN-CSNV interdisciplinary program for GNSS and LAGEOS
ETRUSCO-2 = Extra Terrestrial Ranging to Unified Satellite COnstellations-2, an ASI-INFN co-funded project of technological development for GNSS
3F = Formation Flying Functionality
FFDP = Far Field Diffraction Pattern
G-CALIMES = Galileo-COSMO-SkyMed Absolute Laser Intercalibration with Measurements on Earth and in Space
GNSS = Global Navigation Satellite System
GMES = Global Monitoring for Environment and Security
GSEG = Ground SEGment
HW = HardWare
ILRS = International Laser Ranging Service (http://ilrs.gsfc.nasa.gov/)
INFN = Istituto Nazionale di Fisica Nucleare (http://www.infn.it/indexen.php)
IRNSS = Indian Regional Navigation Satellite System, the Indian GNSS
ISF = Internal Special Facility of the LNF
ITRF = International Terrestrial Reference Frame
LAGEOS = LAser GEOdynamics Satellites-I (by NASA, 1974) & II (by NASA/ASI, 1992)
LEO = Low Earth Orbits
LLR = Lunar Laser Ranging (to Apollo and Lunokhod LRAs)
LNF = Laboratori Nazionali di Frascati dell'INFN, Frascati (Rome), Italy (http://www.lnf.infn.it/user.html/)
LRA = Laser Retroreflector Array (of CCRRs)
MAIT = Manufacture Assembly Integration Testing
NASA-GSCF = National Aeronautics and Space Admin. − Goddard Space Flight Centre
OCS = Optical Cross Section
OGSE = Optical Ground Support Equipment
P_{STC} = Plate for Support and Thermal Control in the SCF
RD = Reference Document

SCF = Satellite/lunar laser ranging Characterization Facility, the OGSE built at LNF by INFN with ETRUSCO
SCF-Test = Set of test procedures to characterize the detailed thermal behavior and optical performance of LRAs with the SCF; BIPR of INFN
SAR = Synthetic Aperture Radar
SCF_Lab = SCF LABoratory, the LNF laboratory consisting of the SCF and of the Clean Room where the SCF is operated
SLR = Satellite Laser Ranging
SW = SoftWare
τ_{CCR} = CCR Thermal Relaxation Time
VA = Velocity Aberration

I-FCX

S. Dabagov (Resp.)

Not received

MANESCO

S. Bellucci (Resp.)

Not received

NESCOFI@BTF
NEutron Spectrometry in COmplex FIelds @ Beam Test Facility

2013 Activity Report

R. Bedogni (70%), D. Bortot (50%), B. Buonomo (20%), A. Esposito (30%), G. Mazzitelli (20%), L. Quintieri (20%), A. Gentile (40%), M. Chiti (20%).
INFN - LNF

J.M. Gomez-Ros (40%)
CIEMAT, Madrid / associato LNF

M.V. Introini, A. Pola
INFN-Milano / Politecnico di Milano

2013 activities

The 2013 activities were focused on achieving two milestones, namely:
Sept. 2013 Building SP^2 and CYSP with associated DAQ systems
Dec. 2013 electronics testing; spectrometer calibration (according to possibilities)
In addition, the design, production and response characteristics of the active thermal neutron detectors are now consolidated. Two types of thermal neutron detectors are now standardized, namely the TNPD (Thermal neutron pulse detector) and TNRD (thermal neutron rate detector). Both SP^2 and CYSP spectrometers were built, equipped with TNPD detectors and the electronics were tested on time. In addition to the SP^2 and CYSP development activity, a side activity has started to disseminate the newly developed thermal neutron detectors in the medical sector, particularly for the neutron dosimetry of the patient undergoing radiotherapy treatment. This activity was co-funded by the Sevilla University.

The “thermal neutron pulse detector” TNPD

The so called “thermal neutron pulse detector” TNPD [1] produces a pulse height distribution, from which the thermal neutron fluence can be derived. Analog signals from TNPDs are sent to the multi-detector board (developed within NESCOFI@BTF) shown in Fig. 1. This includes independent spectrometry chains. Each one is composed by a bias regulator, a charge preamplifier and a shaper amplifier. The amplified signals are transmitted to multi-channel commercial ADC (NI USB 6366). Each analogue signal is digitized with 16 bits and sampling rate 2 Msamples/s.
From the pulse height distribution the neutron-to-photon discrimination is performed and the net thermal neutron signal is extracted. Typical thermal neutron sensitivity: 0.03 cm^2 (counts per unit fluence).

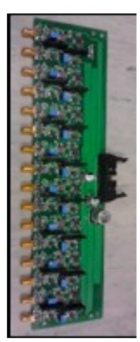

Figure 1. Multi-detector NESCOFI acquisition board. Up to 16 detectors can be controlled through SMA connectors. For every detector a charge preamplifier and a shaper amplifier allow adapting, guassian-shaping an magnifying the charge pulses produced in the semiconductor based thermal neutron detectors. The amplified signals are sent to a multi-channel digitizer (NI USB 6366) controlled through a Labview program. The control software allows simultaneous spectrum calculation for all detectors.

The converted employed in both TNPD and TNRD was developed and optimized in thickness with the special aim of reducing the photon sensitivity without compromising the thermal neutron sensitivity. Typical thermal neutron spectrum from the TNPD is shown in Fig. 2

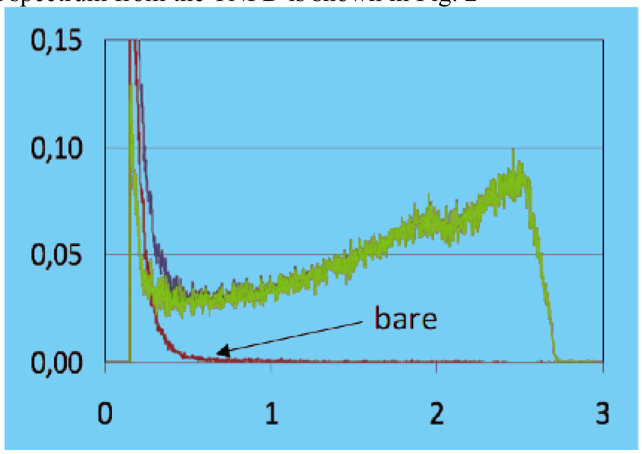

Figure 2. Spectrum of energy deposited in the TNPD. The label “bare” denotes the uncovered detector. The Blue spectrum is the “covered” detector. The green spectrum is the “covered” – “bare” spectrum. X axis is pulse height (V) and Y axis is number of pulses (a.u.).

Characteristics of TNPD are:

- Different detector thicknesses are easy to fabricate and well controllable;
- Optimal sensitivity obtained: 0.03 counts per unit thermal fluence (cm^2);
- Fabrication reproducibility <10%;
- Radiation damage observed for integrated thermal neutron fluence 3E+12 cm^{-2} (measured at TRIGA reactor, ENEA Casaccia).
- A single exposure is sufficient to discriminate the thermal neutron component from the photon one.

The TNPD was further tested against a well-established detector, the ^{6}LiI(Eu) scintillator, at the centre of a set of Bonner spheres. The test was performed at TSL Uppsala [1] where a wide neutron spectrum is produced by bombarding a Be target with 30 MeV protons. Figure 3 demonstrate that the neutron spectra derived with the ^{6}LiI(Eu) scintillator or the TNRD at centre of the Bonner spheres are equivalent.

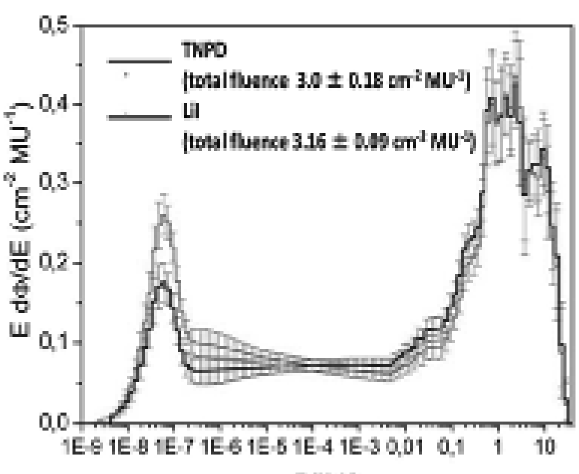

Figure 3. Neutron spectra derived with the ^{6}LiI(Eu) scintillator or the TNRD at centre of the Bonner spheres at the TSL facility (30 MeV protons on Be target). Spectra are in equi-lethargy representation.

The “thermal neutron rate detector” TNRD

The so called “thermal neutron rate detector” TNRD [2] produces a DC voltage level that is proportional to

the thermal neutron flux. Adequate photon rejection is achieved through an intrinsic compensation effect. The lowest measurable thermal neutron flux is <100 $cm^{-2}s^{-1}$.
With respect to the TNPD, the TNRD shows simplified readout and reduced cost. By contrast its sensitivity is lower than that of the TNPD.
The TNRD active area is one cm^2 and its overall dimensions are approx. 1.5 cm x 1 cm x 0.4 cm. Its output is a DC voltage, which is proportional to the thermal neutron fluence rate (for this reason the device is called “rate detector”). This signal is amplified in a low-voltage electronics module especially developed by the project team. The amplifier output is sent to a programmable ADC (NI USB-6218 BNC, 16 bit, up to 250 kS/s) controlled by a PC through a LabView application. Typical time-dependent output is shown in Fig. 4.

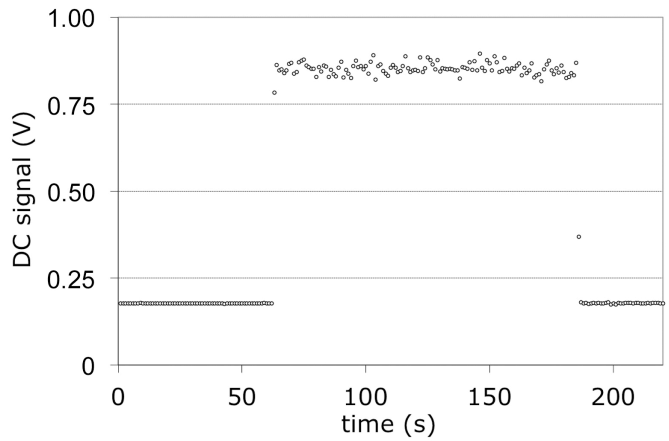

Figure 4. Time-dependent output of the TNRD when exposed in an ex-core thermal neutron beam from the ENEA Casaccia TRIGA reactor at power 46 kW. The step is produced when opening and closing the neutron shutter. The conventional fluence rate is about 6E+4 $cm^{-2}s^{-1}$. The constant voltage level measured in the “shutter closed” configuration corresponds to an offset in the operational amplifier-based circuit used to treat the detector signal.

After manufacturing, every TNRD is calibrated in a moderating cylinder. Typical response is (96±3) $cm^{-2}s^{-1}$ mV^{-1} in terms of conventional thermal flux. To estimate the reproducibility of the manufacturing process, the response of ten TNRDs with nominally identical fabrication characteristics was compared, and its variability is 5% (one s.d.). The response to photon radiation, measured in a reference ^{137}Cs field, is (0.51±0.02) mGy h^{-1} mV^{-1}. Linearity is better than 2% in the range from 7E+2 to 3E+5 $cm^{-2}s^{-1}$.

CYlindrical SPectrometer (CYSP)

The CYSP spectrometer has been designed according to the conclusions of a detailed simulation study made with MCNPX 2.6 [3], using the ENDF/B-VII cross-section library [4] for neutrons with energies below 20 MeV and the room temperature cross-section tables in polyethylene, $S(\alpha,\beta)$. Neutron transport above 20 MeV has been modelled using Bertini intra-nuclear cascade model and Dresner evaporation model [5]. The CYSP spectrometer mainly consists of a series of TNDs (thermal neutron detectors) located along the axis of a polyethylene cylinder that provides spectral information when it is irradiated with a directional neutron beam.
The dimensions of the cylinder as well as the location of detectors have been optimized to achieve spectral resolution and practically eliminate the eventual contribution from epithermal neutrons coming from lateral directions. The collimator and the additional shielding made in borated plastic are included to eliminate such lateral contributions over the whole energy range.
As it is shown in Figure 5, the first part of the CYSP is a collimator 50 in diameter 30 cm in length made of polyethylene. The hole diameter is 16 cm and it is covered by 5 mm thick borated plastic SWX-238. The central capsule of the spectrometer (on the right in figure) is a 35 cm diameter polyethylene cylinder with seven detectors located along the axis. Detector-to-detector distance along the cylindrical axis is 2 cm

approximately. A lead disk has been inserted between 6th and 7th positions to increase the response to high-energy neutrons. Air holes are needed to favour streaming of neutrons towards deep measurement positions. The response matrix is given in Fig. 6. The signal of every detector is reported, per unit incident fluence, as a function of the monochromatic neutron energy. Detector 1 is the shallowest and detector 7 is "behind lead", thus its response increases above approx. 1 MeV.

A prototype of the CYSP was fabricated, equipped with active detectors and tested in reference neutron fields from an Am-Be source (INFN-LNF), monochromatic beams (0.144 MeV, 0,565, 2.0, 3.5, 5.0, 16.5 MeV) and a reference ^{252}Cf source at NPL (UK). The simulated response matrix was confirmed within less than 2%.

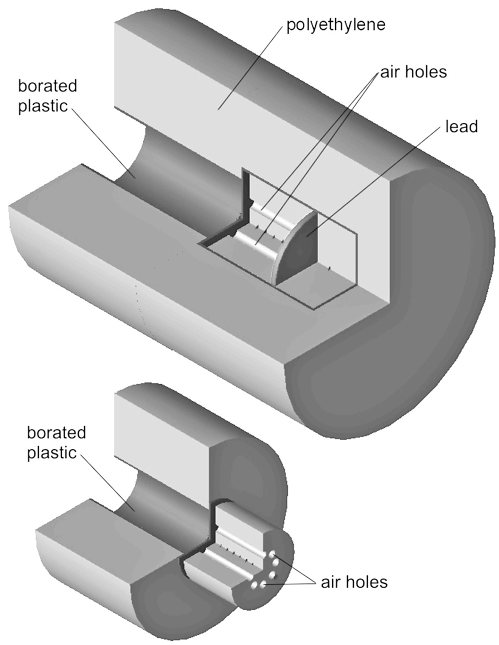

Fig.5. Scheme of the CYSP.

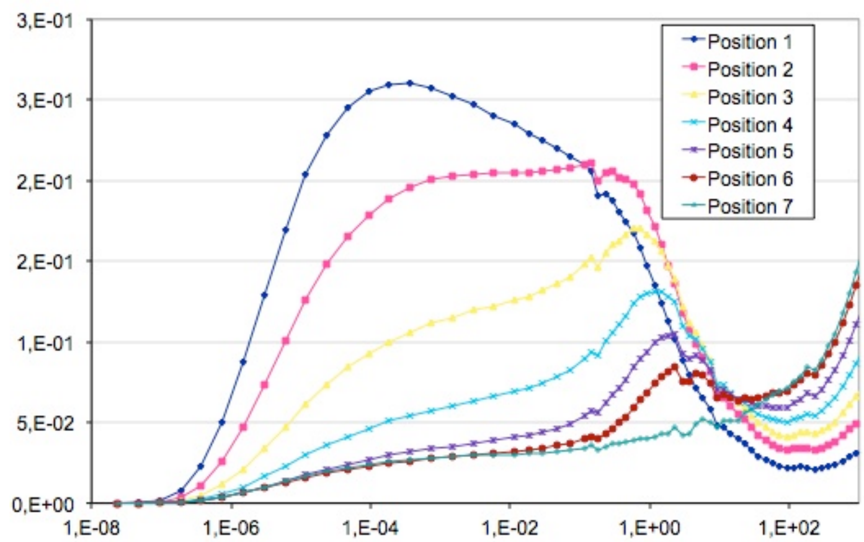

Figure 6. Typical response matrix of the CYSP.

The SPherical Spectrometer (SP^2)

The SP^2 spectrometer consists of thirty-one thermal neutron detectors arranged along three perpendicular

axes at 5 radial distances (5.5, 7.5, 9.5, 11 and 12.5 cm) and at the centre of a polyethylene sphere of diameter 25 cm. An internal 1 cm thick lead shell between 3.5 and 4.5 works as an energy converter via (n,xn) reactions thus enhancing the response above 20 MeV, either for the central detector and for those located at 5.5 and 9.5 cm.
Although the response of a single TND in a given location is clearly not isotropic, a nearly isotropic response is obtained by averaging the readout of detectors located at the same radial response, as it has been discussed in previously published papers [6,7]. The same works also demonstrate the spectrometric capabilities of the device from thermal energies up to hundreds MeV neutrons.
The SP^2 response matrix, intended as the response of each thermal neutron detector per unit incident fluence as a function of the detector position and the irradiation energy, was modelled on the basis of extensive simulations performed with MCNPX 2.6 Monte Carlo code. To validate these calculations, a passive prototype, operating with Dysprosium activation foils, was built and tested in reference monochromatic fields available at PTB. The energies were 0.147, 0.565, 1.2, 5.0 and 14.8 MeV. The details of the experimental campaign are reported in [8]. The simulated response matrix was confirmed within less than 3%.
The active prototype was achieved in May 2013. Active thermal neutron detectors of type TNPD have been embedded in the 25 cm diameter polyethylene + lead sphere, and arranged as sketched in Fig. 7. Detectors occupy positions at radius = 0 (centre), 5.5 cm, 7.5 cm, 9.5 cm, 11 cm, 12.5 cm (on surface).
As in the case of the CYSP spectrometer, signals from detectors were acquired through NESCOFI multi-detector board (see Fig 1) and digitized with NI USB 6366 digitizer.

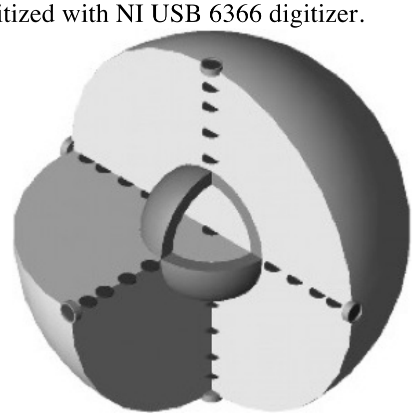

Figure 7. Geoemtry of the SP2 with detector positions. Only one detector is located behind the lead insert. Detectors on surface are back-shielded with 1 mm of Cd with the aim of preventing a possible signal due to neutrons backscattered from the sphere.

Taking advantage of the reference ^{241}Am-Be source available at FISMEL laboratories of INFN-LNF, a partial calibration of the SP^2 was achieved using the shadow-cone technique. Differently than CYSP, the Spherical Spectrometer responds to neutrons coming from all directions, thus well defined irradiation geometries were fixed for calibration purposes. Again, the simulated geometry-dependent response matrix was confirmed within less than 3%.
Similar level of agreement was achieved in field test was organized at the 14.6 MeV quasi monochromatic beam of the ENEA fast neutron generator, obtained at 45° from a T(d,n) target (deuterium energy 260 keV).

Applying the TNRD in the medical sector

A collaboration with Sevilla University, Azienda Ospedaliera San Camillo-Forlanini (Roma) and Ospedale Santa Maria delle Croci (Ravenna) consolidated the use of TNRD in the in-phantom neutron dose measurements during photon radiotherapy sessions. This allowed validating a recently developed risk model for the neutron-induced second cancer in patients [9]. An anthropomorphic phantom was submitted to two standard 15 MV treatments, in abdomen and head (See Fig. 8 for the different gantry positions, corresponding to fractions with equal dose to the isocentre). The TNRD was exposed in four selected point of interest (centre of head, lung, abdomen and skin) and the measured neutron doses were generally in agreement (5% or better) with the values expected from Monte Carlo simulations.

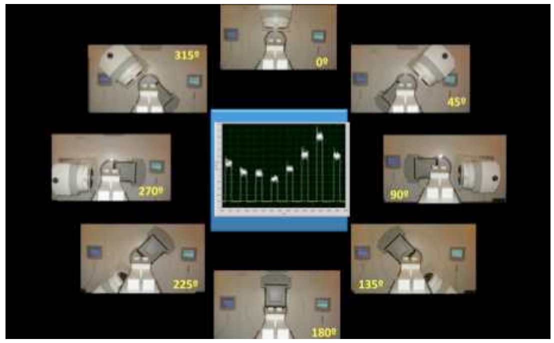

Figure 8. Gantry positions for a typical treatment and corresponding DC signal from the TNRD.

Following the satisfactorily results from this test, the system formed by a single TNRD and its DAQ electronics was extended to five parallel detectors working in parallel to simultaneously measure neutron doses in multiple organs (Co-funded by Sevilla University).

Collaboration and external funds

CIEMAT Madrid: 35,000 equiv-hours CPU time on EULER cluster. A contract for building a dedicated SP2 for CIEMAT is under elaboration.
CRISP (INFN-LNF): 6 k€ (detectors, trips exp. campaigns)
Politecnico di Milano 3 k€ (trips at experimental campaigns) + support for electronics design and testing
Sevilla Universiy: 3 k€ co-funding for parallelization of the TNRD fro medical sector.
Azienda Ospedaliera San Camillo-Forianini (Roma) and Ospedale Santa Maria delle Croci (Ravenna): usage of 15 MV electron LINACs
LNF support:
- 2 man*month at mechanical workshop
- Guest-house: 30 man*night
- Experiments for detector fabrication and characterization performed at FISMEL laboratories.

Project meetings

29 Jan 201, LNF, 2013 NESCOFI launch meeting
15 April 2013, Milan, Mid-year NESCOFI meeting.

International Review Panel

Text of the 2013 reviewer reports

"*It is my pleasure for me to write this letter to truly recommend this project for medical benefits. NESCOFI achieved the stated targets on time and on budget. Looking from thepoint of view of the medical sector, where we are involved, we see important applications for the developed instruments. This is especially true for the present and coming years, due to the increasing interest of the medical community for the second cancers induced by neutrons in radiotherapy patients. The availability of real-time spectrometers, like those developed in the project, would allow to extensively map the oncology accelerator facilities, thus leading routine patient-risk assessment practices which will benefit a significant fraction of population. We recommend to specialize (maybe simplify, considering the reduced energy range of medical linacs) a version of SP^2 for the medical sector only). Concerning in-phantom neutron evaluations, we tested the miniaturized thermal neutron detectors of type TNRD in our phantom NORMA, with promising results in terms of rapidity, accuracy and possibility to multiply the number of simultaneous measurement points. I hope my letter will help you to take a decision. Please do not hesitate to contact me if you have further questions. Yours Sincerely"*

Prof. Francisco Sanchez Doblado, Profesor Catedratico Universidad de Sevilla, paco@us.es

"*Dear Dr. Bedogni,*
It is a pleasure for me to confirm that the project was able to reach a satisfactory level of testing and calibration for both spectrometers in spite of the economical restrictions. The impressive results obtained with CYSP, especially the high degree of accuracy and the significant response differentiation as a function of the energy, suggest that its use in neutron beam-lines or for cosmic rays would produce important and new results. The SP2 has the potentiality for opening the way to a new philosophy of neutron area monitoring for radiation protection, and for this reason I recommend to further develop it, possibly in conjunction with an industry. Results are clear, complete, and produced on time".

Prof. Carles Domingo, Profesor Titular Universitat Autonoma de Barcelona, carles.domingo@uab.cat

Web-site
http://www.lnf.infn.it/acceleratori/public/nescofi/

2013 Publications

Main publications for 2013 are:

NIM A 714 (2013) 110-114.
Radiat. Meas. 50 (2013) 67-70
Radiat. Meas. 50 (2013) 78-81
IEEE Trans. Nucl. Sci. 60 (6) (2013) 4692-4696.

Most of the activity done in 2013 was presented at the 12th Neutron and Ion Dosimetry Symposium (NEUDOS-12), Aix en Provence, 3-7 June 2013. The project obtained one session chair, four orals and three posters. Paper published in 2014.
The applications to medical sector were presented to the SEFM 19 - SEPR 14 (18-21 June 2013, Caceres, Spain) with an invited talk and a poster.
NESCOFI activity was also presented to the Giornata di studio su IRIDE (10-11 June 2013, LNF) and at the Workshop HeRe in Italy, 2-3 Dec. 2013 (ENEA Frascati).

Bibliography

[1] A. Pola, D. Bortot, M.V. Introini, R. Bedogni, A. Gentile, A. Esposito, J. M. Gomez-Ros, E. Passoth, A. Prokofiev. Compact thermal neutron sensors for moderator-based neutron spectrometers. Radiation Protection Dosimetry (2014). doi:10.1093/rpd/nct298.
[2] R. Bedogni, D. Bortot, A. Pola, M. V. Introini, A. Gentile, A. Esposito, J. M. Gomez-Ros, M. Palomba, A. Grossi. A new active thermal neutron detector. Radiation Protection Dosimetry (2014). doi:10.1093/rpd/nct319.
[3] Pelowitz, D.B. (ed.). MCNPX User's Manual Version 2.6. Report LA-CP-07-1473 (2008).
[4] Chadwick, M.B., Oblozinsky, P., Herman, M. et al. Evaluated Nuclear Data File ENDF/B-VII.0. Nuclear Data Sheets 107, 2931-3118 (2006).
[5] Pioch, C., Mares, V., Rühm, W. Influence of Bonner sphere response functions above 20 MeV on unfolded neutron spectra. Radiat. Meas. 45, 1263-1267 (2010).
[6] Gómez-Ros, J.M., Bedogni, R., Moraleda, M., Delgado, A., Romero, A., Esposito, A. A multi-detector neutron spectrometer with nearly isotropic response for environmental and workplace monitoring. Nucl. Instrum. Meth. A 613, 127-133 (2010)
[7] Gómez-Ros, J.M., Bedogni, R., Moraleda, M., Esposito, A., Pola, A., Introini, M.V., Mazzitelli, G., Quintieri, L., Buonomo, B. Designing an extended range single-sphere multi-detector neutron spectrometer. Nucl. Instrum. Meth. A 677, 4-9 (2012)
[8] Bedogni, R., Gómez-Ros, J.M., Pola, A., Introini, M.V., Bortot, D., Gentile, A., Esposito, A., Mazzitelli, G., Quintieri, L. , Buonomo, B. Testing a newly developed single-sphere neutron spectrometer in reference monochromatic fields from 147 keV to 14.8 MeV. Nucl. Instrum. Meth.

A 714, 110-114 (2013).
[9] F. Sánchez-Doblado; C. Domingo; F. Gómez; B. Sánchez-Nieto; J.L. Muñiz; M.J. García-Fusté; M.R. Expósito, R. Barquero; G. Hartmann; J.A. Terrón; J. Pena; R. Méndez; F. Gutiérrez; F.X. Guerre; J. Roselló; L. Núñez; L.Brualla-González; F. Manchado; A. Lorente; E. Gallego; R. Capote; D. Planes; J.I. Lagares; X. González-Soto; F. Sansaloni; R. Colmenares; K. Amgarou; E. Morales; R. Bedogni; J.P. Cano; F. Fernández.Estimation of neutron-equivalent dose in organs of patients undergoing radiotherapy by the use of a novel online digital detector. Phys. Med. Biol.57,pp. 6167 – 6191 (2012).

NEXTARCH

M. Iliescu (Resp.)

Not received

Highlights NORCIA 2013

D. Di Gioacchino (Ric.), G. Gatti (Ric.), A. Marcelli (P.R.) (Resp.), B. Spataro (Ass.)
[*http://www.lnf.infn.it/gr5/website_norcia/home.html*]

In the last century accelerators played a key role in the science and in the society and they will certainly continue playing a key role also in the next decades not only in high-energy physics. More than 15,000 accelerators are in use around the world, more than 97% of these accelerators are used for different industrial and commercial applications and this number is still growing. Actually, electron linacs used for radiotherapy represent one third of all existing accelerators.

In the frame of a large international collaboration among INFN-LNF, SLAC, KEK and UCLA the NORCIA experiment is working to design, fabricate and operate high power X-band accelerating structures: an activity devoted to the research and development of key components existing accelerators and to fulfill the demands of new accelerator devices required to achieve the multi-TeV energies of the future e^+/e^- linear colliders and other foreseen storage rings such as neutrino facilities or x-ray FEL [1-2].

In order to determine the maximum sustainable gradients in normal conducting RF powered particle beam accelerators operating at X-band with extremely low probability of RF breakdown, the NORCIA group has designed and manufactured at the *Laboratori Nazionali di Frascati* two electroformed 11.424 GHz high gradient electroformed structures coated with Au-Ni and with different roughnesses. After the RF electromagnetic characterizations at room temperature these standing wave (SW) linear accelerating structures working are under test at SLAC.

The main cell dimensions and the mechanical drawings of the SW structures are reported in Ref.s [2,3,6,7]. These SW devices have three cells fed by a circular waveguide. The central cell has a twice higher gradient while adjacent cells are used to match the RF power from the input circular waveguide. The mode excited to test the structure is the π-mode. With this arrangement, breakdowns occur predominantly in the high gradient cell while the two other cells have surface conditions unperturbed by the breakdowns [2,3,4]. Table 1 reports the preliminary RF parameters of a Au-Ni electroformed structure measured at SLAC at room temperature. Figures 1 show the electroformed structure with a 70 nm roughness for the low level RF determination and the longitudinal field profiles of the π, π/2 and 0 mode characterizations.

Table 1.

Mode	Frequency [GHz]	Beta	Q_0	Q_{ext}	Q_l
0	11.2692	2.64	7090	2688	1949
π/2	11.3214	2.58	6621	2561	1847
π	11.41454	0.659	5786	8774	3486

Similar results have been obtained also for the second electroformed structure with a 10 nm roughness. In particular, the two structures gave a resistivity about 2.5-3 than the Cu one. Work is in progress at INFN/LNL in order to improve the conductivity of the Au deposited film as a function of the mandrel's shape. We also successfully tested for the first time the possibility to "built in" cooling channels in the irises of these cells.

Since the breakdown phenomenon is an open problem, a dedicated research and development on this field has been launched within the linear-collider community. Collaboration on X band high gradient research and related accelerator technologies, will allow to further advance the X-band technologies and benefit from some important accelerator related projects in the world. In order to improve the higher power performance of the X band structure in terms of the accelerating gradient, the use of the materials with a high tolerance to surface fatigue due to the pulsed heating effects (materials with a higher fusion point) and to avoid the fabrication of soft devices as done in conventional brazing, are required [2,3,4,5,6]. In the framework of a larger collaboration NORCIA is working also to investigate alternative technological approaches such as electroforming, molybdenum sputtering on copper, electron beam welding and multi-layers coatings. In particular, an extensive R&D activity concerning molybdenum coatings is in progress. Mo films were grown by RF magnetron sputtering technique on glass and sapphire substrates at room temperature. The sputtering parameters were optimized specifically addressing the growth of oxygen free Mo layers. Copper coated by molybdenum via sputtering under vacuum is another promising approach to increase the accelerating gradient of RF cavities working at high frequencies. Recently we presented a structural and electronic characterization of Mo coatings obtained via the sputtering method and annealed up to 600 ºC. [8-11] This method is a possible route to obtain homogenous Mo coatings suitable to increase performances of RF cavities working at high frequencies. We combined FIB imaging to visualize at high spatial resolution the morphology of Mo films and to accurately measure their thickness, with transport experiments to measure the resistivity, while XRD and XANES (X-ray Absorption Near Edge Structure) technique were used to evaluate the degree of crystallinity, identify different ordered phases and probe local structure and electronic properties. The characterization of the chemical properties of these coated films has been carried out in cooperation with researchers of the *Sapienza* University, Camerino University and the Diamond Light Source (UK). The achieved results are promising and further enhancements of the conductivity are probably achievable tuning the synthesis and post treatment processes of thick Mo coatings.

[1] A. Grudiev, S. Calatroni, and W. Wuensh, *New local field quantity describing the high gradient limit of accelerating structures*, PRST- Accelerators and Beams 12, 102001 (2009).

[2] V.A. Dolgashev *et al.*, *Status of High Power Tests of Normal Conducting Single-Cell Standing Wave Structures*, Proceeding of IPAC 2010, Kyoto, Japan, 2010, pp. 3810-3812 (*and references therein*).

[3] V. Dolgashev seminar held at LNF (September 2010)

[4] V. Dolgashev and S.G. Tantawi, private commun.

[5] V.A. Dolgashev et al., Geometric dependence of radio-frequency breakdown in normal conducting accelerating structures, Applied Physics Letters **97**, 171501 (2010)

[6] B. Spataro *et al.*, Technological issues and high gradient test results in X-band molybdenum accelerating structures, NIM A **657** (2011) 114-121

[7] B. Spataro *et al.*, High power comparison among brazed, clamped and electroformed X-band cavities, NIM A **657** (2011) 88-93

[8] S. Bini, *et al.*, Molybdenum sputtering film characterization for high gradient accelerating structures, Chin. Phys. C **37** (2013) 097905-07

[9] P. Chimenti, C. Caliendo and B. Spataro, A procedure to obtain a very low Mo films with oxygen contamination, SPARC-RF-12/ 004, June 8, 2012

[10] Y. Xu, *et al*., Structural and morphological characterization of Mo coatings for high gradient accelerating structures, J. Physics: Conference Series **430** (2013) 012091

[11] A. Marcelli *et al.*, submit. to Thin Solid Films (2013)

Figure captions

Figure 1. a) Final X band structure and its cross section after removal of mandrel; b) open channel in the irises visible in a sectioned structure

Figure 2. a) Au-Ni electroformed structure; b) π - mode, on axis field profile; c) π/2 mode, on axis field profile and d) 0 mode, on axis field profile

Figure 1

a) Final X-band structure (left picture) and its cross section (right picture) after removal of mandrel

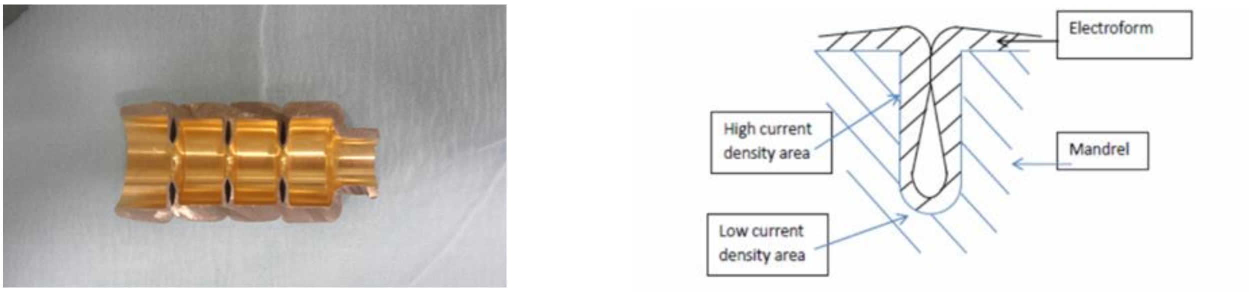

b) open channels in the irises visible in a sectioned structure prototypes

Figure 2

a) Au-Ni electroformed structure

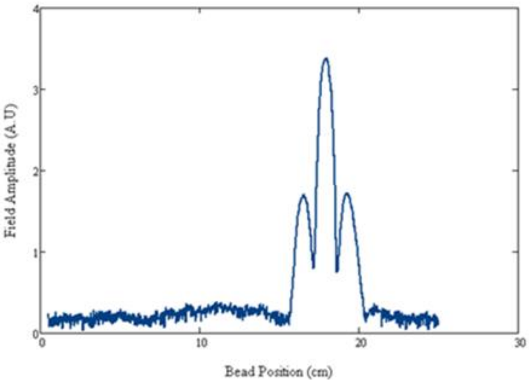

b) π - mode, on axis field profile

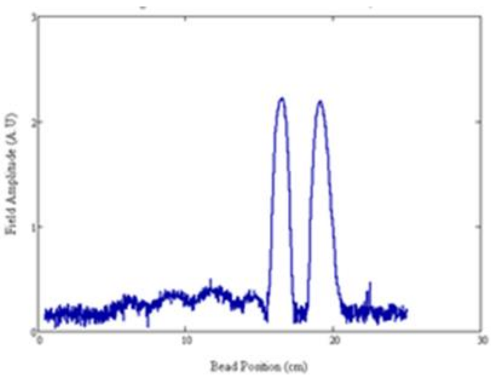

c) π/2 mode, on axis field profile

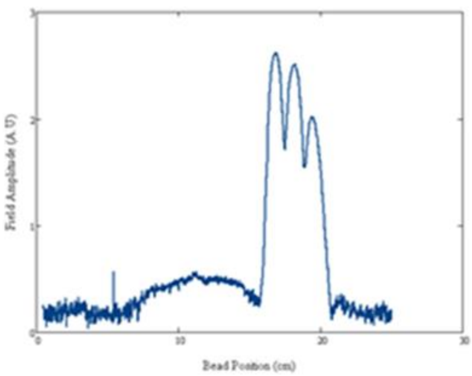

d) Mode 0, on-axis field profile

NTA-ELI

D. Alesini (Resp.)

Not received

NTA-EUROFEL

M. Ferrario (Resp.)

Not received

NTA - IMCA (Innovative Materials and Coatings for Accelerator).

A.Balerna, E. Bernieri, M. Biagini, R.Cimino (Resp.), S. Guiducci, R. Larciprete (Ass.), (LNF-INFN).

The IMCA experiment was started in 2010 in order to develop new materials and coatings with stable and low enough SEY (Secondary Electron Yield) to guarantee full operation of present and future accelerator machines. This issue, in fact, is crucial in controlling Electron Cloud formation and in reducing its effects, that are well known to be a potential bottle-neck to the performances obtainable from particles accelerators. Frascati has a long-standing experience in qualifying materials in terms of surface parameters of interest to e-cloud issues. We are routinely measuring SEY, its dependence from electron energy, temperature and scrubbing dose. We are now able to characterize "in situ" the surface chemical composition and eventual modifications occurring during electron or photon irradiation by using XPS with conventional X-ray source and we are ready to exploit for this purpose the synchrotron radiation beamlines in construction at DAΦNE [1]. Our experimental measurements of the relevant parameters can be also confidently compared to simulations, performed by running the EC codes, in order to elucidate the final consequences on machine performances. Such a combined characterization effort is also suggesting ways to produce low SEY materials coatings. This issue is particularly important in view of the foreseen LHC luminosity upgrades and ILC- Damping ring studies, where e-cloud issues are expected to be present.

We have two running setups: both are now routinely working, operating in UHV conditions being steadily in a vacuum better than 1×10^{-10} Torr after bake-out. The two set-ups are based on a UHV μ-metal chamber, with less than 5 mG residual magnetic field at the sample position. Both are equipped with an Omicron LEED; an electron gun to measure SEY; a Faraday cup to characterize beam currents and beam profiles and both can produce samples with different growing technique inserting them in the measuring system without breaking the vacuum.

One system, built in collaboration with CNR, is designed to deposit thin films and analyze their SEY in connection with XPS at room or higher temperature. This is done by using an Omicron electron analyzer and an X-Ray and a UV Lamps to acquire photoemission spectra and to obtain chemical information on the studied surface. The other system is optimized to perform SEY experiment at cryogenic temperature (down to 8 K) and in connection to angle resolved VUV photoemission studies. For this reason has been equipped over the years with an OMICRON AR65 angle resolving analyzer and a monochromatic VUV source.

In 2013, in collaboration with the major laboratories which are playing an international leading role on the study and characterization of e-cloud effects, we have addressed a series of issues studying different materials. Such activity not only is promoting our Material Science Laboratory in Frascati as one of the most advanced Laboratories in this field, but also provided a quite comprehensive understanding on the physical phenomena governing the SEY and its variations during the various surface modifications.

Some of the most relevant scientific 2013 results are here reported.

1. In close collaboration with CERN, we studied the chemical origin of the scrubbing process of Cu surface representative of LCH beam screen and its dependence on the energy of the primary electrons. We observe a lower efficiency in reducing the SEY when the energy of the scrubbing electrons is less than 20 eV. This may have an impact on the scrubbing strategies for LHC. Also, we finally understand the chemical modification occurring at the surface during electron bombardment. SEY reduction can be assigned to the formation of

graphitic carbon on the surface and low energy electrons seem not to be able to promote such graphitization as the higher energy electrons do. An extensive analysis of those results, first published in 2012 on Physical Review Letters [4] can be found in Physical Review ST-AB 2013 [5].

2. In collaboration with the DAΦNE accelerator division and the DESY vacuum group running PETRA III, we have studied the SEY and the chemical variations of Al samples representative of the two accelerators. PETRA III is a positron ring for very low emittance Synchrotron Radiation and its actual performances seems to be affected by ECE (Electron Cloud Effects). Our study confirms the high SEY value of the Al and that subtle differences in the experimental conditions can affect the reduction phenomenon during scrubbing. The combined SEY and XPS analysis identify in the extremely high reactivity of Al to oxygen the main cause of variability. Due to this reactivity, C does not undergo the graphitization process, as it does on other surfaces, suggesting that Al is not suitable for the construction of accelerators with potential ECE. This work has been published in Physical Review ST-AB 2013 [6].

   Last but not least, in 2013 the proceedings of the fifth electron-cloud workshop ECLOUD12 chaired by R. Cimino and F. Zimmermann has been edited by R.Cimino, G. Rumolo and F. Zimmermann and published as CERN yellow book in 2013. [7].

   In collaboration with the group of Salerno, (formed by S. Petracca, V. Pierro, A. Stabile and F. Velotti) and following the recommendation from group V committee, we start an experimental study on open-cell metal foams. Such materials have been analytically studied and proposed as high synchrotron radiation particle accelerator beam liners for their estimated low gas desorption, their mechanical-structural properties, their expected capability to resist to eddy-current induced stresses,in case of superconducting magnets' failure, their low impedance and possibly low SEY. Experimental validation of all such very promising properties is under way and a student of the University of Benevento, Annalisa Romano will have her master-thesis on this topic.

   Also, the challenges offered by the new high intensity machines show a clear link between e-cloud and wake-fields issues. Within our project, the group of Napoli (formed by R. Fedele, F. Galluccio, M.R. Masullo and V. Vaccaro), is developing a new laboratory method to measure the coupling impedance of high-Q insertion devices below the beam pipe cut-off frequency, when the classical wire method is not reliable. This method should allow a quick and very accurate evaluation of the impedance budget of various insertion structures. The method has been tested on a pill-box cavity and the first results are in good agreement with simulation methods and classical theory so that the collaboration will perform more realistic preliminary tests on UA9 and LHC collimator prototypes.

Conference Talks

- R. Cimino: "Material Science for next generation Accelerator Vacuum systems", Universita' di Napoli, 12-2-2013.
- R. Cimino: "Material Science for next generation Accelerator Vacuum systems", Universita' di Salerno, 6-3-2013.
- R. Cimino: "Material Science for next generation Accelerator Vacuum systems", AIV conference, Catania, 15-5-2013.
- R. Cimino: "status of our understanding of the SEY situation in the LHC ", e-cloud meeting CERN, 22-11-2013.

References

1. LNF Annual Report. This and previous issues.

2. R. Cimino et al., "Experimental efforts at LNF to reduce secondary electron yield in particle accelerators", proceedings of ECLOUD10, 2010.

3. R. Cimino et al., "Can Low-Energy Electrons Affect High-Energy Physics Accelerators?" Phys. Rev. Lett. 93, 14801 (2004).

4. R. Cimino et al., "Nature of the Decrease of the Secondary-Electron Yield by Electron Bombardment and its Energy Dependence" Phys. Rev. Lett. 109 (2012) 064801.

5. R. Larciprete et al. : "Secondary electron yield of Cu technical surfaces: dependence on electron irradiation" Phys. Rev. ST-AT, 16 (2013) 011002.

6. D. R. Grosso et al. : "Effect of the surface processing on the secondary electron yield of Al samples" Phys. Rev. ST-AT 16, 051003 (2013).

7. R. Cimino, G. Rumolo and F. Zimmermann editors: Proceedings of the:"International Workshop on Electron-Cloud Effects (ECLOUD '12)". CERN Yellow Report No. CERN-2013-002 and INFN-12-26/LNF.

NTA-COMB

M. Ferrario (Resp.)

Not received

NTA-SL-EXIN

G. Di Pirro (Resp.)

Not received

The THOMSON SOURCE AT SPARC_LAB

C. Vaccarezza (Resp. Naz.), M.P. Anania (Ass. Ric.), M. Bellaveglia (Art. 23), M. Cestelli Guidi (Art. 23) , D. Di Giovenale (Art. 23) G. Di Pirro, A. Drago, M. Ferrario, A. Gallo, G. Gatti, A. Ghigo, A. Marcelli, E. Pace, L. Palumbo (Ass.), F. Villa (Ass. Ric.).

Participant institutions: other INFN sections (Mi, RM1, RM2, Ba, Ca, Pi, Ts, Fe, Le, Fi, Na, LNS), ENEA-Frascat

In the 2013 the SL-Thomson project has seen the completion of the hardware installation by means of the interaction region finalization and the vacuum connection between the two electron and laser transfer lines.
More over the first steps of the electron beam commissioning have been performed in a few days dedicated shifts between September and October 2013
The SL-Thomson project consists in a monochromatic source of ultra-fast X-ray pulses by Thomson back-scattering (TS) between the SPARC photoinjector high-quality electron beam and the 200 TW laser FLAME laser pulse, see Fig.1. The key points of this configuration are the flexibility and the potential compactness with respect to conventional synchrotron sources.

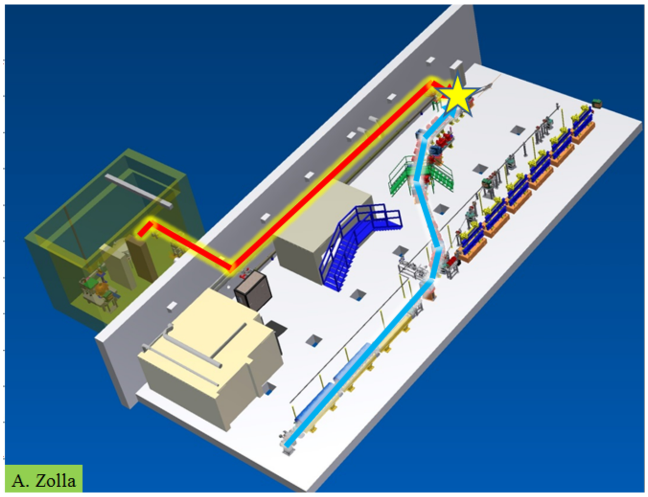

Fig.1 The SPARC-LAB Thomson Source layout

The source is meant to provide X-rays ranging between 20-500 keV able to produce, for example, suitable radiation for medical imaging at the lower energies and the possibility to investigate the inner quantum nature of the Compton process in the higher part of the spectrum.

The Thomson system

To bring the two beams in collision a 30 m long double dogleg electron beamline has been constructed that extracts the electron beam at the exit of the the linac and brings it in the outer bay of the SPARC hall (Fig. 2), while the laser pulse coming from the FLAME building enters the hall behind a protective concrete labyrinth and propagates for around 20 m under vacuum (*10^{-6} Torr*) up to the Interaction Point, Fig. 3. The two beams parameter table is reported below:

- Laser

  - Wavelength 800 nm
  - Compressed pulse energy 5 J
  - Pulse duration/bandwidth 3 -12 (80) ps/nm
  - Rep.Rate 10 Hz
  - Beam quality M2 <1.5
  - Energy stability 10%
  - Pointing stability < 2 µm
  - Synchronization with SPARC photoinjector clock < 1 ps

- Electron Beam

  - Bunch charge 0.2-1.0 nC
  - Energy 28-150 MeV
  - Length 15-20 ps
  - $\varepsilon_{n\,x,y}$ 1-5 µ rad
  - Energy spread 0.1-0.2 %
  - Spot size at IP 5-20 µm
  - Rep.Rate 10 Hz

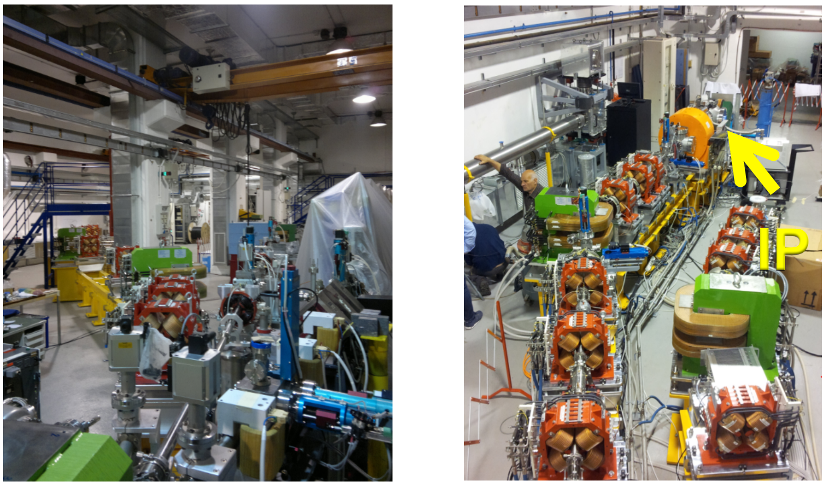

Fig. 2 Pictures of the electron beam line

Fig. 3: Pictures of the photon beam line: the protection wall for the photon pipe insertion (left above), a mirror chamber(left below), the photon beamline inside the SPARC hall.

The Interaction Chamber

A special care has been devoted to the interaction chamber design that in the most compact arrangement provides the housing for both the electron and photon beam focusing systems and for the diagnostic and vacuum pumping as well. In Fig. 4 the CAD 3D design is reported that shows the two beams propagation directions together with the parabolic mirror location (right side) for the focusing of the incoming photons (rightside) while on the leftside the electron beam focusing solenoid is located. In Fig. 5 the Thomson interaction chamber is shown as realized and installed in the beamline.

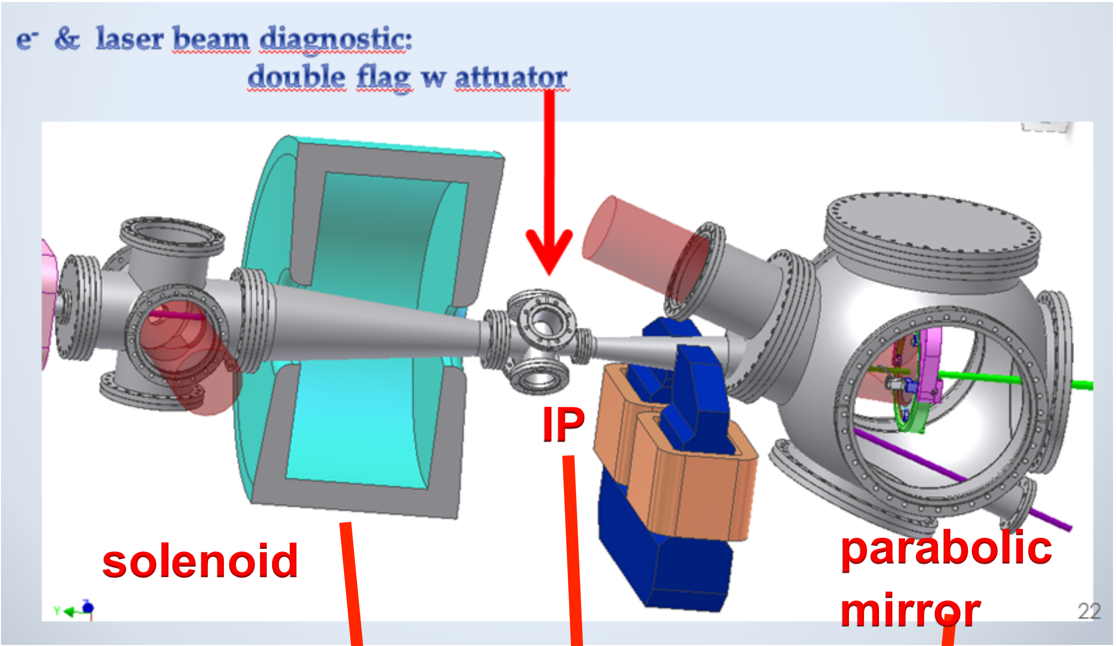

Fig. 4 CAD design of the Interaction chamber.

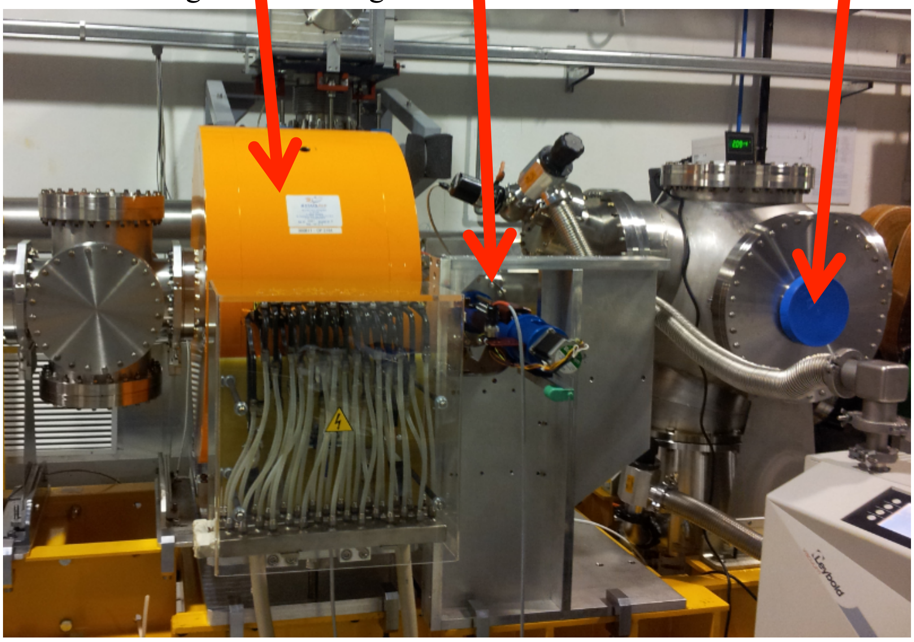

Fig. 5 The installed Thomson Interaction chamber.

Experimental Results

The foreseen first commissoning phase was meant to provide a 200pC electron beam transport at two energies between 80-30 MeV with the final focus obtained by means of the quadrupole triplet upstream the Interaction Point.

The first measurements have been performed in the month of September 2013 with a four day shift: the goal was to transport the electron beam bunches up to the interaction chamber. The measurements have been performed using the electron beam diagnostics of the beam line consisting in fluorescent screen mounted on movable supports for the beam imaging and in Beam Position Monitors to record the beam transverse position along the beamline

Electron Beam transport and measurements

In fig. 6-7 the results of the very first few days of commissioning in September 2013 are reported as the beam pictures grabbed on the Thomson-IP fluorescent screens for two different beam energies: 75 and 50 MeV, while in fig. 8 the beam image on the final dumper screen downstream the IP is reported. The quadrupole focusing has been kept as low as possible in order to minimize the steering effect due to the off-center electron orbit inside the quadrupoles and an rms beam size of σ_x =0.50±0.02 mm and σ_y=0.28±0.02 mm have been obtained as a first attempt at IP for the 150 and 75 MeV beams with a charge Q=230 pC, while a beam size of σ_x =0.18±0.02 mm and σ_y=0.17±0.02 mm has been otained in the 50 MeV case.

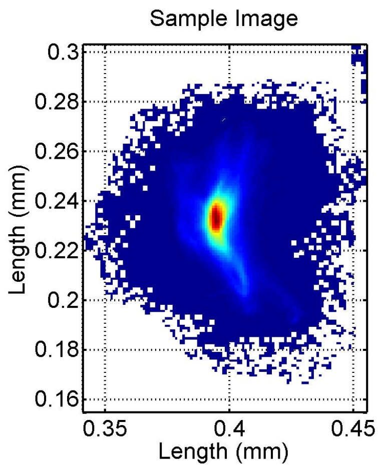

Fig. 6: 75 MeV electron beam on the THMFLG03 screen at the Interaction Point of the SL_Thomson beamline, Q ~ 230 pC, σ_x =0.55±0.02 mm and σ_y=0.36±0.02 mm.

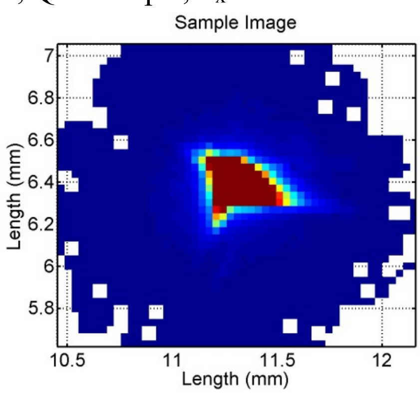

Fig. 7: 50 MeV electron beam on the THMFLG03 screen at the Interaction Point of the SL_Thomson beamline, Q ~ 230 pC, σ_x =0.18±0.02 mm and σ_y=0.17±0.02 mm.

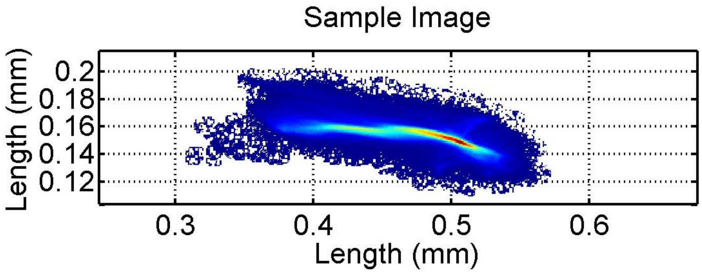

Fig.8: 75 MeV electron beam on the THMFLG04 screen about two meter downstream the final dumper, Q ~ 230 pC, σ_x =1.60±0.02 mm and σ_y=0.34±0.02 mm

Laser Pulse transport @IP

The laser beam transfer line to the interaction region is composed by a series of high reflectivity mirrors inserted in a vacuum pipe 50 m long see fig. 3. The mirrors, 8 inches diameter, are supported by motorized gimbal mounts in order to assure the alignment up to to the off-axis parabola that focuses the laser pulse on the electron beam. The design of the line has been performed with ZEMAX optical code to simulate the effect of the misalignment of the mirrors on the final spot. The FLAME laser beam is extracted from the FLAME target area and guided up to the Thomson IP by means of an under vacuum beamline: the vacuum of the photon beam line is a the level of 10^{-6}Torr suitable for the transport of the compressed laser pulse (≈10fs length) as needed for the plasma acceleration experiment. A concrete wall has been realized in order to stop any radiation draft from the FLAME area towards the SPARC bunker, and to allow people entering in the SPARC hall during the FLAME laser operation and viceversa.

The synchronization system

The Thomson scattering experiment needs an extremely precise synchronization between electron bunch and laser pulse. The relative time of arrival jitter of the two beams is fundamental to obtain a repeatable and efficient interaction. The electrons and photons have to be synchronized with a relative jitter < 500 fs_{RMS}. This is obtained with a standard electrical distribution of the reference signal, already present at SPARC. A Reference Master Oscillator (RMO) with a good phase noise performance (60fs_{RMS}, measured from 10Hz to 10MHz from the carrier) is used to lock the subsystems with different feedback loops.
They can be divided in two general types: slow (bandwidth <10 Hz) and fast (10 Hz to some MHz bandwidth). The formers are used typically to compensate slow drifts caused by thermal elongation of cables and are implemented by means of high resolution stepper motors. The others are designed to compensate the high frequency noise suffered by the systems that is normally due to mechanical vibrations or electrical noise in the RF circuits or power amplifiers (klystron tubes and driver amplifiers).
For the photocathode laser oscillator we have enhanced the performance of the PLL modifying the loop error amplifier, providing a RMO relative phase noise jitter <50fs_{RMS}. We also added a new electronic board to choose the relative delay to the FLAME laser oscillator pulses (already locked to the RMO) to ensure the longitudinal superposition of the electron beam and the photon pulse at the interaction point.

Pubblicazioni:

Petrillo, V.; Bacci, A.; Curatolo, C.; Maroli, C., Serafini.L.; Rossi A.R.
'Time evolution analysis of the electron distribution in Thomson/Compton back-scattering'
JOURNAL OF APPLIED PHYSICS Volume: 114 Issue: 4 Article Number: 043104 Published: JUL 28 2013

Bacci, A.; Alesini, D.; Antici, P.; et al.
'Electron Linac design to drive bright Compton back-scattering gamma-ray sources'
JOURNAL OF APPLIED PHYSICS Volume: 113 Issue: 19 Article Number: 194508 Published: MAY 21 2013

Maroli, C.; Petrillo, V.; Tomassini, P.; Serafini L.
'Nonlinear effects in Thomson backscattering'
PHYSICAL REVIEW SPECIAL TOPICS-ACCELERATORS AND BEAMS Volume: 16
Issue: 3 Article Number: 030706 Published: MAR 27 2013

Petrillo, V.; Chaikovska, I.; Ronsivalle, C.; Rossi, A.R., Serafini L.; Vaccarezza C.
'Phase space distribution of an electron beam emerging from Compton/Thomson back-scattering by an intense laser pulse'
Europhysics Letters Volume: 101 Issue: 1 Article Number: 10008
Published: JAN 2013

NTA-SUPERB

M. Biagini (Resp.)

Not received

ODRI2D: Achievements in 2013

E. Chiadroni (Resp.), M. Castellano (Ass.), D. Di Giovenale (Art. 23), G. Gatti,
R. Pompili (PhD Stud.)

The experiment called ODRI2D aims to determine the transverse emittance in both horizontal and vertical planes in a non-intercepting, non-disturbing way. It studies the angular distribution of the Optical Diffraction Radiation (ODR) resulting from the interference between ODR emitted forward by the first slit (1 mm aperture, normal to the electron beam) and ODR reflected backward from the second slit (0.5 mm aperture, at 45° with respect to the beam). Since the electron beam passes through both slits, this experiment is particularly suitable to be used as online diagnostics for future high repetition rate particles accelerators. In addition, since the ODR angular distribution is sensitive to both beam size and divergence (σ_y and $\sigma_{y'}$), in principle only two stations are required, both non intercepting, to make the equivalent of 4-screen monitor, paving the way to a totally parasitic, single shot, emittance measurement.
The achievements in 2013 concern first the preparation of targets and machining of the holder (Fig. 1), later the installation of the assembled actuator in the new vacuum chamber, placed on the FLASH2 main line after the variable gap undulator (Fig. 2).

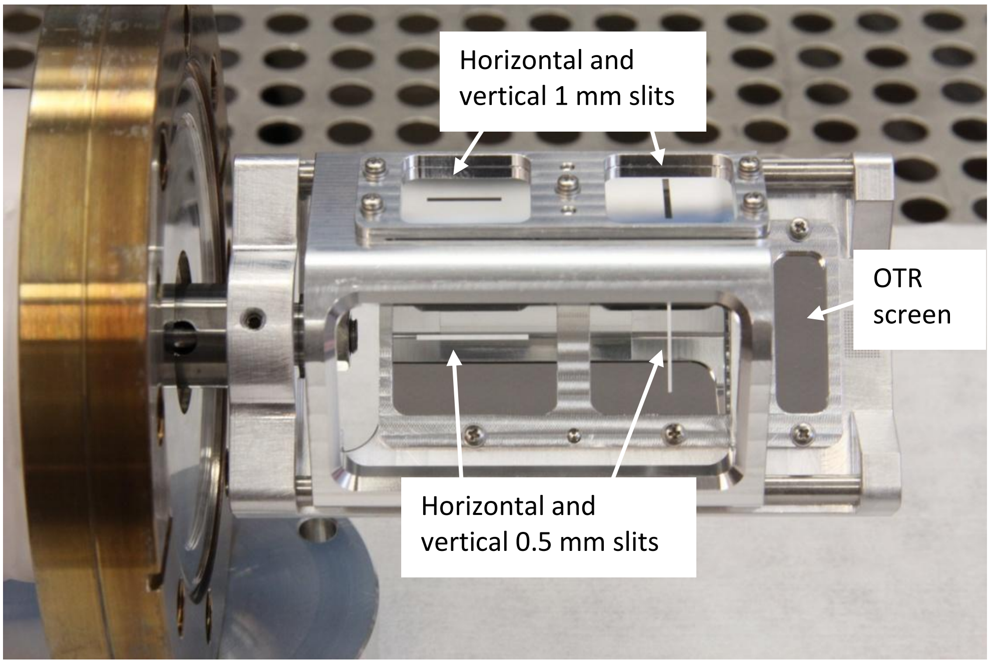

Figure 1:Target holder for both horizontal and vertical emittance measurements.

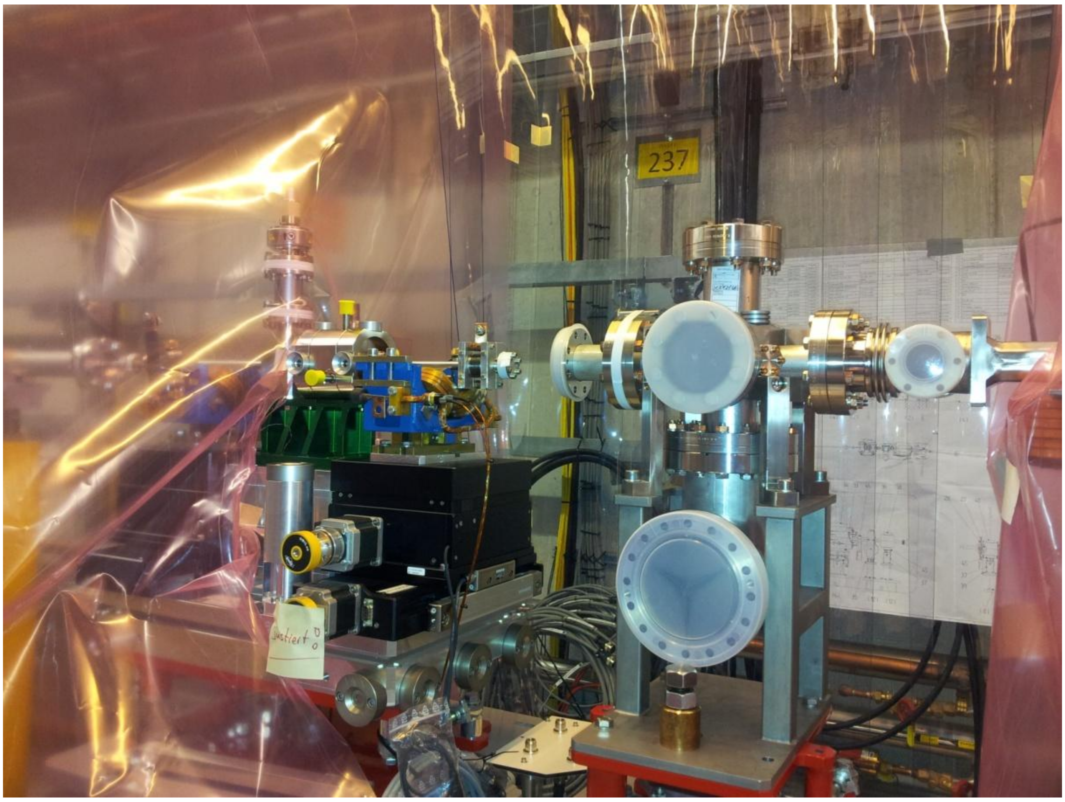

Figure 2: The vacuum chamber housing the holder has been installed on the FLASH2 main line after the variable gap undulator (on the left side of the picture).

RDH activity at LNF in 2013

P. Ciambrone, E. De Lucia, E. Iarocci, I. Mattei, A. Paoloni, A. Sarti, E. Spiriti (Resp.)

1. Introduction

The RDH (**R**esearch and **D**evelopment for **H**adrontherapy) project, approved by the INFN scientific committee fifth, wants to pursue the new phase that Hadrontherapy is entering in Italy after the initial work pionereed at the LNS CATANA INFN initiative. The previous TPS project, approved also by the same scientific committee was also part of the same initial work. The LNF group is involved in the WorkPackages WP5 (Dose monitoring for hadrontherapy) and WP6 (Nuclear fragmentation studies for hadronthrapy) out of the eight in which the RDH project is organized.

The first activity, described in paragraph 2, involves different italian research groups from INFN and "La Sapienza" University in Rome, INFN and Pisa University, INFN Milano and the LNF INFN Laboratory. For what concern the activity in the Carbon nuclear double differential cross section studies, describd in paragraph 3, the group is part of the FIRST (**F**ragmentation of **I**ons **R**elevant for **S**pace and **T**herapy) international collaboration that includes various Italian Universities and INFN centers and research groups from France, Germany and Spain.

The last paragraph briefly describe the studies underway to improve the performances of the detectors used in the past in the FIRST experiment. In particular the sensitivity of the analog monolithic pixel sensors to the released charge from different Z nuclear fragments.

2. Dose monitoring for hadrontherapy

2.1 Introduction

Hadrontherapy is becoming a valuable option in the clinical treatment of solid tumors, using accelerated protons or carbon ions. Several new centers based on hadron accelerators are operational or under construction. The main advantage of this technique, in comparison to the standard radiotherapy with x-ray beams, is the better localization of the irradiation dose in the tumor-affected region sparing healthy tissues and possible surrounding organs at risk. This feature can be achieved because the heavy charged particles loose most of the energy at the end of their range, the Bragg peak (hereafter BP), in comparison to the exponentially decreasing energy release of the x-ray beam. Up to now most of the patients have been treated at centers with proton beams, but routinary use of carbon beams has now started.

New dose-monitoring techniques need to be developed and introduced into clinical use, to meet the improved capability of hadrontherapy to match the dose release with the cancer position. The R&D effort of our group has been then focused to develop novel imaging methods to monitor, preferably in real time, the three-dimensional distribution of the radiation dose effectively delivered during hadrontherapy. This holds true especially for treatments using carbon ion beams since the dose profile is very sensitive to anatomical changes and minor patients' positioning uncertainties. Conventional methods for the assessment of patients' positioning used in all x-ray-based radiation therapy, where a non-negligible fraction of the treatment beam is transmitted through the patient, cannot be used to pursue this task due to the different physics underlying.

The only technique that has been used in a clinical environment so far exploits the collinear emission of photons due to positron annihilation, this is induced by β + decay of several radioactive isotopes (mostly 11 C 15 O) produced as a consequence of projectile and target nuclear fragmentation. This approach, in its first formulation, was performed only after the irradiation. Other techniques have been recently proposed exploiting other secondary radiation sources, such as: prompt photons, emitted after nuclei de-excitation, or charged particles, emitted at large angles after target fragmentation. The correlation of the prompt photons emission shape with the beam path is known in literature both for proton or ^{12}C beam [1], [2], [3], [4], [5] while only recently the correlation of the charged particle emission shape with the released dose has been established [6], [7], [8], [9].

Therefore the measurement of the fluxes of the secondary particles produced by the hadron beam is of fundamental importance in the design of any dose-monitoring device and is eagerly needed to tune Monte Carlo simulations.

The activity of our group has been focusing on these flux measurements, on dedicated Monte Carlo simulation based on the FLUKA software and on the desing and realization of an integrated monitoring system to detect both prompt photons and charged particles, the Dose Profiler, for online dose monitoring in hadrontherapy applications . Feasibility measurements on beam have been performed at LNS-INFN, CNAO and GSI (Darmstadt) laboratories [4],[6],[7],[10],[11].

2.2 The Dose Profiler

The Dose Profiler (DP) has been designed to collect information from prompt neutral and charged radiation, produced during the radiotherapy treatment with protons or carbon ions. Its twofold operation principle will allow to maximize the information on dose deposition, regardless the ion beam in use. Its final purpose is the measurement of the Bragg Peak position. The detector, working as a charged particle tracker and a Compton camera, is made of three sub-detectors: (i) a scintillating fibers tracker, (ii) a plastic scintillator absorber and (iii) a LYSO calorimeter. The tracker, with 6 low-Z scintillating fiber planes with two views, will provide a fast response on the dose pattern, analyzing the emission region of charged particles, mainly protons, and of prompt photons produced from the beam interaction with the patient tissue. Both the charged and the neutral emission shapes can be correlated with the spatial dose release and the Bragg peak position, through calibration with data and corresponding Monte Carlo (MC) simulation. The low-Z plastic scintillator absorber will: reduce the backscattering probability of low-energy electron on LYSO, and therefore tracking inefficiencies; b) prevent low-energy electrons from arriving to the LYSO calorimeter, avoiding photon/electron cluster identification. The high-density LYSO calorimeter will not only detect the neutral secondary component but also measure the energy of charged particles. This information, even with a poor resolution, will be used to weight differently particles that undergo different MS effect inside the patient. Figure 1 shows the operation principle of the dual scheme.

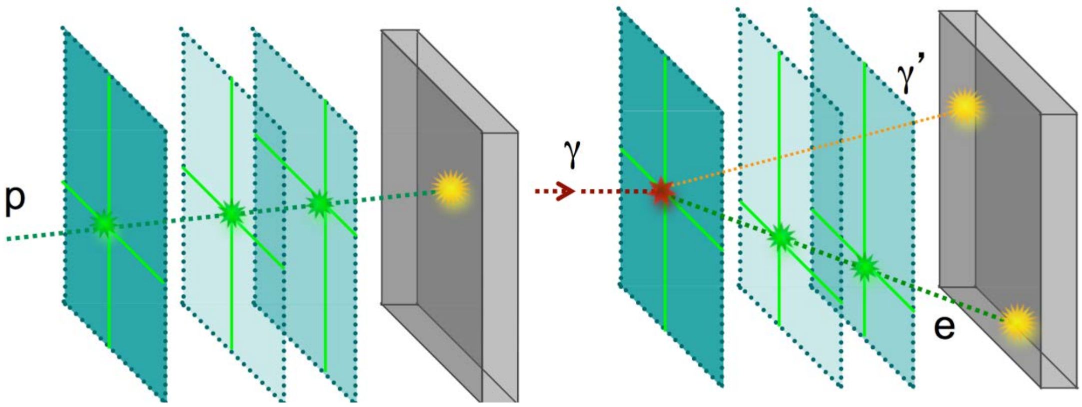

Figure 1: Detection of secondary proton and Compton interaction in tracker

Since the main contribution to the uncertainties on charged particle track reconstruction is due to multiple scattering (MS) through several centimeters of patient tissue, the tracker has been designed to have a spatial resolution of few millimeters. The expected mean value of the electron kinetic energy is few MeV, thus the material budget crossed by electrons must be kept as low as possible to reduce MS straggling, therefore asking for low-Z light material usage.

A decrease of prompt photon emission beyond the Bragg peak was observed by several authors including some of the members of this group [1], [2], [3], [4], [5], confirming a correlation with the beam range and the Bragg peak location. The experimental challenge is therefore the backtracking of few MeV photons, and in this project the photon main interaction process at these energies, the Compton scattering on the

Tracker planes, will be exploited. The neutral mode operation, given the prompt photon measured energy spectrum ranging between 1-10 MeV [4], asks for a careful study and optimization of the tracker materials. At the same time, Compton scattered photon must be detected as well in the high-Z, high density LYSO crystal, to reconstruct its momentum and to close Compton scattering kinematics together with the electron momentum information.

Compactness, reliability, large geometrical acceptance and high tracking efficiency represent the minimum requirements of such detector, considering its foreseen use into clinical workflow.

2.3 Layout optimization

A detailed simulation of the detector has been developed in order to study separately, and with the required precision, the crucial cornerstones eagerly needed for the project development, such as: sub-detector materials, Compton scattering cross section, total readout channels, maximum acceptable angular straggling, reconstruction software training and DP performance benchmarking. In order to find the best DP layout, several configurations with different fiber thickness and spacing between planes have been studied, together with different absorber and LYSO crystal thicknesses and acceptances. The MC software used for the simulations is FLUKA (release 2011.2) [12], [13]. MC data have been organized in ROOT–trees, mirroring the foreseen DAQ output format. In order to find the best tradeoff between spatial resolution and available statistics, a DP realistic geometry has been simulated including: i) tracker planes, each one consisting of 2 orthogonal layers providing the 2D coordinates, for a total of 6x2x256 scintillating fibers; ii) front–end electronic frames; iii) electron-absorber scintillating calorimeter; iv) LYSO calorimeter; v) calorimeter MAPMT photocathode; vi) aluminum frame enclosing the entire detector.

Due to its dual–mode functionality, the simulation allows to choose primary particles: photons and protons are simulated with energies extracted from [4] and [6], [7] secondary particle spectra measured by members of our group. Events are then selected using a realistic trigger condition: at least three tracking planes must be fired or an energy release of $E_{rel} \geq 100$ keV must be detected inside the LYSO calorimeter or in the absorber plane. For each energy release (or track, using the MC nomenclature) the following information is stored: particle ID, charge, mass, type; detector element number; time; initial and final momentum; spatial coordinates of the beginning and the end of the current track in each element of the detector. Moreover, the same information is also recorded at each detector boundary crossing. Quenching effect in the scintillators has been included in the MC according to [14]. Optical photon production and transport inside the LYSO calorimeter has been taken into account. The simulations were performed with a DELL OPTIPLEX 980 with 4 CPUs at 3.6 GHz.

Detector capabilities and criticalities have been assessed with an isotropic photon point-like source and a simplified human head with a proton source inside. The Dose

Profiler layout has been optimized limiting the multiple scattering effect in the tracker layers, increasing the absorber stopping efficiency and minimizing the contribution due to uncertainty on the reconstructed Compton scattered photon depth of interaction inside the calorimeter. For the tracker, scintillating fibers 0.5 x 0.5 mm^2 have been chosen with a 2 cm plane separation and SiPM readout for a total of 128+128 readout channels/plane and 19.2x19.2 cm^2 sensitive area per plane. The absorber will be made of 2x16x(12,5x7,5x200) mm^3 plastic scintillator bars readout by wavelength shifter fibers and SiPM. For the calorimeter 4x4 LYSO matrices will be used with a 1,9x1,9x16 mm^3 active area.

The preliminary results, although obtained with Monte Carlo data only, are very promising showing a spatial resolution on the reconstructed dose release position of the order of 5÷6 mm for promt photons and 2÷3 mm for protons.

3.1 Nuclear fragmentation studies for hadrontherapy

The FIRST collaboration goal is the measurement of fragmentation double differential cross sections on thin targets: projectiles and targets are defined accordingly to the different possible applications (Hadrontherapy or Space Safety).

The LNF group is actively contributing to the FIRST collaboration: E.Spiriti is a member of the Collaboration Board while A.Sarti is the physics analysis coordinator. A first data taking took place in August 2011 at GSI: several millions of collisions of Carbon ions with a thin Carbon or Gold target have been acquired. The relative data-set is currently being analyzed.

The main analysis tasks performed within the LNF group are related to:

- The ToF wall calibration. The Time of Flight (ToF) wall is a scintillator wall, 6 meters after the target, that measures the fragments time of flight and also perform a fragment identification by studying the particle released energy as a function of the ToF. The calibration of innermost modules, heavily irradiated by the small angle fragments that are the most energetic and more abundant, is a tough task, complicated by the presence of module discontinuities. The LNF group has deployed a strategy and the software tools needed to inter-calibrate the ToF response with the information from the VTX detector allowing to properly take into account modules dishomogeneities.

- The VTX detector particle ID algorithms development. The mimosa silicon detector used to reconstruct the fragment tracks just after the target interaction can be used to disentangle heavy and light fragments based on the number of pixels that are fired and attached to a given track for each event. The LNF team took care of the inter-calibration of such fragment ID algorithm, based on the VTX pixels number, using the ToF Z Id calibrated distributions, reducing significantly the cross feed between high and low Z fragments.

- The full MC validation. The MC simulation, developed in Fluka, has been updated to match with the observed data distributions: such validation performed on all the different detectors, has been carried out with the help of the LNF team.

- The mass fit development using unbinned likelihood techniques. In order to measure the cross sections as a function of the fragments production energy and angle, the fragments mass has been chosen as observable: in this way the combinatorial background as well as the contribution from different isotopes can be accounted for, by fitting the invariant mass distributions. The LNF team has developed the technology needed to fit the mass distributions and extract the yields as a function of the fragment ID to be used in the cross section calculation.
- The computation of the cross sections. The LNF team has developed the algorithm to compute the full energy and angular cross sections: the calculations of the efficiencies and the correction for the cross feed contribution has been developed and tested against the events full simulation.

Figure 2 shows the preliminary measurement performed on 22M carbon ions collisions on a carbon target at GSI, for a production angle with respect to the beam direction in the range 1 to 5 degrees. The uncertainties shown in each bin are statistical only.

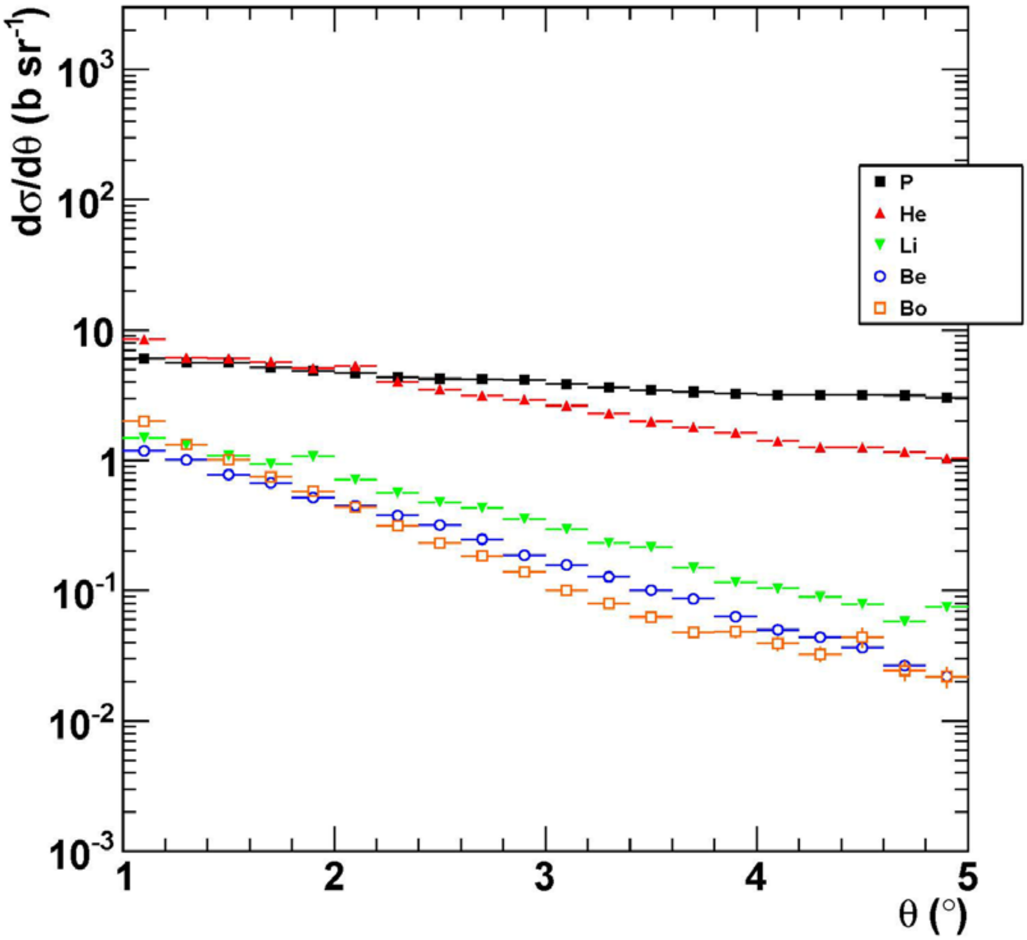

Figure 2: Preliminary measurement of fragmentation cross section as a function of production angles for Z = 1 to Z = 5 fragments in Carbon ion collisions on Carbon target. Uncertainties are statistical only.

Currently the analysis works is aiming to the evaluation of the systematics related to the measurement of the cross sections. The main systematic contributions are expecte from the fragment Z identification, performed using the VTX and ToF wall detectors, the efficiency evaluation (done using the full MC simulation) and the fragment cross feed correction. The measurement is completely systematically dominated and the proper evaluation of this contribution is the final and most important piece before the publication of the result.

Some preliminary results have been presented last October at Seoul [15],while an article is begin prepared and will be published soon.

4.1 Analog MAPS sensitivity to low Z fragments released charge

The FIRST VTX detector used four planes of MAPS (**M**onolithic **A**ctive **P**ixel **S**ensor) with a digital readout. As underlined in the previous paragraph some particle ID were possible regardless the really tiny thickness of the sensitive region. To better evaluate the sensor response to different low Z (Z=1 to Z=6) impinging ions from the particle ID point of view a specific measurement at the Catania (INFN LNS) ion bam at 62 MeV/nucleon energy could not take place due to a fault at the Cyclotron cryogenic system.

Some simulation work to define the design of the measurement was done with the Fluka package with the collaboration of C. Morone from the Rome Tor Vergata University. The available ions 12C was planned to produce (the experimental setup is shown in the pictorial view of the left part of Figure 3) on a PMMA target (blue area), with a thickness slightly larger than the Bragg peak position, all possible fragments at all possible energies.

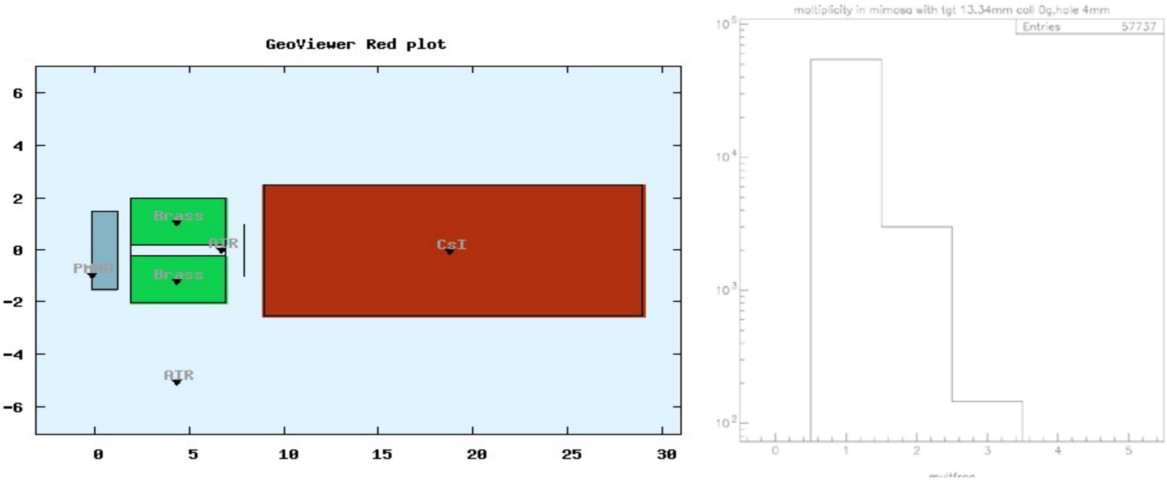

Figure 3: Left side: pictorial view of the simulated setup. Right side: impinging fragment multiplicity in the 3ms integration time of the M18 (Mimosa 18) sensors.

To minimize the fragment multiplicity in the pixel sensor a collimator has been defined with the simulation (green area), then the multiplicity in the Mimosa 18 sensor (thin black area) is shown in the right part of Figure 3. The high spatial resolution of those sensors due the 10 μm pitch and the analog amplitude information they provide could easily allow to disentangle the events with more than one fragment. Those events should be rejected because the following Cesium Iodide sensor (red area) could only measure the energy of the single fragments. Then also the foreseen rate for the different fragments produced was evaluated showing that a reasonable statistics could be acquired in the available beam time.

As soon as the cyclotron will restart, next June, the measurement described will be rescheduled.

References

[1] E. Testa et al., Dose Profile monitoring with carbon ions by means of prompt-gamma measurements, Nucl. Instrum. Meth. B 267 (2009), 993.

[2] C. H. Min et al.,Prompt gamma measurements for locating the dose fal loff region in the proton therapy, Appl. Phys. Lett. 89, 183517 (2006).

[3] M. Testa et al., Monitoring the Bragg peak location of 73 MeV/u carbon ions by means of prompt γ -ray measurements , Appl. Phys. Lett. 93, 093506 (2008).

[4] C. Agodi et al., Precise measurement of prompt photon emission for carbon ion therapy, JINST 7 (2012), P03001 and arXiv:1110.3736v1.

[5] Min, C. H., J. W. Kim, M. Y. Youn, and C. H. Kim, 2007, "Determination of distal dose edge location by measuring right-angled prompt-gamma rays from a 38-MeV proton beam," Nucl. Instrum. Methods Phys. Res. A 580, 562–565.

[6] C. Agodi et al., Charged particle's flux measurement from PMMA irradiated by 80 MeV/u carbon ion beam., PMB 57 (2012) 5667.

[7] C. Agodi et al., Measurement of charged particle's yields from PMMA irradiated by a 220 MeV/u 12C beam, to be submitted for publication.

[8] Gwosch K. et al., Non-invasive monitoring of therapeutic carbon ion beams in a homogeneous phantom by tracking of secondary ions ., PMB 58 (2013) 3755, 3773.

[9] B. Braunn, et al. Nuclear reaction measurements of 95MeV/u ^{12}C interactions on PMMA for hadrontherapy , Nucl. Ins. And Methods B, 269, 22, 2676-2684.

[10] C. Agodi, et al., Study of the time and space distribution of β^+ emitters from 80 MeV/u carbon ion beam irradiation on PMMA, Nuclear Inst. and Methods in Physics Research, B 283 (2012), pp. 1-8.

[11] F. Bellini, et al., Extended calibration range for prompt photon emission in ion beam irradiation, Nuclear Inst. and Methods in Physics Research, A 745C (2014), pp. 114-118.

[12] G. Battistoni et al., The FLUKA code: Description and benchmarking, Proceed. of the Hadronic Shower Simulation Workshop2006, (2007), aIP ConferenceProceed. 896 (2007) 31,49.

[13] A.Ferrari, P.R.Sala, A.Fasso', J.Ranft, FLUKA: a multi particle transport code, Tech. Rep. CERN- 2005-10, INFN/TC05/11, SLAC-R-773 (2005).

[14] Y. Koba et. al., Scintillation Efficiency of Inorganic Scintillators for Intermediate-Energy Charged Particles, Prog. Nucl. Sci. Tech. (2011), Vol.1 218.

[15] Seoul, 2013, IEEE/NSS/MIC/RTSD conference, ``Experiment FIRST: Fragmentation of Carbon Beam at 400 MeV/u''

SL-BEATS2

C. Vaccarezza (Resp.)

Not received

SL-POSSO

S. Dabagov (Resp.)

Not received

SLEAR

F. Celani (Resp.)

Not received

SL_Femtotera: Achievements in 2013

E. Chiadroni (Resp. Locale), M. Cestelli Guidi (Art. 23), A. Nucara (Ass.), G. Gatti,
C. Ronsivalle (Ass.)

The experiment called SL_Femtotera aims at the characterization of advanced THz sources, broad-band (0.15-5 THz) and narrow-band, featuring high peak and fs pulse duration, as both linac and laser based.

The linac-based THz source is produced at SPARC_LAB through radiative phenomena based on relativistic electron bunches as short as 100 fs, produced and manipulated at the SPARC high brightness photo-injector.

Taking advantage of the advanced electron beam manipulation techniques, well-established at SPARC_LAB, both broadband and quasi-narrow band THz radiation is produced for several purposes, e.g. as electron beam longitudinal diagnostics, linear and non-linear spectroscopic applications thanks to the high electric (MV/cm) and magnetic (0.5 T) fields associated to the SPARC THz radiation.

In 2013 a second THz station, placed at the linac exit, has been commissioned at SPARC LAB, housing targets for the production of both Coherent Transition and Diffraction Radiation (CTR and CDR, respectively). Both sources are currently characterized by measuring the radiation spectrum in air both through a set of discrete custom THz filters, placed in front of a THz detector, and an interferometer, either Martin-Puplett, with wire grids to select polarizations, or Michelson, with a 12 μm Mylar beam splitter. Pyrodetectors are used in this case. From the point of view of narrowband THz emission, a train of high brightness electron bunches has been produced and manipulated by means of the laser comb technique, as shown in Fig. 1a) and Fig. 1b). The corresponding autocorrelation function, as measured by a Michelson interferometer, is reported in Fig. 1c), showing the multi-peaked signature characteristics of a multi-bunch train of electrons. The normalized form factor clearly presents peaks at the frequency corresponding to the comb repetition rate and higher harmonics (Fig. 1d).

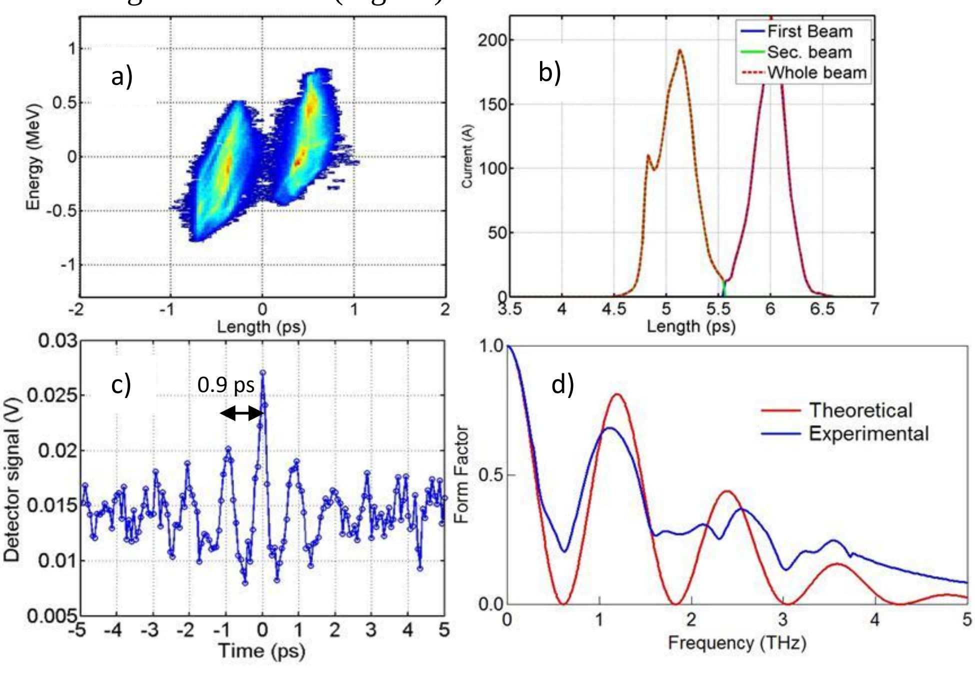

Figure 1: a) Measured longitudinal phase space of a 2-bunches train; b) Measured electron beam current profile. c) Measured autocorrelation function of CTR with a Michelson interferometer; d) measured CTR form factor (blue line) compared with the one expected by double peaked longitudinal distribution (red line).

In 2013 we have also started the activity concerning the development of a laser-based THz source. We have first used the IR part of the SPARC photo-cathode laser, 200 fs long, to generate, via optical rectification, broadband THz pulses, whose shape resembles the optical pulse envelope. The experiment was performed using a bolometer (operating at 4.2 K) to measure the THz radiation produced by a ZnTe crystal (thickness of 1mm). Figure 2 shows the working principle, the measured energy spectrum and the experimental apparatus.

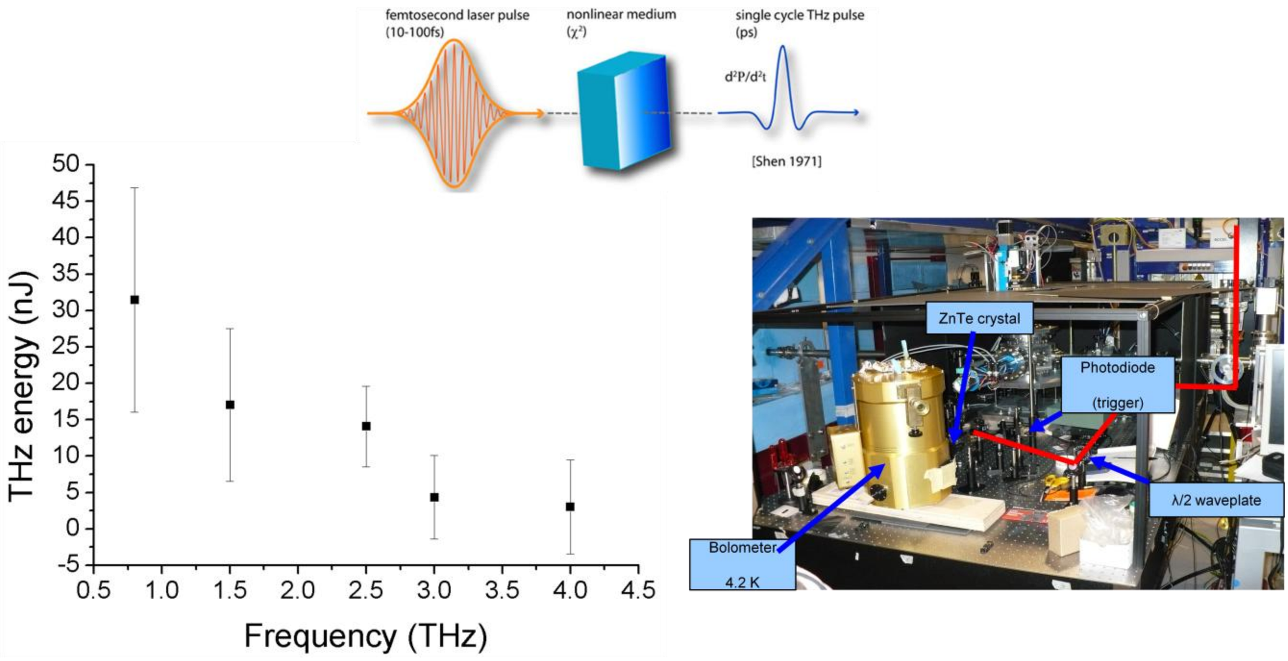

Figure 2: Optical rectification working principle (top), measured energy spectrum (left) and experimental apparatus (right).

Invited Seminar

- E. Chiadroni, *The SPARC_LAB High Peak Power THz Source: Different Methods of Generation and Characterization*, presented at the IRMMW-THz 2013 in Mainz on the Rhine, September 1st – 6th 2013.

- E. Chiadroni, *The SPARC_LAB THz Source driven by High Brightness Electron Beams*, presented at the XCIX Congresso Nazionale della Società Italiana di Fisica, Trieste, September 23rd – 27th 2013.

Publications:

- E. Chiadroni et al., Rev. Sci. Instrum. **84**, 022703 (2013); doi: 10.1063/1.4790429.

- E. Chiadroni et al., Appl. Phys. Lett. **102**, 094101 (2013); doi: 10.1063/1.4794014.

- E. Chiadroni, *The SPARC_LAB THz Source driven by High Brightness Electron Beams*, submitted to Nuovo Cimento C on January 31st 2014, being awarded as “II Premio come Migliore comunicazione alla SIF 2013”, in Section 7a – Fisica degli Acceleratori.

SPACEWEATHER

M.A.Franceschi, T. Napolitano, M.Ricci (Resp.), B.Spataro

The SPACEWEATHER experimental program is devoted to the exploration - through dedicated space missions - of three main research fields:

1. Interaction between terrestrial geophysical events and Earth radiation belts.
2. Physics of the space environment in Earth orbits.
3. Biomedical effects of space radiation on human body.

The main scientific objectives, the instruments and the overall experimental program (missions SI-RAD and ALTCRISS) have been described in detail in the previous reports. Starting from 2013, most of the activity has been dedicated to the project CSES/LIMADOU for the study of the correlation between seismic events and perturbation of the Van Allen belts (Italian-Chinese mission CSES, Chinese Seismo-Electromagnetic Satellite).
The mission CSES, presently in preparatory phase and object of international agreements between INFN, ASI and Chinese Agencies, consists of the realization of a series of detectors (mini-magnetic spectrometer, detector of electric field, detector of magnetic field, detector of low frequency electromagnetic waves). They are designed to study the fast variations of the proton and electron fluxes trapped in the radiation belts due to perturbations caused by seismic events.
The Italian collaboration (Roma Tor Vergata, LNF, Perugia, Bologna, Trento) has the responsibility of the realization of the Electrical Field Detector (EFD) and the High Energy Particle Detector (HEPD).
The objectives of the Project CSES cover several aspects: scientific, engineering and application ones.
The objectives in the scientific aspect of the project are to study the ionospheric perturbations possibly associated with earthquakes and to explore new approaches for short-term and imminent prediction.
The objectives in the engineering aspect of the project are to check the reliability and effectiveness of the proposed electromagnetic satellite monitoring system by utilizing a set of new techniques and equipment, in order to obtain world-wide data of space environment of the electromagnetic field, plasma and energetic particles.
The objectives for the aspect of application of the project are to extract the electromagnetic information possibly associated with the earthquakes of M≥6 within Chinese territory and its neighboring area (1000 km) and that of M≥7 in the global scale; to analyze the features of seismo-ionospheric perturbations, in order to test the possibility for short-term earthquake forecasting experimentally in terms of satellite observation; to provide the data sharing service for international cooperation and scientific community.
In brief, the mission contents of CSES can be summarized as:

1. Measurement of signals from electromagnetic emission and its perturbations in inonosphere;
2. Measurement of the disturbance of plasma in ionosphere, such as: contents, density and temperature of the ions, density and temperature of the electron, total electron contents, etc.
3. Measurement of energetic particles precipitations

Roma Tor Vergata and LNF are in charge for the EFD (design, test, qualification, analysis). After the test and characterization of different sensors by an analog board made in 2012, a complete prototype of the EFD has been realized in 2013, able to measure the electrical signals for 5 frequency-bands, from about constant to 5 MHz.

The detector is composed of a high precision mechanical sphere containing the sensor and an electronic system with the front-end, the digitalization part and a FPGA for data treatment. After a complete set of tests, in the second part of the year a work started for the realization of a second sphere for differential measurements and 4 complete electronic channels.
Work is in progress for further implementation of the DAQ software and for the definition of the work packages to prepare the required documentation and the Technical Design review.
This program has been selected to be funded by the MIUR in the context of the programs "Premiali".

DAΦNE

The DAΦNE Team
D. Alesini, M.E. Biagini, M. Boscolo, B. Buonomo, S. Cantarella (Art. 23), A. De Santis (Art. 23), G. O. Delle Monache, A. Drago, L. Foggetta (Art. 23), O. Frasciello (Ph.D stud), A. Gallo, A. Ghigo, F. Guatieri (Bors.), S. Guiducci, F. Iungo, C. Ligi, G. Mazzitelli, C. Milardi (Resp.),L. Pellegrino, M. Petrarca, R. Ricci, U. Rotundo, C. Sanelli, M. Serio, A. Stecchi, A. Stella, M. Zobov [INFN/LNF]
S. Bini, R. Gargana, A. Michelotti [Cabibbo Lab]

The DAΦNE Technical Staff
G. Baldini, P. Baldini, A. Battisti, A. Beatrici, M. Belli, B. Bolli, L. Cacciotti, G. Ceccarelli, R. Ceccarelli, A. Cecchinelli, S. Ceravolo, P. Chimenti (Ass.), P. Ciuffetti, R. Clementi, O. Coiro, S. De Biase, M. De Giorgi, T. Di Domenico (Bors.), R. Di Raddo, G. Ermini, M.R. Ferrazza, G. Fontana, U. Frasacco, C. Fusco, F. Galletti, E. Gaspari, M. Giabbai, O. Giacinti, E. Grossi, F. Iungo, V. Lollo, M. Marchetti, C. Marini, S. Martelli (Art. 15), M. Martinelli, A. Mazzenga, C. Mencarelli, M. Monteduro, M. Paris, E. Passarelli, S. Pella, D. Pellegrini, G. Piermarini, S. Quaglia, M. Rondinelli, L.A. Rossi (Art. 15), M. Sardone, M. Scampati, G. Sensolini, R. Sorchetti, A. Sorgi, M. Sperati, A. Sprecacenere, S. Strabioli (Art. 15), R. Tonus, T. Tranquilli, M. Troiani, V. Valtriani, R. Zarlenga, A. Zolla

1 DAΦNE activities during 2013

The activities on the DAΦNE collider has been aimed at implementing the upgrade for the KLOE-2 detector. The six months shut-down gave a very useful opportunity to revise the design of the Interaction Region (IR) in terms of mechanical structure and diagnostics as well as to implement a general refurbishing program involving the whole accelerator complex in order to ensure the largest possible up-time (>80%) during the next KLOE-2 physics run.

1.1 New IR installation

The revision of the IR implied several activities in addition to the installation of the new detectors and the relative cabling which has been mainly done by the KLOE collaboration. The main IR evolution with respect to the one used for the KLOE-2 test run can be summarized as follows:

- single vacuum chamber tapered in the section common to the two beams;
- new bellows with improved design to increase robustness;
- additional water cooling near the Interaction Point in order to avoid critical rise of temperature close to the new KLOE-2 Inner Tracker (IT);
- new beryllium screens closer to the beam baseline substituting the old damaged ones;
- temperature probe added in order to have a precise monitoring of the heat dispersion along the beam pipe;

- new shields: tungsten cylindrical shields added around the external legs of the IR and lead toroidal shields in front of the first low-β quadrupole from the IP in order to decrease the amount of background hitting the KLOE-2 detector;
- two new Beam Position Monitor (BPM) symmetrical with respect to the Interaction point (IP) in order to increase the diagnostic in the low-beta region otherwise relying on KLOE information only.

Several modification involved also the mechanics of the IR:

- The cylindrical supports at the two edges of the KLOE Drift Chamber have been completely redesigned in order to stand the additional weight coming from the new detector layer and to accommodate the larger amount of cables coming from them,
- additional carbon-fiber support added to increase the structure stability thus reducing the IR vibration observed during the previous test run with simplified KLOE-2 setup;
- insertion tools have been deeply modified to cope both with the heavier and bulkier of IR the new KLOE-2 detectors and with the enormous amount of cables required for the data acquisition;
- modification of the tail support of the girder;

The assembly of the new IR took place between January and June in a reserved area in the DAΦNE Hall. One of the biggest issue was the short time allocated for every task (almost no contingency). A very aggressive planning and a strong commitment required to be on-time.

The installation has been completed according the schedule. However the first days of operation, started by the end of June, outlined a severe installation error, two out of four permanent dipoles in the IR sections inside the KLOE detector were mounted with wrong orientation. The problem was immediately addressed and solved in order to have the main rings fully operational for the commissioning phase already by the half of September.

1.2 DAΦNE consolidation

The DAΦNE accelerator complex has been working since more than 15 years. Operation during years 2011/2012 has clearly shown that an extraordinary consolidation effort was required in order to provide a secure and reliable data taking for the KLOE-2 experiment with at least 80% up-time. The consolidation effort can be summarized as follows:

- revamping of the DAΦNE auxiliary services;
- upgrade of the control system;
- substitution of supplies for the skew correctors;
- improved diagnostic in the accelerator complex;
- new power supplies for e-cloud suppression providing higher voltage;
- new kicker for the horizontal transverse feedback in the electron ring;
- new scrapers control devices;
- new LINAC Gun;

Figure 1: *New IR assembly and intallation phase. First row: external legs already assembled (left); detail of the region between IP and low-β quadrupoles, copper pipes of the new cooling system and inlets of new BPMs are clearly visible (right). Second row: assembling of the second legs of the IR after KLOE-2 Inner Tracker installation, welding already performed (left); final assembly with all KLOE-2 detectors installed (right). Third row: lifting of the IR fully assembled with detector already cabled (left); IR fully inserted and beam pipe reconnected, the additional struct added to the IR support is the vertical one (right).*

In addition all the DAΦNE subsystems have been maintained and often mended like the magnets power supply (450 devices) or the magnets that had a faulty behaviour during KLOE-2 test run (e.g. injection septa). Magnets of the IR have been realigned; Main Rings ion pumps cabling and related HV power supply has been checked. For the LINAC several intervention took place: replacement of damaged flag windows, replacement of equipments with vacuum leaks

(RF loads and valves), maintenance of modulators and RF equipments, spares availability and functionality checks.

The entire auxiliaries service (cooling, RF power, vacuum) has been revised. A new low level control system has been implemented with new commercial PLCs. Decommissioned components from older devices are now available as spare parts for other units. Single point control system has been developed in order to collect all the information from the entire complex in a local server providing alert in case of faults and logging all the information for offline analysis of system performance. Server has a web-based interface accessible from the internal LNF network.

The upgrade of the DAΦNE control system has the following objectives: improve the existing infrastructure in order to move all the control processes from VME embedded processor to virtual machines; replace the old Sun Solaris servers with new HW based using Linux OS; migrate control processes from the old MacOS7 based platform to new one based on Linux (VMIC or Virtual Machines). This upgrade required the installation of new blade servers hosted in the LNF CED and new network infrastructure inside DAΦNE and a general review of software.

Diagnostic in the DAΦNE Main Rings have been improved by installing four new BPMs and new syncrotron light monitor CCD cameras. The new CCD gated camera provide a faster and cleaner measurements of the transverse beam size. Two BPMs are close to the IP, to measure beam parameters in the low-β region, while the other two have been installed before the injection septa in order to monitor the dispersion in the injection section.

RF system has been fully maintained and revamped with spare parts. Tuner encoder of the cavity have been replaced and the control system of the RF has been fully migrated from old 3rd level Apple LCIII to the new HW. A vacuum leak in one of the two spare Klystrons have been repaired.

A new movement system has been developed, built and installed in the Main Rings. The blades of two devices installed near the IP have been modified to avoid discharge at high current.

The control system of the cryogenic plant has been replaced. Transfer lines allowing anti-solenoidal cooling have been modified to increase reliability of cooling down process and to avoid leakage.

The LINAC gun system was renewed. The pulser unit has been modified so as improve stability and reliability in terms of timing. New control system has been implemented to fully exploit the HW improvements. A new cathode has been installed.

1.3 Machine operations

The LINAC system completed its major maintenance program, as planned. The operations was resumed on June, 3rd. By the end of June LINAC provided BTF users and DAΦNE with the electron beam. Positron beam was not available due to problems with the last accelerating section because of faulty behaviour of the Klystron. After several replacements (two new Klystron tube, a vacuum section between Klystron and LINAC, a RF Wave-guide, and a vacuum gauge) and a complete revision of conditioning procedures the positron beam was delivered at the beginning of November.

DAΦNE Main Rings were operational by the end of July when the installation of the new IR was completed. As mentioned before between July and August, the operation on the Main Rings has been concentrated on solving the alignment problem of the permanent dipole in the IR. Operation restarted by the end of September. During the first two months of operations with electron beam only, the activities was concentrated on: injection optimization, vacuum conditioning and feedback tuning.

Starting from November both beams, electron and positron, were circulating in the DAΦNE Main Rings. Several days of measurements and adjustments started in order to improve machine performances. The first collisions have been observed by the mid of December and a reliable, even not brilliant, instantaneous luminosity was measured ($0.35 \times 10^{32} cm^{-2} s^{-1}$ with 0.5 A per beam). The maximum current stored was 1250 mA and 600 mA for electron and positron beam, respectively.

New measurement of vibration of the beam base-line certified a reduction of a factor of three in vertical oscillation of the IR and a frequency shift from 10 Hz to 15 Hz due to the improved properties of the IR support.

2 Publications

1. D. Alesini, A. Drago, A. Gallo, S. Guiducci, C. Milardi, A. Stella and M. Zobov (INFN-LNF), S. De Santis (BNL). T. Demma (LAL), P. Raimondi (ESRF), " DAΦNE operation with Electron-cloud clearing-electrodes", Phys. Rev. Lett. 110 (2013) 124801.

---

3 DAΦNE History

3.1 Introduction

DAΦNE is an electron-positron Φ *meson factory* operating at Frascati since 1997. Factories are storage ring colliders designed to work at the energies of the meson resonances, where the production cross section peaks, to deliver a high rate of events to high resolution experiments.

The factory luminosity (the number of events per unit time produced by the reaction under investigation divided by its cross section weighted by the acceptance of the detector) is very high, about two orders of magnitudes larger than that obtained at the same energy in colliders of the previous generation. One of the key-points to get a substantial luminosity increase is the use of separated vacuum chambers for the two beams merging only in the interaction regions (IRs). When sharing the same ring the two N-bunch trains cross in $2N$ points and the maximum luminosity is limited by the electromagnetic beam-beam interaction. The unwanted effects of this interaction can be reduced with a very strong focussing (called "low-β") at the interaction point (IP), obtained by means of quadrupole doublets or triplets. However these magnetic structures take up much space and excite chromatic aberrations which must be corrected elsewhere in the ring.

This limitation does not hold for the double ring option, consisting in two separate rings crossing at two low-β points. The number of bunches that can be stored in such a collider is limited only by the geometry of the IR's.

DAΦNE is an accelerator complex consisting of a double-ring collider, a linear accelerator (LINAC), an intermediate damping ring to make injection easier and faster and 180 m of transfer lines connecting these machines. The beam accelerated by the Linac can also be switched into a laboratory called "Beam Test Facility (BTF)", for dedicated experiments and calibration of detectors. Three synchrotron radiation lines, two from bending dipoles and the other from the wiggler are routinely operated by the DAΦNE-LIGHT group in a parasitic mode, providing photons from the infrared to soft x-rays.

3.2 Injection System

In a low energy electron-positron collider, such as DAΦNE, the lifetime of the stored current is mainly limited by the Touschek effect, namely the particle loss due to the scattering of the particles inside the bunches. In the present typical operating conditions the Touschek lifetime is below 1000 s. It is therefore necessary to have a powerful injection system, capable of refilling the beam without dumping the already stored one. In addition, flexibility of operation requires that any bunch pattern can be stored among the 120 available buckets. The injection system of DAΦNE is therefore designed to deliver a large rate of particles in a single bunch at the working energy of the collider. It consists of a linear accelerator with a total accelerating voltage of 800 MV. In the positron mode, electrons are accelerated to ≈ 250 MeV before hitting a tungsten target (called positron converter) where positrons are generated by bremsstrahlung and pair production with an efficiency of $\approx 1\%$. The positrons exit from the target with an energy of few MeV and are then accelerated by the second section of the LINAC to their final energy of ≈ 0.51 GeV. The positrons are then driven along a transfer line and injected into a small storage ring, called Accumulator, at frequency of 50 Hz. Up to 15 positron pulses are stacked into a single bucket of the Accumulator, then injection stops and the bunch damps down to its equilibrium beam size and energy spread, which are much smaller than the LINAC ones. Damping takes ≈ 0.1 s and then the beam is extracted from the Accumulator and injected into the positron main ring at an overall repetition rate of 2 Hz. A powerful and flexible timing system allows the storage of any desired bunch pattern in the collider. In the electron mode, a magnetic chicane deviates the particle trajectory around the positron converter and electrons are directly accelerated to 0.51 GeV and injected into the Accumulator in the opposite direction with respect to positron operation. They are then extracted like in the positron case and injected into the electron main ring through the second transfer line.

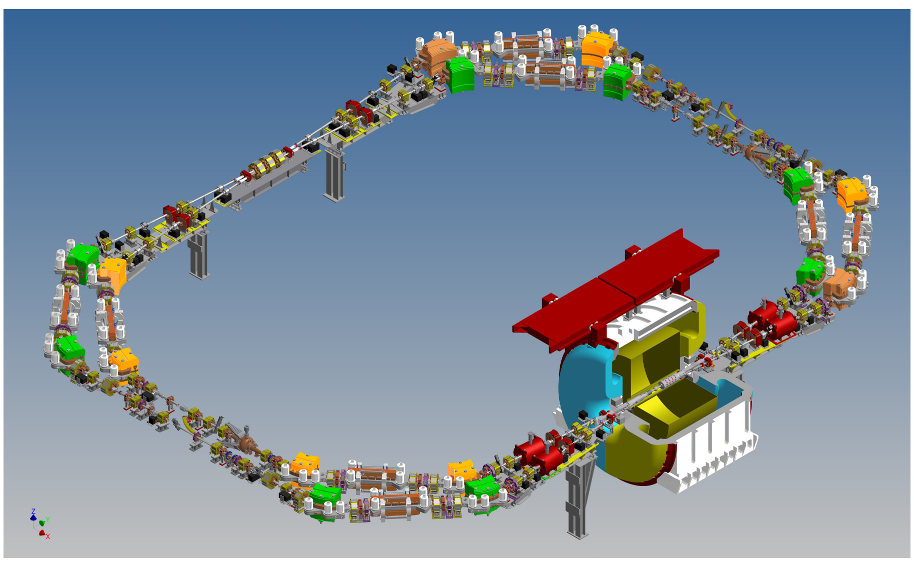

Figure 2: *The DAΦNE Main Rings in the present crab-waist scheme for the KLOE-2 run.*

The Accumulator ring has been introduced in the accelerator complex to increase the injection efficiency, especially for the positrons that are produced by the LINAC at 50 Hz rate in 10 ns pulses with a charge of $\approx$ 0.5 nC. Since the design charge of the main ring at the maximum luminosity is ≈ 1.5 μC and the longitudinal acceptance of the main rings is only 2 ns, the number of 50 Hz pulses necessary to fill the ring is of the order of 10^4. In order to avoid saturation it is therefore necessary that at each injection pulse a fraction smaller than 10^{-4} of the already stored beam is lost, and this is not easy to achieve. The Accumulator instead works with a lower frequency RF cavity and therefore with a larger longitudinal acceptance. In this way the full charge coming from the LINAC can be stored in a single RF bucket. In a complete injection cycle, that has a duration of 500 ms, up to 15 LINAC pulses can be stored in a single Accumulator RF bucket, and after being damped to the ring equilibrium emittances and energy spread, the whole stacked charge can be stored into a single RF bucket of the main ring. In this way the nominal single bunch charge can be stored with only one pulse from the Accumulator, reducing to 120 the number of injection pulses (at 2 Hz) into each main ring. As an additional benefit, the transverse beam size and energy spread of the beam coming from the Accumulator are at least one order of magnitude smaller than those of the LINAC beam, and this strongly reduces the aperture requirements of the main ring and, as a consequence, the overall cost of the collider.

3.3 Main Rings

In the DAΦNE collider the two beam trajectories cross at the interaction point (IP) with an horizontal angle that has been recently increased from ≈ 25 mrad to ≈ 50 mrad. A positron bunch leaving the IP after crossing an electron one will reach the following electron bunch at a distance of half the longitudinal separation between bunches from the IP.

Due to the horizontal angle between the trajectories of the two beams, the distance in the horizontal direction between the two bunches is equal to the horizontal angle times half the longitudinal distance between the bunches in each beam. The beam-beam interaction can be harmful to the beam stability even if the distance in the horizontal direction between bunches of opposite charge is of the order of few bunch widths at points where the β function is high and this sets a lower limit on the bunch longitudinal separation and therefore on the number of bunches which can be stored in the collider. However, the so called *crab waist collision scheme* (CW) recently implemented in the machine alleviates this problem, as it will be exhaustively explained in the following of this report.

By design the minimum bunch separation at DAΦNE has been set to ≈ 80 cm, and the maximum number of bunches that can be stored in each ring is 120. This number determines the frequency of the radiofrequency cavity which restore at each turn the energy lost in synchrotron radiation, which must be 120 times the ring revolution frequency. The luminosity of the collider can therefore be up to 120 times larger than that obtainable in a single ring with the same size and optical functions. Crossing at an angle could in principle be a limitation to the maximum single bunch luminosity. In order to make the beam-beam interaction less sensitive to this parameter and similar to the case of single ring colliders where the bunches cross head-on, the shape of the bunches at the IP is made very flat (typical ranges of r.m.s. sizes are $15 \div 30$ mm in the longitudinal direction, $0.2 \div 1.5$ mm in the horizontal and $2.5 \div 10$ μm in the vertical one). The double ring scheme with many bunches has also some relevant challenges: the total current in the ring reaches extremely high values (5 A in the DAΦNE design, $\approx$ 1.4 A in the DAΦNE operation so far) and the high power emitted as synchrotron radiation needs to be absorbed by a complicated structure of vacuum chambers and pumping systems in order to reach the very low residual gas pressure levels necessary to avoid beam loss. In addition, the number of possible oscillation modes of the beam increases with the number of bunches, calling for sophisticated bunch-to-bunch feedback systems.

The double annular structure of the DAΦNE collider as it is now after the recent modifications to implement the crab waist scheme (described in the following sections) with KLOE is shown schematically in Fig. 2. Both rings lay in the same horizontal plane and each one consists of a long external arc and a short internal one. Starting from the IP the two beams share the same vacuum chamber while traveling in a common permanent magnet defocusing quadrupole (QD) which, due to the beam off-axis trajectory increases the deflection of the two beam trajectories to ≈ 75 mrad. Shortly after the QD, the common vacuum chamber splits in two separated ones

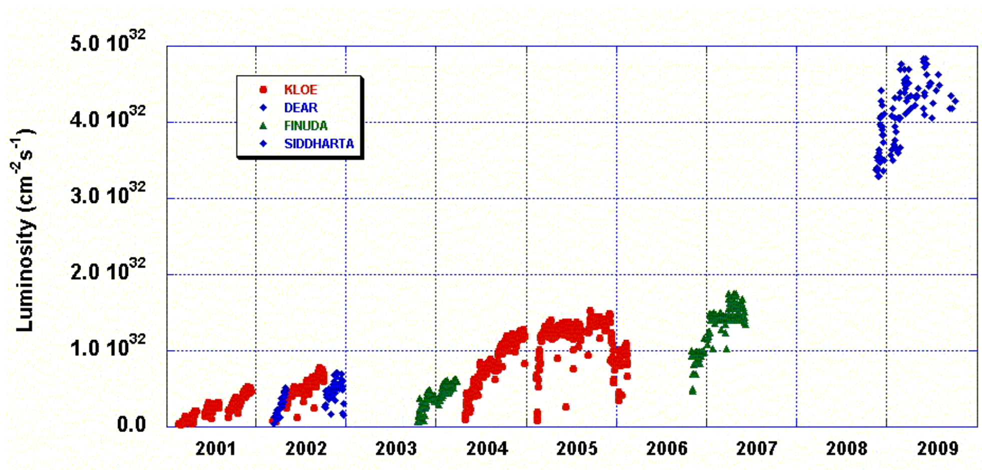

Figure 3: *Peak luminosity at DAΦNE.*

connected to the vacuum chambers of the long and short arcs. Two individual permanent magnet quadrupoles (QFs) are placed just after the chamber separation. Together with the previous QD they constitute the low-β doublets focusing the beams in the IP. The long and short arcs consist of two "almost achromatic" sections (deflecting the beam by ≈ 85.4 degrees in the short arc and ≈ 94.6 degrees in the long one) similar to those frequently used in synchrotron radiation sources, with a long straight section in between. Each section includes two dipoles, three quadrupoles, two sextupoles and a wiggler. This structure is used for the first time in an electron-positron collider and it has been designed to let DAΦNE deal with high current beams.

The amount of synchrotron radiation power emitted in the wigglers is the same as in the bending magnets and the wigglers can be used to change the transverse size of the beams. The increase of emitted power doubles the damping rates for betatron and synchrotron oscillations, thus making the beam dynamics more stable, while the possibility of changing the beam sizes makes the beam-beam interaction parameters more flexible.

The straight section in the long arc houses the kickers used to store into the rings the bunches coming from the injection system, while in the short straight arc there are the radiofrequency cavity and the equipment for the feedback systems which are used to damp longitudinal and transverse instabilities. The vacuum chambers of the arcs have been designed to stand the nominal level of radiation power emitted by the beams (up to 50 KW per ring). They consist of 10 m long aluminum structures built in a single piece: its cross section exhibits a central region around the beam and two external ones, called the antechambers, connected to the central one by means of a narrow slot. In this way the synchrotron radiation hits the vacuum chamber walls far from the beam and the desorbed gas particles can be easily pumped away. The chambers contain water cooled copper absorbers placed where the radiation flux is maximum: each absorber has a sputter ion pump below and a titanium sublimation pump above. The Main Rings have undergone many readjustments during the years to optimize the collider performances while operating for different detectors.

In principle the rings could host two experiments in parallel, but only one at a time has been operated so far. Three detectors, KLOE, DEAR and FINUDA, have taken data until 2007 and logged a total integrated luminosity of ≈ 4.4 fb^{-1} with a peak luminosity of $\approx 1.6 \cdot 10^{32}$ cm^{-2} s^{-1} and a maximum daily integrated luminosity of ≈ 10 pb^{-1}.

KLOE has been in place on the first IP from 1999 to 2006, while DEAR and FINUDA have alternatively run on the second one. The detectors of KLOE and FINUDA are surrounded by large superconducting solenoid magnets for the momentum analysis of the decay particles and their magnetic fields represent a strong perturbation on the beam dynamics. This perturbation tends to induce an effect called "beam coupling", consisting in the transfer of the betatron oscillations from the horizontal plane to the vertical one. If the coupling is not properly corrected, it would give a significant increase of the vertical beam size and a corresponding reduction of luminosity. For this reason two superconducting anti-solenoid magnets are placed on both sides of the detector with half its field integral and opposite sign, in this way the overall field integral in the IR vanishes.

The rotation of the beam transverse plane is compensated by rotating the quadrupoles in the low-β section. In the case of KLOE the low-β at the IP was originally designed with two quadrupole triplets built with permanent magnets, to provide high field quality and to left room to the detector. The structure of the FINUDA IR is quite similar to the KLOE one. Since its superconducting solenoid magnet has half the length (but twice the field) of the KLOE one, the low-β focusing at the IP was obtained by means of two permanent magnet quadrupole doublets inside the detector and completed with two other conventional doublets outside.

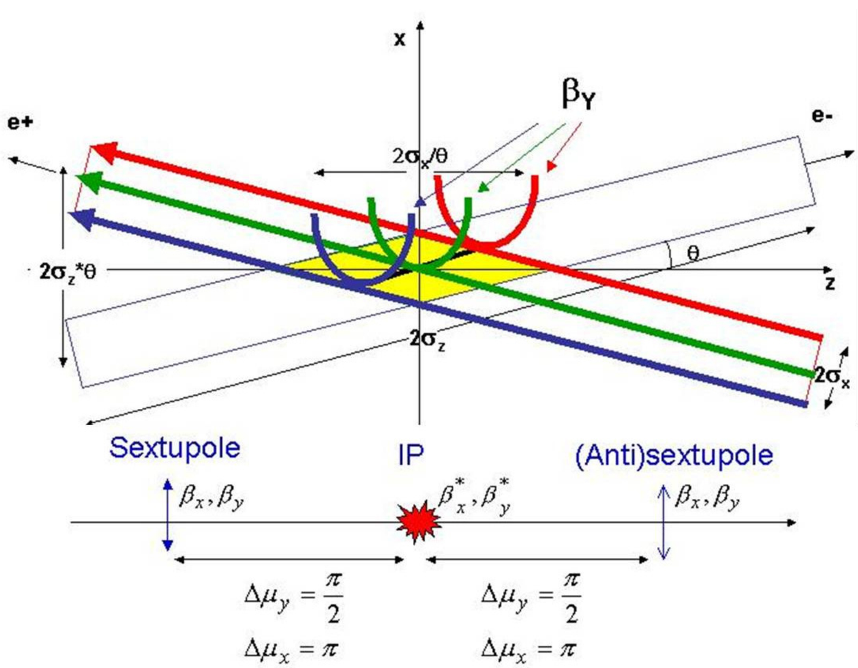

Figure 4: *Crab waist scheme*

The DEAR experiment, which was installed on the IR opposite to KLOE, took data during the years 2002-2003. It does not need magnetic field and therefore only conventional quadrupoles were used for the low-β. FINUDA rolled-in at DEAR's place in the second half of 2003 and took data until spring 2004. It was then removed from IP2 in order to run the KLOE experiment with only one low-β section at IP1, and rolled-in back in 2006 for a second data taking run ended in June 2007. After that the detector has been rolled-out again, and presently there are no detectors installed in IR2. The two chambers are vertically separated so that the two beams do not suffer from parasitic interactions in the whole IR2. A summary of the peak luminosity during these runs is shown in Fig. 3.

3.4 The large Piwinski angle and crab waist collision scheme at DAΦNE

In standard high luminosity colliders the key requirements to increase the luminosity are: very small vertical beta function β_y at the IP, high beam intensity I, the small vertical emittance ϵ_y and large horizontal beam size σ_x and horizontal emittance ϵ_x required to minimize beam-beam effects. The minimum value of β_y is set by the bunch length to avoid the detrimental effect on the luminosity caused by the hour-glass effect. It is very difficult to shorten the bunch in a high current ring without exciting instabilities. Moreover, high current implies high beam power losses, beam instabilities and a remarkable enhancement of the wall-plug power. In the CW scheme of beam-beam collisions a substantial luminosity increase can be achieved without bunch length reduction and with moderate beam currents. For collisions under a crossing angle θ the luminosity L and the horizontal ξ_x and vertical ξ_y tune shifts scale as:

$$L \propto \frac{N\xi_y}{\beta_y} \propto \frac{1}{\sqrt{\beta_y}} \tag{1}$$

$$\xi_y \propto \frac{N\sqrt{\beta_y}}{\sigma_z\theta}; \tag{2}$$

$$\xi_x \propto \frac{N}{(\sigma_z\theta)^2} \tag{3}$$

The Piwinski angle ϕ is a collision parameter defined as:

$$\phi = \frac{\sigma_z}{\sigma_x}\tan\left(\frac{\theta}{2}\right) \approx \frac{\sigma_z}{\sigma_x}\frac{\theta}{2} \tag{4}$$

with N being the number of particles per bunch. Here we consider the case of flat beams, small horizontal crossing angle $\theta << 1$ and large Piwinski angle $\phi >> 1$. In the large Piwinski angle and Crab Waist scheme described here, the Piwinski angle is increased by decreasing the horizontal beam size and increasing the crossing angle. In such a case, if it were possible to increase N proportionally to $\sigma_z\theta$, the vertical tune shift ξ_y would remain constant, while the luminosity would grow proportionally to $\sigma_z\theta$. Moreover, the horizontal tune shift ξ_x would drop like $1/\sigma_z\theta$. However, the most important effect is that the overlap area of the colliding bunches is reduced, as it is proportional to σ_x/θ (see Fig. 4). Then, the vertical beta function β_y can be made comparable to the overlap area size (i.e. much smaller than the bunch length):

$$\beta_y \approx \sigma_x/\theta << \sigma_z \tag{5}$$

We get several advantages in this case:

- Small spot size at the IP, i.e. higher luminosity L.
- Reduction of the vertical tune shift ξ_y with synchrotron oscillation amplitude.
- Suppression of synchrobetatron resonances.

There are also additional advantages in such a collision scheme: there is no need to decrease the bunch length to increase the luminosity as proposed in standard upgrade plans for B- and Φ-factories. This will certainly help solving the problems of HOM heating, coherent synchrotron radiation of short bunches, excessive power consumption etc. Moreover, parasitic collisions (PC) become negligible since with higher crossing angle and smaller horizontal beam size the beam separation at the PC is large in terms of σ_x.

Table 1: DAΦNE Beam parameters for KLOE (2006) and SIDDHARTA (2008-2009)

PARAMETERS	KLOE Run	SIDDHARTA Run
L [cm^{-2}s^{-1}]	$1.5 \cdot 10^{32}$	$4.5 \cdot 10^{32}$
N_{part}/bunch	$2.65 \cdot 10^{10}$	$2.65 \cdot 10^{10}$
I_{bunch} [mA]	13	13
ϵ_x [10^{-9} m $\cdot$ rad]	340	260
ϵ_y [10^{-9} m $\cdot$ rad]	1.5	1
σ_x [μm]	760	200
σ_y [μm]	5.4	3.5
σ_z [mm]	25	17
β_x^* [m]	1.7	0.25
β_y^* [mm]	17	9
θ [mrad]	2×12.5	2×25

However, large Piwinski angle itself introduces new beam-beam resonances which may strongly limit the maximum achievable tune shifts. At this point the crab waist transformation enters the game boosting the luminosity, mainly because of the suppression of betatron (and synchro-betatron) resonances arising (in collisions without CW) through the vertical motion modulation by the horizontal oscillations. The CW vertical beta function rotation is provided by sextupole magnets placed on both sides of the IP in phase with the IP in the horizontal plane and at $\pi/2$ in the vertical one (see Fig. 4).

For comparison, the parameters used during the last DAΦNE run with the KLOE detector (2005-2006) are shown in Table 1. As discussed above, in order to realize the CW scheme in DAΦNE, the Piwinski angle ϕ should be increased and the beam collision area reduced: this is achieved by increasing the crossing angle θ by a factor 2 and reducing the horizontal beam size σ_x. In this scheme the horizontal emittance ϵ_x is reduced by a factor 1.5, and the horizontal beta function β_x lowered from 1.5 to 0.2 m. Since the beam collision length decreases proportionally to σ_x/θ, the vertical beta function β_y can be also reduced by a factor 3, from 1.8 cm to 0.6 cm. All other parameters are similar to those already achieved at DAΦNE.

3.5 Hardware upgrades for the Crab Waist test at DAΦNE with the SIDDHARTA run

DAΦNE has been upgraded to allow the CW collision scheme test with the SIDDHARTA run during the summer shutdown of 2007.

The major upgrades on the machine are summarized as:

- new IR1 geometry for the CW test;
- new IR2 geometry with two completely separated vacuum chambers with half moon profile;
- new shielded bellows;
- the four e^+ e^- transverse feedbacks have been upgraded;
- solenoid windings in the two long IRs sections of the e^+ ring;
- new calorimeter for luminosity measurement and tuning;
- new longitudinal position of the two IRs horizontal collimators;

- new injection kickers.

The need of a new IR geometry is essentially due to have a very small β_y (9 mm) and a large crossing angle (25 mrad per beam). Splitter magnets installed in the original design have been removed thanks to the large crossing angle in the CW scheme. Defocusing and focusing quadrupoles (QD, QF) on both sides of the IP have been placed to obtain the required low-β structure. Further trajectory separation is provided by two small dipole correctors upstream and downstream the quadrupole doublets, while other three quadrupoles are used to match the betatron functions in the arcs.

The low-β section quadrupoles near the IP are of permanent magnet (PM) type. The QDs are located near the IP where the beams share a common vacuum chamber, while the QFs are positioned where the chambers are splitted and each one acts on a single beam. Therefore a total of two QDs and four QFs is required to get the two doublets around IP1. Four corrector dipoles provide a deflection of 9.5 mrad to match the inlet and outlet arc chamber flanges.

CW sextupoles are placed at ~ 9.3 m far from the IP1. Bending dipoles facing the IRs have been rotated and their field adjusted according to requirements. They have been powered with independent supplies to match these requirements.

For the SIDDHARTA experiment a new aluminium alloy (AL6082T6) chamber with two thin windows (0.3 mm 0.02 thickness) in the top and bottom sides has been designed and built.

Electromagnetic simulations have shown the presence of trapped modes which add resonant contributions to the beam coupling impedance in the Y-chamber junctions, the regions where the two separate ring pipes merge in the common vacuum chamber near the IP. In the worst possible scenario, that occurs when a beam spectrum line at a frequency equal to a multiple to the bunch repetition rate is in full coupling, the joule loss does not exceed 200 W. To keep this effect under control the Y-chambers have been equipped with cooling pipes.

This additional cooling circuit allows to remove the beam induced HOM heating and, if necessary, to reduce it by detuning the mode frequencies with respect to the dangerous beam spectrum lines.

A new design of the central IR2 beam pipe has been implemented, the two vacuum chambers are completely separated and their cross section has an half moon profile.

The main Bhabha monitor consists of a 4-modules sandwich calorimeter, made of lead and scintillator. Four modules of calorimeters surround the final permanent quadrupole magnets, located at a distance of 32.5 cm on both sides of the IR, as shown in Fig. **??**. They cover an acceptance of $18 \div 27$ degrees in polar angle, and are segmented in azimuthal angle in five sectors, 30 degrees wide.

Two gamma monitor detectors are located 170 cm away from the IR, collecting the photons radiated by electron or positron beam. The detectors are now made of four PbW04 crystals (squared section of 30×30 mm^2 and 110 mm high) assembled together along z, in order to have a 30 mm face towards the photon beam, and a total depth of 120 mm corresponding to about 13 X_0. Thanks to the high rate, those detectors are mainly used as a fast feedback for the optimization of machine luminosity versus background, since the relative contribution of background is changing with the machine conditions. A total systematic uncertainty on the luminosity measurement of 11% can be estimated.

3.6 Luminosity achievements during the SIDDHARTA run

The commissioning of the upgraded machine started in November 2007. At the end of the year the ring vacuum was almost recovered, the beams were stored in the upgraded rings, all the sub-systems went quickly to regime operation.

Table 2: DAΦNE luminosity performances with the CW scheme and low-β parameters compared to the KLOE and FUNUDA runs. SIDDHARTA data taking does not profit of the fast injection rate system, that would increase $L_{\int logged}$.

	SIDDHARTA March 08 ÷ Nov 09	KLOE May 04 ÷ Nov 05	FINUDA Nov 06 ÷ Jun 07
L_{peak} [cm^{-2}s^{-1}]	4.5	1.5	1.6
$L^{MAX}_{\int day}$ [pb^{-1}]	15.24	9.8	9.4
$L^{MAX}_{\int hour}$ [pb^{-1}]	1.033	0.44	0.5
$I^{-\ MAX}_{coll}$ [A]	1.4	1.4	1.5
$I^{+\ MAX}_{coll}$ [A]	1	1.2	1.1
$n_{bunches}$	105	111	106
$L_{\int logged}$ [fb^{-1}]	2.9	2.0	0.966
β^*_x [m]	0.25	1.5	2.0
β^*_y [m]	0.009	0.018	0.019
ϵ_x [10^{-6} m·rad]	0.25	0.34	0.34
ξ_y	0.0443	0.025	0.029

The first collisions in the CW scheme have been obtained in February 2008, with the first experimental confirmation of the potentiality of the new configuration in terms of specific luminosity growth and reduction of the beam-beam detrimental effects.

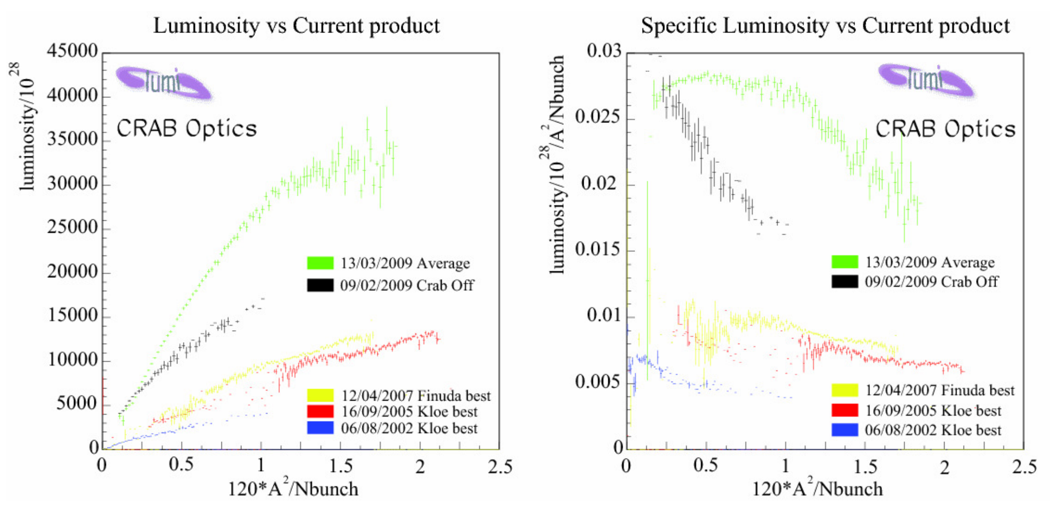

Figure 5: *Comparison of the upgraded DAΦNE perfomance (green) with respect to the results during previuos KLOE (blue, red) and FINUDA runs (yellow).*

DAΦNE luminosity as a function of the colliding bunches compared to past runs is reported in Fig. 5. Blue and red dots refer to the two KLOE runs, with the initial triplet low-β IR quadrupoles and with the new IR doublet, respectively. Yellow dots refer to the FINUDA run; in green is the

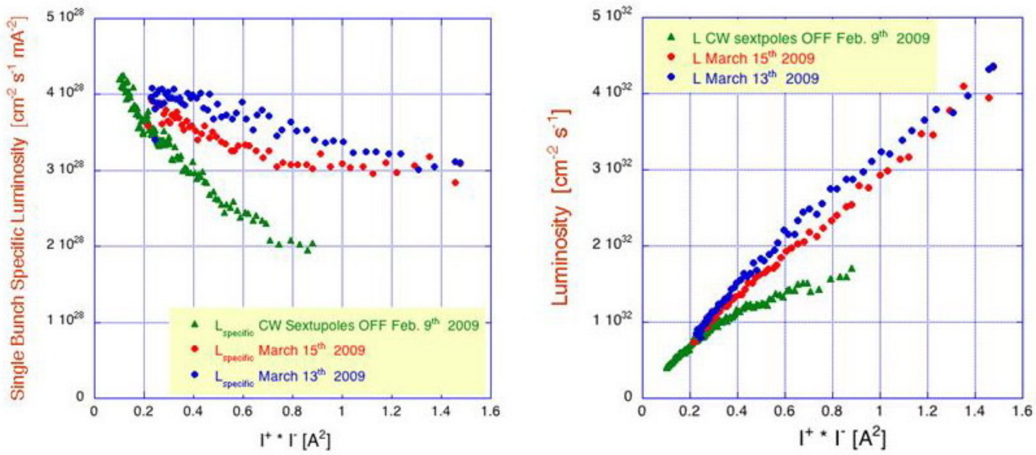

Figure 6: *Single bunch specific luminosity (left) and luminosity (right) versus the product of the colliding currents for two of the best run and for the crab waist sextupoles off.*

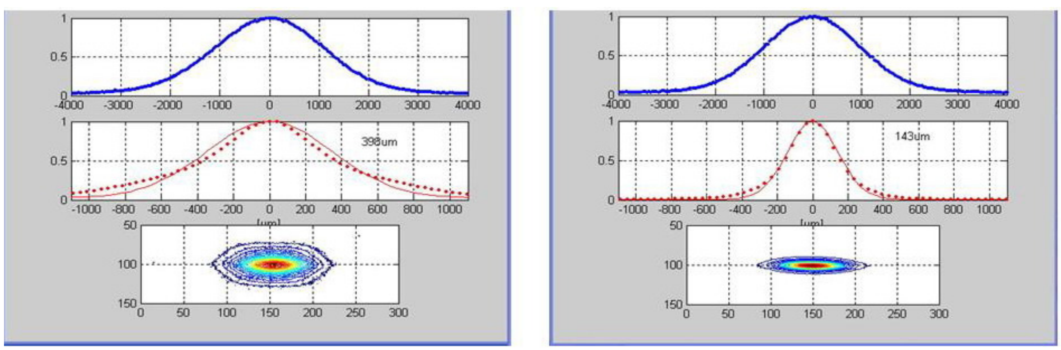

Figure 7: *Transverse positron beam profile as measured at SLM with crab sextupoles off (left) and crab sextupoles on (right) for beams in collisions (103 bunches).*

luminosity with the CW scheme. The gain provided by the new IR gets higher with the products of the currents and the difference with respect to collisions with the crab sextupoles off can reach 50%. During 2009 the peak luminosity has been progressively improved by tuning the collider and increasing the beam currents; the maximum value achieved is $\approx 4.5 \cdot 10^{32}$ cm^{-2}s^{-1} measured in several runs with good luminosity to background ratio. The present peak luminosity is close to the nominal one predicted by numerical simulations. The highest single bunch luminosity achieved is $\approx 5 \cdot 10^{30}$ cm^{-2}s^{-1} measured with 20 bunches in collisions instead of the usual 105. The single bunch specific luminosity, defined as the single bunch luminosity divided by the product of the single bunch currents, at low currents exceed by 4 times the best value measured during the past DAΦNE runs (present values are red and blue dots in Fig. 6). It gradually decreases with colliding beam currents, as can be seen in Fig. 6. This reduction can be only partially explained by the growing beam size blow up due to the beam-beam interaction. Another factor comes from the fact that in the large Piwinski angle regime the luminosity decreases with the bunch length, which in turn is affected by the ring coupling impedance. The impact of the Crab-Waist sextupoles can be recognized comparing runs taken with CW sextupoles on and off (Fig. 6). At low current the luminosity is the same in the two cases and higher than the one measured with the original collision scheme. As the product of the stored currents exceed 0.3 A, the luminosity with CW sextupoles off becomes lower and a corresponding transverse beam size blow up and beam lifetime reduction are observed as a consequence of the uncompensated beam-beam resonances. The convolved vertical beam size at the IP in collision has been measured by means of a beam-beam scan technique. The measured Σy of 5.6 μm is compatible with the value obtained by using the coupling value ($k = 0.7\%$) as measured at the Synchrotron Light Monitor (SLM), being the single vertical beam size at the IP1 of the order of 4 μm.

Fig. 7 reports another proof of the crab sextupoles effectiveness, where the positrons transverse beam profile measured at the synchrotron light monitor with crab sextupoles OFF (left plot) and with crab sextupoles ON (right plot) is shown. The measurement refers to collision in a strong-weak regime (1 A electrons beam current against 0.1 A of positrons beam current): it is evident that the transverse beam size is smaller and its shape remains Gaussian during collision with the sextupoles ON.

The crab waist sextupoles proved to be of great importance for the collider luminosity increase, since much lower luminosity is achieved with crab sextupoles off, with a larger blow up and a sharp lifetime reduction is observed for single bunch currents greater than 8-10 mA. This is in agreement with beam-beam simulations taking into account the DAΦNE nonlinear lattice. The results achieved at DAΦNE have pushed several accelerator teams to study and consider the implementation of this scheme on their machines. Besides, the physics and the accelerator communities are discussing a new project of a Super B-factory with luminosity as high as 10^{36} cm^{-2}s^{-1}, i.e. by about two orders of magnitude higher with respect to that achieved at the existing B-factories at SLAC and KEK.

3.7 Hardware modifications for the KLOE-2 run

During 2009 the new interaction region design for KLOE has been completed and several components of the new hardware have been acquired. In beginning 2010 the KLOE detector has been rolled in on IR1.

The new IR magnetic layout, sketched in Fig. 8, has been designed in order to maximize the beam stay clear letting the beam trajectory pass as much as possible through the center of the magnetic elements. The field integral introduced by the solenoidal detector is almost cancelled by means of two anti-solenoids, installed symmetrically with respect to the IP in each ring, which provide compensation also for off-energy particles. Due to the larger crossing angle, the vertical displacement of the beam in the IR is about an order of magnitude larger than in the last KLOE run. To keep the beam vertical trajectory within reasonable values, two permanent magnet dipoles (PMD) have been added just after the first permanent magnet horizontally focusing quadrupole, inside the detector magnetic field, in each one of the four IR branches (see Fig. 8). The PMDs are based on a modular design in view of a possible KLOE-2 run at a lower solenoidal field. Since the two beams are vertically deflected in opposite directions by the KLOE solenoid, they provide a horizontal magnetic field directed towards the center of the ring in the positron ring and towards the outside in the electron one. Four new skew quadrupoles have been added on the IR, just outside the KLOE magnet, to provide fine tuning for the coupling compensation.

The shimmed plates added on the wiggler poles in 2004 have been removed and the poles displaced alternately in the horizontal direction by ± 8 mm with respect to the wiggler axis in order to keep the beam trajectory as much as possible centered with respect to the pole axes. Due to the reduction of the gap and of the overall length of the magnetic circuit, this new configuration allows to reach, at a current of 450 A, a magnetic field still higher than that achieved at 550 A in the previous configuration with shimmed plates inserted. A further improvement has been obtained

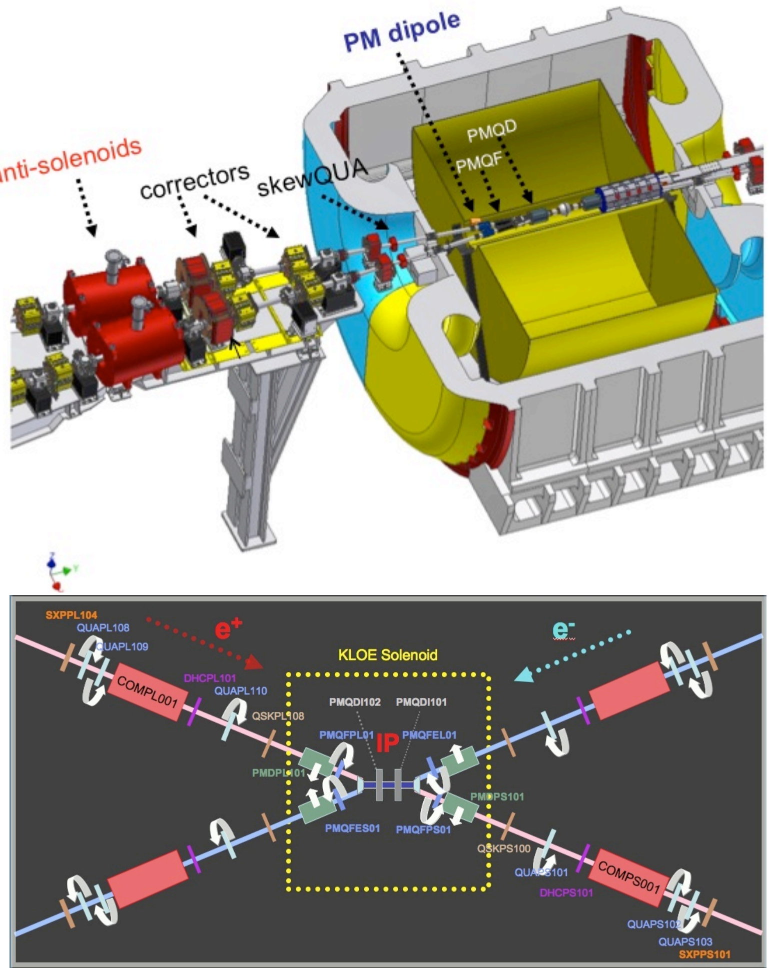

Figure 8: *(Top) The KLOE-2 detector and the new DAΦNE Interaction Region 1. (Bottom) Schematic drawing of the DAΦNE Interaction Region 1 magnetic layout.*

by powering in series all the 7 poles of the wigglers, while before each couple of terminal poles was powered independently. This has been obtained by short-circuiting one out of the five windings in the terminal poles coils and correcting the field integral in each wiggler below 1 Gm by tuning the end pole clamps aperture. In this way eight power supplies are no more necessary and the cycling procedure at startup is much more reliable. All the DAΦNE wigglers have been removed, modified and measured.

New stripline electrodes have been designed and inserted in the wiggler and dipole vacuum chambers of the positron ring. These electrodes, powered by DC voltages, counteract the parasitic electron cloud formation, which helps in increasing the positron beam current threshold.

The exhausted LINAC gun cathode has been replaced with a new one.

The modifications on the machine for the KLOE-2 run have been completed at the beginning of May. At the end of June the KLOE magnet has been partially warmed-up to allow the installation of the anti-solenoids cryogenic transfer lines. Since then, and up to mid November, several problems at the cryogenic plant and its ancillary systems occurred, preventing the KLOE solenoid energization. In September a magnetic setup without the KLOE magnet, but using the anti-solenoids, has been found to allow the DAΦNE beam conditioning. Up to about 1 A of positrons has been stored in the main ring with this optics, while the electron current was limited to ≈ 0.1 A due to ion trapping. On November 16th, the KLOE magnet was cooled and energized and beam conditioning in the nominal configuration was started with currents around 0.8 A stored at the same time in both rings, with half circumference filled in each one to avoid beam-beam interactions.

The first phase of the main ring commissioning has been done with the KLOE detector off. The lack of focusing from the solenoid has a strong impact on the ring optics, which had to be deeply modified. In November all the six DAΦNE bunch-by-bunch feedback systems have been upgraded to new software and hardware versions. The two (electron and positron) longitudinal feedbacks have been completely replaced with new ones, with the goal to have more compact systems with updated hardware components and new software programs compatible with the currently used operating system. These efforts are motivated also by reaching lower noise in detecting and better performance in damping the beam longitudinal oscillations. The vertical feedback systems have been equipped with 12-bit AD and DA converters in place of the 8-bit old units to reduce the quantization noise impact in the system gain. The positron ring horizontal feedback power has been doubled (1 kW now) providing about 40% increase in the kick strength. Furthermore, the horizontal feedback kicker has been replaced with a device with a double length stripline and reduced plate separation, providing larger shunt impedance at the low frequency typical of the positron horizontal unstable modes. The kicker has been also moved in a position with a higher horizontal β value.

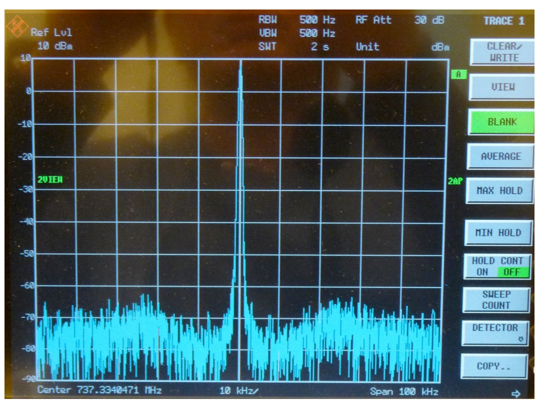

Figure 9: *Beam spectrum snapshot.*

3.8 DAΦNE commissioning for the KLOE-2 run

DAΦNE upgrade for the KLOE-2 run has been completed in July 2010. KLOE cool-down started on the second half of April 2010, however several problems involving the cryo-plant prevented to energize the detector till October 25^{th}.

From November 2010 until June 2011 there have been several faults involving:

- injection septum of the positron ring;
- linac gun cathode and D modulator of the injection system;
- cooling system of the KLOE magnet power supply;

- vertical orbit oscillation in both rings.

These faults slowed down the commissioning and caused two major unscheduled shut-down periods. On January 11^{th} the 34 degrees injection septum of the positron ring got permanently damaged due to a water leakage together with a fault in the alarm system. Since no spare part was available it has been impossible to store the positron beam for three months. However, the accident had a positive drawback: the new septum coil has been optimized by reducing the coil gap and changing the geometrical dimension of the conductor, thus achieving a 50% reduction in the wall plug power with respect to the original device.
The cooling system of the KLOE magnet power supply experienced a faulty behaviour (from February 20^{th} to March 30^{th}), which has been linked, eventually, to the internal oxidation of the cooling circuit, that has been fixed in two weeks.

The Linac had several problems concerning the D modulator system, essential for positron production and the gun cathode, which required several replacements till to run out of spare parts by mid-May. This circumstance forced the last, and more relevant, unscheduled shut-down four months long.

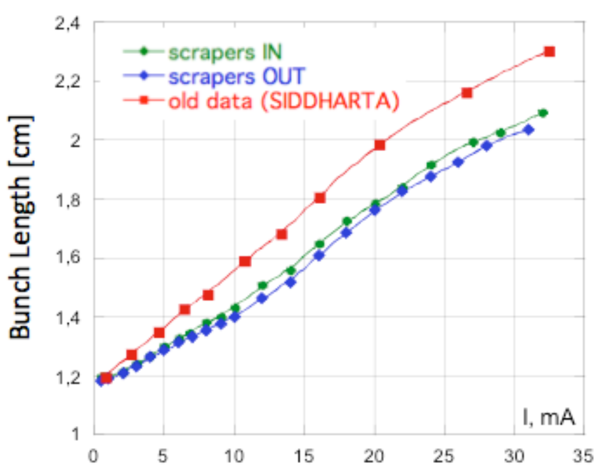

Figure 10: *Bunch length measurements in the electron ring.*

Suspending the DAΦNE activity gave a useful opportunity to start an extensive program of maintenance and consolidation involving almost all the collider subsystems.
It is the case of the test and replacement activities involving several Linac components such as: radio frequency loads in the gun area, modulators with their high power units, buncher phase shifter, diagnostic tools and cathode test station.
Concerning magnetic elements: all the four 34 degrees septa have been replaced and four correctors in the IR replaced with devices having better field quality.
About mechanics and layout many vibration measurements have been done in the Interaction Region area to sort out the source of the vertical oscillation observed, on both beams. Measurement analysis indicated how to consolidate the Interaction Region supports halving the vertical oscillation.

Alignment has been revised in several sections of the main rings relying on beam measurement analysis.
The cryogenic plant has been maintained with a standard cleaning procedure.

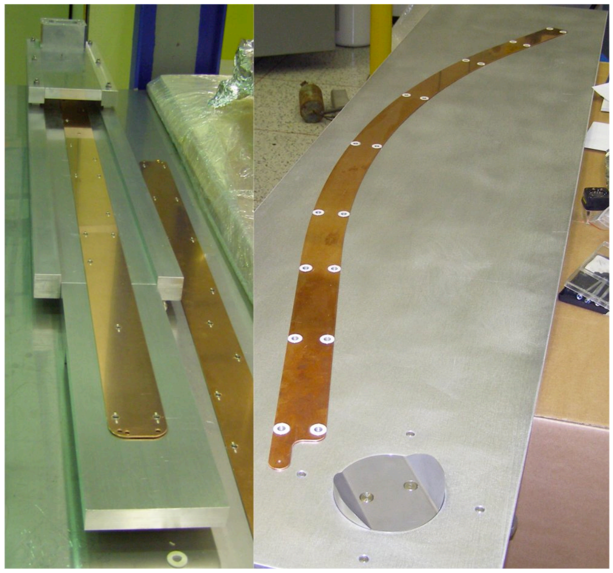

Figure 11: *Pictures of the electrodes inserted in the chambers of the dipole (on the right) and in the wiggler (left picture).*

Concerning controls: the fluid plant low-level interface has been upgraded and front-end controls for several class of elements have been ported to new more performing processors.
A lot has been done to reduce and optimize the demand for electric power. In fact the electric power necessary to run DAΦNE is $\approx 3.34\ MW$ now, which is $\approx 2.56\ MW$ lower than during the last KLOE run with a consequent reduction of $\approx 2.0\ Meuros$ on the electric bill due for a 200 days long run.

Although the collider uptime has been very limited, especially for the positron ring, some relevant work has been done to test the upgraded systems and to tune the Main Rings optics.

As for all circular colliders, the DAΦNE beam longitudinal dynamics is very much affected by the Low Level Radio-Frequency (LLRF) control. In particular, the dynamics of the beam barycentre motion (the coupled bunch zero-mode) is very sensitive to the large RF cavity detuning required to compensate the reactive beam loading, which is particularly huge at DAΦNE where the operating conditions are characterized by relatively low accelerating gradients ($\approx\ 200\ kV$) e large stored currents (up to $2\ A$). For this reason a fully analog RF feedback loop has been added to the LLRF system and commissioned on both e^+ and e^- rings, resulting in a drastic limitation of the synchrotron zero-mode coherent frequency shift that have affected the operation of the collider in the past. The measured beam spectrum around the RF 2^{nd} harmonics is shown in Fig. 9, where the sidebands of the longitudinal barycentre motion appear much lower and broader compared to what we observed in the past before the feedback implementation. The efficiency of the RF system has been also increased since no extra cavity detuning is necessary with direct RF feedback in operation. The RF systems of both rings are now operating reliably in the new configuration.

The ring impedance has been estimated relying on bunch length measurements as a function of bunch current. Numerical fits based on potential well as well as microwave regime converge to a ring coupling impedance of 0.3Ω; it was 0.4Ω during the previous run (see Fig. 10).

One of the main limitations in the maximum stored current of the positron ring has been identified in previous runs, in a horizontal instability due to the electron cloud effect. To mitigate such instability, metallic -copper- electrodes have been inserted in all dipoles and wigglers chambers

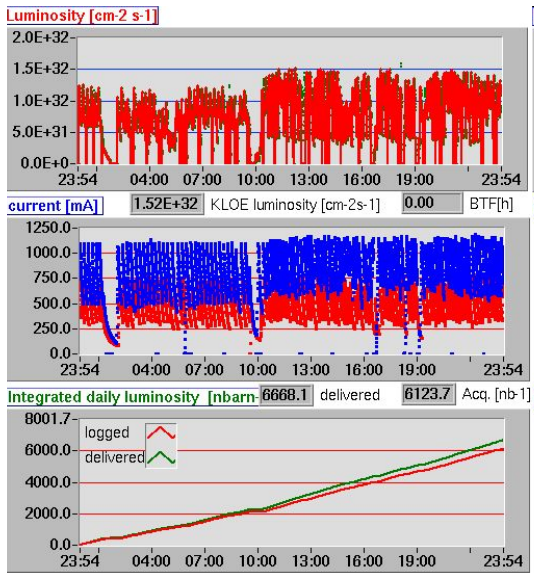

Figure 12: *(Top) Luminosity, (Middle) beam currents, (Low) Integrated luminosity for the best day, Dec.* 17^{th} *2011.*

of the machine and have been connected to external dc voltage generators in order to absorb the photo-electrons. With a dc voltage of about 200 V applied to each electrode we expect a reduction of such density by two orders of magnitude that will contribute to reduce substantially the source of the instability. The pictures of the electrodes inserted in the dipole and wiggler chambers are shown in Fig. 11.

The dipole electrodes have a length of 1.4 or 1.6 m depending on the considered arc (short or long), while the wiggler ones are 1.4 m long. They have 50 mm width, 1.5 mm thickness and their distance from the chamber is about 0.5 mm. This distance is guaranteed by special ceramic supports made in SHAPAL and distributed along the electrodes. This ceramic material is also thermo-conducting in order to partially dissipate the power released by the beam to the electrode through the vacuum chamber. Moreover, the supports have been designed to minimize their beam coupling impedance as well as to sustain the strip. First experimental measurements on the electrodes effectiveness in mitigating the electron cloud effects in the positron beam are very encouraging.

The new configuration of the wiggler magnets, based on shifted poles has proved to be effective in reducing the non-linear terms in the magnetic field (B) . The field quality has been tested by measuring the beam tune shift induced by a horizontal closed orbit bump at the wiggler place. This bump, including the two dipoles adjacent to the wiggler, slightly changes the ring energy: this effect has been carefully compensated tuning the frequency of the RF cavity. The orbit position at the wiggler centre has been obtained by averaging the readout from two beam position monitors (BPM) placed at the magnet end side. For large values of the bump the BPMs non-linearity have been taken into account and properly corrected. The measured horizontal and vertical tune shifts exhibit a clear linear behaviour.

The lattice for the KLOE-2 run with the crab-waist scheme has been optimized and matched to the real beams, relying on optics measurements (beta functions, dispersion, chromaticity, coupling, betatron tunes). The lowest value of the betatron coupling that has been measured is as small as 0.14% with a $\sigma_y = 75\mu m$ at the syncrotron light monitor. The vertical beam-beam luminosity scan showed that vertical orbit oscillation does not affect beam size at the IP, $\sigma_y = 3\mu m$

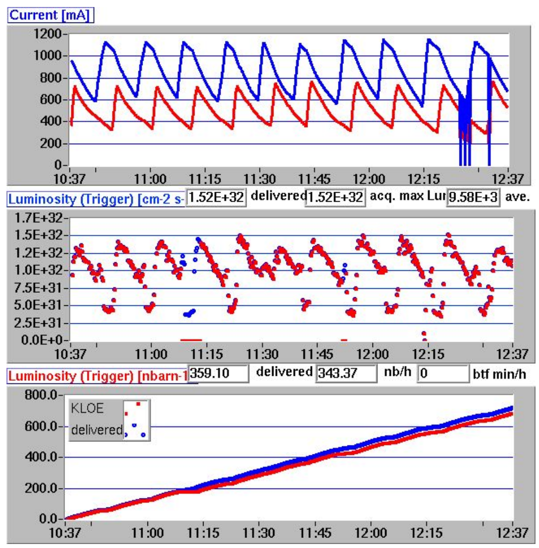

Figure 13: *Best two hours for KLOE-2 run.*

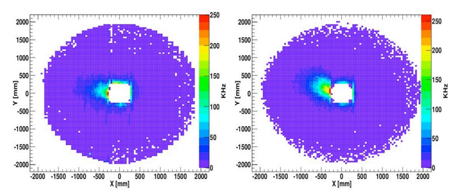

Figure 14: *Transverse profile of the backward EmC rates. Left and right plots are data and MC, respectively.*

has been measured at IP. The new configuration of the wiggler magnets, based on shifted poles has proved to be effective in reducing the non-linear terms in the magnetic field. Luminosity is still not at nominal value due to different reasons, however beam-beam is not a limiting factor, and crab-waist sextupoles work well, as expected.

The luminosity has been optimized by storing 100 bunches in collision at low current. The single bunch specific luminosity at low currents is of the order of about $\approx 4.5 \cdot 28$ cm^{-2} s^{-1}, the same as the one measured during the crab-waist test without the detector solenoid. The DAΦNE performances at the end of December 2011 reproduced the best ones obtained during the previous KLOE run. In fact, up to now the maximum peak luminosity is $1.52 \cdot 10^{32}$ cm^{-2} s^{-1}, obtained on December 17th 2011, with $I^- = 0.93$ A and $I^+ = 0.719$ A stored in 100 bunches. This value can be compared to the same luminosity $1.53 \cdot 10^{32}$ cm^{-2} s^{-1} with $I^- = 1.4$ A and $I^+ = 1.2$ A with 111 bunches, achieved during the KLOE run in 2005. The same day (December 17th) has been also the best day in terms of daily integrated luminosity (see Fig. 12).

The plot with the highest luminosity per hour is shown in Fig. 13. The best hourly integrated luminosity is 0.359 pb^{-1}, which might provide 8.62 pb^{-1} per day.

However, an efficient data taking requires not only high luminosity but also background rates induced in the detector as low as possible.

The two collimators mostly effective are the one upstream the IR and the one just after the old IP2, as predicted also by numerical simulations. The beam stay clear at these two collimators

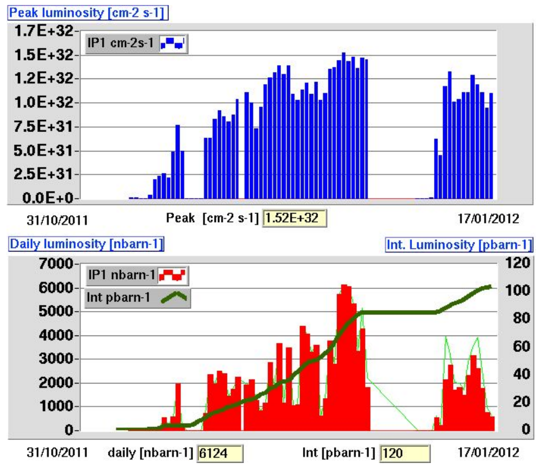

Figure 15: *Summary of current and luminosity during year 2011.*

has been reduced to intercept Touschek scattered particles that would be lost at the IR. They proved to be very much effective in reducing background showers. However, after careful orbit optimization and collimator tuning, an additional lead shielding 1 *cm* thick has been added around the inner layer (QCAL) of the KLOE-2 detector to prevent background contamination in the physics events without reducing the detector acceptance. A full Monte Carlo (MC) simulation that allows a direct comparison between the expected and measured background rates at the KLOE electromagnetic calorimeter (EmC) has been developed in the new KLOE-2 configuration. The data/MC background rates are in agreement within a factor of two in the different regions of the KLOE EmC and the main features of the shapes are well reproduced (see Fig. 14). A good agreement for the Touschek lifetime is found between measured and calculated lifetime with scrapers inserted at the experimental set. On the contrary, the comparison without scrapers shows a disagreement of about a factor 1.9, which might be explained by a misalignment of the on-energy beam orbit that induced beam scraping in the IP2 section. This allows us to expect some margins of optimization, especially by correcting orbit and dynamic aperture.

The summary of current and luminosity during year 2011 is shown in Fig. 15. In order to push the collider performances in terms of luminosity, multibunches and high current operation must be consolidated and improved by tuning the working points in the two rings, the coupling at the IP for the two beams, the non-linear beam dynamics and, last but not least, beam-beam interaction. Background has been improved especially at high current and mainly for the positron ring. Dedicated studies may help to optimize the collimator configuration and to understand the possibility to introduce additional shieldings between the beam pipe and the detector.

3.9 DAΦNE setup and data taking tests with the KLOE-2 detector

DAΦNE activity in year 2012 has been aimed at completing the machine commissioning and at starting the detector data taking. However the machine operation has been seriously slowed down by several technical problems and faults that outlined a clear need for planning a radical consolidation program involving the whole accelerator complex.

On mid January a sudden rise, more than 90 ℃, occurred in the temperature of the beam pipe inside the detector, which was compatible with the lack of electrical continuity in the bellows of the section common for the two beams. It occurred close by the low-β defocusing quadrupole installed at the incoming side of the electron beam. In order to avoid a rather long machine shutdown, an attempt has be done to fix the problem by pushing the two halves of the IR from outside the detector, thus achieving a considerable reduction of the temperature variation in the range $25 \div 55$ ℃. This excursion, albeit reduced, has been causing sudden and unpredictable variation in the vertical tune and non-reproducibility in the betatron function measurements. In fact the low-β QDs are permanent magnet made by a SmCo alloy and experience a rather relevant variation in the gradient with the temperature of the order of ~ 0.0004 m^{-2} ℃$^{-1}$.

Many faults affected the cooling system causing also water leakages in the wiggler magnets of the electron ring, which, in turn, required several not simple soldering interventions to fix holes and to replace two end poles coils.

In the first months of the year in spite of the considerable downtime several encouraging results have been obtained in terms of luminosity. The maximum values achieved for peak, hourly and daily integrated luminosity have been: $L_{peak} = 1.53 \times 10^{32}$ (with colliding currents $I^- = 840$ mA and $I^+ = 810$ mA stored in 100 bunches), $L_{\int 1hour} = 0.350$ pb^{-1} and $L_{\int day} = 7$ pb^{-1}. The specific luminosity, at low current, exceeded by more than a factor of 2 the best value measured during the KLOE run in 2005 (see Fig. 16).

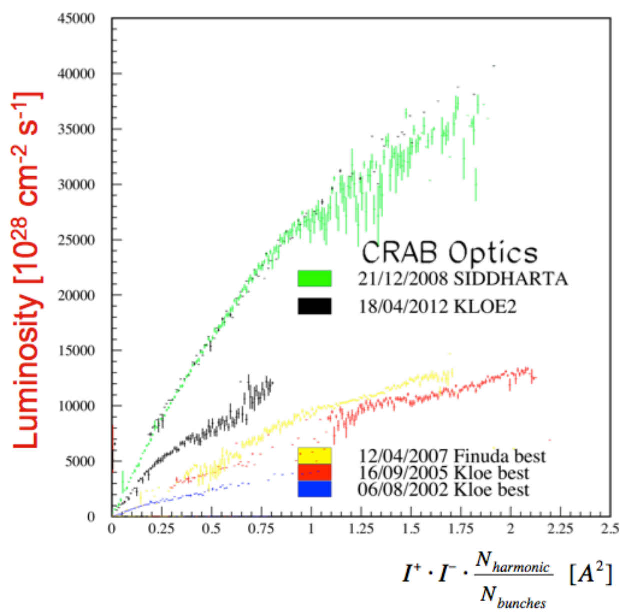

Figure 16: *Luminosity versus the product of the colliding currents normalized to the number of colliding bunches. Data refer to runs acquired before (bottom) and after (top) implementing the Crab-Waist scheme.*

DAΦNE is the first collider operating routinely with long electrodes, for e-cloud mitigation, installed in all dipole and wigglers vacuum chambers. These electrodes not only permitted a more stable operation with the positron beam, but have also allowed unique measurements such as e-cloud instabilities growth rate, transverse beam size variation, and tune shifts along the bunch train, demonstrating their effectiveness in mitigating the e-cloud induced effects. All measurements have been done with positive voltage polarity. The power supplies connected to the electrodes absorb electrons from the cloud. Betatron tune measurements taken by a spectrum analyzer have shown an average tune shift, especially in the horizontal plane, when switching off the electrodes. For this reasons a more sophisticated analysis has been done using the front-end data of the bunch-by-bunch feedbacks, which can measure the tune-shift for each bunch in the train [1]. The results are presented in Fig. 17.

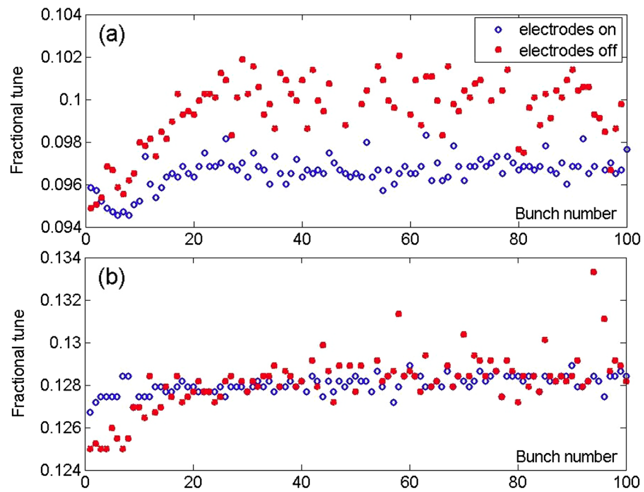

Figure 17: *Bunch by bunch measurements of horizontal (a) and vertical (b) fractional tunes for a positron current of the order of* $\sim$ *500 mA.*

When the electrodes are off horizontal tunes show a typical modulation along the train induced by the e-cloud density variation. The measured values increase progressively and reach a steady state regime after $\sim$ 20 bunches. The head-tail tune spread is about $0.006 - 0.008$. Switching the electrodes on the tune shift reduces by a factor of 2-3, but still the tune spread is not completely cancelled. This is likely due to the fact that the electrodes in the wigglers cover only 67% of the total magnet length. On the contrary the vertical tune spread is notably smaller and the electrodes almost completely cancel it.

A clear effect due to the single bunch e-cloud instability has been detected measuring the vertical beam size at the synchrotron light monitor by gradually turning off the electrodes. The observed beam size increases from about 110 μm with electrodes on, to more than 145 μm with the electrodes off. The e-cloud plasma can interact with RF waves transmitted in the vacuum chamber changing the phase velocity of the waves. The e-cloud changes the electromagnetic properties of vacuum, which can induce a shift of the resonant frequencies modes trapped in the chamber. In principle, from these shifts it is possible to evaluate the e-cloud density. Resonant TE-like modes are trapped in the DAΦNE arcs and can be excited through button pickups. A first measurement of these resonant modes has been done at DAΦNE for several beam currents with the electrodes on and off [?]. A preliminary analysis of the data has given the following results: (a) all modes have a positive frequency shift with the positron beam current and it is between 100 and 400 kHz depending on the modes taken into account; (b) switching on the electrodes the frequency shift can be partially cancelled for almost all modes; (c) the quality factor of the modes decreases with positron current.

The power supplies connected to the electrodes absorb cloud electrons. The current delivered by the generator has been measured as a function of the generator voltage for different beam currents. The result is given in Fig. 18.

Relying on numerical predictions, confirmed by measurement, it was evident that, in order to store positron beam currents higher than 1 A, voltages of the order of 250 V (presently available) are no longer adequate to completely absorb and suppress the e-cloud in DAΦNE.

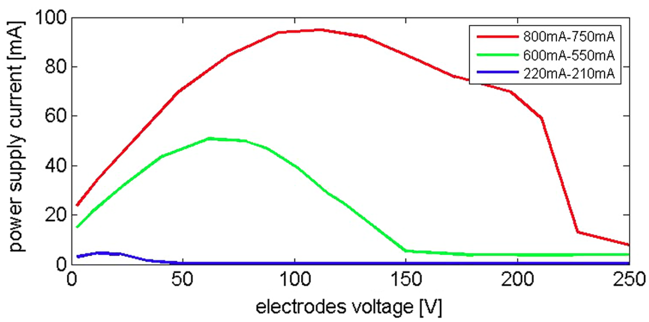

Figure 18: *Current supplied by the DC generator as a function of the applied voltage and beam current; the e-cloud is completely adsorbed when* $I = 0$.

Since the effectiveness of the e-cloud suppression does not depend on the voltage polarity it is preferable using negative voltages in order to avoid damages, caused by electron bombardment of the electrodes, and power supply overcurrent.

On July a medium intensity earthquake caused a relevant misalignment in the IR vanishing large part of the achievements obtained during the previous part of the commissioning: luminosity reduced dramatically and, in the positron ring, even beam injection was problematic. These circumstances forced an anticipated summer shutdown which has been exploited to undertake several activities. The detector end-caps have been opened to measure and restore the nominal position of the low-β elements. The electromagnetic quadrupoles in the IR have been checked too.

An endoscopic inspection of the low-β vacuum chamber confirmed the presence of broken bellows at the place where the temperature rise had been observed. However that component has not been replaced because the operation required the disassembly of the whole IR. An additional air-flow based cooling system has been installed in the IR to stabilize the temperature level. The functionality of the low-level system supervisor, based on old components no longer in production, has been restored by using part from another broken equipment.

Concerning the experimental detector, a half cylinder pure carbon target has been inserted inside the detector drift chamber to study the kaon-nuclei interaction process by using the KLOE-2 apparatus. This study, in fact, can lead to interesting scientific results by acquiring a rather modest data sample of the order of $\sim$ 100 pb^{-1}, for this reason it was quite compatible with the preliminary tests needed before the main KLOE-2 data taking.

DAΦNE operation restarted on mid September. The optics of the two rings has been refined as well as the alignment of electromagnetic quadrupoles in the IR and the Crab-Waist sestupoles by using beam based alignment techniques.

In less than three months performances in terms of peak luminosity have been recovered, $L_{peak} = 1.44 \times 10^{32}$ m^{-2} s^{-1}, while hourly and daily integrated luminosity had even some improvements achieving the values: $L_{\int 1hour} = 0.415$ pb^{-1} (Fig. 19) and $L_{\int day}$ 8 pb^{-1} respectively (Fig. 20).

By the end of the year two important tests have been done concerning the effectiveness of the Crab-Waist sextupoles in presence of a strong solenoidal field introduced by the detector, and the maximum achievable luminosity putting 10 bunches in collision.

All the tests concerning the Crab-Waist sestupoles have been done in collision. A clear increase in the transverse vertical dimension of the electron beam, σ_y^-, has been observed as the Crab-Waist sextupoles strength is reduced in the corresponding ring, see Fig. 21; at the same time σ_y^+ decreases as a consequence of the reduced beam-beam kick.

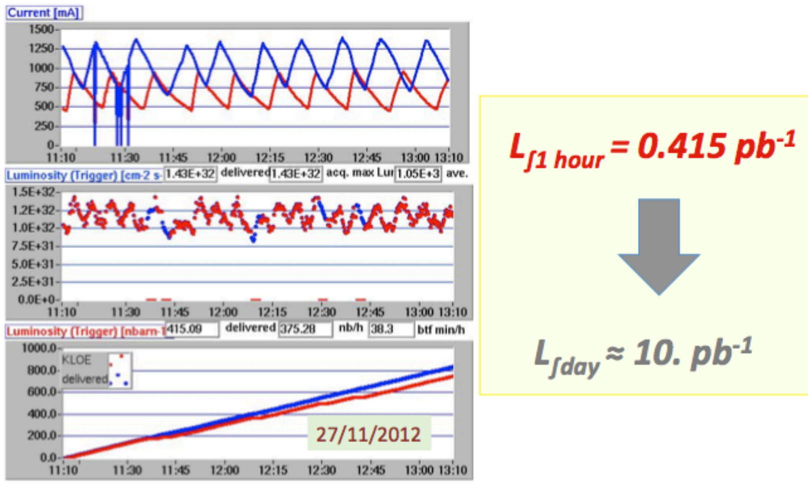

Figure 19: *Best hourly integrated luminosity.*

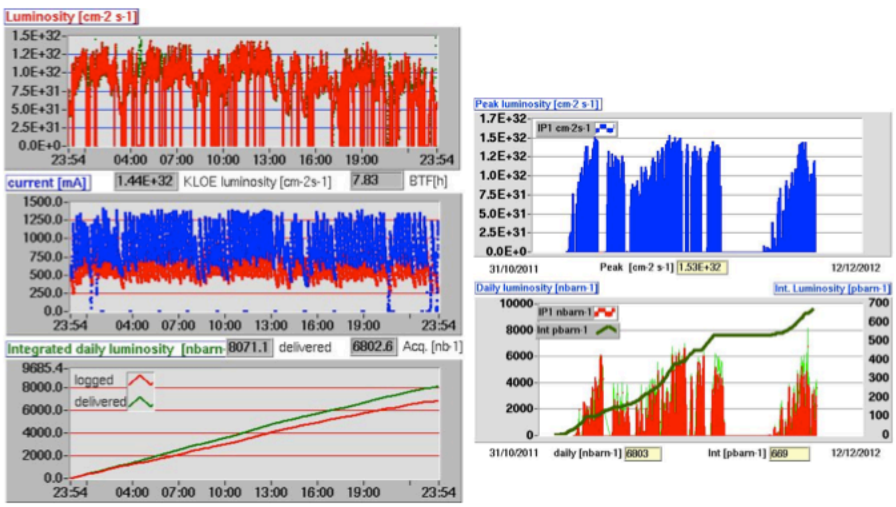

Figure 20: *Best daily run (left), peak luminosity (right top), daily integrated luminosity (right bottom).*

A consistent behavior is observed when the Crab-Waist sextupoles are progressively turned off in both rings, see Fig. 22. In this case the transverse vertical beam dimensions become larger for both beams.

Data from the machine γ-monitor and from the detector, see Fig. 23, point out an evident reduction in the luminosity when the Crab-Waist sextupoles are off. These observations all together give a clear evidence about the Crab-Waist sextupoles capability in keeping under control the coupling resonances due to collision with large horizontal crossing angle even in presence of a large detector having a strong solenoidal field.

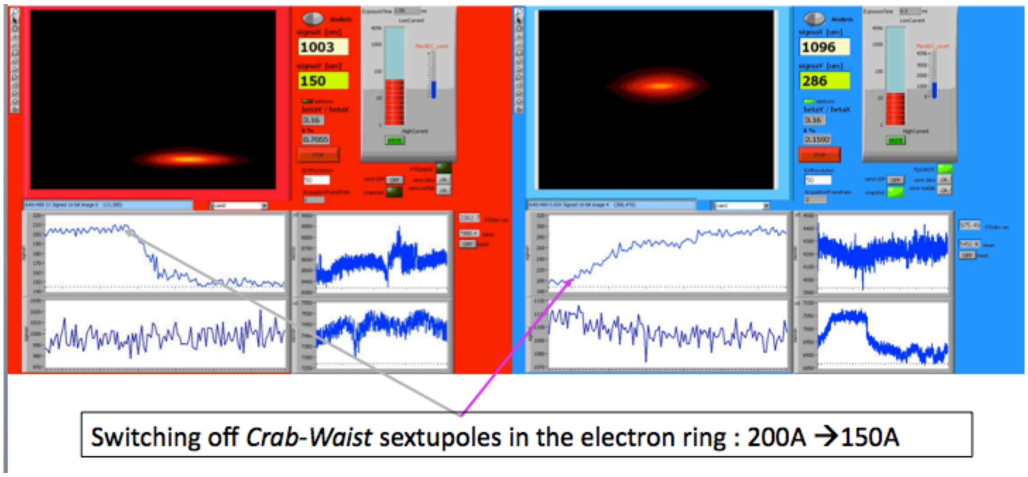

Figure 21: *Vertical beam dimension of the colliding beams as Crab-Waist sextupoles are switched off in the electron ring.*

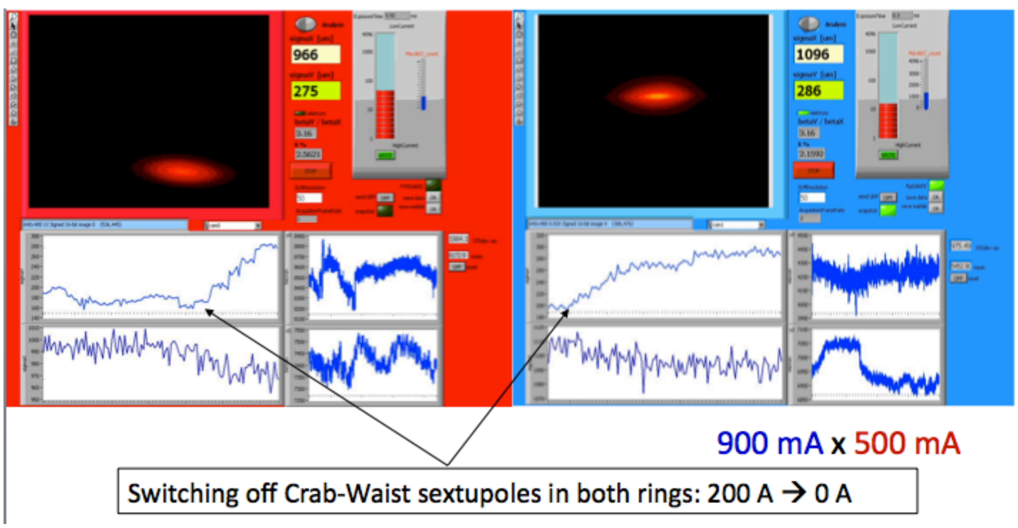

Figure 22: *Vertical beam dimension of the colliding beams as Crab-Waist sextupoles are switched off in both rings.*

Collisions with 10 consecutive bunches permit to measure the maximum achievable luminosity independently from the effects introduced by multi-bunch operations. The maximum value obtained by now in this configuration with the KLOE-2 optics has been 2.19×10^{31} cm^{-2} s^{-1}, which devises the possibility to achieve a peak luminosity of the order of $\sim 2.5 \times 10^{32}$ cm^{-2} s^{-1} by optimizing 110 bunches operations. This test has been also relevant in showing that the present limit in the measured peak luminosity does not depend on the beam-beam or on the Crab-Waist collision scheme.

By beginning of November, contextually with the machine studies, the data taking activity has started. This phase has been quite relevant to optimize the collider background, to improve adiabatically the collisions as well as to deliver to the KLOE-2 detector the 100 pb^{-1} integrated

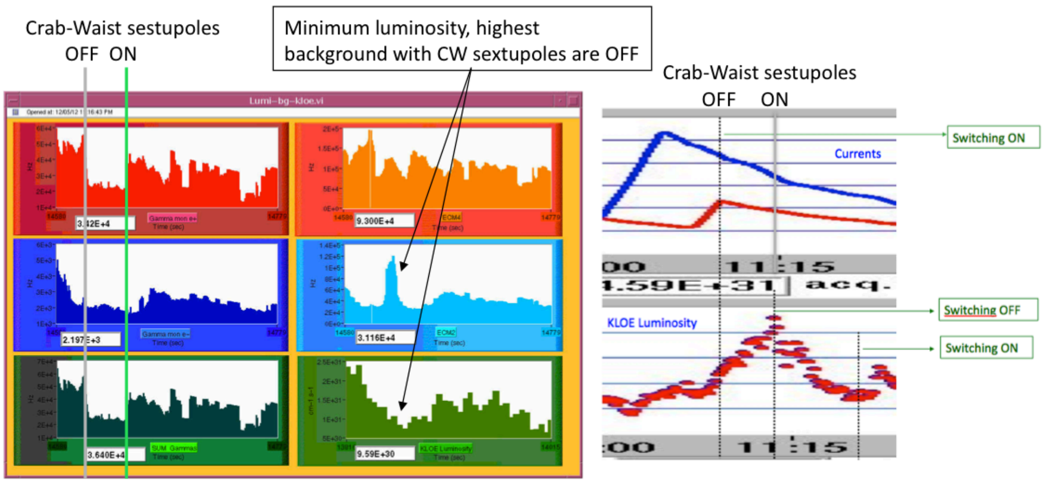

Figure 23: *luminosity evolution as measured from the DAΦNE γ-monitor (left) and from the KLOE detector (right), while switching on the Crab-Waist sestupoles in both rings.*

luminosity required for the experiment with the carbon target.

Consolidation Plan

The DAΦNE accelerator complex has been working for more than 15 years. Recent operation experience has clearly shown that an extraordinary consolidation effort is required in order to provide a 80% uptime in the next years and secure a reliable data taking for the KLOE-2 experiment. A brainstorming on DAΦNE refurbishment started on past spring, stemming from a detailed analysis of the fault occurrences and a critical revision of all the subsystems containing old or out of production parts.

A list of mandatory items has been defined and the relative costs have been evaluated. The more relevant items are:

- Revamping of the low level control system.
- Control system upgrade.
- New power supplies for the skew correctors.
- Improved diagnostic in the accelerator complex.
- Power supplies for e-cloud suppression replaced with devices providing higher voltage.
- New kicker for the transverse feedback in the electron ring.
- Improved design for the vacuum chamber of the low-β section and the relative support.

The consolidation plan has been endorsed and funded by the INFN management. This revamping program will be implemented during the six months long shut starting on January 2013, which has been planned to complete the KLOE-2 detector upgrade.

BTF

P. Valente (Resp.), B. Buonomo, L. Foggetta (art. 23)

The Beam-Test Facility was operational only in the second half of 2013 due to the long shutdown of the DAFNE complex. However, it was possible to deliver about 160 beam-days to 14 user groups, starting from the beginning of June up to mid December. At the same time as providing beam to the users, a significant amount of improvement work has been performed:

- the BTF vacuum sub-system was integrated in the main LNF supervisor with a general revision of the interlock mechanism;

- the photon-tagging system was partially dismounted in order to allow the maintenance of the silicon based detectors ASIC and front-end hardware;

- the BTF network has been redesigned and users and staff computers have been virtualized;

- the LINAC HODOSCOPE and the LINAC BPM hardware and software have been revised, in order to improve BTF operations;

- The GEM compact TPC has been permanently installed with all final service elements (gas system, electronics, rails and mechanics) and with DAQ running in stand-alone, providing a point resolution of about 80 um along the drift coordinate. This was successfully used, e.g. by channeling experiments (see Figure);

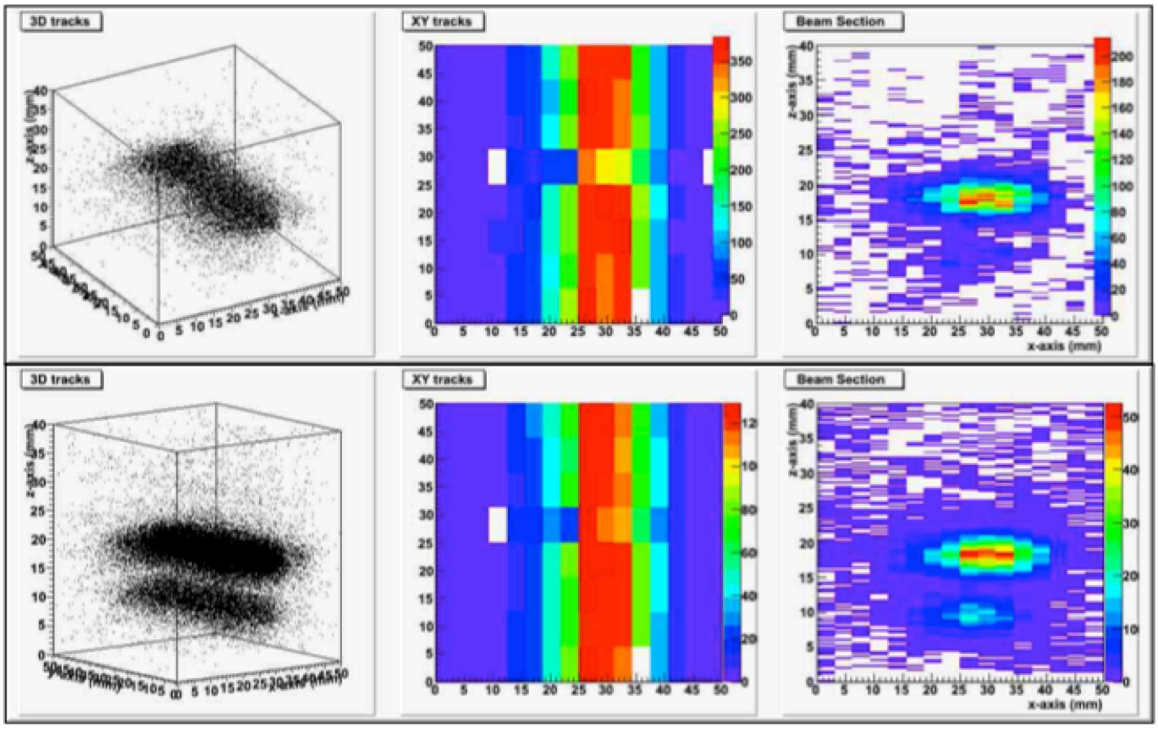

- Installation and test of MEDIPIX detector (Timepix) to increase transverse beam detection granularity for beam position/size monitoring and optimization (see Figure).

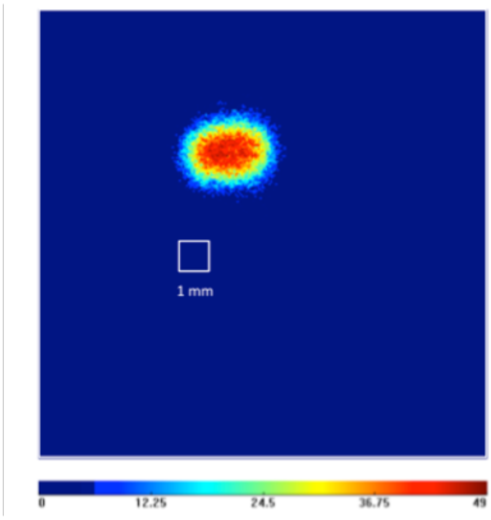

In addition, the BTF calorimeter system has been re-calibrated for providing precise multiplicity measurement. A new triggering and coincidence distribution system was also studied.

First operative tests in collaboration with the !CHAOS teams were performed on BTF magnets and beam, in preparation of the implementation of the !CHAOS controls framework in the BTF environment (for controlling magnets and other devices, and for the acquisition of diagnostics detectors).

DAΦNE-Light Laboratory and Activity

A. Balerna (Resp.), M. Cestelli Guidi (Art. 23), R. Cimino, A. De Sio (Osp.),
A. Grilli (Tecn.), R. Larciprete (Ass.), E. Pace (Ass.), M. Pietropaoli (Tecn.),
A. Raco (Tecn.), V. Sciarra (Tecn.), V. Tullio (Tecn.), G. Viviani (Tecn.).

1 Summary

The scientific activity at the DAΦNE-Light laboratory, in 2013, was mainly performed using conventional sources, due to the DAΦNE shutdown. The experimental teams that got access to the DAΦNE-Light laboratory were from Italian Universities and research Institutions, and some of them also from EU countries within the INFN-FAI framework. The experimental activities, performed in 2013, were dedicated to some upgrades of the beamlines with new instrumentations, and also to the completion of the upgrade of the UV beamline and of the experimental chambers of the two new XUV beamlines that will hopefully be commissioned in 2014. Some tests, using synchrotron radiation, were possible only during few days of the last months of 2013.

2 Activity

2.1 SINBAD - IR beamline

The experimental activity on the SINBAD IR beamline mainly concerns micro-imaging and FTIR (Fourier transform InfraRed) spectroscopy in different research areas, including material science and THz applications, biology, radiobiology, live cell imaging, cultural heritage and geophysics. All these studies are possible owing to the imaging capabilities of the IR microscope coupled to the synchrotron source. Due to the long DAΦNE stand-by, during the last year, researches on the IR beamline were carried out using conventional sources. The institutions involved were mainly Italian teams. Some of the international collaborations were financed by INFN-FAI fundings. Due to the late beginning, for INFN, of the FP7 transnational access project CALIPSO and to the technical problems of DAΦNE, EU users will hopefully start receiving beamtime in 2014.
Some of the scientific results obtained at the SINBAD IR beamline are here summarized:

1. *North American microtektites are more oxidized than tektites.*

   Gabriele Giuli (University of Camerino)

   Iron oxidation states and coordination numbers have been determined by micro-X-ray absorption near edge spectroscopy (XANES) on the cores of a large group of microtektites from the Australasian, Ivory Coast, and North American (NA) tektite strewn field. The difference between the Fe oxidation state of tektites and microtektites from the North American strewn fields suggests that some factors in the formation of the North American microtektites were different than for the North American tektites and for microtektites in the other strewn fields. The 2D map of the intensity of the 3600cm^{-1} FTIR absorption band is shown in Fig. 1, with warmer colors representing higher peak intensities and, thus, higher water contents. The warmer colors at the border of the two samples correspond to the epoxy resin surrounding the microtektite spherules. With the exception of a single sample (a dumbbell shaped tektite) displaying anomalous domains enriched in water, the microtektites analyzed display no significant variations of the water content going from the core toward the rim of the spherules. The determined water content of these microtektites fall within the range of tektites from the same strewn field. The lack of significant water enrichment in microtektites, with respect to tektites, further reinforces the suggestion that these samples are not altered and the Fe oxidation state is not the result of sea water alteration.

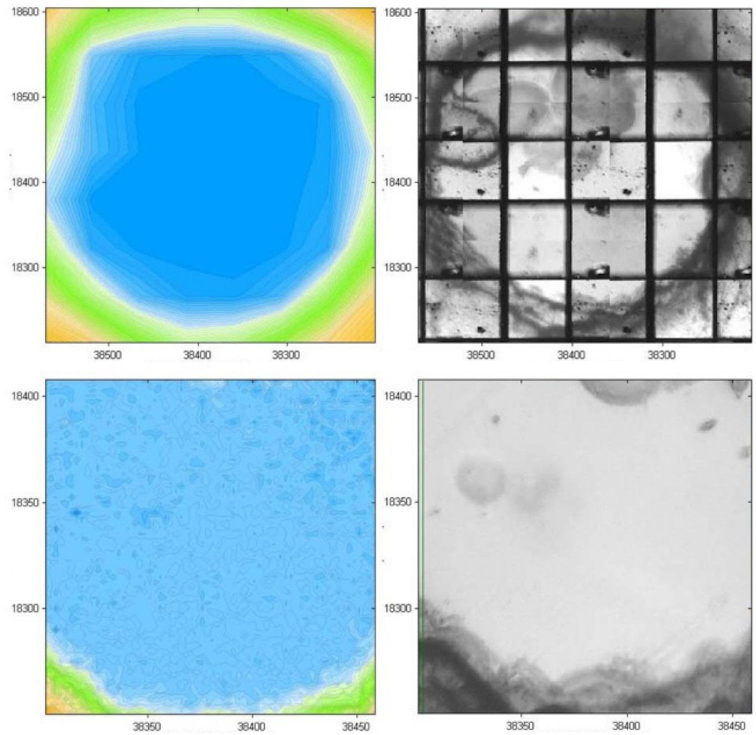

Figure 1: (a) FT-IR mapping of the NA microtektite. The map was recorded using a motorized micrometric sample stage, a single element MCT detector and a 80 μm aperture in the focal plane of the IR microscope. The image size is $\sim$400x400 μm and shows the spatial distribution of the absorption band centered at 3600 cm^{-1} indicating the O-H stretching mode in water molecules. (b) FT-IR Imaging of a smaller area of the same sample (170x170 μm) obtained with a Focal Plane Array detector, showing the spatial distribution of the same OH absorption. The image was recorded without slits. Both images indicate the absence of water inside the measured samples.

2. *Development of new spectroscopic in-situ techniques for the study of dehydration of minerals.*

   University of Roma Tre - Dipartimento di Geologia

   The loss of H_2O and other molecular groups (CO_2, ${SO_4}^{2-}$, ${CO_3}^{2-}$, etc.), typically involved in high-temperature transitions of many minerals, as well as the loss of structural H+ (like for amphiboles and phyllo-silicates) associated with red-ox phenomena, are matter of strong interest among the scientific community. The only way to understand in detail the mechanisms of such processes is by the use of the *in-situ* FTIR technique, in order to measure the variations of light elements at ppm scale, real-time and directly in temperature. The aim of the present work is to set up new micro-analytical techniques to enable us to cover the stability field of almost all of the geological materials. This achievement is possible by the use of equipment specially modified to reach 1200°C, instead of the temperature of 600°C possible with conventional accessories. Initially the technique was applied to the study of the high temperature behavior for several mineralogical species, silicatic and non-silicatic, natural and synthetic, in order to point out the interactions of different functional groups (H_2O, OH^-, CO_2, $SO_4{}^{2-}$ and $CO_3{}^{2-}$) with different structures. Thermal analysis has been applied to halotrichites, a group of hydrated sulphates. Natural amphiboles with different proportions between Fe^{2+} and Mg have been analyzed. A synthetic amphibole (Fe-richterite) was studied and the obtained data (Fig. 2a) were in strong agreement with those from high temperature diffraction (Fig. 2b).

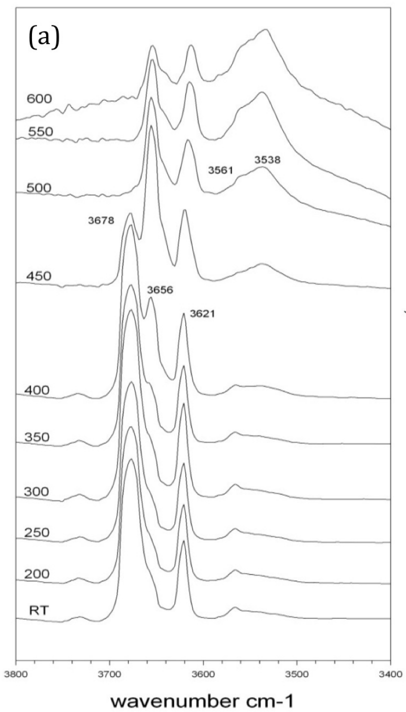

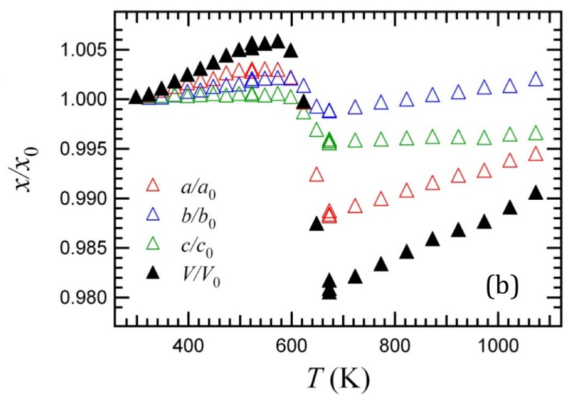

Figure 2: (a) Synthetic Fe-richterite, absorption FTIR spectra measured at room after rapid cooling starting from the temperature indicated for each curve. For the spectra obtained at temperature greater than 400°C, the vertical axis has been exaggerated because of their very low intensities. Such a solution has been chosen to qualitatively visualize the thermal evolution of the principal OH-stretching region absorption bands. (b) Synthetic Fe-richterite, cell parameters variations with temperature, from single cristal diffraction data refinement carried out at Istituto di Cristallografia CNR Pavia.

3. *A crystal-chemical study of cordierite, synthesis and stability at variable H_2O and CO_2 concentration: geological and technological applications.*

   University of Roma Tre - Dipartimento di Geologia

   Microporous and mesoporous minerals are very important materials from both a geological and a technological viewpoint. In this context, cordierite represents the only case of a widespread microporous mineral able to trap significant amounts of molecular H_2O and CO_2 under extreme geological conditions, spanning from the amphibolite facies to ultra-high temperature metamorphism to crustal anatexis . The analysis of volatiles in cordierite can be a very useful tool to define the composition of coexisting fluids during its formation, thus

knowledge of their diffusion mechanism through the structure is crucial in petrologic studies. This knowledge may also have significant implications on technological issues such as the design of new strategies for the permanent sequestration of atmospheric CO_2.
The experiments were carried out in tandem on natural cordierite and synthetic CO_2-free beryl, isostructural with cordierite. All samples were treated in CO_2-saturated atmosphere at different pressure, temperature and time (PTt) conditions using a non end-load piston-cylinder at INGV (Rome). The run products were oriented using a spindle stage, cut and doubly polished and analyzed using polarized micro-FTIR spectroscopy at INFN-LNF (Frascati) equipped with using a Focal Planar Array (FPA) of detectors in order to study the distribution of CO_2 across the sample and quantify its content. Preliminary data showed that pressure play a major role on the diffusion of gaseous CO_2 in both cordierite and beryl, whereas the effect of both temperature and time is less pronounced. The FPA data show that the diffusion of CO_2 occurs exclusively along the structural channels running along the c-axis direction (Fig. 3). Notably, the calculated diffusion coefficients (D) are in the order of 10^{-13}, 10^{-15} m^2/s. Sample cracks formed during the experimental runs speed up the gas diffusion; measured CO_2 contents along these cracks are up to 4 times higher.

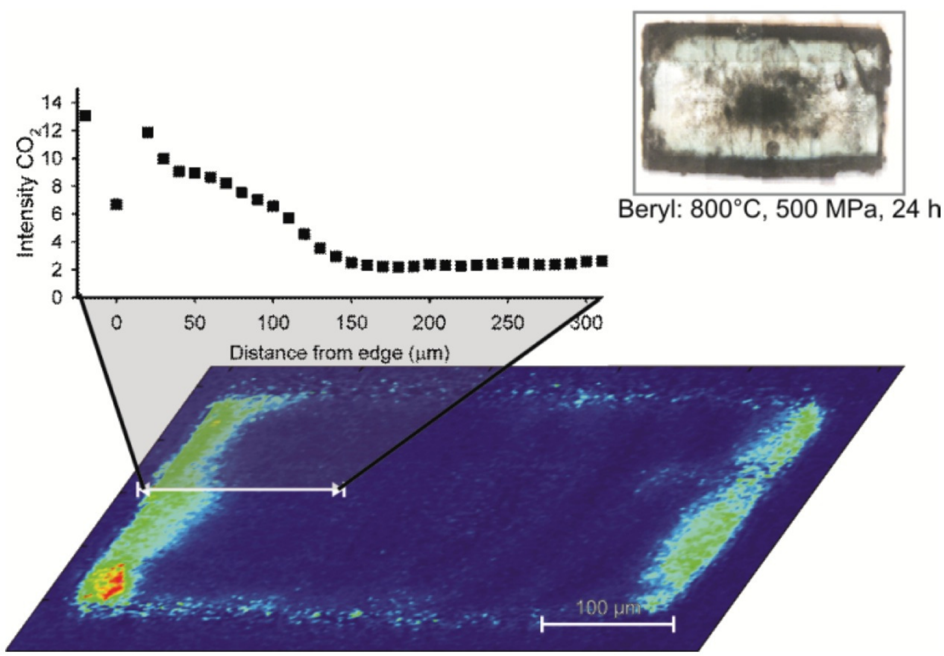

Figure 3: FPA image and FTIR diffusion profile of CO_2 concentration in a synthetic beryl treated at 700°C and 500 MPa for 24 hours.

Several CO_2-rich cordierite samples were heat-treated up to 1200°C using a Linkam heating stage to investigate the rate of CO_2 evacuation as a function of temperature. *In-situ* FTIR spectra showed that the process of CO_2 loss starts around 800°C. Isothermal experiments on 60 m thick slabs pointed out that the CO_2 loss at room-pressure is a very slow and energetic process (Fig. 4); E_a 283±17 kJ/mol measured via FTIR in-situ micro-spectroscopy are over two times larger than the activation energies measured for cordierite dehydration.

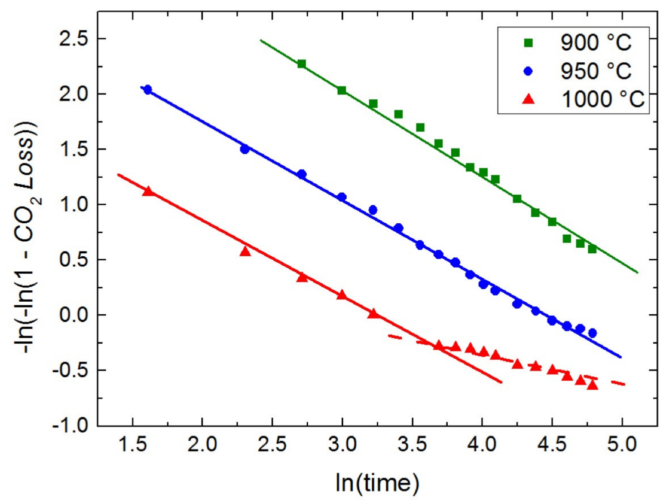

Figure 4: Avrami plot of the CO_2 loss over time during 2 hour isothermal experiments for three different temperatures.

4. *SR-FTIR imaging of single cell / fiber interaction for recognition of amphibole-related lung pathogenesis.*

   University of Bordeaux

   In this series of experiments, the aim is to analyze specifically the ECM (extracellular matrix) of lung cells facing the presence and toxicity of long fibers in their environment, notably considering the production of extracellular matrix, which is a major biochemical aspect of fibrosis development in asbestosis. This ECM is difficult to analyze using conventional cell biology means due to its molecular composition, containing collagens and other fibrillar proteins as well as glycoproteins. These macromolecules are organized as a network and their purification does not allow analyzing a native form. This is mandatory to allow describing the molecular composition of ECM and its changes over time when the cell produces specific ECM for trapping a toxic fiber. A first series of measurements with A549 lung cells exposed to low but gradual amounts of mineral fibers - Crocidolite* $Na_2(Fe^{3+})_2(Fe^{2+})_3Si_8O_{22}(OH)_2$ and Tremolite $Ca_2Mg_5Si_8O_{22}(OH)$ - with 0 (control), 1, 5, and 10 μg/cm^2 of fibers were performed. First IR images show that lipid/protein ratio is higher in controls compared to 1, and 5 μg/cm^2 of fibers (P<0.05), but lower with 10 μg/cm^2 of fibers (P<0.05). These preliminary results are consistent with a previous study using the same methodology (paper under press), where cells exposed to fibers at amounts > than 10 μg/cm^2 exhibited toxicity parameters. At this stage of the experimental development of the single cell imaging by SR-FTIR microscopy it is thus hypothesized that cell already have to adapt to the presence of amphiboles at very low amounts. If confirmed by next experiments using synchrotron radiation for acquisition of high-quality spectral images from cells, one should therefore consider that official exposition levels to mineral fibers might be revised in industry and public safety regulations.

During 2013 two students performed part of their activity at the SINBAD beamline:

1. Dr. Francesca Marchio has spent three months in our laboratory for a Master stage ″Progetto MaTeRiA Master SPRINT PON a3_00370/F″ in the framework of the STAR FEL project.
2. Deborah Schierano from University of Florence started working on her Master Thesis on ″Atmospheres in a test tube″, on the setup of the instrumentation to realize a database of FTIR spectra of gas atmospheres in different pressure and temperature conditions, to be used for comparison with the spectra collected by existing and future space missions.

2.2 DXR1 - Soft X-ray Beamline

The DAΦNE soft X-ray beamline, DXR-1, is mainly dedicated to soft X-ray absorption spectroscopy. The X-ray source of this beamline is one of the 6-poles equivalent planar wiggler devices installed on the DAΦNE electron ring (0.51 GeV) for the vertical beam compaction. The 6 wiggler poles and the high storage ring current (higher then 1 Ampere) give a useful X-ray flux for measurements well beyond ten times the critical energy. The useful soft X-ray energy range is 900 eV - 3000eV where the lower limit is given by the Beryl crystals used in the double-crystal monochromator and the higher limit is given by the wiggler working conditions. Some check tests were performed on all the elements of the beamline after the long shut down at the end of 2013 when the beam conditions became more stable. In order to control the new working conditions also some XANES measurements were performed in the presence of good and stable beam conditions (Fig. 5).

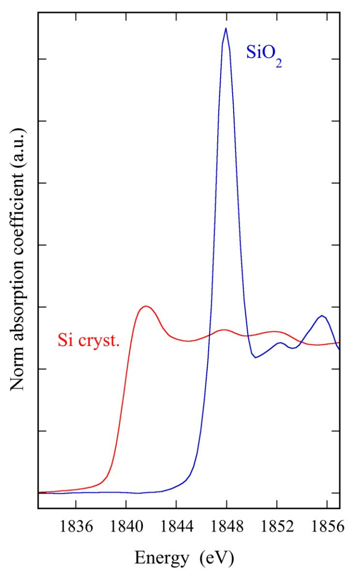

Figure 5: Normalized XANES spectra of crystalline Si and SiO_2 reference compounds.

The soft X-ray beamline has been equipped in 2013 with microfocus W x-ray source (Fig. 6) that will be used to test samples and also to perform XRF measurements using the available SDD detector. A vacuum compatible experimental chamber to test samples containing low Z materials as been purchased and will be aligned and completed in 2014.

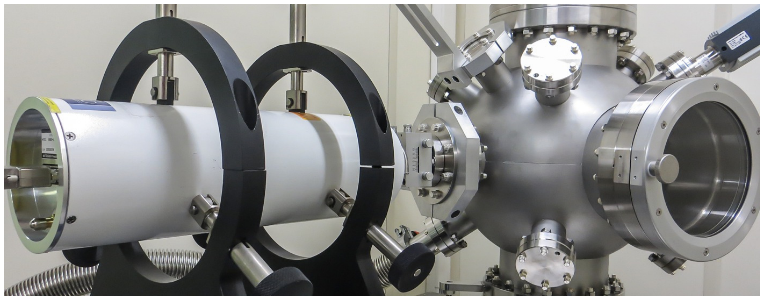

Figure 6: The microfocus x-ray source and the new experimental chamber.

2.3 DXR2 -UV branch Line

The synchrotron radiation (SR) photon beam from a wiggler installed on the DAΦNE storage ring is split by a grazing incidence Au-coated mirror ($\theta_i = 40$ mrad, cut-off energy about 800 eV), in order to provide the X-ray and UV beamlines. The reflected UV radiation travels through the UV beamline and ends in a 63 mm diameter MgF_2 window. The UV-VIS beamline operates on an extended spectral range from 120 nm to 650 nm, spectral regions commonly referred to as Visible, UV-A, UV-B and UV-C. There are three experimental stations: one operates in the VUV (UV-B and UV-C) region between 120 nm and 200 nm (monochromatic radiation), the second covers the range 200-650 nm (VIS, UV-A, UV-B) with monochromatic radiation and the third covers the same spectral range but in white light or broadband typically for experiments of irradiation or aging. The same spectral range can be also covered by conventional light sources like gas discharge lamps that have emission spectra not continuous as synchrotron radiation, but have particularly intense emission lines. The three stations can also be used in test operations and calibration of components of optical systems even of large size, of photon detectors having standard sizes and of thin layers or multilayers. It is possible to carry out measurements of reflectivity, transmissivity and absorption of thin layers. This beamline is particularly suitable for experiments of photochemistry and photobiology related to the characterization of inorganic and organic materials, the alteration of organic molecules and inorganic complexes as an effect of irradiation experiments and aging. The UV region of this beamline has been used for photochemistry experiments to study molecules of astrobiological interest. This kind of experiments was also performed in combination with the use of the SINBAD IR beamline to monitor in real time the UV irradiation effects. An on-going project for a photochemical facility at the DAΦNE-L laboratory combines the UV and the IR beamlines. The accessible wavelength region for the photochemical experiments is 180-400 nm. In the framework of the analyses of dielectric materials, as diamond for electronic devices and detector, and of biological materials, a table-top Scanning Electron Microscope (mini-SEM) has been purchased and will be set up and put in operation during 2014. The advantage of such an instrument is the option of low- vacuum operation, which is very useful to make high-resolution images of samples like bacteria and biological materials with no need of deposition of conductive layers.

2.4 New XUV beamlines and laboratory

Aim of this laboratory is to host two bending magnet beamlines covering the photon energy range from 30 eV to 1000 eV. One beam line will cover the low energy part of this interval (30-200 eV) and is called LEB (Low Energy Beam line), the other will cover the range from 60 eV to 1000 eV and is called HEB (High Energy Beam line). Both beam lines are in UHV and directly connected to the vacuum of the main DAΦNE ring. All the safety protocol and control systems are ready and tested. Since the beginning of the year, the two beam lines were ready to start commissioning with synchrotron light. Such initial commissioning was not even started due to the lack of a stable orbits and beam from DAΦNE in 2013. The complex procedures of commissioning the two XUV beamlines will start as soon as the necessary beam conditions will become available. Meanwhile, the two *state of the art* end stations, whose construction was nearly completely funded without using resources from the DAΦNE-L laboratory, are still being implemented and successfully used. Both experimental set-up have been equipped with commercial laboratory sources (X-ray lamp and He-discharge lamps), electron sources and all the needed tools to perform not only detailed tests on their functionality but also experiments. Also a *state of the art* micro-Raman station founded combining DAΦNE-L and IMCA-NTA economic resources is routinely being used. At the moment the experimental chambers are mainly used to perform experiments on SEY (Secondary Electron Yield) reduction versus electron bombardment, surface conditions and Carbon deposition, which are the objectives of the IMCA Project (see this annual report for a detailed description of this activity) and are done in collaboration with R. Larciprete (ISC-CNR), Iaia Masullo (INFN-NA) and CERN vacuum Group. The laboratory has been recently equipped with an in air scanning tunneling microscope (STM) shown in Fig. 7.

Figure 7: In air scanning tunneling microscope (STM) from RHK to be soon available.

This instrument, acquired by combining differently obtained economic resources, can and will be upgraded in 2014 to be used in UHV, incrementing the appeal and the available techniques of the XUV laboratory. Annalisa Romano, from University of Benevento, has spent 4 months in the XUV laboratory to perform her bachelor thesis work.

3 List of Conference Talks

1. F. Radica, F. Bellatreccia, G. Della Ventura, C. Freda, G. Cinque, M. Cestelli Guidi, ″FTIR imaging of carbon dioxide diffusion in cordierite-like structures″, Goldschmidt Conference,

Firenze, 25 - 30 August, 2013

2. A. Balerna ″The DAΦNE-Light synchrotron radiation facility ″, SILS XXI in FisMat2013: Italian National Conference on Condensed Matter Physics, Milano, September 9-13, 2013.

3. F. Radica, F. Bellatreccia, G. Della Ventura, G. Cinque, M. Cestelli Guidi, C. Freda, ″SR-FTIR imaging of carbon dioxide diffusion in cordierite-like structures″, SILS XXI in FisMat2013: Italian National Conference on Condensed Matter Physics, Milano, September 9-13, 2013.

4. M. Cestelli-Guidi, ″Applications of syncrotron light analysis ″, 3rd International Conference Frontiers in Diagnostic Technologies - Frascati, November 25-27, 2013.

4 Lectures

1. M. Cestelli-Guidi, ″Un nuovo approccio analitico al micro-imaging IR: raggiungere i limiti strumentali″, Workshop: Innovazione tecnologica per la diagnostica dei Beni Culturali: macro-imaging IR e micro XRF - Dip. di Ingegneria, Univ. La Sapienza, Roma, 15 Marzo 2013.

2. M. Cestelli-Guidi, ″La generazione di immagini spettrali. Dalla teoria alla pratica″, Scuola di Spettroscopia IR Applicata alla Diagnostica dei Beni Culturali: II edizione - Venaria Reale (TO), 15-18 Ottobre 2013.

5 Publications

1. T. Fornaro, J. R. Brucato, E. Pace, M. Cestelli Guidi, S. Branciamore, A. Pucci , ″Infrared spectral investigations of UV irradiated nucleobases adsorbed on mineral surfaces″, Icarus, **226**, 1068 (2013)

2. G. Giuli, M. R. Cicconi, S. G. Eeckhout, C. Koeberl, B. P. Glass, G. Pratesi, M. Cestelli-Guidi and E. Paris, ″ North-American microtektites are more oxidized than tektites.″, American Mineralogist, **98**, 1930 (2013)

3. G. Della Ventura, G. Ventruti, F. Bellatreccia, I. Bilotti, F. Scordari, M. Cestelli Guidi ″FTIR and Raman spectroscopy of sideronatrite, a sodium-iron hydrous sulfate.″, Mineralogical Magazine, **77**, 499 (2013)

4. E. Pace, M. Cestelli Guidi, A. De Sio, L. Gambicorti, A. Grilli, M. Pietropaoli, A. Raco, G. Viviani ″An innovative photochemical facility at DAΦNE-L″, J. of Phys: Conf. Series, **425**, 072024 (2013)

5. D.R. Grosso, M. Commisso, R. Cimino, R. Larciprete, R. Flammini, R. Wanzenberg, ″Effect of the surface processing on the secondary electron yield of Al alloy samples.″, Phys. Rev. Spec. Top.-Accelerators and Beams, **16**, 051003 (2013)

6. R. Larciprete, D.R. Grosso, M. Commisso, R. Flammini, R. Cimino ″Secondary electron yield of Cu technical surfaces: Dependence on electron irradiation″, Phys. Rev. Spec. Top.-Accel. and Beams, **16**, 011002 (2013)

BY-NanoERA

(Institutional Development of Applied Nanoelectromagnetics: Belarus in ERA Widening)

S. Bellucci (Resp. INFN), R. Baldini (Tecn.), S.Bistarelli (Laur.), M. Mastrucci (Bors. Tecn.), A. Cataldo (Bors.), G. Giannini (Osp.), F. Micciulla (Osp.), E. Stefanutti (dott.)

External collaborating Institutions:

Institute of Nuclear Problems of Belarusian State University,
Institut fuer Festkoerperphysik, Technische Universitaet Berlin,
Central Laboratory of Physico-Chemical Mechanics, Bulgarian Academy of Sciences, Sofia,
Institute of Electronic Structure and Laser (IESL), Heraklion, Crete,
Belarusian Institute of System Analysis and Information Support of Scientific Technical Sphere,
Science & Technology Park "Metolit" at Belarusian National Technical University.

We participate as a partner (the INFN unit) to the Coordination and support actions of the FP7-INCO-2010-6. BY-NanoERA has a duration of 36 months and started its activities on 1st January 2011. The consortium binds together four Universities, two Research Organizations and an industry (Science & Technology Park).

Project objectives:

The main objectives of the project BY-NanoERA are to prove necessity and promising capability of nanoelectromagnetics in the core objective of FP7 Theme 4 'Nanosciences,Nanotechnologies, Materials and new Production Technologies – NMP' and to develop a concept of nanoelectromagnetics as a perspective direction in NMP. We also wish to establish network with research centers in Member States or Associated Countries in the field of applied nanoelectromagnetics aimed with the progress in solving concrete scientific problems and submission of joint research projects, as well as to organize a set of workshops and seminars on nanoelectromagnetics.

Publications by LNF Authors in the Year 2013

A study of random resistor-capacitor-diode networks to assess the electromagnetic properties of carbon nanotube filled polymers, DS Bychanok, AG Paddubskaya, PP Kuzhir, SA Maksimenko, C Brosseau, J Macutkevic, S Bellucci, Applied Physics Letters, Volume 103, Page 243104

Transport mechanisms and dielectric relaxation of epoxy nanocomposites in dc to microwave range, Stefano Bellucci, D Bychanok, P Kuzhir, S Maksimenko, J Macutkevic, C Brosseau, 2013 International Semiconductor Conference (CAS), Volume 1, Pages 35-40, Editor IEEE.

Nanocarbon broadband analysis, temperature dependent dielectric properties and percolation thresholds, S Bellucci, J Macutkevic, PP Kuzhir, A Paddubskaya, SA Maksimenko, A Cataldo, F

Micciulla, J Banys, 2013 International Conference on Electromagnetics in Advanced Applications (ICEAA), Pages 536-539, Editor IEEE

Carbon foams, nano-thin carbonaceous films and nanocarbon based polymer composites: Microwave applications, PP Kuzhir, SA Maksimenko, T Kaplas, Y Svirko, A Celzard, J Macutkevic, F Micciulla, S Bellucci, 2013 International Conference on Electromagnetics in Advanced Applications (ICEAA), Pages 415-418, Editor IEEE

Equivalent electric circuits for the simulation of carbon nanotube-epoxy composites, Biagio De Vivo, Patrizia Lamberti, Vincenzo Tucci, P Kuzhir, S Maksimenko, Stefano Bellucci, Number 99 Pages 1-1, Editor IEEE

Epoxy Resin/Carbon Black Composites Below the Percolation Threshold J Macutkevic, P Kuzhir, A Paddubskaya, S Maksimenko, J Banys, A Celzard, V Fierro, E Stefanutti, A Cataldo, F Micciulla, S Bellucci, Journal of Nanoscience and Nanotechnology, Volume 13, Pages 5434-5439

Electrical transport in carbon black-epoxy resin composites at different temperatures, J Macutkevic, P Kuzhir, A Paddubskaya, S Maksimenko, J Banys, A Celzard, V Fierro, S Bistarelli, A Cataldo, F Micciulla, S Bellucci, Journal of Applied Physics, Volume 114, Pages 033707.

Characterizing epoxy composites filled with carbonaceous nanoparticles from dc to microwave, D Bychanok, P Kuzhir, S Maksimenko, S Bellucci, C Brosseau, Journal of Applied Physics, Volume 113, Pages 124103-124103-6

Broadband dielectric/electric properties of epoxy thin films filled with multiwalled carbon nanotubes, Jan Macutkevic, Polina P Kuzhir, Alesia G Paddubskaya, Juras Banys, Sergey A Maksimenko, Eleonora Stefanutti, Federico Micciulla, Stefano Bellucci, Journal of Nanophotonics, Volume 7, Pages 073593-073593

List of Conference Talks by LNF Authors in the Year 2013

S. Bellucci, Nanotechnology and Advanced Materials as enablers of applications in Health: possible activities within priority health of HORIZON2020, Closing Meeting BY-NanoERA, Octorber 2013, Institute of Nuclear Problems of Belarusian State University

S. Bellucci et al., Advanced mechanics of heat-resistant boron containing phosphate ceramics: toward nuclear and aerospace applications, ICCS17 17th International Conference on Composite Structures (ICCS/17), at the University of Porto, Porto, Portugal, 17-21 June 2013.

S. Bistarelli et al., AFM characterization and cytotoxic effects induced by multiwalled carbon nanotubes on human breast adenocarcinoma cell line, International workshop on Nanoscience and nanotechnology 2013, Laboratori Nazionali di Frascati, 30 September-4 October 2013.

LHCPhenoNet: Advanced Particle Phenomenology in the LHC

G. Corcella, V. Del Duca (Resp.)

The research topics investigated within the LNF sub-node of the INFN node of the LHCPhenoNet network can be divided into two main realms:

- theoretical and phenomenological aspects of collider physics for LHC (G. Corcella, V. Del Duca);
- mathematical methods in quantum field theory (V. Del Duca);

The projects tackled in 2013 in the two research areas above are listed below:

i) Z' boson production at the LHC, assuming that the Z' bosons can decay into supersymmetric particles [1, 2];

ii) computation of multi-loop scattering amplitudes in gauge theories, using advanced concepts of modern algebra, like the symbol map [3];

iii) universality of the infrared divergences of QCD amplitudes [4, 5];

iv) a subtraction scheme for the computation of cross sections to NNLO in α_S in a process independent way [6].

References

[1] G. Corcella and S. Gentile, "Heavy Neutral Gauge Bosons at the LHC in an Extended MSSM," Nucl. Phys. B **866** (2013) 293 [Erratum-ibid. **2013** (2013) 554] [arXiv:1205.5780 [hep-ph]].

[2] G. Corcella, "Searching for supersymmetry in Z' decays," EPJ Web Conf. **60** (2013) 18011 [arXiv:1307.1040].

[3] V. Del Duca, L. J. Dixon, C. Duhr and J. Pennington, "The BFKL equation, Mueller-Navelet jets and single-valued harmonic polylogarithms," JHEP **1402** (2014) 086 [arXiv:1309.6647 [hep-ph], arXiv:1309.6647].

[4] V. Del Duca, G. Falcioni, L. Magnea and L. Vernazza, "High-energy QCD amplitudes at two loops and beyond," arXiv:1311.0304 [hep-ph].

[5] V. Del Duca, G. Falcioni, L. Magnea and L. Vernazza, "Beyond Reggeization for two- and three-loop QCD amplitudes," arXiv:1312.5098 [hep-ph].

[6] V. Del Duca, G. Somogyi and Z. Trocsanyi, "Integration of collinear-type doubly unresolved counterterms in NNLO jet cross sections," JHEP **1306** (2013) 079 [arXiv:1301.3504 [hep-ph]].

Communication and Outreach

R. Centioni (Resp.), S. Reda (Bors.), M. Scudieri (Art. 15), E. Santinelli (Art. 15)

SIDS - Scientific Information and Documentation Service

Throughout the year the LNF provide basic education in physics by means of a vast outreach program for the general public, teachers and students.

These activities are made possible by the enthusiastic involvement of INFN-LNF people: graduate students, postdocs, researchers, engineers and technicians.

We remember 2013 as the year the European Physical Society (EPS) declared AdA (Anello di Accumulazione), the first particle-antiparticle accelerator ever built, Historic Site. The celebration took place at the Frascati National Laboratories (LNF), with the unveiling of the Plaque by the European Physical Society and two important seminars as part of the Bruno Touschek Memorial Lectures. Prof. Samuel C. C. Ting (MIT, Nobel Prize for Physics 1976) held a scientific seminar "Latest results from AMS" (in English) and Prof. Luigi Rolandi (CERN), held the seminar "Il bosone di Higgs un anno dopo la sua scoperta" (in Italian) for general public and schools. All the data and pictures are available at http://www.lnf.infn.it/edu/AdA_EPSHistoricSite/

L. Cifarelli (SIF Vipresident) and F. Ferroni (INFN President) unveil the EPS Plaque

The events are organized both inside - (Visits, Open Day, Physics Lessons, European Researchers Night and special appointments addressed to high school teachers and students such as Incontri di Fisica and Stages) - and outside LNF (Seminars at schools, local libraries, etc).

1) **Visits** www.lnf.infn.it/edu/visite to LNF are a well established tradition. They consist of a brief historical presentation of the Laboratories and their activities on site and abroad, and of a guided tour to the experimental areas and the open air museum. Visits are organized for both students in

their last high school year and pupils (age: 10-14) and they usually last about 3 hours. This year the pupils' program, named Quasar Project, hosted about 900 kids.
Not just Italian schools but also schools from all over the world book visits. During 2013 about 5000 people visited the LNF.
(Scientific Coordinator: D. Babusci and B. Sciascia for the Quasar Project)

2) The **Open Day** www.lnf.infn.it/edu/settimana/ consists of a full day program of guided tours inside LNF, conferences, public lectures, expositions and scientific videos. Most of the LNF employees are then in action to present their research centre, answer questions and take care of their guests.
This year's LNF Open Day was on April 22, 2013, hosting about 900 people.
(Care of SIDS-Ufficio Comunicazione ed Educazione Scientifica).

Open Day 2013 (INFN-LNF Photo)

4) **Seminars** www.lnf.infn.it/edu/seminaridivulgativi/ aimed to high school students and the general public are held every couple of months by important personalities of the scientific field at the LNF's Bruno Touschek Auditorium. Among this year's guests, we were glad to have A. de Rujula and M. Mangano from CERN, who illustrated the last results achieved by LHC. Upon request, LNF researches will also hold lessons in schools and libraries. A special agreement exists with the Frascati's library and the IKEA store.
In 2013 Seminars involved about 1500 students all over Italy.


A. de Rujula' Seminar 2013 (INFN-LNF Photo)

5) **Incontro con l'Autore** www.lnf.infn.it/edu/ica/ LNF organize meetings with authors who present their scientific books. On October 11th, 2013, Catalina Curceanu presented her new book *Dai buchi neri all'adroterapia: un viaggio nella fisica moderna* at LNF Frascati.

6) **European Researchers' Night** http://www.frascatiscienza.it/ organized by FrascatiScienza. The SIDS is involved in setting up guided tours at LNF.
The European Researchers' Night took place on September 27th, 2013 and hosted about 1000 people with a program of guided tours, conferences and performances.

7) **Incontri di Fisica** www.lnf.infn.it/edu/incontri/ has been organized since 2001. The event is a three-days course for high school teachers and people involved in scientific research dissemination. About 200 participants from all over Italy, attend this event every year. The goal is to stimulate teachers' professional training and provide an occasion for interactive and hands-on contact with the latest developments in physics.
The program consists of plenary lessons, presentation of INFN-LNF activities, visits to LNF experimental area and discussion. The peculiarity of this course is represented by the group work, focused on a theoretical lesson and hands-on activity or data analysis of a real experiment. This way, teachers have a direct contact with researchers and they can use typical experimental instrumentation employed in contemporary physics.
Teachers, authorized by the Minister of Education, receive a certificate of participation.
All the programs are published on the LNF web site (lessons, videos, photos).
LNF October 9th -11th, 2013.
(Organizing Committee: D. Babusci, R. Centioni, C. Curceanu (Chair), P. Di Nezza, U. Dosselli, R. Fabrianesi (AIF), C. Gatti, G. Venanzoni – Secretariat: E. Santinelli, M. Scudieri)

8) **Stages for students** www.lnf.infn.it/edu/stagelnf have been organized since 2000 for high school students in their last years. Students are selected by their teachers on the basis of their curriculum but above all on the basis of their interest and motivation.
In direct contact with their tutors (1 tutor / 2 students), students are involved in theoretical lessons and practical operations. They acquire knowledge and understanding of INFN research activities in an interactive modality.
At the end of the stage they will get a Certificate of Participation.

The LNF offers a number of different stages:

- The Stage Masterclass is organized on behalf of IPPOG Masterclasses International Project. It lasts 5 full days, usually in February. Students, in one group of 40, follow lessons on modern physics and analyze data from the ALICE experiment at CERN.
This year's Stage Masterclass was at LNF between February 25nd and March 1st.
(Scientific Coordinators: D. Domenici (Resp), P. Di Nezza)

- The International Masterclass is open for 45 of the best students in their last year(s) of high school/college, from every European country. It usually lasts about 4 days and it involves lectures on Modern Physics and its applications in our society, and activities to be performed in laboratories. Participants have, as well, the opportunity to visit the main experiments and accelerating facilities of the LNF. The official language is English. LNF, LNF February 4th-7th, 2013
(Scientific Coordinator: C. Curceanu);

- The Winter Stages take place during the school year and they consist of 9 appointments, once a week. 24 students - February 4th – March 16th, 2013.
(Scientific Coordinator: C. Curceanu);

- The Summer Stages are organized in June, at the end of the school year, and last 10 days.
Summer Stages – 128 students - LNF June 10th -21nd, 2013.
(Scientific Coordinator: D. Babusci);

-**AISTAP Summer Camp** organized by LNF for students (age:13-18), belonging to the *Associazione Italiana per lo Sviluppo del Talento e della Plusdotazione*. In 2013 for the first time, this 3 days camp took place between July 10th and 12th, involving about 20 students in a program of conferences, guided tours and experimental activities.
More info http://www.lnf.infn.it/edu/stagelnf/2013/prog_AISTAPsumcamp13.html
(Scientific Coordinator: C. Curceanu);

Participation in the stages program has increased over the last 10 years: since 2000, 1235 students attended the stages. In the year 2000, LNF hosted 12 students from just one local school, while in the year 2013, 288 students from over 90 different schools all over Italy and from abroad came to Frascati.

Tab. 1

Year	Students	Females	Males	School	INFN Tutors
2000	12	1	11	1	7
2001	14	3	11	1	14
2002	57	15	42	8	50
2003	56	11	45	14	22
2004	114	34	80	21	25
2005	154	42	112	29	56
2006	161	48	113	46	58
2007	163	45	118	51	55
2008	161	47	114	51	63
2009	177	40	137	54	67
2010	166	36	130	60	60
2011	184	61	184	60	70
2012	206	59	147	72	59
2013	288	78	210	90	84

The LNF monitor the successes of the various initiatives proposed, mostly through questionnaires (each one specific to the event) and keep track of the progresses using dedicated databases, thanks to which it is possible to perform simple statistical analysis.

9) **Web page**

On the LNF web site are reported all the events organized: tutors lessons, videos, photos, reports that, together with the educational material and the general information about the LNF research activities, introduce the general public and schools to modern physics and INFN-LNF research, so to bridge the gap between science and society.

Tab. 2 - Number of participants to LNF events during 2013

EVENTS (2010)	**PARTICIPANTS**
Visits	5000
Open Day	900
Seminars (at LNF and outside)	1500
European Researchers' Night	1000
Incontri di Fisica for high school teachers	210
Stages for high school students	288

Aknowledgments

Many thanks to the LNF Director and the Heads of Accelerator, Research and Technical Divisions. Special thanks to all LNF Tutors and Services and to Ms Beatrice Zuaro for the help in editing this document.

CONFERENCES, WORKSHOPS and MEETINGS

International conferences, workshops and meetings hosted and/or organized by LNF:

1. *XI Workshop on Resistive Plate Chambers and Related Detectors (RPC2012)* LNF, 5-10 February 2012.
2. *ALICE HLT Physics Workshop*, LNF 9-11 February 2012.
3. *ALICE Physics Week 2012-LNF*, LNF 15-20 March, 2012.
4. *3rd SuperB Collaboration Meeting* LNF 19-23 March, 2012.
5. *Radiative Corrections and Generators for Low Energy Hadronic Cross Section and Luminosity* LNF 16-17 April, 2012.
6. *Management of radioactive waste: from transmutation to bioremediation*, LNF 16-23 April, 2012.
7. *Commissione Scientifica Nazionale II*, LNF 16-18 April, 2012.
8. *XVI Frascati Spring School "Bruno Touschek"*, LNF 7-11 May, 2008.
9. *Frontier objects in Astrophysics and Particle Physics*, Vulcano 28 May - 2 June, 2012.
10. *ECLOUD'12*, LNF 5-8 June, 2012.
11. *Open Problems in Quantum Mechanics - QF2012*, LNF 20-22 June 2012.
12. *New Trends in Algebraic Quantum Field Theory*, LNF 12-14 September, 2012.
13. *MC-PAD*, LNF 19-22 September, 2012.
14. *Channeling 2012*, Alghero 23-28 September, 2008.
15. *Nanoscience and Nanotechnology 2012*, LNF 1-4 October, 2012.
16. *r-ECFA*, LNF 5 October, 2012.
17. *Dark Forces at Accelerators - Dark 2012*, LNF 16-19 October, 2012.
18. *International Technical Laser Workshop 2012 (ITLW-12)*, LNF 5-9 November 2012.
19. *2nd Joint HiLumi LHC-LARP Annual Meeting*, LNF 14-16 November, 2012.
20. *Bruno Touschek Memorial Lectures 2012* LNF 7 December, 2012.
21. *6th SuperB Collaboration Meeting* LNF 11-14 December, 2012.
22. *JLab12 e gli altri esperimenti: punti di incontro e prospettive future*, LNF 18-19 December, 2012.

INFN INTERNAL NOTES

INFN-13-01/PI
SuperB Collaboration (F. Forti et al.), *SuperB Detector Technical Design Report*

INFN-13-02/CCR
R. Veraldi et al., *Analisi Preliminare sull'Evoluzione del Sistema di Mailing dell'INFN*

INFN-13-03/LNF
D. Di Gioacchino et al., *Radiation damage: evaluation of cosmic rays fluxes and high intensity radiation beams*

INFN-13-04/LNF
ILC Global Design Effort and World Wide Study, *International Linear Collider - Technical Design Report*

INFN-13-05/LNF
A. Mottana, A. Marcelli, *Fifty years since the first European synchrotron radiation-derived XAFS spectrum (Frascati, 1963)*

INFN-13-06/GE
F. Alessandria et al., *Technical Design Report of the Superconducting Dipole for fair SIS300*

INFN-13-07/PG
B. Checcucci, F. Cantini, *Guida al "Sistema di catalogazione e gestione delle Dotazioni Tecnologiche INFN per fini di Trasferimento Tecnologico"*

INFN-13-08/GE
M. Conte, A.U. Luccio, *About the Extraction of Beams with a Very Small Momentum Dispersion*

INFN-13-09/LNF
A.V. Franchi et al., *Test for the Measurement of Diffusion Coefficient of Water in Kapton Foils for the Gem Detector of the Upgraded High-Pseudorapidity Muon Detection in CMS*

INFN-13-10/LNF
G. Raffone, *Manifold Design of the GEM Detectors for a Uniform Gas Flow*

INFN-13-11/LNF
G. Raffone, *CHE and Related Stresses in GEM Foils*

INFN-13-12/GE
F. Ameli et al., *Digital Hydrophone Signal Acquisition and Analysis for KM3NET*

INFN-13-13/CLAB
M.E. Biagini et al., *Tau/Charm Factory Accelerator Report*

INFN-13-14/CNAF
C. Galli, *Piano per la Migrazione Sistemistica dell'Impianto di Contabilità INFN dalla release R11i a 32 bit alla R12.1.3 a 64 bit*

INFN-13-15/CNAF
C. Galli, *Disaster Recovery INFN: Configurazione di una soluzione High Availability con Oracle Data Guard 11g*

INFN-13-16/LNF
C. Polese et al., *Instruments and methods for XRF analysis of multilayer materials*

INFN-DIV-13-01/LNF
C. Gatti, *La scoperta del Bosone di Higgs: la versione di ATLAS*

INFN-13-17/GE
M. Osipenko et al., *Comparison of fast amplifiers for diamond detectors*

INFN-DIV-13-02/LNF
M. Beretta, C. Bloise, M. Dreucci, C. Gatti, S. Martellotti, *Misura della vita media del Muone*

INFN-13-18/LNF
S. Wang, Z. Wu, A. Marcelli, D. Di Gioacchino, *The AC multi-harmonic magnetic susceptibility measurement setup at the LNF-INFN*

INFN-13-19/LNF
S. Di Matteo, L. Sperandio, *Evaluation of the Anomalous X-Ray Energy in VIP Experiment*

INFN-13-20/LNF
S. Di Matteo, L. Sperandio, *Evaluation of the anomalous X-ray energy in VIP experiment: some values from Dirac-Fock method*

INFN-13-21/LNF
C. Curceanu, L. De Paolis, S. Di Matteo, H. Elnaggar, L. Sperandio, *Evaluation of the X-ray transition energies for the Pauli-Principle-violating atomic transitions in several elements by using the Dirac-Fock method*

INFN-13-22/LNF
M. Antonelli, P. Raimondi, *Snowmass Report: Ideas for Muon Production from Positron Beam Interaction on a Plasma Target*

INFN-13-23/LNF
M. Pallotta, *Per se definition of Dirac's Delta funcion*

POPULAR PHYSICS NOTES

In 2013 has been inaugurated the series of popular publications aimed at teachers and students of high school students and the general public.

INFN-DIV-13-01/LNF
C. Gatti, *La scoperta del Bosone di Higgs: la versione di ATLAS*

INFN-DIV-13-02/LNF
M. Beretta, C. Bloise, M. Dreucci, C. Gatti, S. Martellotti, *Misura della vita media del Muone*

2013 LNF GENERAL SEMINARS

LNF Seminars Committee: M. Boscolo (Resp.), U. Dosselli (LNF director),
T. Spadaro (CSN1 local coord.) , A. Paoloni (CSN2 local coord.) , A. Fantoni (CSN3 local coord.),
S. Bellucci (CSN4 local coord.) , S. Dell'Agnello (CSN5 local coord.),
D. Babusci, (SIDS resp.), M. Legramante (secr.)

LNF General Seminars are listed below. In addition to the general seminars program we successfully continued the *LNF mini-workshop series* initiated in 2012 with the idea of deepen selected topics which we believe are of interest for the laboratory. In total, seven mini-workshops have been organized covering different research areas, from space physics to high energy physics, as well as applied physics (https://agenda.infn.it/categoryDisplay.py?categId=636).

1 List of the 2013 LNF General Seminars:

1. Emilie Passemar (Los Alamos National Laboratory, USA):
   "Vus from τ: status and perspectives at new facilities", 10 January.
2. Theo Demma (Laborateur de l'Accelerateur Lineaire CNRS-IN2P3):
   " Collective Effects in the 50 MEV Thomx compact storage ring", 17 January.
3. Wolfram Weise (ECT*):
   " Strangeness in Low-Energy QCD and Dense Baryonic Matter ", 11 March.
4. Caterina Bloise (INFN-LNF):
   "Highlights from Moriond EW2013", 13 March.
5. Max Klein (Liverpool University):
   " Physics and Realisation of the LHeC" 21 March.
6. Alessandro Stecchi (INFN-LNF):
   "!CHAOS: a new approach to Control Systems" , 25 March.

Figure 1: *Poster of the Seminar given by Giovanni Jona-Lasinio.*

7. John Cesaratto (SLAC):
   "Recent Measurements of a 4 GS/s Intra-bunch Vertical Feedback System at the SPS", 26 March.

8. Robert Jan Veenhof (CERN):
   " Simulation of gas detectors and related physical processes", 9 April.

9. Werner Riegler (CERN):
   " Signal Formation in Particle Detectors", 9 April.

10. Leticia Cunqueiro (INFN-LNF):
    " Probing the QGP with ALICE at the LHC", 18 April.

11. Paul Robert Bolton (Kansai Photon Science Institute, Japan Atomic Energy Agency):
    "Kansai Photon Science Institute and Progress with Laser-acceleration of Protons", 23 April.

12. Viorel Sandu (National Institute of Materials Physics, Bucharest-Magurele):
    "Tritium in Superconductors", 8 May.

13. Franco Cervelli (Univ. Pisa):
    " Precision measurement of the positron fraction in primary cosmic rays with the AMS-02 detector", 10 May.

14. Tiberio Ceccotti (CEA):
    " Ultra High Intensity laser-matter interaction at CEA Saclay", 16 May.

15. Michael Sokoloff (Cincinnati Univ):
    " Precise Measurements of D-Meson Properties", 5 June.

16. Giovanni Jona-Lasinio (Univ. La Sapienza) (see poster in Fig. 1):
    "Le molecole chirali: un caso di rottura spontanea di simmetria", 6 June.

17. P. di Nezza (INFN-LNF):
    "Summary of the International Nuclear Physics Conference (INPC 2013)" ,13 June.

Figure 2: *Movie on Bruno Touschek.*

18. Roberto Petronzio (Univ. Roma Tor Vergata):
    "Il progetto tau charm: un acceleratore italiano per la fisica del sapore con applicazioni interdisciplinari"

19. Kamal Seth (Northwestern University):
    "Timelike Form Factors of Pions, Kaons and other Hadrons", 3 July.

20. Giorgio Saccoccia (ESA):
    "ESTEC and its role within the European Space Agency", 19 September.

21. Bogdan Wojtsekhowski (TJNAF):
    "Search for Heavy Photon", 26 September.

22. Kirill Prokofiev (New York Univ.):
    " Status and prospects of the Higgs boson studies in the Atlas experiment at the LHC" , 1 October.

23. Marco Ricci and Francesco Ronga (LNF):
    "Highlights from ICRC2013, the International Cosmic Ray Conference" , 24 October.

24. Simone Liuzzo (ESRF):
    "Optimization studies and error budget for the ESRF upgrade lattice", 4 November.

25. Allen Caldwell (Max Planck Institut):
    " Plasma wakefields - a revolution in particle acceleration" , 7 November.

26. P. Lenisa (Univ. Ferrara and INFN):
    " Search for Electric Dipole Moments with Polarized Beams in Storage Rings", 20 November.

27. Sante Carloni (Karlova Univ.) :
    "PDF Dark Universe and Marvels of Gravity: exploring the idea of a geometric interpretation of the Dark Phenomenology"

28. Francesco Gullo (Yahoo Labs, Spain):
”From Patterns in Data to knowledge Discovery: what Data Mining can do”, 26 November.

29. Caterina Biscari (ALBA-CELLS, INFN-LNF):
” ALBA, the Spanish Synchrotron Light Source”, 9 dicembre.

30. Emanuela Schisani (Agenzia Promozione Ricerca Europea):
” Bandi ERC 2014: caratteristiche e regole di partecipazione”, 11 December.

31. Gioacchino Ranucci (INFN-MI):
” Caratteristiche e obiettivi dell’esperimento di oscillazione di neutrino JUNO - Jiangmen Underground Neutrino Observatory” , 12 December.

32. Introduzione di A. Ghigo e G. Pancheri (INFN-LNF): Proiezione del film ”Bruno Touschek con AdA a Orsay: Storie delle prime collisioni tra elettroni e positroni in un laboratorio”, 16 December.

2 LNF Mini-workshop series list:

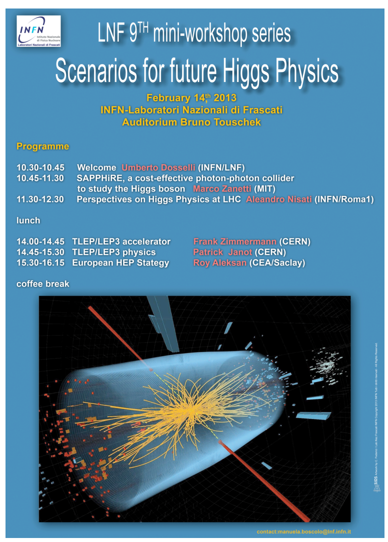

Figure 3: *9th LNF Mini-Workshop on Future Higgs Factories.*

1. **Challenges in Higgs Phenomenology (24 January)**
Overview:
The Mini-workshop ‘Challenges in Higgs phenomenology’ will address the above issues and the recent results on the Higgs boson searches at 7 and 8 TeV will be presented by both CMS and ATLAS collaborations. On the theoretical side, special attention will be paid to Higgs production in vector boson fusion and to the role played by the inclusion of higher-order radiative corrections.

   Programme:

   (a) Terrance Maynard Figy (Manchester Univ.):
   ”Higgs boson production via vector boson fusion”,

(b) Francesco Fabozzi (INFN-NA):
"Search for the Standard Model Higgs boson at CMS ",

(c) Andrea Gabrielli (INFN-ROMA1):
"Status of the Standard Model Higgs boson searches with the ATLAS detector".

2. **Scenarios for future Higgs Physics (14 February)** (see poster in Fig. 3)
Overview:

After the discovery at the LHC of a new boson with a mass of 125 GeV, the high-energy physics community is investigating the idea of precisely assessing its properties by means of a future accelerator complex devoted to the production of a high statistics of such bosons, a so-called Higgs factory. This one-day workshop puts a focus on the most recent studies in this field, in particular aiming at comparing in depth the prospects of on-going studies on the Higgs boson at the LHC with the needed and affordable sensitivity potential of a future Higgs factory. Different Higgs-factory machine design options will be compared.

Programme:

(a) Marco Zanetti (MIT):
"SAPPHIRE, a cost-effective photon-photon collider to study the Higgs boson"

(b) Aleandro Nisati (INFN-ROMA1):
"Perspectives on Higgs Physics at LHC"

(c) Frank Zimmermann ((CERN):
"TLEP/LEP3 Accelerator"

(d) Patrick Janot ((CERN):
"TLEP/LEP3 Accelerator"

(e) Roy Aleksan (CEA):
"European HEP Stategy"

3. **Planck Mission Results (29 May)**

(a) Alessandro Melchiorri (ROMA1):
"Cosmological Constraints from the Planck satellite mission "

(b) Sabino Matarrese (PD):
"Constraints on the Physics of the Early Universe from the Planck Satellite Mission"

4. **Presentazione dei progetti di ricerca PED4PV e CIGS Thin Film (Ricerca su tecnologie e materiali innovativi per applicazioni in ambito fotovoltaico" (18 Giugno)**
Overview:

I progetti in studio intendono sviluppare una nuova tecnologia di produzione di celle fotovoltaiche che abbiano un assorbitore in Cu(InGa)Se2 in sostituzione del silicio cristallino bulk. Il Cu(InGa)Se2 essendo un semiconduttore a gap diretto ha potenzialit molto superiori al silicio come riduzione del pay back energetico , per la sua possibilit di ottenere elevate efficienze con un adatta architettura del dispositivo, per la possibilit di essere depositato su supporti facilmente integrabili nelledilizia. Allo scopo si vuole industrializzare un tecnica di deposizione di film sottili fin ora utilizzata solo per lo studio di materiali complessi : La Pulsed Electrons Deposition (PED) . La nuova apparecchiatura potr semplificare il processo di produzione dei dispositivi e principalmente abbatterne i costi che oggi limitano la diffusione di questi dispositivi. Lapplicazione della PED non si limita alla deposizione dei calcogenuri ma una tecnica applicabile alla ablazioni di molti materiali complessi.

Programme:

(a) Umberto Dosselli (LNF director):
Welcome

(b) Flavio Lucibello (INFN-LNF):
Presentazione progetti

(c) Mariano Zarcone (INFN-LNF):
La tecnologia Thin Film, il CIGSe, La PED un nuovo strumento per depositare i materiali complessi

(d) Alberto Clozza, Marco Milucci (INFN-LNF):
Cosa si fa ai LNF: Deposizione di film per Sputtering

(e) Massimiliano Bazzi, Emanuele Sbardella (INFN-LNF):
Cosa si fa ai LNF: Elettronica per Pulsed Electron Deposition

(f) Discussione e conclusioni

5. **INFN-Space/3 (18 September)** (see poster in Fig. 4)

Figure 4: *INFN-Space 3 Workshop.*

6. **The Higgs Physics (23 October)** (see poster in Fig. 5)

Figure 5: *Poster of the 9th LNF mini-workshop series.*

(a) Umberto Dosselli (LNF director):
"Welcome "

(b) Gino Isidori (INFN-LNF):
"Theoretical Overview on Higgs Physics"

(c) Fabio Cerutti (LBNL):
"Higgs Properties at the LHC "

(d) Alain Blondel (Geneve Univ):
"Higgs Factories "

(e) Frederic Teubert (CERN):
"Probing the Higgs mechanism with flavour physics: status and perspectives"

7. **Detectors for the LHC Upgrade (28 November)** (Fig. 6)

(a) Vitaliano Chiarella (INFN-LNF):
"Introduction "

(b) Helmut Burkhardt (CERN):
"High-Lumi LHC"

(c) Giovanni Bencivenni (LNF):
"Gaseous Detectors R&D for the Muon Systems Upgrade at LHC"

(d) Guido Volpi (INFN Pisa):
"Trigger for LHC Run II and beyond"

(e) Markus Keil (CERN):
"Next generation of silicon pixel detectors for the upgrade of the LHC experiments"

(f) Francesca Cavallari (INFN-ROMA1):
"Calorimetry challanges in view of LHC upgrades"

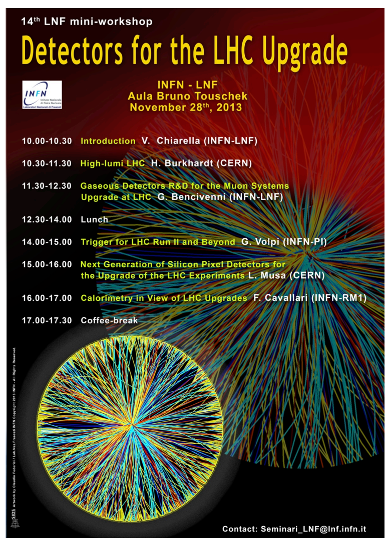

Figure 6: *14th LNF Mini-Workshop.*

The General Services and Technical Division 2013

F. Angeloni (Art. 15), M. Arpaia, G. Bisogni, F. Bocale, M. Campoli, S. Cantarella (Art. 23), A. Cassarà, P. Celli, O. Cerafogli, A. Chiarucci, A. Clozza, V. Crisanti, A. De Paolis, A. Donkerlo, G. Ferretti, M.A. Franceschi, C. Fusco, M. Giorgi, E. Iacuessa, M. Marchetti, U. Martini, M. Matteo (Art. 15), S.G.A. Monacelli, M. Monteduro, T. Napolitano, E. Passarelli, R. Ricci, A. Riondino, M. Rondinelli, U. Rotundo, M. Ruggeri, C. Sanelli (Head, Tech. Div.), F. Sanelli, M. Santoni (as of February), A. Sorgi, A. Tacchi, R. Tonus, R. Valtriani

Retired in 2013: G. Bernardi, L. Iannotti, P. Panattoni

1 Introduction

The mandate of the General Services and Technical Division is the facility management of the Frascati Laboratories, and, at the same time, the Division must guarantee all the necessary support to experiments and accelerating machines in their research and technical activities, mainly in the field of mechanics, electric systems and HVAC systems. The Division can also supply technical and scientific support in the following technologies: ultra-high vacuum, beam diagnostics systems, magnets and power supplies for accelerating machines as civil engineering and service plants.

During 2013, the Division collaborated, supported and gave consultancies with many experimental activities, such as AMADEUS, ATLAS, BES III, CCR, CNAO, CUORE, ETRUSCO II, FISMEL, FLAME, ICARUS, JEM-EUSO, KAONNIS, KLOE2, LHCb, MAE-INDIA, MOONLIGHT, NA62, NANOPAD, NESCOFI@BTF, NEXT, PANDA, SIDDHARTA, SPACEWEATHER, SPARC, TPS, UA9, VIP2.

The Division strongly supported the SPARC-LAB and DAFNE complex, upgrading many systems and performing normal and extraordinary maintenance during the long shut-down. A great job was accomplished, as requested by the INFN Management at the beginning of the year, in the study of a possible tau-charm machine as alternative to the Super-B flagship project of INFN. In addition, the Division also supplied technical assistance to the INFN Headquarters in Rome and, but only for some services, to the INFN Central Administration.

2 General Services Dept.

The General Services Dept. of the LNF deals with the organization and management of the general operational activities of the LNF and the Central Administration of the INFN, such as:

1. ENEA Canteen + Bar/Canteen LNF
2. Cleaning Service
3. Guards Service
4. Gardening Service
5. Porterage
6. Reuse of discarded furniture
7. Child care center
8. Buses
9. Coffee breaks and lunches
10. Deratization and pest control

11. Purchase of hygienic materials and rental of no-dust carpets
12. Purchase and cleaning of work clothes
13. Drink water dispensers rental
14. Microbiological analyses of LNF bar food & equipment
15. Lease, insurances, maintenance and documentation of LNF vehicles
16. Emission of badges for staff & guests of LNF & AC and several other INFN structures
17. Liaising with the City of Frascati for licenses, authorizations and taxes
18. Liaising with the ENEA Frascati Center.

In addition to routine activities, during 2013 the Dept. has dealt with:

- organization of the new LNF Canteen premises;
- preparation of the public tender for Guards & Security Services;
- organization of facilities for the EPS – AdA Historic Site Event of December 5th, 2013: installation of the marquee in collaboration with the supplying firm; organization of the catering; preparing the gardens & terrain; coordination of restoration activities of the area of the monuments;
- cleaning up of the gardens around Villa Laura after the renewal of its roof;
- extraordinary pruning of the pine trees.

Collaboration with the Research Groups in the organization of meetings and conferences – coffee breaks, lunches, conference room preparation, participants transport (*Summer Internships, Spring School, Researchers' Night, Eurofel, Iride, WGRC, Incontri di Fisica, NN2013, PSHP2013 etc.*).

The General Services Dept. of the LNF consists of two persons: Ms Anna Tacchi (Dept. Head) and Mr Massimo Santoni (collaborator), who joined the Dept. in February.

3 Central Stores and Purchasing Dept.

The Central Stores and Purchasing Dept. supervises the purchasing and stocking of goods of the Central Stores as well as those of the Metal Stores, and incoming and outgoing articles; development and extension of the stocked articles. The LNF, the Central Administration and some INFN Sections and groups have access to the LNF Stores.

Moreover, the Dept. carries out market researches upon request of the users for the extension and upgrade of the articles in stock, maintains quality standards of stocked articles, and performs maintenance and updating of its web pages, including the online General Catalogue database for the general users. Extensive use of Consip, mainly through MEPA, has been made.

During the 2013 accounting period the Central Stores and Purchasing Dept. has transferred a total amount of € 142.000,00 for stock materials replenishment as follows:

- € 62.000,00 on Cap. 130110 (standard consumables),
- € 80.100,00 on Cap. 130120 (research consumables).

Furthermore, the Dept. has spent approx. € 78.300,00 for its ordinary activities, including mail handling services and management of small services such as the fork lift and small office equipment.

These activities have entailed the preparation and emission of over 100 RdA, to which should be added approx. 100 orders to contracted firms for minor purchases.

4 Building Management Dept.

In the course of the year 2013, the renovation works on the roof of Villa Laura and the ADONE guest houses have been completed.

Routine maintenance and repairs as well as extraordinary maintenance has been executed on the LNF buildings in order to preserve the value of the LNF assets. Other repair and maintenance works involving modifications, adaptations and renovations on LNF buildings have been carried out upon requests of the various LNF experimental groups.

5 Mechanical Design and Construction Dept.

The Mechanics Design and Construction Group (SPCM) is composed of five Units: Mechanical Design, Carpentry and Soldering, Machine Shop, Metrology and Alignment, Material Store.
During 2013, the SPCM lost again some staff: one person was retired, and another was transferred within the Technical Division; Metrology in particular continued to suffer lack of personnel and its activity has stopped since June 2012.

The SPCM performs the following tasks:

- mechanical design of experimental apparatuses and detectors, using CAD/CAE software and FEM analysis;
- construction of prototypes and structures with the support of various soldering techniques and numeric control machine tools;
- production of high precision mechanical components, relying on manual and numeric control machine tools equipped with CAM control;
- high precision dimensional check, material strength test, large structures and apparatuses optical alignment;
- acquisition and storing of mechanical components, tooling, metallic and plastic materials of workshop common use.

During 2013, the SPCM has supplied support to several experimental activities, playing a role of direct responsibility in the design, production, construction or installation: CUORE (Cryogenic Underground Observatory for rare Events) at LNGS for the study of Neutrinoless Double Beta Decay (engineering coordination and integration of the whole experimental apparatus), JEM-EUSO (Extreme Universe Space Observatory onboard Japanese Experiment Module) to be installed aboard the International Space Station for the study of Ultra High Energy Cosmic Rays (photo detector module and focal surface layout and mechanics).

Many other activities were supported as well, though with no direct involvement in terms of responsibility: ATLAS, DAFNE, ETRUSCO2, FISMEL, KAONNIS, KLOE2, MAE-INDIA, MU2E, NA62, NANOPAD, NESCOFI@BTF, NEXT, PANDA, SPARC, UA9, VIP2 were supported in terms of mechanical design or construction.

To conclude, some 70 short-term actions were taken by the SPCM personnel to support experimental activities, in case of unplanned production, interventions or urgent repairs.

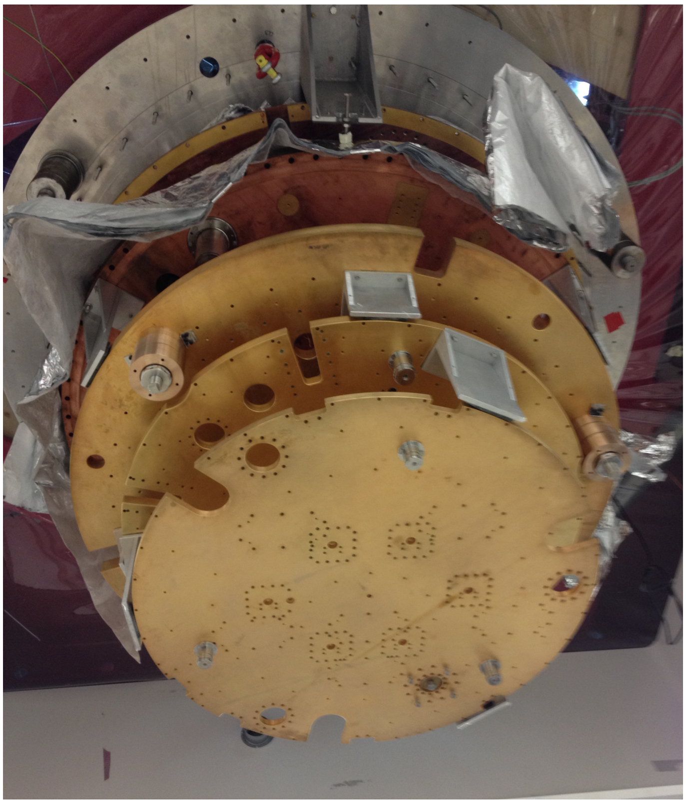

CUORE: Cryostat top plates assembly @LNGS

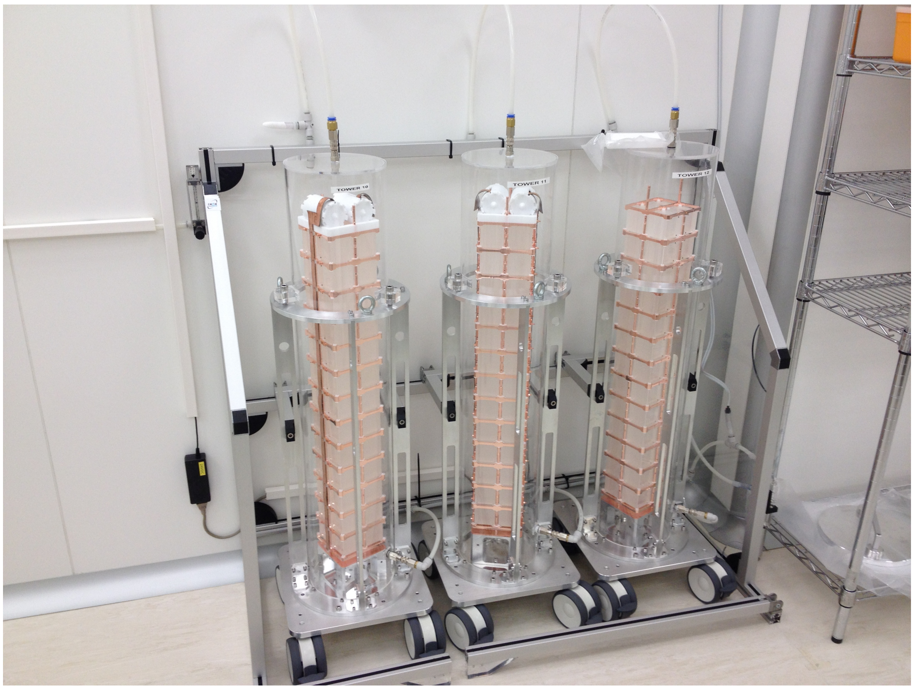

CUORE: Detector Towers (3 over 19), stored @LNGS

6 Heating, Ventilation, Air Conditioning Department

The HVAC Dept. is in charge of the operation and maintenance of the auxiliary plants, comprising water cooling plants, water treatment facilities, compressed air and other gases production and distribution systems, HVAC plants for accelerators and experimental halls.

The group is also in charge of the HVAC Building Management (civil plants), and tap water distribution for the whole Lab.

Procurements for new installations, from technical specifications definition to the follow-up of tender procedures, construction, commissioning, start-up, performance tests and standard operations constitute part of the work scope of the Dept.

In 2013 the group has provided support to DAFNE, KLOE, BTF, SPARC, FLAME, ATLAS and the LNF Data Center.

During the year, the installation work for the upgrade of the Frascati Data Center has been completed, arranging the new hall to host the ATLAS TIER2. A back-up system for cooling IT structures has been installed, which resulted in the possibility to run the facility also during water cut problems due to the mains fault.

The revamping of the SPARC supervisory and control system for Cooling and HVAC plants has been executed. The revamping of the PLCs system for the management of the Fluid Plants related to the DAFNE accelerator complex has been conducted in close collaboration with the Electric Systems Dept.

7 Electric Systems Department

The Dept. manages the LNF electrical installations from the high voltage power supply to end users and the lighting. The 150 kV substation and the eight cabins are operated by staff, who also cover emergency calls and fault fixing. Routine safety and functional maintenance activities are usually performed by external contractors under the Dept.'s supervision. Maintenance involves several skilled scheduled activities on switchboards, transformers, medium voltage devices, safety lighting, UPS, emergency generating sets and electrical devices of Dafne and Sparc cooling systems, but also small repairs or changes requested by users.

The Department also services the INFN Rome Headquarters offices' installation.

In 2013, the Dept. has been involved in the revamping of the Dafne Auxiliaries Control System, which has been studied since October 2012, and which has been carried out during the first half of 2013. This system integrates Cooling, HVAC, Vacuum, RF and the Magnets safety system. All the control levels of the 9 cooling system switchboards have been renewed.

This activity aimed to improve the control systems, to fix some problems, substitute obsolete components of control and regulation that were expensive and out of production, and save spare parts, not available any more, necessary for the maintenance of the previous magnet safety system.

The activity implied a joint effort of different departments, including reverse engineering, field devices test and fault fixing. The Electrical Dept. coordinated the activities, the studies and the tests. A better exploitation of the devices is obtainable in terms of energy efficiency.

The Dept. also takes care of the telephone service. In 2013 the telephone switchboard has been upgraded and now is VoIP ready.

The technical direction of the electrical power supply contract involves continuous contacts with public utility companies and increasingly accurate load and budget forecasts. The LNF laboratories and the Central Administration burnt out about 19 GWh in the 2013, against a cost of 3,55 M€.

Some technical support was supplied to other INFN Data Centers through CCR.

8 Other technical-scientific support activity

During 2013 a lot of work has been done on the Tau/Charm project. In particular, a preliminary design of the vacuum system of the machine complex has been carried out going in detail with LINAC, Transfer Lines, Damping Ring and Main Rings vacuum system. The main result of this activity is the Tau/Charm Factory Accelerator Report, arXiv 1310.6944.

The activities related to the VIP experiment proceeded with the realization of the experimental setup, which is now under data acquisition test. Moreover, some other activities related to the VIP experimental area, located in Laboratori Nazionali del Gran Sasso, have been carried out.

The experimental activities of the PED4PV project have started in 2013. The PED4PV project aims to demonstrate that the Pulsed Electron Deposition (PED) technique is a valid and innovative method to realize thin film based Photo Voltaic (PV) cells. Scope of the task, performed at the LNF, is the deposition of Molybdenum thin film as back contact on several substrates of various nature, such as: glass, stainless steel, copper, bronze, ceramic, cement. For this purpose a dedicated thin film deposition system has been realized, with which several samples have been made. The activity is going on, with good results.


Figure 1 Deposition Chamber


Figure 2 160x160 mm Ceramic Substrate with Mo coating

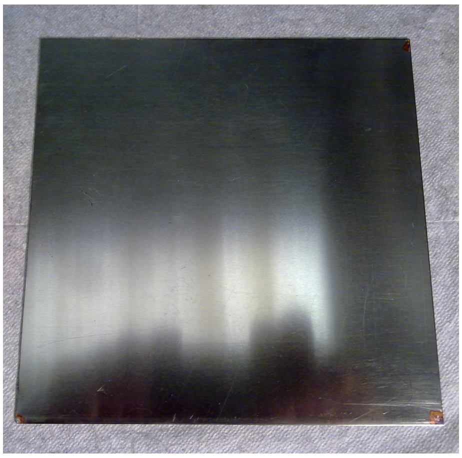

Figure 3 160x160 mm copper substrate with Mo coating

9 Some Statistics

ACTIVITY REQUESTS STATISTICS

During 2013, a total number of **848** registered requests reached the Technical and General Services Division, either through the General Users Form (543 requests), the SPCM 'small jobs request procedure' (147 requests), or through a 'flash mail' system for several standard requests (illumination repairs, conference coffee breaks requests, HVAC repairs, and tenocode modifications) (158 requests).

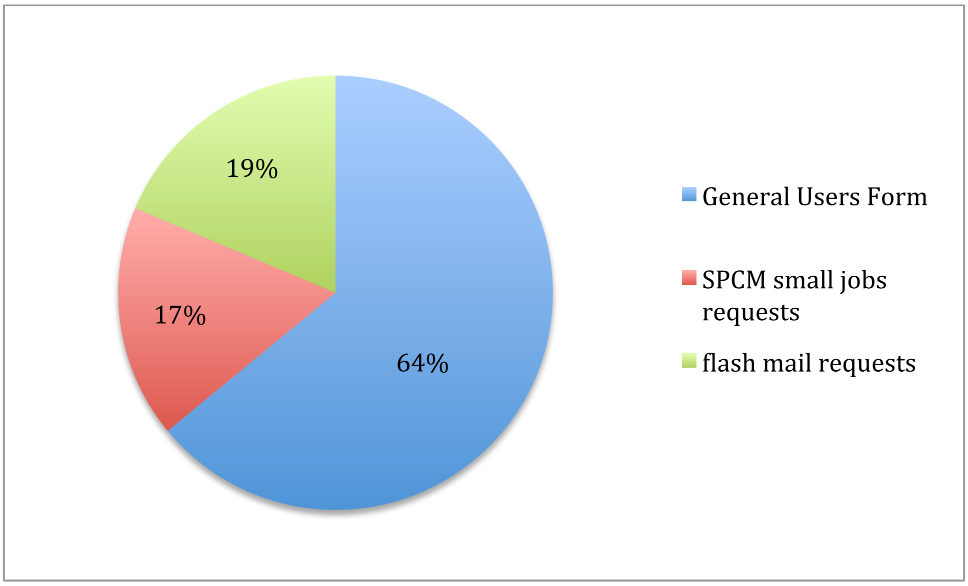

Not included in this number are the scheduled maintenance activities on the research and general facilities of the LNF, and any work executed by the Electric Systems Dept. on request of the INFN Head Quarters in Rome.

The following departments were involved in the requests:

Depts. Involved	requests	%
General Services Dept.	272	32,08
Electric Installations Dept.	204	24,06
SPCM	147	17,33
Building Dept.	143	16,86
HVAC Dept.	80	9,43
SMCA	2	0,24
total	**848**	**100,00**

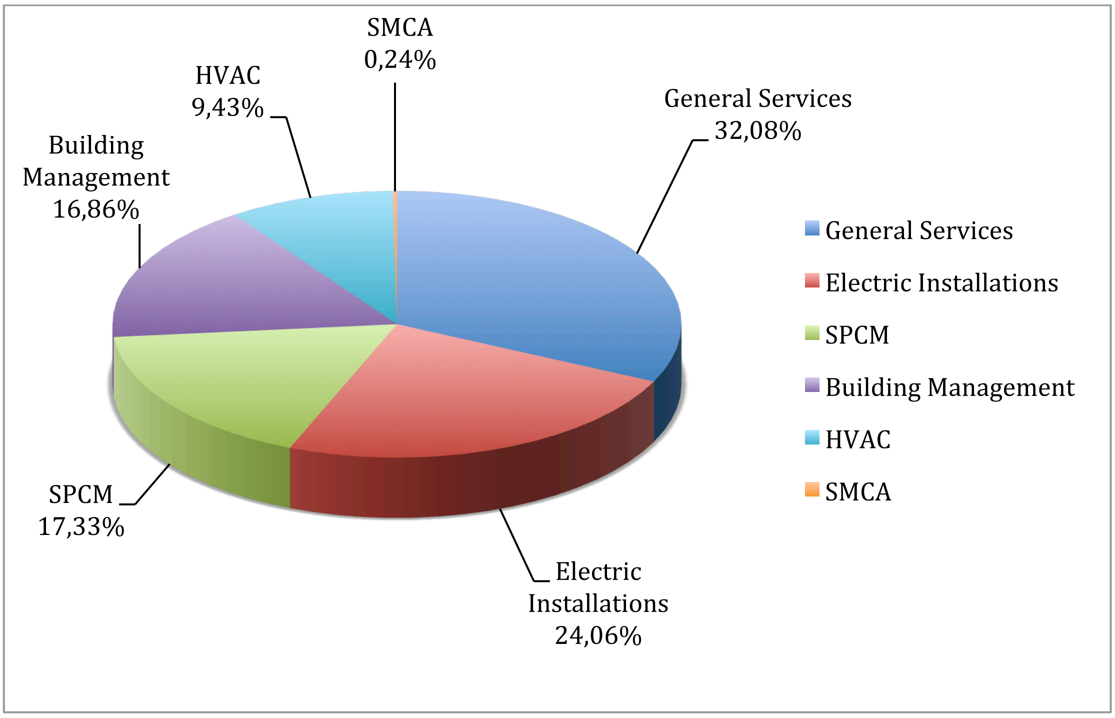

We may better specify the requests, dividing between requests for support of scientific activities and general facility management requests:

Dept.	Facility Mgt.	Scient.Supp.
General Services Dept.	272	
Building Dept.	143	
Electric Dept. - telephones	94	
HVAC Dept. Heating & AC	65	15
Electric Dept. – elect. repairs	55	55
SPCM		147
total	**629**	**217**

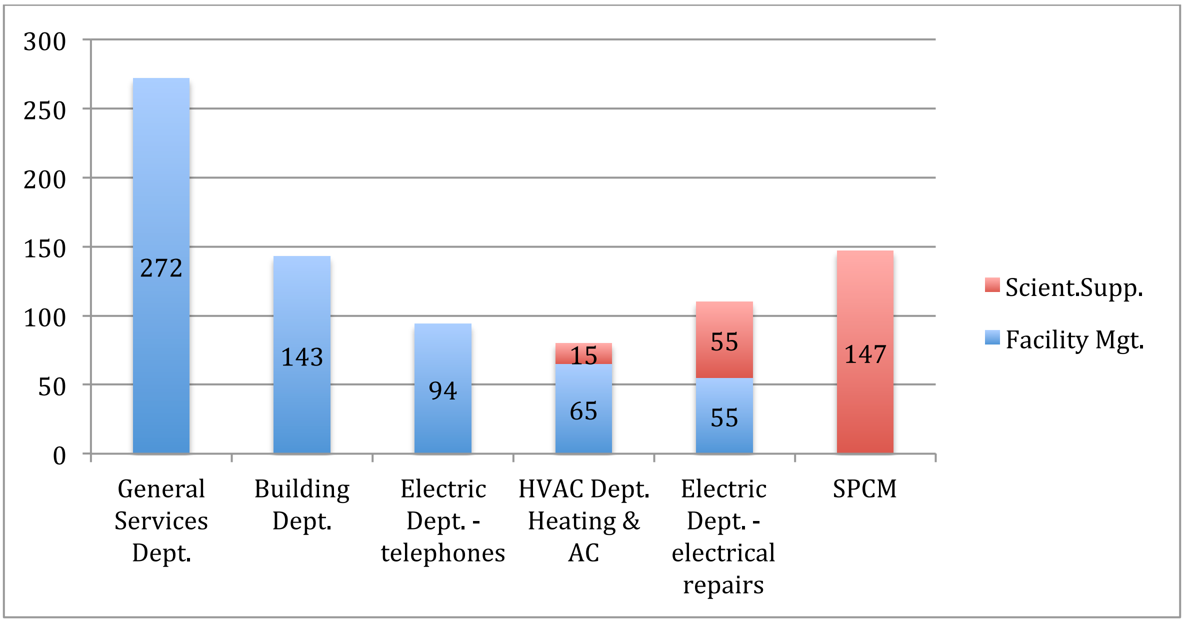

As may be expected, the Research Division was the main requester for support activities (45%), whereas the Accelerator Division came second with 17%:

Origin of requests	**qty**	**%**
Research Division	378	44,58
Accelerator Division	147	17,33
Technical Division*)	105	12,38
unspecified origin	88	10,38
LNF Directorate	39	4,60
Administrative HQ	24	2,83
Health & Radiation Safety	23	2,71
SPARC	16	1,89
HR Dept.	10	1,18
Admin. Dept.	9	1,06
Safety & Protection	9	1,06
total	**848**	**100**

*) A number of activities generated within the Technical Division but pertaining to the whole of the LNF have been registered as requests originating from the Technical Division (12%).

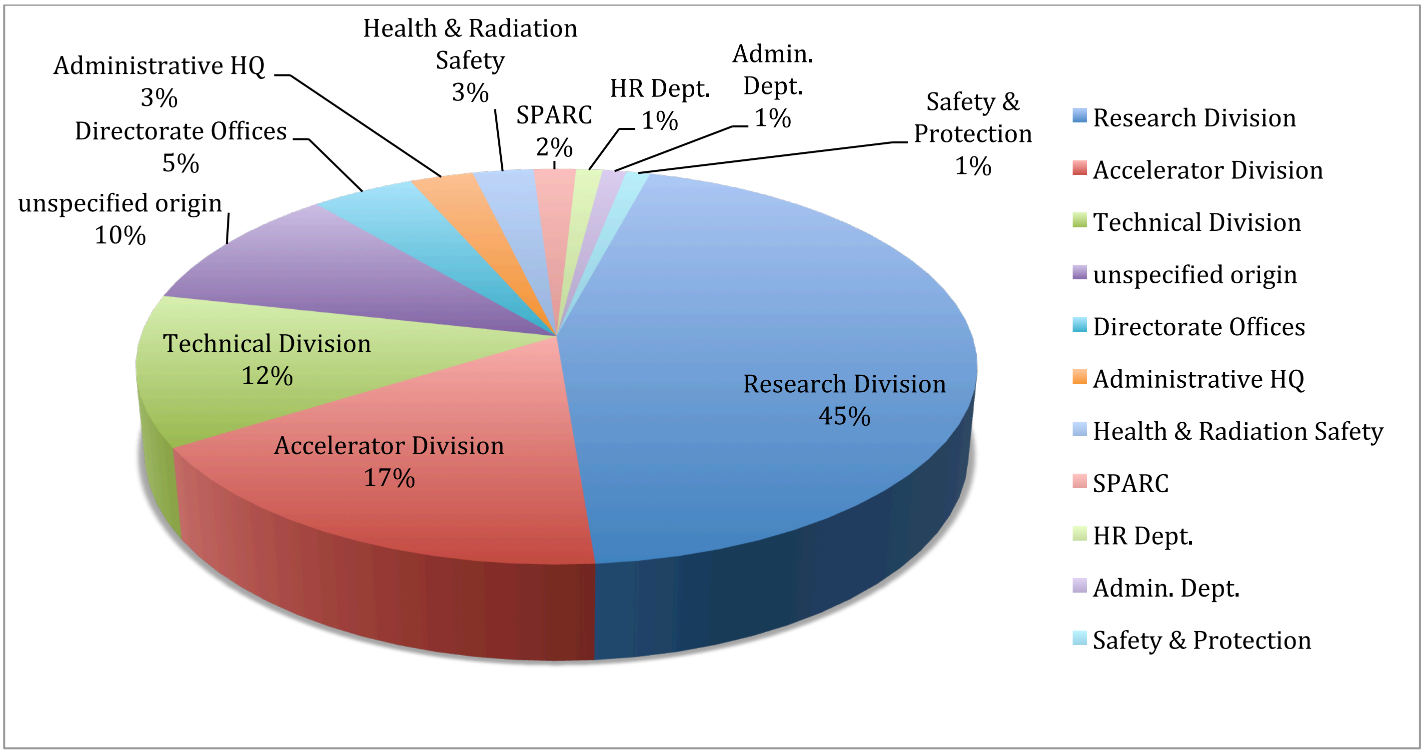

JOB COMPLETION TIMES

No statistics are available of the times of response/solution of the 158 flash mail requests. Of the remaining 690 requests, 653 have been closed with an overall average completion of 38 days (this was 39 days in 2012):

AVERAGE TIME OF JOB COMPLETION	
DEPT.	**DAYS**
SPCM	13
General Services	29
Telephone Systems	35
Electric Systems	46
Building Management	56
HVAC	56
SMCA	66
Piping Systems	251
Overall	**38**

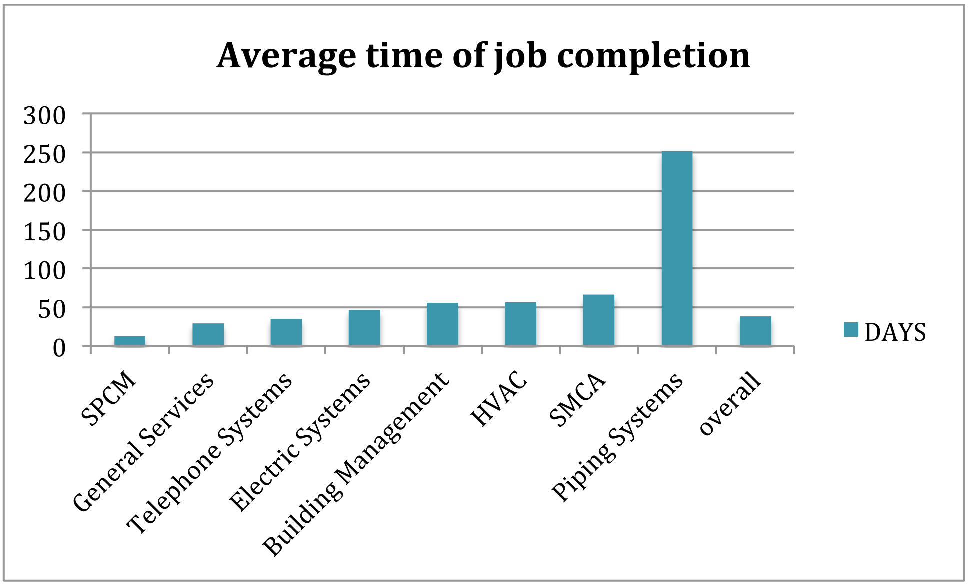

FINANCE

In 2013 the Technical Division almost €4.000.000 (2012: €4.402.108,54), between the General Stores budget (Magazzini – see section 3.), the Division's main budget, other Division budgets (e.g. water supplies, insurances, phone bills, cleaning services, guards services, ...) and non TD-budgets (e.g. Accelerator Division, Infrastrutture Sperimentali, ...).

Budget	**2013**	**2012**
General Stores budget	€74.917,37	€83.682,01
TD main budget	€1.331.975,44	€1.454.537,04
Other TD budgets	€2.326.855,16	€2.430.611,56
Other non TD budgets	€255.542,23	€433.277,93
TOTAL	**€3.989.290,20**	**€4.402.108,54**

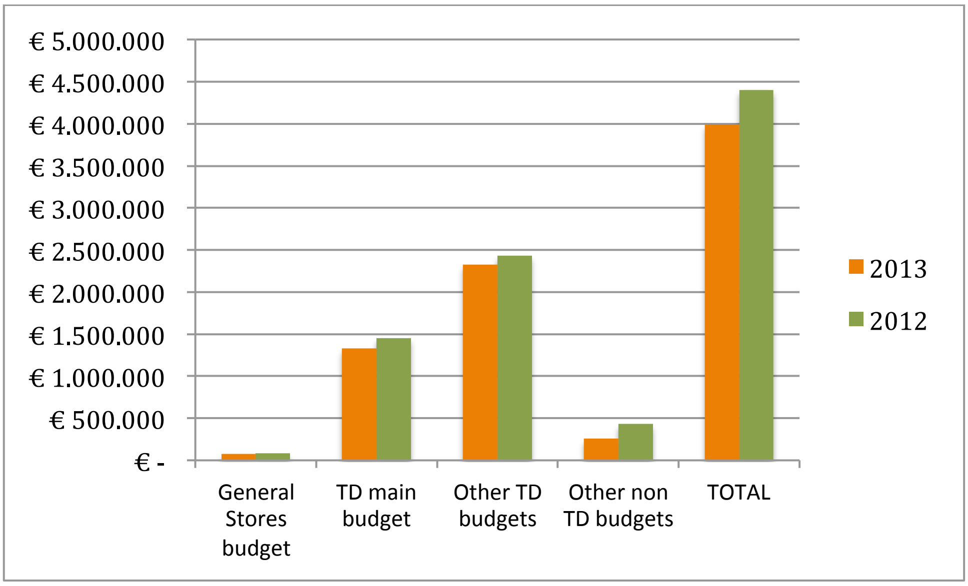

The Division departments have issued orders on the General Stores budget and the TD main budget as follows:

Dept.	**Spent 2013**
HVAC & Piping Systems	€369.497,07
Building Mgt	€321.266,56
Electric Systems	€263.472,25
Gen. Services	€213.381,88
Gen. Stores	€153.153,73
SPCM	€50.307,26
Other	€35.212,88
TOTAL	**€1.406.291,63**

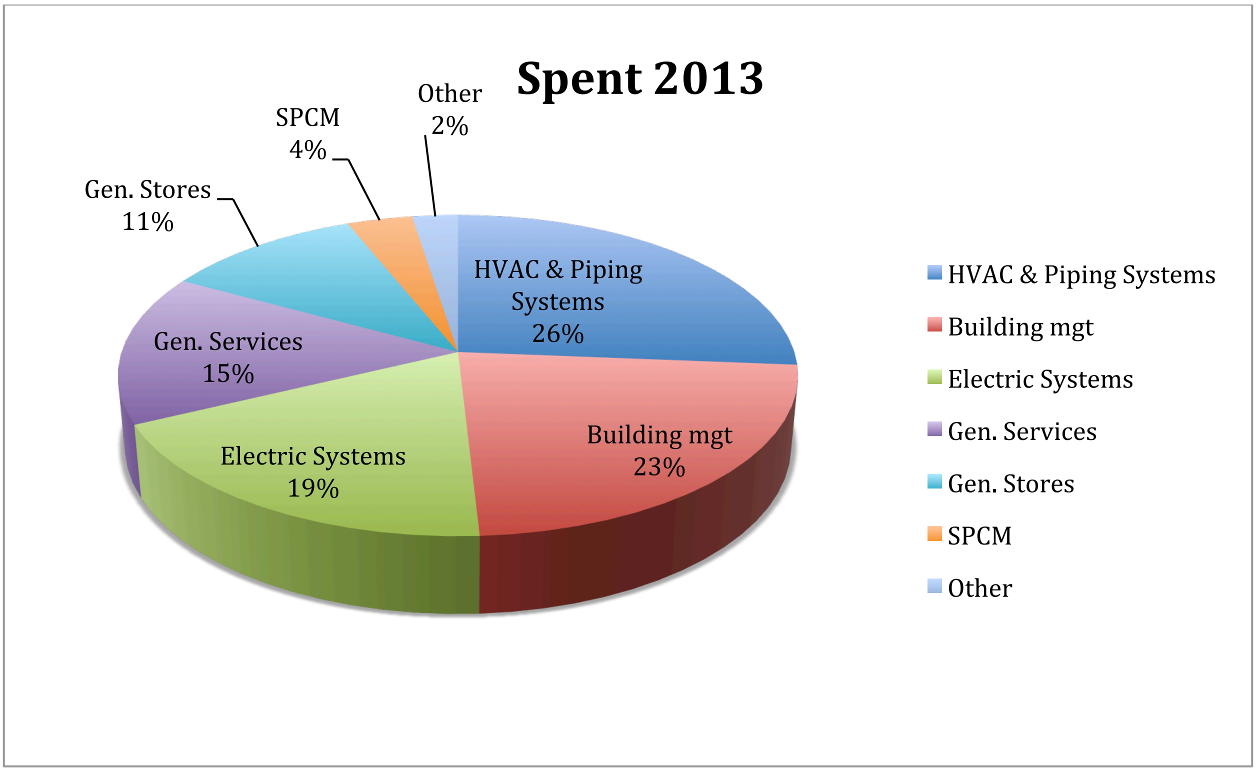

A total of 304 purchasing orders have been issued by the Technical Division Departments:

Dept.	**Purchasing Orders**
HVAC & Piping Systems	**81**
Gen. Stores	**72**
Gen. Services	**39**
Electric Systems	**37**
Building Mgt	**25**
SPCM	**25**

Other	**25**
TOT.	**304**